Mathematical modelling of hybrid biomedical imaging by mechanical perturbations

Laurent Seppecher

ED 386 : Ecole doctorale de sciences mathématiques de Paris-Centre

Thèse de doctorat

Modélisation de l'imagerie biomedicale hybride par perturbations mécaniques

Présentée pour obtenir le grade de

Docteur de l'Université Pierre et Marie Curie

Spécialtité : Mathématiques Appliquées

par

Laurent SEPPECHER

Soutenue publiquement le 20 Juin 2014 devant le jury composée de

M. Habib AMMARI	Directeur de thèse
M. Josselin GARNIER	Codirecteur de thèse
M. Otmar SCHERZER	Rapporteur
M. John SCHOTLAND	Rapporteur
M. Stéphane MALLAT	Examinateur
Mme. Laure SAINT-RAYMOND	Examinatrice
M. JIN KEUN SEO	Examinateur

Contents

Résumé

Dans cette thèse, nous introduisons et développons une approche mathématiques originale des techniques d'imagerie biomédicale dites «hybrides». L'idée et d'appliquer une méthode d'imagerie mal posée, tout en perturbant le milieu à imager par des déplacements mécaniques. Ces déplacements provenant d'une équation de type onde élastique perturbent les mesures effectuées. En utilisant ces mesures perturbées, et profitant du caractère local des perturbations mécaniques, il est possible d'augmenter considérablement la résolution de la méthode de base. Le problème direct est donc un couplage d'une EDP décrivant la propagation utilisée pour la méthode de base et d'une seconde décrivant les champs de déplacement mécaniques. Dans toutes cette thèse, on fait l'hypothèse d'un milieu mécaniquement homogène afin d'assurer le contrôle et la géométrie des ondes perturbatrices utilisées.

A partir des mesures perturbées, une étape d'interprétation permet de construire une donnée interne au domaine considéré. Cette étape nécessite en général l'inversion d'opérateurs géométriques intégraux de type Radon, afin d'utiliser le caractère localisant des perturbations utilisées. A partir de cette donnée interne, il est possible d'initier une procédure de reconstruction du paramètre physique recherché.

Dans le chapitre 1, il est question d'un couplage entre micro-ondes et perturbations sphériques. Dans les chapitres 2, 3 et 4, nous étudions l'imagerie optique diffuse toujours couplée avec des perturbations sphériques. Enfin dans le chapitre cinq, nous donnons une méthode originale de reconstruction de la conductivité électrique par un couplage entre champs magnétique et perturbations acoustiques focalisées.

Abstract

This thesis aims at developing an original mathematical approach for modeling hybrid biomedical imaging modalities. The core idea is to run an ill-posed imaging method while perturbing the medium using mechanical displacements. These displacements described by an elastic wave equation perturb the collected measurements. Using these perturbed measurements and taking advantage of the perturbation localizing effect, it is possible to significantly overcome the resolution of the basic method. The direct problem here is a coupling between a PDE describing the propagation used for the basic method and a second one describing the mechanical displacements fields. In the whole thesis, we only consider mechanically homogeneous medium in order to assure the control and the geometry of the perturbing wavefronts.

From these perturbed measurements, an interpretation step leads to an internal data map inside the considered medium. This step usually requires inversion of geometric integral operators such as Radon transform. This allows to use the geometrical localizing behavior of the perturbations. From this internal data, one can start a recovering procedure for the unknown physical parameter. This recovering step involves a new non physical PDE, non linearly coupled with the main modality equation.

In the first chapter, we study a coupling between micro-waves and spherical perturbations. In chapter 2, 3 and 4, we propose a model for diffuse optical imaging coupled with spherical perturbations. In chapter 5, we introduce a new method for imaging the electric conductivity by a coupling between magnetic field and focused acoustic perturbations.

Introduction

This thesis aims at developing an original mathematical and numerical framework for modeling biomedical imaging modalities based on mechanical perturbations of the medium.

Many kinds of waves propagate in biological tissues over certain frequency ranges. Each of them can be used to provide an image of a specific physical parameter. Low-frequency electromagnetic waves are sensitive to electrical conductivity; optical waves tell about optical absorption, ultrasonic waves reveal tissue's density, mechanical shear waves indicate how tissues respond to shear forces. However, single-wave imaging modalities are known to suffer from low specificity as well as intrinsic instabilities and low resolution. These fundamental deficiencies are impossible to eliminate, unless additional a priori information is incorporated. Single-wave imaging modalities can only be used for anomaly detection. Expansions techniques for data analysis, which reduce the set of admissible solutions and the number of unknowns, allow robust and accurate reconstruction of the location and of some geometric features of the anomalies, even with moderately noisy data.

One promising way to overcome the inherent limits of single-wave imaging and provide a stable and quantitative reconstruction of a physical parameters distribution is to combine different wave-imaging modalities [3]. A variety of multi-wave imaging approaches are being introduced and studied. In such approaches, two or more types of physical waves are involved in order to overcome the individual deficiencies of each of them and to combine their strengths. Because of the way the waves are combined, multi-wave imaging can produce a single image with the best contrast and resolution properties of the two waves.

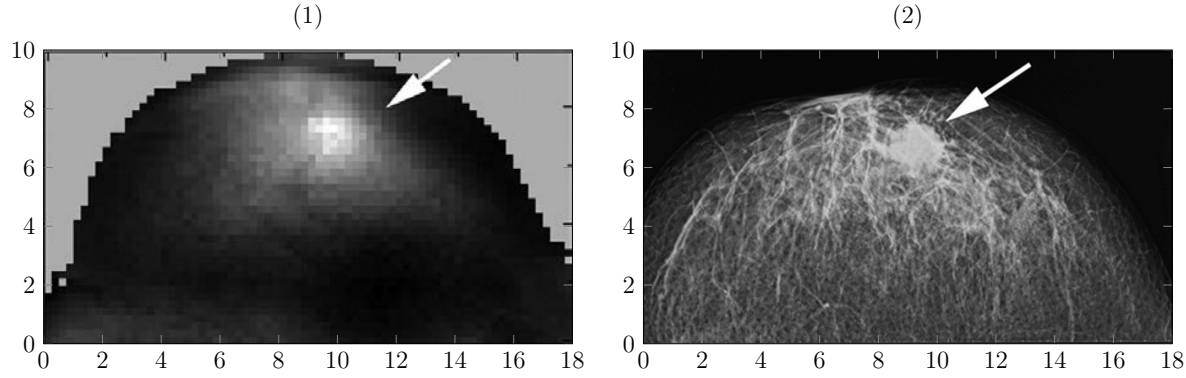

Figure 1: Comparison between Near Infra-Red diffuse light tomography image (1) and a scanner (X-rays attenuation) image (2) of the same breast tumor. This illustrates the inherent lack of resolution of the diffuse optical tomography method.

Three different types of wave interaction can be exploited in multi-wave imaging [55]: (i) the interaction of one kind of wave with tissue can generate a second kind of wave; (ii) a low-frequency wave that carries information about the desired contrast can be locally modulated by a second wave that has better spatial resolution; (iii) a fast propagating wave can be used to acquire a spatio-temporal sequence of the propagation of a slower transient wave.

Multi-wave imaging approaches are particularly useful for obtaining three physical parameters that until recently have been difficult to map with satisfactory spatial resolution: electrical conductivity, optical absorption, and shear modulus.

In this thesis, we introduce a new multi-wave imaging approach. By mechanically perturbing the medium we prove both analytically and numerically stability and resolution enhancement for reconstructing electrical and optical tissue parameters. We show how the high contrast of the microwave, optical, and electrical tomographies can be coupled to the high resolution of the acoustic propagation in soft tissues. The use of mechanical perturbations of the medium modeled by acoustics equations in fluids enhance the resolution to the order of the front width of the acoustic wave, which propagates inside the object.

It is also worth emphasizing that our approach in this thesis is different from the imaging by controlled perturbations [3, 6, 13, 17, 43, 58, 110], where local changes of the parameters of the medium are produced by focalizing an ultrasound beam. Both techniques lead to resolution enhancements. In imaging by controlled perturbations, the resolution is of order the size of the focal spot while here it is of the order of the width of the wave front of the wave propagating in the medium.

The core idea of our approach in this thesis is quite different from imaging by controlled perturbations. It is based on taking microwave, optical or electrical boundary measurements while an acoustic wave is propagating inside the medium and then changing the material parameter of the medium. We show that by cross-correlating boundary measurements it is possible to significantly overcome the resolution limits in microwave imaging, optical and electrical tomographies.

Our purpose is threefold. First, we carefully derive mathematical models for these emerging multi-wave modalities. Second, we analyze these mathematical models and study important uniqueness and stability issues of the associated reconstruction problems. Third, we design image reconstruction algorithms and analytically and numerically investigate their robustness.

Overview of the thesis

Chapter 1

In this chapter, we develop new mathematical tools and inversion methods to address a new biomedical imaging modality called acousto-electromagnetic tomography. This method is based on taking microwave boundary measurements while an acoustic wave is propagating inside the medium and then changing the electromagnetic parameter of the medium. We show that by cross-correlating boundary measurements it is possible to significantly overcome the classical Rayleigh resolution limit in microwave imaging.

For simplicity, we only consider transverse magnetic (TM) waves. For modelling TM-waves in microwave imaging we use a scalar Helmholtz equation in two dimensions together with a Sommerfeld radiation condition. The objective is to image the permittivity of a

dielectric object. The object is confined in a bounded domain Ω and is illuminated by a plane wave of given incidence and the scattered field is measured on the boundary of Ω. Boundary measurements are carried out at one given frequency. In the cross-correlation of boundary measurements, the normal derivatives of the scattered fields are needed. In practice, they are not measured. However, they can be constructed using the exterior capacity operator for the domain Ω; see [93]. Since the electromagnetic waves are propagating in the whole space, their derivatives on the boundary can be expressed in terms of their traces, *i.e.*, the boundary measurements. The sources of the acoustic waves are placed on a circle or a sphere outside the object to be imaged. The medium is supposed to be acoustically homogeneous.

By mechanically perturbing the medium, we show that it is possible to achieve a significant resolution enhancement. We provide a new inversion formula for the permittivity distribution from cross-correlations between the electromagnetic boundary measurements in the perturbed medium and in the unperturbed one. We present numerical results to illustrate the resolution and the stability performances of the proposed reconstruction algorithm.

Chapters 2, 3, and **??** are devoted to optical imaging. Diffuse optical tomography is an emerging biomedical modality that uses diffuse light to probe structural variations in the optical properties of tissue [27]. The associated inverse problem for diffuse waves consists of recovering the absorption properties of a medium of interest from boundary measurements of the light intensity. The most important current applications of diffuse optical imaging are detecting tumors in the breast and brain imaging [33]. In diffuse optical imaging, the resolution is in general low. The aim of Chapters 2, 3, and **??** is to model a new method, called ultrasound-modulated diffuse optical tomography, for reconstructing the optical absorption coefficient of a medium from boundary measurements.

Chapter 2

In this chapter, we develop an efficient fixed point reconstruction algorithm for ultrasound-modulated diffuse optical tomography. In diffuse optical imaging, the resolution is in general low. By mechanically perturbing the medium, we show that it is possible to achieve a significant resolution enhancement. When a spherical acoustic wave is propagating inside the medium, the optical parameter of the medium is perturbed. Using cross-correlations of the boundary measurements of the intensity of the light propagating in the perturbed medium and in the unperturbed one, we provide an iterative algorithm for reconstructing the optical absorption coefficient. Using a spherical Radon transform inversion, we first establish an equation that the optical absorption satisfies. This equation together with the diffusion model constitutes a nonlinear system. Then, solving iteratively such a nonlinear coupled system, we obtain the true absorption parameter. We prove the convergence of the algorithm and present numerical results to illustrate its resolution and stability performances.

Chapter 3

This Chapter aims to generalize the acousto-optic process for inclusions. We tackle the nonlinear optical reconstruction problem for discontinuous optical distributions. We develop a mathematical framework for the reconstruction problem in the case where the optical absorption distribution is a perturbation of a piecewise constant function. We introduce an iterative reconstructing algorithm of Landweber-type and prove its convergence and stability.

For doing so, we introduce a weak Helmholtz decomposition and interpret in a weak sense the cross-correlation measurements.b

Chapter 4

The aim of this chapter is to prove that the algorithm presented in Chapter 2 can be extended for a very general class of discontinuous absorption maps. Starting from the same differential boundary measurements

$$M_v = \int_\Omega (a_v - a)\Phi\Phi_v$$

where v is the smooth displacement field, Φ the light fluance and Φ_v. We consider the case where a has bounded variations and under some additional hypothesis, we understand the first order term in the asymptotic formula when $\|v\|_{L^\infty}$ goes to zero. Look for the same kind of algorithm than in Chapter 2 we manage to decrease the smoothness of the unknown absorption to be recovered. We give a new fixed point algorithm proving that the absorption is the fixed point of a contracting map in $H^s(\Omega)$ where $s < 1/2$. This allows the reconstruction of a much wider class of absorption maps admitting discontinuities. By a clever change of variable, we study two coupled linear elliptic PDEs interpreted in the classical variational point of view. In this chapter, the global Lipschitz stability of the whole imaging process is proved. We give some numerical examples to illustrate the ability of this new algorithm.

Chapter 5

In this Chapter, we provide a mathematical analysis and a numerical framework for Lorentz force electrical conductivity imaging. Ultrasonic vibration of a tissue in the presence of a static magnetic field induces an electrical current by the Lorentz force. This current can be detected by electrodes placed around the tissue; it is proportional to the velocity of the ultrasonic pulse, but depends nonlinearly on the conductivity distribution. The imaging problem is to reconstruct the conductivity distribution from measurements of the induced current. To solve this nonlinear inverse problem, we first make use of a virtual potential to relate explicitly the current measurements to the conductivity distribution and the velocity of the ultrasonic pulse. Then, by applying a Wiener filter to the measured data, we reduce the problem to imaging the conductivity from an internal electric current density. We first introduce an optimal control method for solving such a problem. A new direct reconstruction scheme involving a partial differential equation is then proposed based on viscosity-type regularization to a transport equation satisfied by the current density field. We prove that solving such an equation yields the true conductivity distribution as the regularization parameter approaches zero. We also test both schemes numerically in the presence of measurement noise, quantify their stability and resolution, and compare their performance. Our results in this chapter dramatically improve the stability and resolution of electrical impedance imaging.

The results in Chapers 1, 2, 3 and 5 are published as[8, 9, 18, 19].

Main notations

$BV(\Omega)$	is the set of bounded variation functions in Ω. See definition 4.1.1.
$\mathcal{C}^n(\Omega)$	with $n \in \mathbb{N}$ is the set of function n times differentiable in $\Omega \subset \mathbb{R}^d$.
$\mathcal{C}^{n,\alpha}(\Omega)$	with $n \in \mathbb{N}$, $\alpha \in [0,1[$, $\Omega \subset \mathbb{R}^d$ is the set of function f n times differentiable in $\Omega \subset \mathbb{R}^d$ and such that $f^{(n)}$ is α-Holder in Ω.
$\mathcal{C}_S^{n,\alpha}(\Omega)$	is the set of functions of class $C^{n,\alpha}$ in $\Omega \backslash S$ where S is a smooth surface of class $\mathcal{C}^{n+1}$. It is a model set for piecewise Holder regularity. See definition 5.4.1.
$\mathcal{D}(\Omega), \mathcal{D}'(\Omega)$	respectively the set $\mathcal{C}_c^\infty(\Omega)$ and its topological dual, the set of distributions in Ω.
$\mathcal{S}(\mathbb{R}^d), \mathcal{S}'(\mathbb{R}^d)$	respectively the Schwartz space and its topological dual, the set of temperated distributions.
$\mathcal{E}(\mathbb{R}^d), \mathcal{E}'(\mathbb{R}^d)$	respectively the set $\mathcal{C}^\infty(\mathbb{R}^d)$ and its topological dual, the set of compactly supported distributions.
D	is the derivative operator for scalar distributions. The symbol ∇ will be only used if the derivative belongs to a functional space.
$\mathrm{D}_l, \mathrm{D}_j, \mathrm{D}_c$	respectively the Lebesgue part, the jump part and the Cantor part of the derivative of a function with bounded variations. See subsection 4.1.1.
d_x	is the Fréchet differential operator with respect to the vectorial variable x.
∂_{x_i}	is the partial derivative operator with respect to the scalar variable x_i.
$H^s(\Omega), H^s_{\mathrm{loc}}(\Omega)$	with $s \geq 0$, respectively $W^{s,2}(\Omega)$ and $W^{s,2}_{\mathrm{loc}}(\Omega)$.
$H^s_K(\Omega)$	$s \in \mathbb{R}$, is the set of distribution supported in the compact $K \subset \Omega$ and with H^s regularity. See subsection 4.6.2.
$\mathcal{H}^\alpha, \mathcal{H}^\alpha_S$	respectively the Hausdorff measure of dimension $\alpha > 0$ in $\mathbb{R}^d$ and it restriction to a subset $S \subset \mathbb{R}^d$. $\mathcal{H}^\alpha_S(A) = \mathcal{H}^\alpha(A \cap S)$.
$\mathcal{R}, \vec{\mathcal{R}}$	respectively the spherical means Radon transform operator and the outgoing flow transform operator. See subsection 4.1.3

$SBV(\Omega)$	is the special class of bounded variation functions on Ω. See definition 4.1.2.
$SBV^p(\Omega)$	with $p \in [1, +\infty]$. See definition 4.1.3.
σ	is the classic surface measure on the considered surface. It is equal to the Hausdorff measure $\mathcal{H}^{d-1}$ restricted to the considered surface.
$\lvert\cdot\rvert_{TV(\Omega)}$	or $\lvert\cdot\rvert_{BV(\Omega)}$ is the total variations semi-norm of $BV(\Omega)$. The real number $\lvert f\rvert_{TV(\Omega)}$ corresponds to $\lvert \mathrm{D}a\rvert(\Omega) = \int_\Omega \lvert \mathrm{D}a\rvert$.
$W^{s,p}(\Omega), W^{s,p}_{\mathrm{loc}}(\Omega)$	with $s \geq 0$ and $p \in [1, +\infty]$, respectively the fractional order Sobolev space and $W^{s,p}_{\mathrm{loc}}(\Omega) := \{f \in L^p_{\mathrm{loc}}(\Omega),\ \forall x \in \Omega,\ \exists \varepsilon > 0,\ f \in W^{s,p}(B(x, \varepsilon))\}$.

Chapter 1

Acousto-microwave tomography, a model problem

Introduction

The purpose of this first chapter is to illustrate with a first simple model, the different aspects of a mathematical study of imaging by mechanically perturbing the medium. The imaging problem considered here is to reconstruct from boundary measurements the electromagnetic parameter $q(x)$ involved in the Helmholtz equation

$$\triangle\varphi + \omega^2 q\varphi = 0 \tag{1.1}$$

in a bounded domain $\Omega \subset \mathbb{R}^d$, for $d = 2, 3$, where ω is the operating frequency.

Using controlled mechanical perturbations of Ω, we define the data as the evaluation of the outward normal derivative $\partial_\nu\varphi$ on $\partial\Omega$, which change due to the mechanical perturbations.

Being one of the modern techniques in medicine, microwave tomography (MWT) has significant advantages over x-rays, computed tomography (CT), and nuclear magnetic resonance (NMR) imaging; see [42]. Microwave imaging has good contrast since malignant anomalies have very different electric properties than the background healthy tissues. Moreover, it does not require either ionizing radiation or contrast agents and is an inexpensive and a transportable modality. However, it suffers from poor space resolution limited by the Rayleigh criterion when compared to x-rays, CT or NRM tomography. It is well-known that the main problem using microwaves in classical tomography methods is that it is impossible to get a better resolution than half the wavelength. Typically, the operating frequency of microwaves is between 1 GHz and 200 GHz, and this imposes a wavelength of microwaves between 1.5 mm and 300 mm. Then, if we want to image small objects or use low-frequency microwaves for physical or biological reasons, we need a way to increase resolution of classical methods.

It is shown in this chapter how the high contrast of the microwave tomography can be coupled to the high resolution of the acoustic propagation in soft tissues. The use of mechanical perturbations of the medium modeled by acoustics equations in fluids enhance the resolution to the order of the front width of the acoustic wave, which propagates inside the object. This chapter aims at developing a mathematical and numerical framework for a new hybrid imaging technique called acousto-microwave tomography. The resolution and stability enhancements are illustrated both analytically and numerically.

In order to model this emerging hybrid biomedical technique, we start with time-harmonic Maxwell's equations

$$\nabla \times \left(\frac{1}{\mu}\nabla \times E\right) - \omega^2 \varepsilon E = 0, \tag{1.2}$$

where E is the electric field, ε is the electric permittivity, μ the magnetic permeability, and ω the operating frequency. In order to simplify this vectorial equation, we only consider polarized transverse magnetic waves and arrive at the scalar model

$$\nabla \cdot \left(\frac{1}{\mu}\nabla \varphi\right) + \omega^2 \varepsilon \varphi = 0 \tag{1.3}$$

with φ being the complex amplitude of the electric field. Moreover, we consider nonmagnetic objects, i.e., with a constant magnetic permeability μ and a variable electric permittivity ε that we want to image. This choice is not crucial because all the following computations can be done with both μ and ε variable. By changing the frequency, we can separate the information about these two parameters. Moreover, in biological tissues, the permittivity ε is much more contrasted than the permeability μ.

Denote by $q(x) = \mu\varepsilon(x)$. The electric amplitude φ satisfies

$$\triangle \varphi + \omega^2 q \varphi = 0 \quad \text{in } \Omega. \tag{1.4}$$

In acousto-microwave tomography microwave, we take boundary measurements while an acoustic wave is propagating inside the medium and then changing the permittivity of the medium. Our main idea is to cross-correlate boundary measurements in order to significantly overcome the Rayleigh resolution limit.

Denote by $v : \Omega \longrightarrow \mathbb{R}^d$, a displacement field such that $|v| < \text{dist}(\text{supp}v, \partial\Omega)$. The permittivity distribution q changes to q_v defined implicitly by

$$q_v(x + v(x)) = q(x), \quad \forall x \in \Omega. \tag{1.5}$$

The electric field changes to φ_v which satisfies

$$\triangle \varphi_v + \omega^2 q_v \varphi_v = 0 \quad \text{in } \Omega. \tag{1.6}$$

Now, multiplying (1.4) by $\overline{\varphi_v}$ and the conjugate of (1.5) by φ and integrating both identities by parts, we immediately get the so called cross correlation formula:

$$\int_{\partial\Omega} (\partial_\nu \varphi \overline{\varphi_v} - \partial_\nu \overline{\varphi_v} \varphi) = \omega^2 \int_\Omega (q_v - q)\varphi \overline{\varphi_v}. \tag{1.7}$$

Assuming that the term on the left-hand side can be measured as a boundary integral term, we have access to the complex number

$$M_v = \int_\Omega (q_v - q)\varphi \overline{\varphi_v}. \tag{1.8}$$

Now considering that v changes with time (wave traveling), the choice of the source, the shape of the signal sent, etc, we can measure this quantities in a lot of configurations and from this knowledge, try to reconstruct the permittivity distribution q.

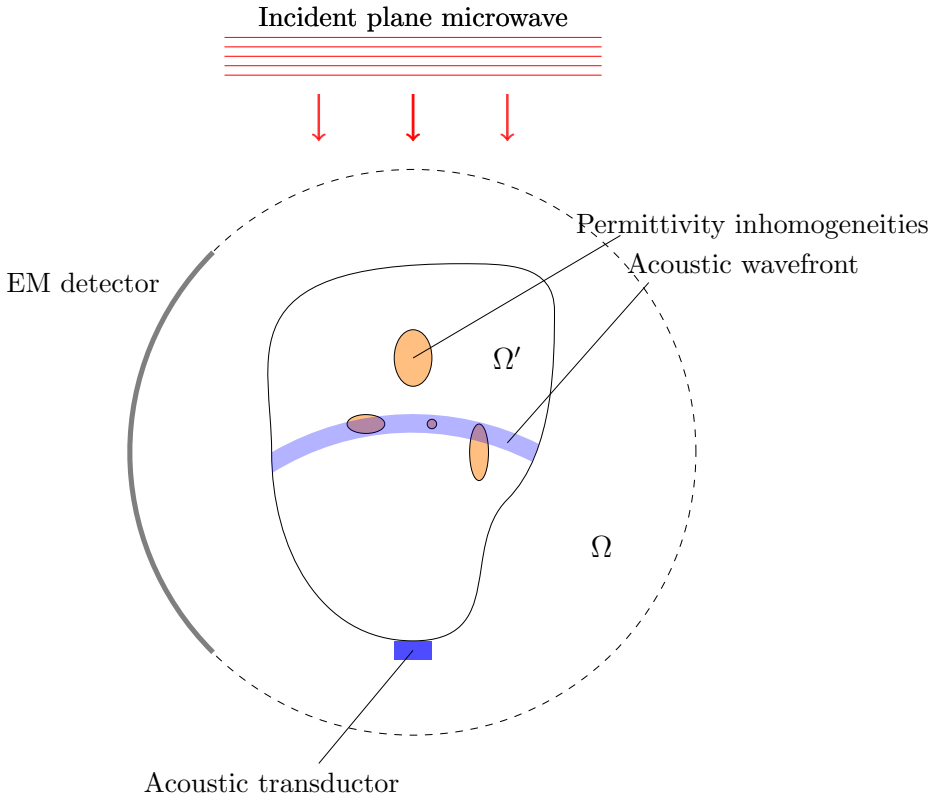

Figure 1.1: The support of v is the blue arc and the difference $\varphi_v - \varphi$ is generated in the intersection of the support of permittivity variations and the support of v. The electromagnetic (EM) detector measures the variations of φ_v on $\partial\Omega$ while the wavefront is traveling through the object.

The chapter is organized as follows. In the first section, we discuss inherent difficulties of well posing the direct problem for the Helmholtz equation. We discuss the choice of working in free space instead of a bounded domain. Under the assumption of Born approximation, we give several stability results for the solution to use latter. In the second section we establish an asymptotic formula for (1.7) and interpret the measurements as an approximation of a much simpler quantities. In the third section we derive a model for the displacement field v which is created by a pressure wave traveling in a mechanically homogeneous medium. The spherical symmetry of the displacement brings a spherical symmetry to the measurement. The fourth section introduces the spherical means Radon transform and provides asymptotic formula involving the radial derivative of the Radon transform of q. This formula is first written for q smooth then extended to the piecewise constant case using the smoothing properties of the spherical means Radon transform. In the fifth section, we illustrate the resolution and the stability of the reconstruction through the inversion of the spherical means Radon transform by a filtered back propagation algorithm. The chapter ends with some concluding remarks.

1.1 Helmholtz equation in heterogeneous media

We assume that the variations of q is compactly supported in Ω. In other words, there exists a positive constant $q_0 > 0$ and a function $s \in L^\infty(\Omega)$ supported in $K \subset \Omega$ such that $||s||_\infty < 1$ and

$$q(x) = q_0(1 + \delta s(x)), \quad \forall x \in \Omega, \tag{1.9}$$

where δ is a positive constant.

There are two classical frameworks for studying the Helmholtz equation. We can consider a wave propagation problem in Ω with several kinds of boundary conditions such as Dirichlet, Neumann, or Robin boundary conditions. We can also consider a free space propagation problem extending q in $\mathbb{R}^d \backslash \Omega$ by q_0. The choice of the model depends on the physical constraints about the measurement of the electromagnetic wave. In this chapter, we choose to deal with the free space propagation problem. The treatment of the bounded problem with boundary conditions could follow exactly the same arguments and methodology presented here provided a uniform assumption with respect to the medium changes on the well-posedness of the Helmholtz equation.

1.1.1 Model problem

Here, we extend q by q_0 in $\mathbb{R}^d \backslash \Omega$ and assume that the medium is illuminated by a plane wave $\varphi_I(x) = Ae^{-ik\cdot x}$.

We look for solutions to the Helmholtz equation in the form

$$\varphi = \varphi_I + \varphi_S, \tag{1.10}$$

where φ_S is called the scattered wave and satisfies

$$\triangle \varphi_S + \omega^2 q \varphi_S = -\omega^2 (q - q_0)\varphi_I \quad \text{in } \mathbb{R}^d, \tag{1.11}$$

together with the outgoing Sommerlfeld radiation condition at infinity.

Proposition 1.1.1 *Consider $f \in L^2_c(\mathbb{R}^d)$ and $q \in L^\infty(\mathbb{R}^d)$ such that $0 < q_{min} \leq q$ and $supp(q - q_0) \subset K$ compact. Then the problem*

$$\begin{cases} \triangle \varphi_S + \omega^2 q \varphi_S = f \quad in\ \mathbb{R}^d \\ \lim\limits_{|x|\to\infty} |x|^{\frac{d-1}{2}} \left(\dfrac{x}{|x|} \cdot \nabla - i\omega\sqrt{q_0} \right) \varphi_S(x) = 0 \ uniformly\ in\ x/|x| \end{cases}$$

has a unique solution in $H^2_{loc}(\mathbb{R}^d)$.

Proposition 1.1.2 *Define the function $\Gamma \in W^{1,1}_{loc}(\mathbb{R}^d)$ by*

$$\Gamma(x) = \begin{cases} \dfrac{i}{4} H_0^{(1)}(\omega\sqrt{q_0}|x|) & if\ d = 2, \\ \dfrac{e^{i\omega\sqrt{q_0}|x|}}{4\pi|x|} & if\ d = 3, \end{cases}$$

where $H_0^{(1)}$ is the first Hankel function. This function is the unique solution of the problem

$$\begin{cases} \triangle \Gamma + \omega^2 q_0 \Gamma = \delta_0 \quad in\ (\mathcal{D}'(\mathbb{R}^d), \\ \lim\limits_{|x|\to\infty} |x|^{\frac{d-1}{2}} \left(\dfrac{x}{|x|} \cdot \nabla - i\omega\sqrt{q_0} \right) \Gamma(x) = 0 \ uniformly\ in\ x/|x|. \end{cases}$$

Moreover, the unique solution $u_0 \in H^2_{loc}(\mathbb{R}^d)$ of

$$\begin{cases} \triangle u_0 + \omega^2 q_0 u_0 = f \quad in\ \mathbb{R}^d, \\ \lim\limits_{|x|\to\infty} |x|^{\frac{d-1}{2}} \left(\dfrac{x}{|x|} \cdot \nabla - i\omega\sqrt{q_0} \right) u_0(x) = 0 \ uniformly\ in\ x/|x|, \end{cases} \tag{1.12}$$

where $f \in L^2_c(\mathbb{R}^d)$ can be written as

$$u_0 = \Gamma * f,$$

and satisfies the estimate

$$\|\varphi_0\|_{H^1(B_a)} \leq c_\Gamma(2a) \|f\|_{L^2(\mathbb{R}^d)}, \tag{1.13}$$

where B_a is the ball of radius a and $c_\Gamma(a) = \|\Gamma\|_{W^{1,1}(B_a)}$.

We have now the tools to establish a stability estimate for the scattered wave φ_S. This would be necessary for establishing the asymptotic formulas in the next sections.

1.1.2 Stability estimate

Consider a function $f \in L^2_c(\Omega)$ and assume that q is written as $q = q_0(1+\delta s)$ with $s \in L^\infty(\Omega)$, $||s||_\infty < 1$ and $\text{supp}(s) = K \subset \Omega$. Denoting u the unique solution in $H^2_{loc}(\mathbb{R}^d)$ of the problem

$$\begin{cases} \triangle u + \omega^2 q u = f \quad \text{in } \mathbb{R}^d \\ \lim\limits_{|x|\to\infty} |x|^{\frac{d-1}{2}} \left(\dfrac{x}{|x|} \cdot \nabla - i\omega\sqrt{q_0} \right) u(x) = 0 \text{ uniformly in } x/|x|, \end{cases} \tag{1.14}$$

the following stability result holds.

Proposition 1.1.3 *For any $\omega > 0$, there exists $\delta_0 > 0$ such that, for any $0 \leq \delta < \delta_0$, the solution of (1.14) satisfies the estimate*

$$\|u\|_{H^1(\Omega)} \leq C \|f\|_{L^2(\mathbb{R}^d)},$$

where C depends on δ_0 and Ω.

Proof. Let us introduce a positive number a such that $\Omega \subset B_a$. The solution u satisfies

$$\triangle u + \omega^2 q_0 u = f - \omega^2 q_0 \delta s u,$$

which by using the Green function representation gives

$$u = \Gamma * f - \omega^2 q_0 \delta \Gamma * (su) = \varphi_0 + Tu.$$

Here, φ_0 is the solution of (1.12) with $T : H^1(B_a) \longrightarrow H^1(B_a)$ is the continuous operator given by

$$Tu = -\omega^2 q_0 \delta \Gamma_\omega * (su).$$

Using the fact that $s \leq 1$ and $\mathrm{supp}(s) \subset B_a$, we have

$$\begin{aligned} \|Tu\|_{H^1(B_a)} \leq \omega^2 q_0 \delta \quad & \|\Gamma_\omega\|_{W^{1,1}(B_{2a})} \|su\|_{L^2(\mathbb{R}^d)} \leq \omega^2 q_0 \delta \|\Gamma_\omega\|_{W^{1,1}(B_{2a})} \|s\|_{L^p(B_a)} \|u\|_{H^1(B_a)} \\ & \leq C_p C_\Gamma(2a) \omega^2 q_0 \delta K^{1/p} \|u\|_{H^1(B_a)}, \end{aligned}$$

with $p > d$ and C_p the continuity modulus of the Sobolev injection $H^1(B_a) \hookrightarrow L^p(B_a)$. The operator norm of T is controlled by

$$\|T\|_{\mathcal{L}(H^1(B_a))} \leq C_p C_\Gamma(2a) \omega^2 q_0 \delta K^{1/p}.$$

Let us choose $\delta_0 < \delta_{max} := \left[C_p C_\Gamma(2a) \omega^2 q_0 K^{1/p}\right]^{-1}$. For any $0 \leq \delta < \delta_0$, we have $\|T\|_{\mathcal{L}(H^1(B_a))} < 1$. The solution u can then be written as $u = (I - T)^{-1} \varphi_0$. Since $\mathcal{L}(H^1(B_a))$ is a Banach space, we have

$$(I - T)^{-1} = \sum_{k=0}^{+\infty} T^k,$$

and then

$$\left\|(I - T)^{-1}\right\|_{\mathcal{L}(H^1(B_a))} \leq \sum_{k=0}^{+\infty} \|T\|^k_{\mathcal{L}(H^1(B_a))} = \frac{1}{1 - \|T\|_{\mathcal{L}(H^1(B_a))}} = \frac{\delta_{max}}{\delta_{max} - \delta}.$$

Moreover, estimate (1.13) gives

$$\|\varphi_0\|_{H^1(B_a)} \leq C_\Gamma(2a) \|f\|_{L^2(\mathbb{R}^d)}.$$

From

$$\|\varphi_S\|_{H^1(B_a)} \leq \left\|(I - T)^{-1}\right\|_{\mathcal{L}(H^1(B_a))} \|\varphi_0\|_{H^1(B_a)},$$

the result follows. □

Let the total field $\varphi = \varphi_I + \varphi_S$ with $\varphi_I(x) = Ae^{-ik\cdot x}$ and $|k| = \omega\sqrt{q_0}$. The function φ_S is the unique solution in $H^2_{loc}(\mathbb{R}^d)$ of

$$\begin{cases} \triangle\varphi_S + \omega^2 q\varphi_S = -\omega^2(q-q_0)\varphi_I \quad \text{in } \mathbb{R}^d, \\ \lim\limits_{|x|\to\infty} |x|^{\frac{d-1}{2}} \left(\dfrac{x}{|x|}\cdot\nabla - i\omega\sqrt{q_0}\right)\varphi_S(x) = 0 \text{ uniformly in } x/|x|. \end{cases} \tag{1.15}$$

Write $q = q_0(1+\delta s)$ with $s \in L^\infty(\Omega)$, $||s||_\infty < 1$ and $\text{supp}(s) = K \subset \Omega$. The following estimate holds.

Corollary 1.1.4 *For any $\omega > 0$, there exists $\delta_0 > 0$ such that, for any $0 \le \delta < \delta_0$, the scattered field φ_S satisfies*

$$\|\varphi_S\|_{H^1(\Omega)} \le CA\omega^2\delta|K|^{1/2}, \tag{1.16}$$

where C is a constant depending on δ_0 and Ω.

This corollary ensures that if the variations of q are not too large in amplitude and in support, then the scattered wave is of the order of these variations. In the next section, we assume that the variations are small and use the fact that $\varphi_S = o(\varphi_I)$ to develop an asymptotic formula for the cross-correlation formula (1.7).

1.2 Cross-correlation formula

The direct cross-correlation formula on the boundary between the field φ and the modified one φ_v given by (1.7) is quite difficult to use. The boundary integral is complicated and from a physical point of view it is not clear that this quantity is indeed measurable. Moreover, the right-hand side provides internal information about q but the term $\varphi\overline{\varphi_v}$ is not controlled. Under the assumption of small variations for q, we provide an asymptotic version of this identity.

Under the free space framework, using an incident plane wave $\varphi_I(x) = Ae^{-k\cdot x}$ with $|k| = \omega^2 q_0$, the electric field φ is decomposed as $\varphi = \varphi_I + \varphi_S$ where φ_S is the unique solution of (1.15) and the displaced electric field φ_v is decomposed as $\varphi = \varphi_I + \varphi_{S,v}$ where $\varphi_{S,v}$ is the unique solution of

$$\begin{cases} \triangle\varphi_{S,v} + \omega^2 q_v\varphi_{S,v} = -\omega^2(q_v-q_0)\varphi_I \quad \text{in } \mathbb{R}^d, \\ \lim\limits_{|x|\to\infty} |x|^{\frac{d-1}{2}} \left(\dfrac{x}{|x|}\cdot\nabla - i\omega\sqrt{q_0}\right)\varphi_{S,v}(x) = 0 \text{ uniformly in } x/|x|. \end{cases} \tag{1.17}$$

An interesting question here is to control how far this modified scattered field $\varphi_{S,v}$ is from the original one φ_S. The following result is a direct application of Proposition 1.1.3 to the equation satisfied by the difference $\varphi_v - \varphi$.

Proposition 1.2.1 *For any $\omega > 0$, there exists $\delta_0 > 0$ such that for any $0 \le \delta < \delta_0$, the difference $\varphi_{S,v} - \varphi_S$ satisfies*

$$\|\varphi_{S,v} - \varphi_S\|_{H^1(\Omega)} \le CA\omega^2\delta|supp v \cap K|^{1/2},$$

where C depends on δ_0 and Ω

Theorem 1.2.2 *When the contrast δ goes to zero, the following approximation holds:*

$$\frac{1}{A\omega^2} Re\Big[\int_{\partial\Omega} e^{ik\cdot x}\left(\partial_\nu - ik\cdot n\right)(\varphi - \varphi_v)\Big] = \int_\Omega (q_v - q) + O\left(\omega^2\delta^2 |supp v \cap K|^{1/2}|K|^{1/2}\right). \quad (1.18)$$

Here, the remainder is bounded by $C\left(\omega^2\delta^2|supp v\cap K|^{1/2}|K|^{1/2}\right)$ with C depending on δ_0 (cf. Proposition 1.1.3) and Ω.

Proof. Using the decomposition of φ and φ_v we write the term on the left-hand side as

$$\int_{\partial\Omega} (\partial_\nu \varphi \overline{\varphi_v} - \partial_\nu \overline{\varphi_v}\varphi) = \alpha + \beta + \gamma$$

with

$$\alpha = \int_{\partial\Omega} (\partial_\nu \varphi_I \overline{\varphi_I} - \partial_\nu \overline{\varphi_I}\varphi_I), \qquad \beta = \int_{\partial\Omega} (\partial_\nu \varphi_I \overline{\varphi_{S,v}} + \partial_\nu \varphi_S \overline{\varphi_I} - \partial_\nu \overline{\varphi_I}\varphi_S - \partial_\nu \overline{\varphi_{S,v}}\varphi_I),$$
$$\gamma = \int_{\partial\Omega} (\partial_\nu \varphi_S \overline{\varphi_{S,v}} - \partial_\nu \overline{\varphi_{S,v}}\varphi_S).$$

We note that

$$\alpha = -\int_{\partial\Omega} ik\cdot\nu A^2 = -iA^2 \int_{\partial\Omega} k\cdot\nu = 0.$$

Then,

$$\beta = \int_{\partial\Omega} \left[(\partial_\nu \varphi_S \overline{\varphi_I} - \partial_\nu \overline{\varphi_{S,v}}\varphi_I) - ik\cdot\nu(\varphi_I \overline{\varphi_{S,v}} + \overline{\varphi_I}\varphi_S)\right].$$

and so

$$\begin{aligned}\mathrm{Re}(\beta) &= \mathrm{Re}\int_{\partial\Omega} \left[(\partial_\nu \varphi_S \overline{\varphi_I} - \partial_\nu \varphi_{S,v}\overline{\varphi_I}) - ik\cdot\nu(\overline{\varphi_I}\varphi_S - \overline{\varphi_I}\varphi_{S,v})\right] \\ &= A\ \mathrm{Re}\int_{\partial\Omega} e^{ik\cdot x}(\partial_\nu - ik\cdot\nu)(\varphi_S - \varphi_{S,v})(x)\mathcal{H}^{d-1}(dx).\end{aligned}$$

Now calculating the cross correlation between φ_S and $\varphi_{S,v}$ on $\partial\Omega$, we get

$$\gamma = \omega^2 \int_\Omega (q_v - q)\varphi_S \overline{\varphi_{S,v}} + \omega^2 \int_\Omega (q_v - q)\overline{\varphi_I}\varphi_S + \omega^2 \int_\Omega (q_v - q_0)(\overline{\varphi_I}\varphi_S - \varphi_I \overline{\varphi_{S,v}}).$$

Then, by using Corollary 1.1.4, it follows that

$$\begin{aligned}|\mathrm{Re}(\gamma)| \le & CA^2\omega^4\delta^2|K|^{1/2}|\mathrm{supp} v\cap K|^{1/2}\left(1 + C\omega^2\delta|K|^{1/2}\right) \\ & + \omega^2\delta|K|^{1/2}\left\|\mathrm{Re}(\overline{\varphi_I}\varphi_S - \varphi_I\overline{\varphi_{S,v}})\right\|_{L^2(\Omega)}.\end{aligned}$$

From

$$|\mathrm{Re}(\overline{\varphi_I}\varphi_S - \varphi_I\overline{\varphi_{S,v}})| \le |\mathrm{Re}(\overline{\varphi_I}\varphi_S - \overline{\varphi_I}\varphi_{S,v})| \le |\overline{\varphi_I}\varphi_S - \overline{\varphi_I}\varphi_{S,v}| \le A|\varphi_S - \varphi_{S,v}|$$

Proposition 1.2.1 yields

$$|\mathrm{Re}(\gamma)| \leq CA^2\omega^4\delta^2|K|^{1/2}|\mathrm{supp}v \cap K|^{1/2},$$

where the constant C depends on Ω and δ_0.

Next, let us investigate the real part of the term on the right-hand of (1.7), which can be decomposed as

$$\begin{aligned}\mathrm{Re}\int_\Omega (q_v - q)\varphi\overline{\varphi_v} &= \mathrm{Re}\int_\Omega (q_v - q)\varphi_I\overline{\varphi_I} + \int_\Omega (q_v - q)(\varphi_I\overline{\varphi_{S,v}} + \mathrm{Re}\overline{\varphi_I}\varphi_S + \varphi_S\overline{\varphi_{S,v}}) \\ &= A^2\int_\Omega (q_v - q) + \mathrm{Re}\int_\Omega (q_v - q)(\varphi_I\overline{\varphi_{S,v}} + \overline{\varphi_I}\varphi_S + \varphi_S\overline{\varphi_{S,v}}).\end{aligned}$$

From

$$\left|\int_\Omega (q_v - q)(\varphi_I\overline{\varphi_{S,v}} + \overline{\varphi_I}\varphi_S + \varphi_S\overline{\varphi_{S,v}})\right| \leq CA^2\omega^2\delta^2|\mathrm{supp}v \cap K|^{1/2}|K|^{1/2},$$

by dividing by $A^2\omega^2$ we get the desired approximation. □

Theorem 1.2.2 gives a meaningful formula linking a simple operator on the boundary applied on $\varphi - \varphi_v$ to the quantity $\int_\Omega (q_v - q)$. If only $\varphi - \varphi_v$ is measured on $\partial\Omega$, then $\partial_\nu(\varphi - \varphi_v)$ can be computed using the fact that $\varphi - \varphi_v$ satisfies the homogeneous Helmholtz equation outside Ω together with the Sommerfeld radiation condition. Actually, the exterior capacity operator relates $\partial_\nu(\varphi_S - \varphi_{D,v})$ to $(\varphi_S - \varphi_{S,v})|_{\partial\Omega}$; see [93]. In the following, we assume that the quantity

$$M_v = \int_\Omega (q_v - q), \tag{1.19}$$

is known for many given v. The imaging problem is to reconstruct the permittivity distribution q from $M_v[q]$. We can notice that formally $M_v \approx -\int_\Omega \nabla q \cdot v$ if v is small, so it is clear that we would assume a certain regularity for q in order to make the reconstruction possible. We also would need enough displacement functions v in order to invert the problem. As said in introduction, the functions v are solutions to acoustics equations which model mechanical waves in fluids. Moreover, we assume that ω is acoustically homogeneous. The aim of the next section is to find a set of admissible displacements v for solving the imaging problem.

1.3 Spherical acoustic waves

In this section we see how the displacement function v can be created by a short spherical acoustic wave and what its typical form is. The state of a fluid is characterized by macroscopic quantities such as the density, the fluid velocity, the pressure, and the temperature. The conservation laws of mass and momentum have the form:

$$\left\{\begin{array}{rcl} \dfrac{\partial\rho}{\partial t} + \nabla\cdot(\rho V) & = & 0 \quad \text{in } \mathbb{R}^3, \\ \dfrac{\partial\rho V}{\partial t} + \nabla\cdot(\rho V\otimes V) + \nabla P & = & 0 \quad \text{in } \mathbb{R}^3, \end{array}\right. \tag{1.20}$$

where ρ is the density, V the velocity field, and P the pressure. System (1.20) is complemented by a state equation that gives the pressure as a function of the density and the

temperature. When the flow is isentropic, the pressure is a function of the density only, $P = P(\rho)$. The flow is isentropic if it is adiabatic, which means that no heat is transferred to or from the fluid, and reversible, that is, the flow conditions can return to their original values.

The acoustic wave equations are obtained by linearizing the fluid dynamics equations for small disturbances around a fluid at rest. We denote by p_0 and ρ_0 the unperturbed pressure and density, with the unperturbed velocity equal to 0 and we consider small perturbations of the pressure and density. Denoting $P = p_0 + p$, $\rho = \rho_0 (1 + s)$, we get the linearized system

$$\begin{cases} \dfrac{1}{K_0}\dfrac{\partial p}{\partial t} + \nabla \cdot v &= 0 \quad \text{in } \mathbb{R}^3, \\ \rho_0 \dfrac{\partial v}{\partial t} + \nabla p &= 0 \quad \text{in } \mathbb{R}^3, \end{cases}$$

where K_0 is the bulk modulus of the medium defined in terms of the equation of state

$$K_0 = \rho_0 \left(\frac{\partial P}{\partial \rho}\right)(\rho_0).$$

The linearized version of the equation of state $P = P(\rho)$ gives $p = K_0 s$.

As we are looking for spherical waves, we assume an initial conditions of the form

$$V(x,0) = 0, \qquad p(x, t=0) = p_0(x) = \frac{1}{\eta} f\left(\frac{|x|^2}{\eta^2}\right), \tag{1.21}$$

where $f \in \mathcal{C}^\infty\left(\mathbb{R}^d, \mathbb{R}^+\right)$ satisfying $\text{supp} f \subset [-1,1]$ and η is the support radius of the initial condition (that will be taken small at the end of the analysis). The solution of the acoustic wave system has the form

$$\begin{cases} p(x,t) = \dfrac{\partial}{\partial t}\left[\dfrac{t}{4\pi}\displaystyle\int_{\partial B} p_0(x + cts) d\sigma(s)\right], \\ V(x,t) = -\dfrac{1}{\rho_0}\nabla\left[\dfrac{t}{4\pi}\displaystyle\int_{\partial B} p_0(x + cts) d\sigma(s)\right], \end{cases}$$

where B is the ball centered at 0 and with radius 1 and c is the speed of sound defined by $c = \sqrt{K_0/\rho_0}$. We have

$$\int_{\partial B} p_0(x_0 + cts) d\sigma(s) = \frac{2\pi}{\eta}\int_0^2 f\left(\frac{(|x| - ct)^2}{\eta^2} + \frac{2ct|x|}{\eta^2} r\right) dr.$$

As soon as $ct > \eta$, this can be rewritten as follows:

$$\int_{\partial B} p_0(x_0 + cts) d\sigma(s) = \frac{\pi\eta}{ct|x|} F\left(\frac{(|x| - ct)^2}{\eta^2}\right),$$

where

$$F(r) = \int_r^\infty f_0(r') dr'.$$

Note that F is a smooth function compactly supported in $[0,1]$. Therefore, we find that the velocity field is given by

$$V(x,t) = \frac{1}{4\rho_0 c}\frac{x}{|x|}\left[\frac{2}{\eta}\frac{|x| - ct}{|x|} f\left(\frac{(|x| - ct)^2}{\eta^2}\right) + \frac{\eta}{|x|^2} F\left(\frac{(|x| - ct)^2}{\eta^2}\right)\right].$$

When $ct \gg \eta$, this becomes

$$V(x,t) \approx \frac{1}{2\eta\rho_0 c}\frac{|x|-ct}{|x|^2} f\left(\frac{(|x|-ct)^2}{\eta^2}\right) x$$

up to a term of relative order $\eta^2/(ct)^2$. Remember that $V(x,t)$ is the fluid velocity at position x. If a particle is at x at time 0, then its position $X(x,t)$ at time t satisfies

$$\frac{\partial X(x,t)}{\partial t} = V\left(X(x,t),t\right), \qquad X(x,0) = x.$$

Using the assumption that the amplitude of the displacement is small we can linearize around the original position and obtain that the position satisfies

$$\frac{\partial X(x,t)}{\partial t} = V(x,t) \quad \text{or} \quad X(x,t) = x + \int_0^t V(x,t')dt',$$

and it is therefore given by

$$X(x,t) = x + \frac{\eta}{4\rho_0 c^2}\frac{x}{|x|} F\left(\frac{(|x|-ct)^2}{\eta^2}\right).$$

As the displacement field is written $x \to x + v(x,t)$, we find

$$v(x,t) = \frac{\eta}{4\rho_0 c^2}\frac{x}{|x|} F\left(\frac{(|x|-ct)^2}{\eta^2}\right).$$

For instance, if the initial condition is

$$p_0(x) = e^{-|x|^2/\eta^2},$$

then we get

$$v(x,t) = \frac{\eta}{4\rho_0 c^2}\frac{x}{|x|} e^{-(|x|-ct)^2/\eta^2}.$$

In the previous analysis, the initial condition p_0 was chosen to be centered at 0. If p_0 is nonnegative-valued, $y \in \Omega$ is the center, then the displacement field is given by

$$v_y(x,t) = \frac{\eta}{|x-y|} w\left(\frac{|x-y|-ct}{\eta}\right)\frac{x-y}{|x-y|},$$

and defined for $x \in \mathbb{R}^d \backslash \{y\}$ and $t \gg \eta/c$. The support of the displacement field can be seen as a thin spherical shell growing at a constant speed c. This can be approximated up to a term of order $\eta/(ct)$ by

$$v_y(x,t) = \frac{\eta}{ct} w\left(\frac{|x-y|-ct}{\eta}\right)\frac{x-y}{|x-y|}. \tag{1.22}$$

In this formulation, w is the shape function and is such that $w \in \mathcal{C}^\infty(\mathbb{R}, \mathbb{R}^+)$ and $\text{supp}(w) \subset [-1,1]$ and η is a positive parameter representing the thickness of the wavefront. Note that, in order to have a wavefront with nonzero thickness, initial conditions of the form (1.21) are required.

Posing $r = ct$ and defining the spherical coordinates elements $\xi \in S^{d-1}$, $\rho \in]0, +\infty[$ we assume that we can use the maps

$$v_{y,r,\eta}(y + \rho\xi) = \frac{\eta}{r} w\left(\frac{\rho - r}{\eta}\right) \xi. \tag{1.23}$$

For $y \in Y$ and $\rho > r_0 > 0$. Y will be a smooth manifolds surface the domain of interest satisfying $\text{dist}(Y, K) > r_0$. It interesting to notice that even if v is small when η is small, it is not the case for its derivative $d_x v$. We make the following assumptions on w:

$$\begin{cases} w \in \mathcal{C}^\infty(\mathbb{R}, \mathbb{R}^+), \\ \text{supp}(w) \subset [-1, 1], \\ w < 1, \\ w' > -1. \end{cases} \tag{1.24}$$

Proposition 1.3.1 *The Jacobian of the map $x \longmapsto x + v(x)$ satisfies*

$$\det(Id + dv_{y,r,\eta}(y + \rho\xi)) = 1 + \frac{1}{r} w'\left(\frac{\rho - r}{\eta}\right) + p_{\eta,r}\left(\frac{\rho - r}{\eta}\right)$$

with $p_{\eta,r}(\tau) \leq \dfrac{\eta}{r}$ for all $\tau \in [-1, 1]$.

Proof. The desired identity follows from the fact that dv is explicit and diagonal in the orthonormal basis $(\xi, e_2, \ldots, e_d)$ where $(e_2, \ldots, e_d) \subset \xi^\perp$. □

Although the derivations in this section are in three-dimensions, we will use for the sake of simplicity the same form of the displacement field in the numerical experiments carried out in two dimensions.

In the next section we use the typical form of the displacement functions introduced here to reduce the imaging problem to the inversion of a spherical means Radon transform.

1.4 Recovering the spherical means

For a continuous function f in $\mathbb{R}^d$, we define its spherical means transform

$$\mathcal{R}[f](y, r) = \int_{S^{d-1}} f(y + r\xi) d\sigma(\xi), \tag{1.25}$$

for any $y \in \mathbb{R}^d$ and $r > 0$. This transform has good properties in terms of invertibility that we will discus later. The aim of this section is to prove that under some smoothness assumption on q, its spherical means transform $\mathcal{R}[q]$ can be recovered from the measurement map. For now on, we assume that q is given everywhere in $\mathbb{R}^d$ and is measurable on all the spheres. We define the measurement map as

$$M_\eta(y, r) = \int_\Omega \big(q_{v_{y,r,\eta}}(x) - q(x)\big)\, dx \tag{1.26}$$

where $v_{y,r,\eta}$ is defined in (1.23) is such that $|v_{y,r,\eta}| < \text{dist}\big(\text{supp}(q - q_0), \partial\Omega\big)$. Recalling that $q_v(x + v(x)) = q(x)$, a change of variables gives

$$
\begin{aligned}
M &= \int_\Omega \big(q(x) - q\big(x + v(x)\big)\big) \det(Id + dv(x))dx \\
&= \int_{r-\eta}^{r+\eta} \int_{S^{d-1}} \big[q(y+\rho\xi) - q\big(y + \rho\xi + v(y+\rho\xi)\big)\big] \det(Id + dv(y+\rho\xi))\rho^{d-1} d\rho d\sigma(\xi) \\
&= \eta \int_{-1}^{1} \Big[\mathcal{R}[q](y, r+\eta\tau) - \mathcal{R}[q]\big(y, r+\eta\tau + \frac{\eta}{r} w(\tau)\big)\Big] \Big[1 + \frac{1}{r} w'(\tau) + p_{\eta,r}(\tau)\Big] (r+\eta\tau)^{d-1} d\tau.
\end{aligned}
$$

At first order in η/r, it follows that

$$
\begin{aligned}
&M_\eta(y, r) = \\
&\eta r^{d-1} \int_{-1}^{1} \Big[\mathcal{R}[q](y, r+\eta\tau) - \mathcal{R}[q]\big(y, r+\eta\tau + \frac{\eta}{r} w(\tau)\big)\Big] \Big[1 + \frac{1}{r} w'(\tau)\Big] d\tau \left(1 + O\left(\frac{\eta}{r}\right)\right).
\end{aligned} \tag{1.27}
$$

We are now ready to give asymptotic formulas to link the measurement map $M_\eta(y, r)$ to the spherical mean Radon transform of q. Let us first investigate the smooth case.

1.4.1 Smooth case

If q is smooth then so is $\mathcal{R}[q]$ and we can approximate the difference in (1.27) by

$$
-\frac{\eta}{r} w(\tau) \partial_r \mathcal{R}[q](y, r).
$$

From this, we prove the following approximation theorem which allows us to recover $\mathcal{R}[q]$ if q is smooth enough. This result gives us a simple formula to directly recover the spherical means Radon transform of q from the measurements by integrating over r.

Theorem 1.4.1 *Suppose that $q \in \mathcal{C}^{1,\alpha}\big(\overline{\Omega}\big)$. Let us fix $y \in \Omega$ and let $r_0 > 0$. Suppose also that $q(x) = q_0$ for $x \in B(y, r_0)$, where B is the ball of center y and radius r_0. Then, for all $r > r_0$ and $\eta < r_0$, we have*

$$
\mathcal{R}[q](y, r) = q_0 - \frac{1}{\eta^2 \|\tilde{w}\|_{L^1}} \int_{r_0}^{r} \frac{M(y, \rho)}{\rho^{d-2}} d\rho + \mathcal{O}(\eta^\alpha), \tag{1.28}
$$

where $\tilde{w}(\tau) = w(\tau)\left(1 + \frac{1}{r} w'(\tau)\right)$. Here, the remainder $\mathcal{O}(\eta^\alpha)$ is bounded by $C\eta^\alpha r$, where C depends only on q, r_0, and $\|w\|_\infty$.

Theorem 1.4.1 follows from the following two lemmas.

Lemma 1.4.2 *Suppose that $q \in \mathcal{C}^{1,\alpha}(\overline{\Omega})$. Let us fix $y \in \Omega$. We have for $\eta < r$:*

$$
\left| \frac{M(y, r)}{\eta^2 r^{d-2}} + \int_{-1}^{1} \tilde{w}(\tau) \frac{\partial \mathcal{R}[q]}{\partial r}(y, r+\eta\tau) d\tau \right| \leq C \left(\frac{\eta}{r}\right)^\alpha \|\tilde{w}\|_{L^1},
$$

where $\tilde{w}(\tau) = w(\tau)\left(1 + \frac{1}{r} w'(\tau)\right)$ and C depends only on q.

Proof. Let us denote

$$\tilde{M}(y,r) = \eta r^{d-1} \int_{-1}^{1} \left[\mathcal{R}[q](y, r+\eta\tau) - \mathcal{R}[q]\left(y, r+\eta\tau+\frac{\eta}{r}w(\tau)\right)\right]\left(1+\frac{1}{r}w'(\tau)\right)d\tau,$$

which satisfies

$$M(y,r) = \left[1+\mathcal{O}\left(\frac{\eta}{r}\right)\right]\tilde{M}(y,r).$$

We have

$$\begin{aligned}
&\left|\frac{M(y,r)}{\eta^2 r^{d-2}} + \int_{-1}^{1}\tilde{w}(\tau)\frac{\partial\mathcal{R}[q]}{\partial r}(y, r+\eta\tau)d\tau\right| \\
&\leq C_0\frac{\eta}{r}\left|\frac{\tilde{M}(y,r)}{\eta^2 r^{d-2}}\right| + \left|\frac{\tilde{M}(y,r)}{\eta^2 r^{d-2}} + \int_{-1}^{1}\tilde{w}(\tau)\frac{\partial\mathcal{R}[q]}{\partial r}(y, r+\eta\tau)d\tau\right| \\
&\leq \left(1+C_0\frac{\eta}{r}\right)\left|\frac{\tilde{M}(y,r)}{\eta^2 r^{d-2}} + \int_{-1}^{1} w(\tau)\frac{\partial\mathcal{R}[q]}{\partial r}(y, r+\eta\tau)d\tau\right| \\
&+ C_0\frac{\eta}{r}\left|\int_{-1}^{1}\tilde{w}(\tau)\frac{\partial\mathcal{R}[q]}{\partial r}(y, r+\eta\tau)d\tau\right|,
\end{aligned}$$

where C_0 is a positive constant depending only on d. Since $r \mapsto \mathcal{R}[q](y,r)$ is a $\mathcal{C}^1$ function, using the finite increment theorem it follows that for all $r > 0$, η and for all $\tau \in [-1,1]$, there exists $\gamma \in [0, (\eta/r)w(\tau)]$ such that

$$\mathcal{R}[q]\left(y, r+\eta\tau-\frac{\eta}{r}w(\tau)\right) - \mathcal{R}[q](y, r+\eta\tau) = -\frac{\eta}{r}w(\tau)\frac{\partial\mathcal{R}[q]}{\partial r}(y, r+\eta\tau-\gamma).$$

Then,

$$\begin{aligned}
&\left|\mathcal{R}[q]\left(y, r+\eta\tau-\frac{\eta}{r}w(\tau)\right) - \mathcal{R}[q](y, r+\eta\tau) + \frac{\eta}{r}w(\tau)\frac{\partial\mathcal{R}[q]}{\partial r}(y, r+\eta\tau)\right| \\
&\qquad \leq \frac{\eta}{r}w(\tau)\left|\frac{\partial\mathcal{R}[q]}{\partial r}(y, r+\eta\tau) - \frac{\partial\mathcal{R}[q]}{\partial r}(y, r+\eta\tau-\gamma)\right| \\
&\qquad \leq \kappa\frac{\eta}{r}\gamma^{\alpha}w(\tau) \leq C\left(\frac{\eta}{r}\right)^{\alpha+1}\|w\|_{L^\infty}^{\alpha}w(\tau),
\end{aligned}$$

where

$$\kappa = ||\partial_r\mathcal{R}[q](y,\cdot)||_{\mathcal{C}^{0,\alpha}\left(]0,+\infty[\right)}, \tag{1.29}$$

and the constant C depends only on q. Here, we have used the fact that $r \mapsto \mathcal{R}[q](y,r) \in \mathcal{C}^{1,\alpha}\big(]0,+\infty[\big)$. Now integrating over $[-1,1]$ we get

$$\begin{aligned}
&\left|\int_{-1}^{1}\left[\mathcal{R}[q]\left(y, r+\eta\tau-\frac{\eta}{r}w(\tau)\right) - \mathcal{R}[q](y, r+\eta\tau) + \frac{\eta}{r}w(\tau)\frac{\partial\mathcal{R}[q]}{\partial r}(y, r+\eta\tau)\right]\left(1+\frac{1}{r}w'(\tau)\right)d\tau\right| \\
&\leq 2C\left(\frac{\eta}{r}\right)^{\alpha+1}\|w\|_{L^\infty}^{\alpha}\|\tilde{w}\|_{L^1},
\end{aligned}$$

i.e.,

$$\left|\frac{\tilde{M}(y,r)}{\eta^2 r^{d-2}} + \int_{-1}^{1}\tilde{w}(\tau)\frac{\partial\mathcal{R}[q]}{\partial r}(y, r+\eta\tau)d\tau\right| \leq 2C\left(\frac{\eta}{r}\right)^{\alpha}\|w\|_{L^\infty}^{\alpha}\|\tilde{w}\|_{L^1},$$

where C depends only on q. Moreover, since ∇q is bounded,

$$\int_{-1}^{1} w(\tau)\frac{\partial \mathcal{R}[q]}{\partial r}(y, r+\eta\tau)d\tau$$

is bounded by $C\|\tilde{w}\|_{L^1}$ and the proof is complete. □

Lemma 1.4.3 *Under the same assumptions as in Lemma 1.4.2, the following inequality holds when $\eta \ll r$:*

$$\left|\frac{M(y,r)}{\eta^2 r^{d-2}} + \|\tilde{w}\|_{L^1}\frac{\partial \mathcal{R}[q]}{\partial r}(y,r)\right| \leq C\eta^{\beta}\big(\|w\|_{L^\infty}^{\alpha}+1\big)\|\tilde{w}\|_{L^1}$$

with C depending only on q.

Proof. From

$$\left|\|\tilde{w}\|_{L^1}\frac{\partial \mathcal{R}[q]}{\partial r}(y,r) - \int_{-1}^{1}\tilde{w}(\tau)\frac{\partial \mathcal{R}[q]}{\partial r}(y,r+\eta\tau)d\tau\right|$$

$$\leq \int_{-1}^{1}\tilde{w}(\alpha)\left|\frac{\partial \mathcal{R}[q]}{\partial r}(y,r) - \frac{\partial \mathcal{R}[q]}{\partial r}(y,r+\eta\alpha)\right|d\alpha \leq \kappa\eta^{\alpha}\int_{-1}^{1}\tilde{w}(\tau)|\tau|^{\alpha}d\tau \leq \kappa\eta^{\alpha}\|\tilde{w}\|_{L^1},$$

where κ is given by (1.29), Lemma 1.4.2 yields the desired estimate. □

Finally, integrating over r, we deduce Theorem 1.4.1 from the above lemmas.

1.4.2 Piecewise constant case

In medical applications, it may not be realistic to suppose regularity for q. Indeed, human body is made of different parts of different materials like bones, muscles, fat, aqueous fluid, etc. All of these different kinds of materials are adjacent to or confined in one another. Thus, we obviously have to deal with discontinuities of the parameter q. A good model is to consider q as a piecewise constant function. It is also acceptable to consider that all the parts where q is constant have a smooth enough boundary. We shall discuss about this model of piecewise constant distributions later in this thesis.

In this subsection, we suppose that there exists a finite partition $(A_i)_{i\in\mathbb{N}}$ of Ω such A_0 is Lipschitz and that for all $i \in \mathbb{N}^*$, ∂A_i is $\mathcal{C}^1$ and $q|_{A_i}$ is constant. The question is now to know how smooth is $\mathcal{R}[q]$ for such a piecewise constant q. Is it smooth enough in order to have the same kind of approximation as in Theorem 1.4.1? Clearly, a pointwise approximation of $\partial_r\mathcal{R}[q]$ is not available. We just have to take a spherical inclusion with constant parameter q inside and outside to see that $\mathcal{R}[q]$ is not differentiable. However, under an acceptable assumption, we can say that, for almost all $y \in \Omega$, $r \mapsto \mathcal{R}[q](y,r)$ is continuous. This a consequence of the smoothing effect of the operator $\mathbb{R}$ that we will discuss later. The following result gives the continuity of $r \longmapsto \mathcal{R}[q](y,r)$ for almost all $y \in \mathbb{R}^d$.

The following result is proved in Appendix 1.6.2.

Theorem 1.4.4 *Suppose that q satisfies the conditions above. There exists a numerable set $\mathcal{N} \subset \mathbb{R}^d$, such that for all $y \in \mathbb{R}^d\backslash\mathcal{N}$, the real function $r \mapsto \mathcal{R}[q](y,r)$ is continuous on $(0,+\infty)$.*

With this theorem in hand, we can consider that for any chosen $y \in \mathbb{R}^d$, the function $r \mapsto \mathcal{R}[q](y,r)$ is continuous. But as we will see later, this regularity is not sufficient to have the same approximation as in Theorem 1.4.1. Actually, we need at least a $\mathcal{C}^{0,\alpha}$-regularity with some $\alpha > 0$. If we study the spherical means Radon transform of $\mathbf{1}_{\mathcal{A}}$ where $\mathcal{A}$ is a $\mathcal{C}^1$ bounded domain and $\mathbf{1}_{\mathcal{A}}$ denotes its characteristic function, then it can be proved that if $S(y,r_0)$, the sphere of radius r_0 and center y, and $\partial\mathcal{A}$ are not tangent to each other, then the function $r \mapsto \mathcal{R}[\mathbf{1}_{\mathcal{A}}](y,r)$ is $\mathcal{C}^1$ at $r = r_0$. In order to estimate the singularities in the tangent case, we calculate the behavior of $r \mapsto \mathcal{R}[\mathbf{1}_{\mathcal{A}}](y,r)$ around $r = 1$, where $\mathcal{A} = B(x,c)$, $0 < c < 1$, $x = (c, 0, \ldots, 0)$, and $y = (1, 0, \ldots, 0)$. In dimension 2, a straightforward calculation shows that

$$\mathcal{R}[\mathbf{1}_{\mathcal{A}}](y,r) \underset{r\to 1^-}{\sim} 2\sqrt{\frac{c}{1-c}}\sqrt{1-r}$$

and in dimension 3,

$$\mathcal{R}[\mathbf{1}_{\mathcal{A}}](y,r) \underset{r\to 1^-}{\sim} 2\pi\frac{c}{1-c}(1-r).$$

Hence that gives us a $\mathcal{C}^{0,1/2}$-regularity in the two-dimensional case and a $\mathcal{C}^{0,1}$-regularity in three dimensions. Thus, in the following we will consider that $r \mapsto \mathcal{R}[\mathbf{1}_A](y,r)$ is $\mathcal{C}^{0,\alpha}$ for almost all $y \in \Omega$ with $1/2 \leq \alpha \leq 1$.

Theorem 1.4.5 *Suppose that q is piecewise constant and that $\mathcal{R}[q] \in \mathcal{C}^{0,\alpha}\left(\overline{\Omega}\right)$ where $1/2 \leq \alpha \leq 1$. Let us fix $y \in \Omega$ and $r_0 > 0$. Suppose that $q(x) = q_0$ for $x \in B(y,r_0)$, where B is the ball of center y and radius r_0. Then, for all $r > r_0$ and $\eta \ll r_0$, we have*

$$\mathcal{R}[q](y,r) = q_0 - \frac{1}{\eta^2 \|w\|_{L^1}} \int_{r_0}^{r} \frac{M(y,\rho)}{\rho^{d-2}} d\rho + \mathcal{O}(\eta^\alpha), \tag{1.30}$$

where the remainder $\mathcal{O}(\eta^\alpha)$ is bounded by $C\eta^\alpha r^2$ with C depending only on q, r_0, and $\|w\|_{L^\infty}$.

Proof. By the definition of M, we have

$$\frac{1}{\eta^2}\int_{r_0}^{r} \frac{M(y,\rho)}{\rho^{d-2}} d\rho = (1 + \mathcal{O}(\eta))\, I_{r_0,\eta}(y,r),$$

where

$$I_{r_0,\eta}(y,r) = \frac{1}{\eta}\int_{-1}^{1}\int_{r_0}^{r} \rho \left[\mathcal{R}[q]\left(y, \rho + \eta\tau - \frac{\eta}{\rho}w(\tau)\right) - \mathcal{R}[q](y, \rho + \eta\tau)\right] d\rho d\tau.$$

Therefore,

$$\begin{aligned} &|I_{r_0,\eta}(y,r) + \|w\|_{L^1}\mathcal{R}[q](y,r) - \|w\|_{L^1}\mathcal{R}[q](y,r_0)| \\ &\leq \int_{-1}^{1} \left|\frac{\mathcal{A}}{\eta} - \frac{\mathcal{B}}{\eta} + \mathcal{R}[q](y,r)w(\tau) - \mathcal{R}[q](y,r_0)w(\tau)\right| d\tau \end{aligned}$$

with

$$\mathcal{A} = \int_{r_0}^{r} \rho\mathcal{R}[q]\left(y, \rho + \eta\tau - \frac{\eta}{\rho}w(\tau)\right) d\rho, \qquad \mathcal{B} = \int_{r_0}^{r} \rho\mathcal{R}[q]\left(y, \rho + \eta\tau\right) d\rho.$$

We introduce the following change of variables $\rho \to \theta = \rho - \frac{\eta}{\rho}w(\tau)$, *i.e.*,

$$\rho = \frac{1}{2}\left(\theta + \sqrt{\theta^2 + 4\eta w(\tau)}\right) = \theta\left(1 + \frac{\eta}{\theta^2}w(\tau) + \mathcal{O}\left(\eta^2\right)\right),$$

$$d\rho = \frac{1}{2}\left(1 + \left(1 + 4\frac{\eta}{\theta^2}w(\tau)\right)^{-1/2}\right)d\theta = \left(1 - \frac{\eta}{\theta^2}w(\tau) + \mathcal{O}\left(\eta^2\right)\right)d\theta.$$

Then,

$$\rho d\rho = \left(1 + \mathcal{O}\left(\eta^2\right)\right)\theta d\theta.$$

Using this change of variables, we rewrite

$$\mathcal{A} = \int_{r_0 - \eta w(\tau)/r_0}^{r - \eta w(\tau)/r} \left(1 + \mathcal{O}\left(\eta^2\right)\right)\theta \mathcal{R}[q]\left(y, \theta + \eta\tau\right)d\theta$$

and hence,

$$\begin{aligned}\mathcal{A} - \mathcal{B} \;=\; & \int_{r_0 - \eta w(\tau)/r_0}^{r_0} \theta \mathcal{R}[q]\left(y, \theta + \eta\tau\right)d\theta - \int_{r - \eta w(\tau)/r}^{r} \theta \mathcal{R}[q]\left(y, \theta + \eta\tau\right)d\theta \\ & + \mathcal{O}\left(\eta^2\right)\int_{r_0 - \eta w(\tau)/r_0}^{r - \eta w(\tau)/r} \theta \mathcal{R}[q]\left(y, \theta + \eta\tau\right)d\theta,\end{aligned}$$

or equivalently,

$$\mathcal{A} - \mathcal{B} = \mathcal{C} - \mathcal{D} + \mathcal{E}\mathcal{O}\left(\eta^2\right)$$

with

$$\mathcal{C} = \int_{r_0 - \eta w(\tau)/r_0}^{r_0} \theta \mathcal{R}[q]\left(y, \theta + \eta\tau\right)d\theta, \quad \mathcal{D} = \int_{r - \eta w(\tau)/r}^{r} \theta \mathcal{R}[q]\left(y, \theta + \eta\tau\right)d\theta,$$

and

$$\mathcal{E} = \int_{r_0 - \eta w(\tau)/r_0}^{r - \eta w(\tau)/r} \theta \mathcal{R}[q]\left(y, \theta + \eta\tau\right)d\theta.$$

Since $\mathcal{R}[q](y, r)$ is continuous, there exist $\gamma_1 \in [0, \eta w(\tau)/r_0]$ and $\gamma_2 \in [0, \eta w(\tau)/r]$ such that

$$\begin{aligned}\mathcal{C} &= (r_0 - \gamma_1)\mathcal{R}[q]\left(y, r_0 + \eta\tau - \gamma_1\right)\eta w(\tau)/r_0, \\ \mathcal{D} &= (r - \gamma_2)\mathcal{R}[q]\left(y, r + \eta\tau - \gamma_2\right)\eta w(\tau)/r.\end{aligned}$$

Thus

$$\begin{aligned}\left|\frac{\mathcal{C}}{\eta} - \mathcal{R}[q](y, r_0)w(\tau)\right| &\leq w(\tau)\left|\left(1 - \frac{\gamma_1}{r_0}\right)\mathcal{R}[q](y, r_0 + \eta\tau - \gamma_1) - \mathcal{R}[q](y, r_0)\right| \\ &\leq \left|\mathcal{R}[q](y, r_0 + \eta\tau - \gamma_1) - \mathcal{R}[q](y, r_0)\right| + \frac{\eta}{r_0^2}\left\|q\right\|_{L^\infty}\left\|w\right\|_{L^\infty} \\ &\leq k\eta^\alpha \frac{\|w\|_{L^\infty}^\alpha}{r_0^\alpha} + \eta\frac{\|q\|_{L^\infty}}{r_0^2}\|w\|_{L^\infty} \leq C\eta^\alpha,\end{aligned}$$

where $k := ||\mathcal{R}[q](y, \cdot)||_{\mathcal{C}^{0,\alpha}((0,+\infty))}$ and C depends only on q, $\|w\|_\infty$, and r_0. Similarly,

$$\left|\frac{\mathcal{D}}{\eta} - \mathcal{R}[q](y, r)w(\tau)\right| \leq C\eta^\alpha$$

with C depending only on q, $\|w\|_\infty$, and r_0. Moreover,

$$|\mathcal{E}| \leq \left\|q\right\|_{L^\infty} r^2.$$

Finally, it follows that

$$\left|\frac{\mathcal{A}}{\eta}-\frac{\mathcal{B}}{\eta}+\mathcal{R}[q](y,r)w(\tau)-\mathcal{R}[q](y,r_0)w(\tau)\right|\leq C_1\eta^\alpha+C_2r^2\eta\leq Cr^2\eta^\alpha,$$

where C, C_1 and C_2 depend on r_0, $\|w\|_\infty$, and q. Then, integrating over α yields

$$|I_{r_0,\eta}(y,r)+\|w\|_{L^1}\mathcal{R}[q](y,r)-\|w\|_{L^1}\mathcal{R}[q](y,r_0)|\leq Cr^2\eta^\alpha.$$

As $\mathcal{R}[q]$ is bounded, the estimate above leads to the conclusion. □

1.5 Numerical results

This section illustrates numerically our main findings in this chapter. In particular, we shall see here the resolution enhancement compared to the Rayleigh criteria, which is the resolution limit for a purely microwave imaging. Let us choose $\Omega=]-1,1[$ and $q_0=1$. The permittivity q is given by the first picture in Figure 1.2. Taking $y\in S^1$ $r_0=0.1$, $r\in]r_0,2[$ and $\eta<r_0$, we choose the following simple form for the acoustic displacement

$$v_{y,r,\eta}(y+\rho\xi)=\frac{r_0}{r}\eta\exp\left(\frac{\eta^2}{(\rho-r)^2-\eta^2}\right)\xi,$$

which satisfies conditions (1.23) and (1.24). For any $y\in S^1$ and $r\in]r_0,2[$ and $\eta<r_0$ we compute the map $v_{y,r,\eta}$ and the map q_v-q. The we compute the approximated differential scattered field $\psi_v=\varphi_{S,v}-\varphi_S$, that is, the solution to

$$\begin{cases}\triangle\psi_v+\omega^2q_0\psi_v=-\omega^2(q_v-q)\varphi_I\quad\text{in }\mathbb{R}^d,\\ \lim\limits_{|x|\to\infty}|x|^{\frac{d-1}{2}}\left(\dfrac{x}{|x|}\cdot\nabla-i\omega\sqrt{q_0}\right)\psi_v(x)=0\text{ uniformly in }x/|x|\end{cases}$$

with $\omega=1$ and $\varphi_I(x)=e^{-ik\cdot x}$. Note that we use here the Born approximation to replace q by q_0. This is just for the simplicity of the computation but does not change significantly the results for small contrast. Then, using Theorem 1.2.2, we deduce the function $M(y,r)$ from

$$M:=\int_\Omega(q_v-q)\approx\mathrm{Re}\int_{\partial\Omega}e^{ik\cdot x}(\partial_\nu-ik\cdot\nu)\psi_v.$$

As q is piecewise constant and its spherical means Radon transform $\mathcal{R}[q]$ is $\mathcal{C}^{0,\alpha}$, we apply Theorem 1.4.1 to obtain $\mathcal{R}[q]$ from M using

$$\mathcal{R}[q-q_0](y,r)\approx-\frac{1}{\eta^2\|w\|_{L^1}}\int_{r_0}^r M(y,\rho)d\rho,$$

which gives approximately $\mathcal{R}[q]$, as shown in the third picture in Figure 1.2.

As we can see the support of $\mathcal{R}[q-q_0]$ does not fit with the one expected due to the successive approximations and the numerical errors. To fix it, we impose a simple coherence condition,

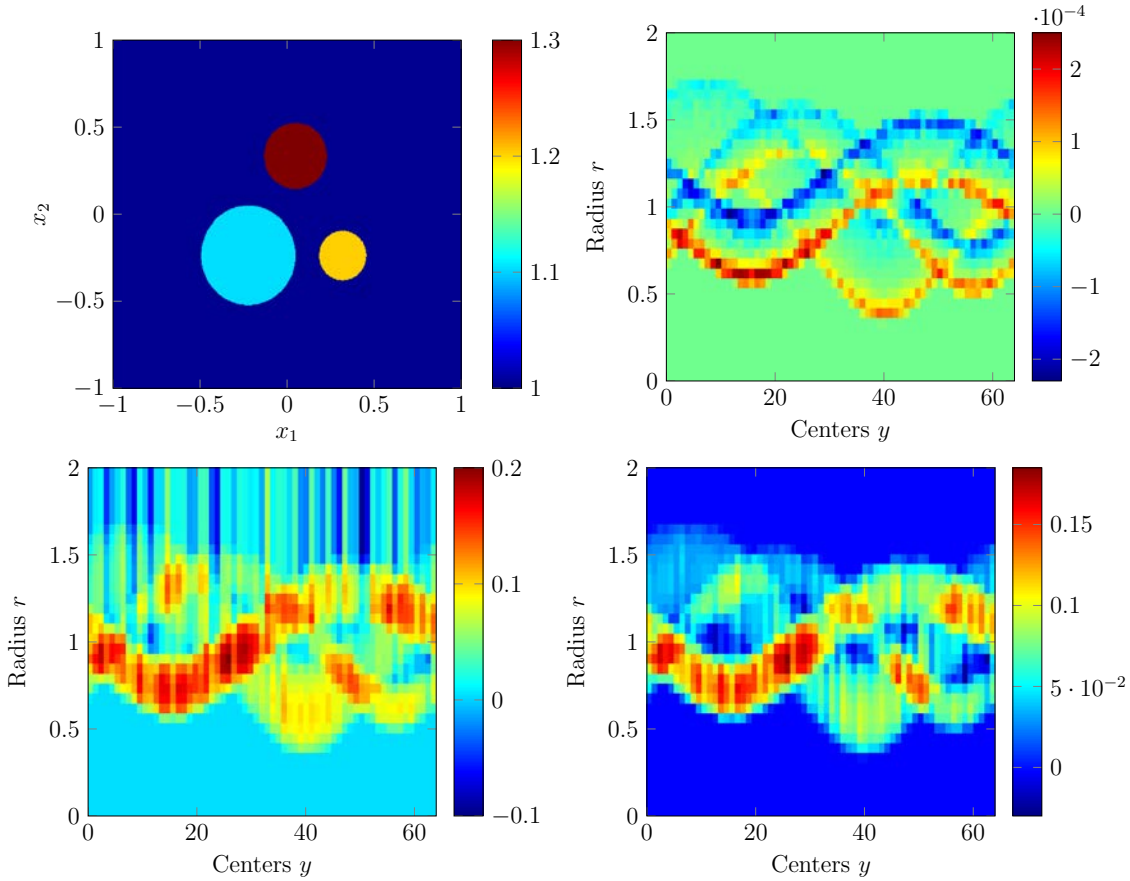

Figure 1.2: From left to right, top to bottom. (1) The permittivity distribution to be reconstructed in $\Omega =]-1,1[^2$. (2) The approximate measurement function $M(y,r)$ with 64 centers y equidistributed on the unit circle, obtained from simulated boundary measurements. (3) The uncorrected Radon transform of the permittivity obtained by direct application of formula (1.30). (4) The Radon transform of the permittivity corrected by applying formula (1.32).

$$\int_0^2 M(y,\rho)d\rho = 0, \quad \forall y \in S^1. \tag{1.31}$$

To do so, we denote $M^+ = \max(M,0)$ and $M^- = -\min(M,0)$ and introduce a correction coefficient by

$$a(y) = \left(\int_0^2 M^+(y,\rho)d\rho\right)^{-\frac{1}{2}} \left(\int_0^2 M^-(y,\rho)d\rho\right)^{\frac{1}{2}}$$

and define the corrected measurement function by

$$\begin{cases} M_{corr}(y,r) = a(y)M^+(y,r) - \dfrac{1}{a(y)}M^-(y,r) & \text{if } a(y) \text{ is defined and } a(y) \neq 0, \\ M_{corr}(y,r) = 0 & \text{otherwise,} \end{cases} \tag{1.32}$$

which satisfies the coherence condition (1.31). In the fourth picture in Figure 1.2, we can see the approximate spherical means Radon transform computed using the corrected measurement function. Now we just have to invert the operator $\mathcal{R}$ using a filtered back projection algorithm.

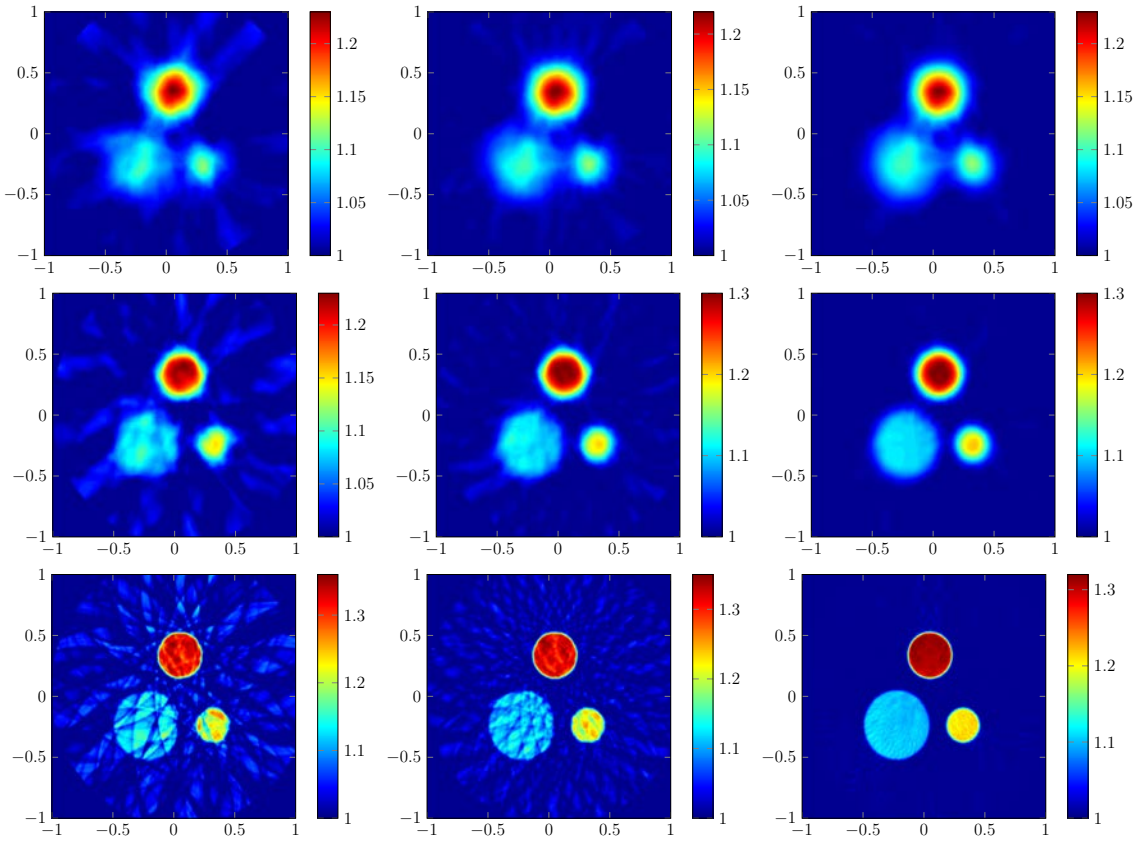

Figure 1.3: Reconstruction of the permittivity with acoustic sources y on the unit circle. From top to bottom, the wavefront size η is 0.1, 0.05 and 0.001 and from left to right the number of acoustic sources is 16, 32, and 128.

It is worth emphasizing that the resolution is much better that what we could have with purely microwave tomography. Here, the wavelength of the microwave is of order of the size of Ω. Our resolution here is fixed by the acoustic pulse size η. As our approximation in Theorem 1.4.5 is of order η^α with $\alpha \in]0,1[$, it is interesting to numerically estimate this order. In Figure 1.5, we represent the error with respect to η and the assumption $\alpha = 1/2$ in dimension 2 for deriving approximation (1.30) seems to be satisfactory.

To illustrate the stability of the algorithm, we add some white noise to the measurement function M; see (1.4). It seems that the smoothing effect of a large acoustic pulse brings more stability than for thin pulses. Actually, there is a compromise to find between resolution and stability as illustrated by Figure 1.5.

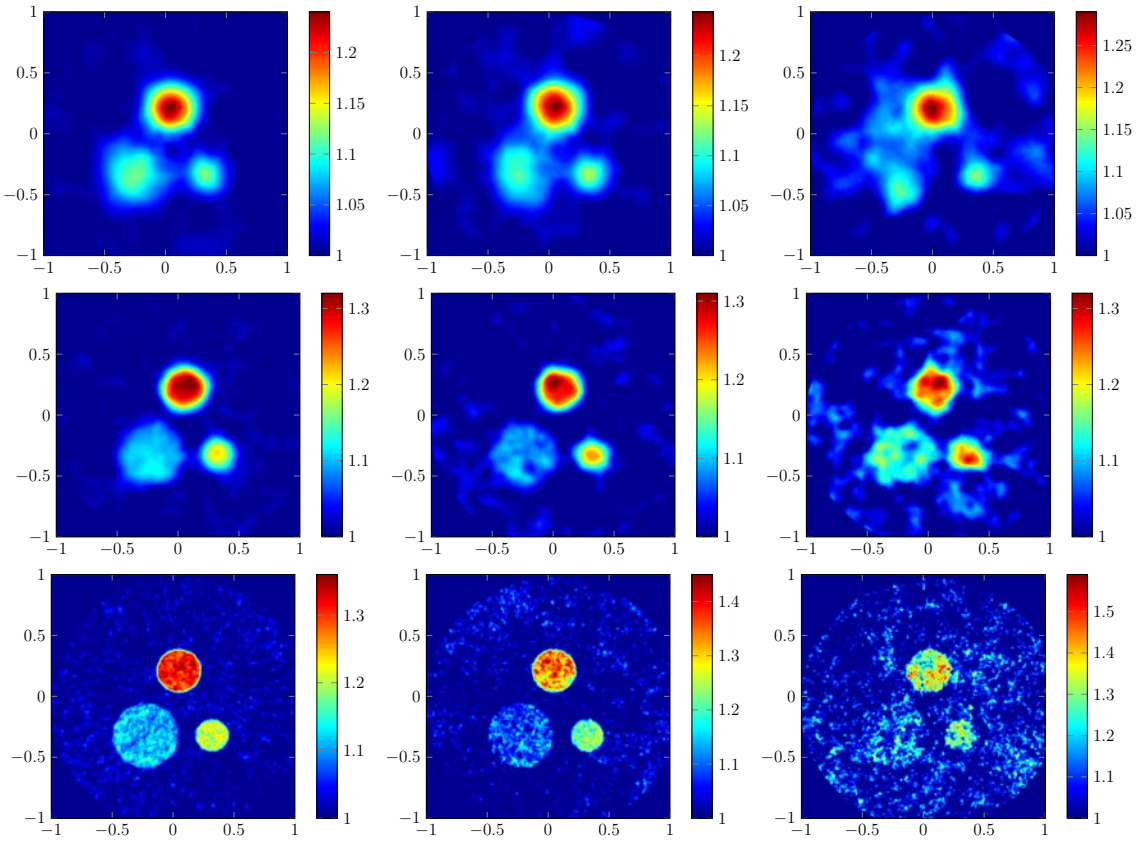

Figure 1.4: Reconstruction of the permittivity from noisy measurements. A white Gaussian noise is added to the measurements. From top to bottom, the wavefront size η is 0.1, 0.05 and 0.001 and from left to right, the noise/signal ratio is 0.1, 0.2, and 0.5.

1.6 Appendix

1.6.1 Sperical means Radon transform

For f a piecewise continuous function on $\mathbb{R}^d$ and $E \subset \mathbb{R}^d$, we can define the spherical means Radon transform of f over E by

$$\mathcal{R}[f](y,r) = \int_{S^{d-1}} f(y + r\xi) d\sigma(\xi) \qquad y \in E,\ r > 0,$$

where σ is the surface measure over S^{d-1}. A lot of work has been done over the inversion problem of the spherical means Radon transform, in particular, when the centers are taken on a sphere. Let B_a be the ball of center 0 and radius a and $S_a = \partial B_a$. If we look at $\mathcal{R}$ as the map

$$\begin{aligned} \mathcal{R} : \mathcal{D}(B_a) &\longrightarrow \mathcal{D}\big(S_a \times]0, +\infty[\big) \\ f &\longmapsto \left((y,r) \longmapsto \int_S f(y + r\xi) d\sigma(\xi) \right), \end{aligned}$$

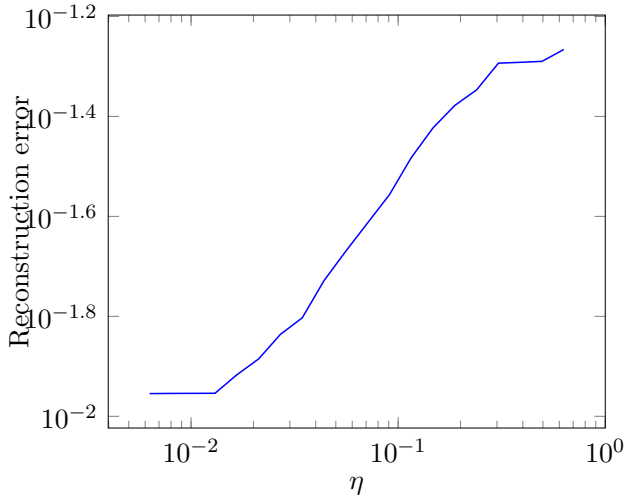

Figure 1.5: Error of the reconstructed permittivity in $L^2(\Omega)$ with respect to the wavefront size η for 64 acoustic centers. The flat on the top part corresponds to a maximal error when the reconstructed q is totally different from the true one. The flat on the bottom part is a saturation due to others parameters of the simulation such as the number of acoustic centers used. The bend of the affine part is about 0.49.

then we have the following inversion formula for $d = 3$ [52]:

$$f(x) = \frac{1}{2\pi a} \nabla \cdot \int_{S_a} y \frac{\frac{\partial}{\partial r}(r\mathcal{R}[f])(y, |x-y|)}{|x-y|} d\sigma(y), \tag{1.33}$$

while for $d = 2$ [53],

$$f(x) = \frac{1}{2\pi a} \int_{S_a} \int_{-2a}^{2a} \frac{r\frac{\partial}{\partial r}(\mathcal{R}[f])(y,t)}{|x-y|-t} dt\, d\sigma(y). \tag{1.34}$$

1.6.2 Proof of Theorem 1.4.4

In order to prove Lemma 1.4.4 we need the following result.

Lemma 1.6.1 *Let B and S be the unit open ball and the unit sphere of $\mathbb{R}^d$, $d = 2, 3$. Let σ be the Euclidean surface measure over S. Let $A \subset B$ be an open measurable set such that $\overline{A}$ is a manifold with boundary. Then, the function f defined by*

$$f(r) = \int_S \mathbf{1}_A(r\xi) d\sigma(\xi), \quad r \in [0, 1),$$

satisfies

$$\lim_{r \to 1^-} f(r) = \sigma(\overline{A} \cap S).$$

Proof. We denote by $T = \overline{A} \cap S$ and its boundary $\partial T = T \cap \overline{T \backslash S}$. We have $\sigma(\partial T) = 0$. We will use the fact that the surface Hausdorff measure $\mathcal{H}^{d-1}$ restricted over S is equal to

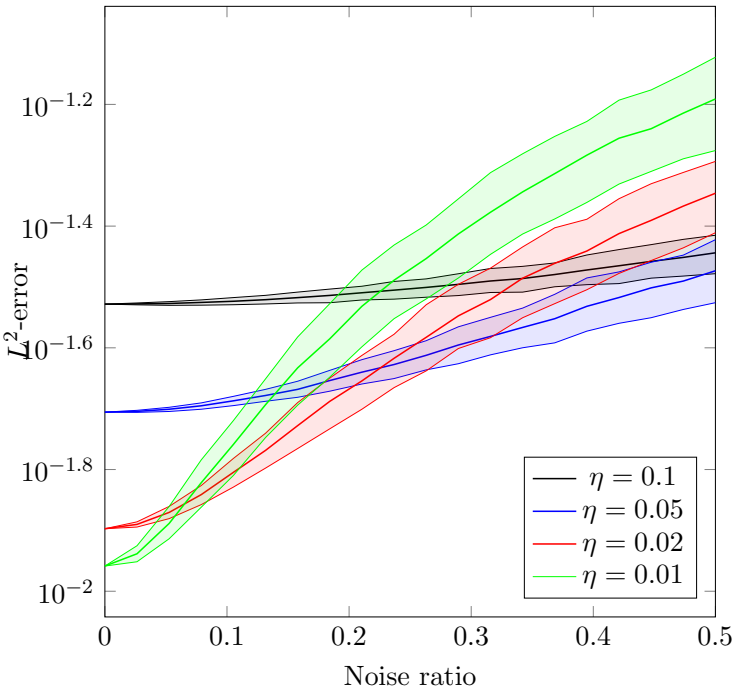

Figure 1.6: Error of the reconstructed permittivity in $L^2(\Omega)$ with respect to the relative white noise on measurements. Each point is obtained by a statistic on 300 realizations of the noise. The lower and upper bounds of the colored parts represents the lower and upper decile.

σ and then $\mathcal{H}^{d-1}(\partial T) = 0$. For all $\varepsilon > 0$, we denote by $\Omega_\varepsilon(\mathbb{R}^d)$ the set of open balls of $\mathbb{R}^d$ of diameters smaller than ε. For $D \subset \mathbb{R}^d$, we let

$$\mathcal{F}_\varepsilon(D) = \left\{ (C_i)_{i\in I},\ I \subset \mathbb{N},\ \forall i \in I,\ C_i \in \Omega_\varepsilon(\mathbb{R}^d),\ D \subset \bigcup_{i\in I} C_i \right\},$$

and define

$$\mathcal{H}^{d-1}_\varepsilon(D) = \inf \left\{ \sum_{i\in I} \alpha_{d-1} r(C_i)^{d-1}, (C_i)_{i\in I} \in \mathcal{F}_\varepsilon(D) \right\},$$

where $r(C_i)$ is half the diameter of C_i and α_{d-1} the volume of the $d-1$ unit ball. This quantity converges when $\varepsilon \to 0$ and its limit is the $d-1$ Hausdorff measure of D denoted $\mathcal{H}^{d-1}(D)$. In our proof, we have here

$$\lim_{\varepsilon\to 0} \mathcal{H}^{d-1}_\varepsilon(\partial T) = 0.$$

Let $\varepsilon > 0$ and $(C_i)_{i\in I} \in \mathcal{F}_\varepsilon(\partial T)$. We set $V = \bigcup_{i\in I} C_i$ open and containing ∂T and denote $U = V \cap S$. We let $T_- = T \backslash U$ and $T_+ = T \cup U$. Note that T^- is a closed set and $T^- \subset T \backslash \partial T$. Write

$$\begin{aligned} f(r) &= \int_{T_-} \mathbf{1}_A(r\xi) d\sigma(\xi) + \int_U \mathbf{1}_A(r\xi) d\sigma(\xi) + \int_{S\backslash T_+} \mathbf{1}_A(r\xi) d\sigma(\xi) \\ &= f_{T_-}(r) + f_U(r) + f_{S\backslash T_+}(r). \end{aligned}$$

Now we want to prove that there exists $r_0 \in]0,1[$ such that for all $r \in]r_0,1[$,

$$f_{T_-}(r) = \sigma(T_-), \tag{1.35}$$
$$f_U(r) \in [0, \sigma(U)], \tag{1.36}$$
$$f_{S\backslash T_+}(r) = 0. \tag{1.37}$$

(i) Suppose that (1.35) is false. There exists a sequence (r_n) converging to 1 such that $f_{T_-}(r_n) < \sigma(T_-)$ for all $n \in \mathbb{N}$. We have $\sigma(\frac{1}{r_n}A \cap T_-) < \sigma(T_-)$ and then $T_-\backslash\frac{1}{r_n}A \neq \emptyset$. Let us take $x_n \in T_-\backslash\frac{1}{r_n}A$. Up to extracting a subsequence, we can say that the sentence (x_n) converges to $x \in T_-$ because T_- is closed. Using the definition of T_- we can say that $x \in T\backslash\partial T$. We have $x \in \partial A$. Indeed, on the one hand, $x \in T$ so that $x \in \overline{A}$, and on the other hand, $x = \lim x_n$ with $x_n \in (\frac{1}{r_n}A)^c$, which implies that $x \in A^c$. Since $x \in \partial A$ and $\overline{A}$ is manifold with boundary, there exists $\eta > 0$ such that $B(x,\eta) \cap A$ is homeomorphic to $\mathbb{R}^d$ and we can choose η small enough to ensure $B(x,\eta) \cap S = B(x,\eta) \cap T = B(x,\eta) \cap \partial A$. This implies that $B(x,\eta) \cap (B\backslash A) = \emptyset$. The sequence $(r_n x_n)$ is in $r_n T^- \backslash A \subset B\backslash A$ and converges to x, which leads to a contradiction.
(ii) Item (1.36) is straightforward.
(iii) Suppose that (1.37) is false. There exists a sequence (r_n) converging to 1 such that $f_{S\backslash T_+}(r_n) > 0$. This implies that $\frac{1}{r_n}A \cap (S\backslash T_+) \neq \emptyset$. Let us take x_n in this set. Up to extracting a subsequence, we can consider that (x_n) converges to $x \in S\backslash T_+$, which is closed. But $(r_n x_n)$ is a sequence of A and converges also to x. Thus $x \in S \cap \overline{A} = T$, which is a contradiction since $T \subset T_+$.

Now we get from (1.35), (1.36), and (1.37) that, for $r \in]r_0,1[$,

$$\sigma(T_-) \leq f(r) \leq \sigma(T_-) + \sigma(U)$$

which leads to

$$\sigma(T) - \sigma(U) \leq f(r) \leq \sigma(T) + \sigma(U).$$

We can now control $\sigma(U)$ by

$$\sigma(U) \leq \sum_{i\in I} \sigma(C_i \cap S) \leq C \sum_{i\in I} \alpha_{d-1} r(C_i)^{d-1},$$

where C is a positive constant. Next, taking the inf over the families $(C_i)_{i\in I}$ we obtain that

$$\sigma(T) - \mathcal{H}^{d-1}_\varepsilon(\partial T) \leq \liminf_{r\to 1^-} f(r) \leq \limsup_{r\to 1^-} f(r) \leq \sigma(T) + \mathcal{H}^{d-1}_\varepsilon(\partial T).$$

Finally, sending ε to zero, we get the result. □

Remark 1.6.2 *Lemma 1.6.1 is also true if we take $A \subset \mathbb{R}^d\backslash B$, and therefore,*

$$\lim_{r\to 1^+} f(r) = \sigma(\overline{A} \cap S).$$

Corollary 1.6.3 *Let $A \subset \mathbb{R}^d$ be an open measurable set such that $\overline{A}$ is a manifold with boundary. If the function*

$$f(r) = \int_S \mathbf{1}_A(r\xi) d\sigma(\xi)$$

is not continuous at 1, then $\sigma(\partial A \cap S) > 0$.

Proof. Let us denote $A_- = A \cap B$ and $A_+ = A \backslash \overline{B}$. Lemma 1.6.1 and Remark 1.6.2 lead to

$$\lim_{r \to 1^-} f(r) = \sigma(\overline{A_-} \cap S), \quad \lim_{r \to 1^+} f(r) = \sigma(\overline{A_+} \cap S).$$

Moreover, $f(1) = \sigma(A \cap S)$. Now, from $A \cap S \subset \overline{A_-} \cap S$ and $A \cap S \subset \overline{A_+} \cap S$ we get

$$\sigma(A \cap S) \leq \sigma(\overline{A_-} \cap S), \quad \sigma(A \cap S) \leq \sigma(\overline{A_+} \cap S).$$

Since by assumption these two inequalities cannot both be equalities, we can consider that $\sigma(A \cap S) < \sigma(\overline{A_-} \cap S)$ (resp. $\sigma(A \cap S) < \sigma(\overline{A_+} \cap S)$). So there exists a set $\Omega \in S$ open in S such that $\Omega \subset \overline{A_-} \backslash A$ (resp. $\Omega \subset \overline{A_+} \backslash A$). Hence $\Omega \subset \partial A$ and thus $\Omega \subset \partial A \cap S$, which implies that $\sigma(\partial A \cap S) > 0$.

□

Proof of Theorem 1.4.4. Let $y \in \mathbb{R}^d$. We suppose that $r \longrightarrow \mathcal{R}[q](y, r)$ is not continuous at r_0. The map q is supposed to be defined by

$$q(x) = \sum_{i \in I} q_i \mathbf{1}_{A_i}(x),$$

with I being finite, q_i being constants, and A_i being $\mathcal{C}^1$-domains. So there exists $i \in I$ such that $r \mapsto \mathcal{R}[\mathbf{1}_{A_i}](y, r)$ is not continuous at r_0. As $\overline{A}_i$ is a manifold with boundary, we can use Corollary 1.6.3 to obtain that $\sigma_{r_0}(\partial A_i \cap S_{r_0}) > 0$. Therefore, for all $(y, r_0) \in \mathbb{R}^d \times (0, +\infty)$ such that $r \mapsto \mathcal{R}[q](y, r)$ is not continuous at r_0, there exists $i \in I$ and $V \subset \partial A_i$ such that the surface measure of V is positive and the curve center is y. Since I is finite and the surface measure of ∂A_i is finite too, it follows that there exists no more than a numerable set of centers y such that $r \mapsto \mathcal{R}[q](y, r)$ is not continuous. □

1.6.3 Diffraction tomography

In this section we present a standard reconstruction method from purely electromagnetic measurements, known as diffraction tomography, and show the superiority of the acousto-electromagnetic tomography in terms of resolution.

Let φ'_I be given by

$$\varphi'_I(x) = e^{-ik' \cdot x},$$

where k' satisfies $|k'|^2 = \omega^2 q_0$. Using the Born approximation, one can show that

$$\int_{\partial\Omega} \left(\partial_\nu \varphi_S \overline{\varphi'_I} - \varphi_S \partial_\nu \overline{\varphi'_I} \right) \approx -\omega^2 \int_\Omega (q - q_0)(x) e^{i(k+k') \cdot x} \, dx, \tag{1.38}$$

where φ_S is the solution of (1.15). Then (1.38) yields the Fourier transform of $q - q_0$ at $k + k'$. If the object is illuminated from many different directions $k/|k|$ and $k'/|k'|$ varies over the unit sphere, one can fill up a ball of diameter 2ω in the Fourier domain, and therefore, the reconstructed $q - q_0$ from (1.38) by direct Fourier inversion is a low pass version of the true one and the resolution of the reconstructed image is π/ω; see [3].

Figure 1.6.3 shows the reconstructed images using diffraction tomography for the same phantoms as in Figures 1.2 and 1.4. In order to obtain comparable image resolutions, much

higher frequencies ω should be used in the case of purely electromagnetic tomography. This clearly illustrates the superiority of the acousto-electromagnetic process in terms of the resolution. On the other hand, it should be emphasized that diffraction tomography uses many incidence directions while only one direction is enough for acousto-electromagnetic tomography.

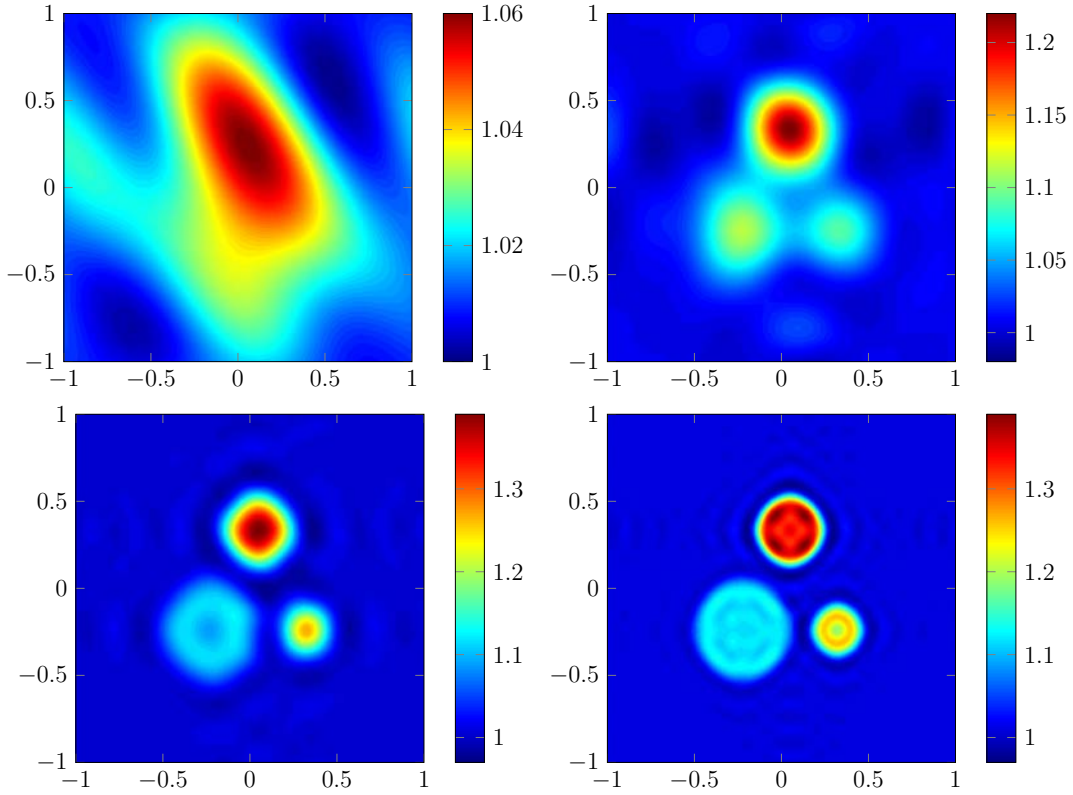

Figure 1.7: Reconstruction of the permittivity with the classical microwave tomography framework for frequency ω fixed at 10, 20, 50 and 100. Note that in our method, we work with $\omega = 1$.

1.6.4 Reconstruction from limited-view data

In this section we show how to modify our approach in the case of limited-view data. Assume that the electromagnetic measurements can be done only on an open part Γ of $\partial\Omega$. Denote by $\Gamma^c = \partial\Omega \setminus \overline{\Gamma}$. Let $\Omega' \Subset \Omega$ be an open set with $\mathcal{C}^2$ boundary and let $\Omega \setminus \overline{\Omega'}$ be connected. It is known that the set $\mathcal{V}$ of solutions to the Helmholtz equation, $\Delta + \omega^2 q_0$, with boundary data 0 on Γ^c is dense in $L^2(\Omega')$ in the set of all solutions; see [25, 26].

Here, to fix ideas, we consider φ_S and $\varphi_{D,u}$ to be the solutions of the Helmholtz equations with Dirichlet boundary conditions:

$$\begin{cases} \triangle\varphi_S + \omega^2 q\varphi_S = -\omega^2 q_0 \delta s \varphi_I & \text{in } \Omega, \\ \varphi_S = 0 & \text{on } \partial\Omega, \end{cases}$$

and

$$\begin{cases} \triangle\varphi_{S,v} + \omega^2 q_u \varphi_{S,v} = -\omega^2 q_0 \delta s_u \varphi_I \quad \text{in } \Omega, \\ \varphi_{S,v} = 0 \quad \text{on } \partial\Omega, \end{cases}$$

and measure $\partial(\varphi_S - \varphi_{S,v})/\partial n$ on Γ. In order to guarantee existence and uniqueness of solutions to the above equations, one should assume that δ is small enough and $\omega^2 q_0$ is not a Dirichlet eigenvalue for $-\Delta$ on Ω.

Assume that δs is supported in Ω'. Let $\Phi \in \mathcal{V}$ be such that $||\Phi - Ae^{-ik\cdot x}||_{L^2(\Omega')} = o(\delta)$. Following the proof of Theorem 1.2.2, one can show that the following approximation holds

$$\frac{1}{A\omega^2}\mathrm{Re}\left[\int_\Gamma \Phi \frac{\partial}{\partial n}(\varphi_S - \varphi_{S,v})\, d\sigma\right] \approx \int_\Omega (q_u - q). \tag{1.39}$$

Therefore, from the (weighted) limited-view measurements in the left-hand side of (1.39) one can reconstruct by exactly the same approach as the one described in this chapter an image of $q = q_0(1 + \delta s)$. To numerically compute the special test function Φ one can minimize over ψ, such that $(\Delta + \omega^2 q_0)\psi = 0$ in Ω, the discrepancy functional

$$J[\psi] := ||\psi - Ae^{-ik\cdot x}||^2_{L^2(\Omega')} + \mu||\psi||^2_{L^2(\Gamma^c)},$$

with $\mu > 0$ being a regularization parameter. Note that if the data is collected over a broad range of frequencies, then the optimal control techniques in the time-domain developed in [4] can be used.

Chapter 2

Ultrasound-modulated diffuse optical tomography

Introduction

Diffuse optical tomography is an emerging biomedical modality that uses diffuse light to probe structural variations in the optical properties of tissue [27]. The associated inverse problem for diffuse light propagation consists of recovering the absorption properties of a medium of interest from boundary measurements of the light intensity. The most important current applications of diffuse optical imaging are detecting tumors in the breast and brain imaging [33].

Around the red/infrared wavelength, the light is highly scattered in living tissues. At macroscopic scale, its propagation does not fit with a wave model. A classical approach is to consider the directional density of light energy $L(x,t,\xi)$ at position x at time t in the direction ξ. This quantity satisfies radiative transfer equation [102]. Define the fluence or intensity as the average of L over all the direction

$$\Phi(x,t) = \int_{S^{d-1}} L(x,t,\xi) d\sigma(\xi), \tag{2.1}$$

where S^{d-1} is the unit sphere in dimension d.

Under the diffusion approximation, this quantity is solution of the diffusion problem

$$\frac{1}{c}\partial_t \Phi - \nabla \cdot (D\Phi) + \mu_a \Phi = S, \tag{2.2}$$

where c is the light speed in the void, $D = \big(3(\mu_a + \mu_s')\big)^{-1}$, μ_a is the absorption coefficient, μ_s' the reduced scattering coefficient, and S represents an eventual light source; see [102]. The purpose of the diffuse optical tomography is to identify the coefficient μ_a and/or μ_s' from boundary measurements using many different illuminations.

Let Ω be a smooth bounded domain of $\mathbb{R}^d$, for $d = 2, 3$, representing our domain of interest. An external illumination is represented by a Robin type boundary condition of the form

$$l\partial_\nu \Phi + \Phi = g \qquad \text{on } \partial\Omega, \tag{2.3}$$

where g is the illumination intensity and $l > 0$ is the extrapolation length computed from the radiative transfer equation at the boundary. If the illumination is constant with respect to time, then the light intensity in Ω quickly gets its permanent regime because $1/c$ is very small compared to D and μ_a. In this case, the light intensity is a solution of the problem

$$\begin{cases} -\nabla \cdot (D\Phi) + \mu_a \Phi = 0 & \text{in } \Omega \\ l\partial_\nu \Phi + \Phi = g & \text{on } \partial\Omega. \end{cases} \tag{2.4}$$

As D and μ_a belongs to $L^\infty(\Omega)$ and are bounded from above and below by positive constants, it Lax-Milgram theorem shows that this problem is well posed and for any $g \in H^{1/2}(\partial\Omega)$ there exists a unique solution in $H^1(\Omega)$.

For now on, in order to simplify the problem, we assume that the scattering coefficient D is constant. Denoting the attenuation rate $a = \mu_a/D$, we consider the simplified problem

$$\begin{cases} -\triangle \Phi + a\Phi = 0 & \text{in } \Omega, \\ l\partial_\nu \Phi + \Phi = g & \text{on } \partial\Omega. \end{cases} \tag{2.5}$$

This choice is motivated by the fact that in the breast tumor detection problem, the reduced scattering coefficient μ_s' is much higher than the absorption μ_a and it does not variate much. Due to the high concentration of blood vessels in tumors, the contrast is good on the absorption coefficient μ_a.

The main purpose of this chapter is to recover the coefficient a in (2.5) from light boundary measurements using acoustic perturbations of the medium. The reconstruction of a from purely optical measurements is severely ill-posed and lacks certain resolution and stability properties. Using acoustically-induced perturbations of the domain, it is expected to enhance both resolution and stability for the reconstruction of the absorption coefficient a.

In the hybrid method developed in this chapter, only one illumination g is needed. We introduced an acoustic perturbation whose only effect is to generate a small internal displacement in Ω. This displacement field will travel in the domain and will perturb the light measurements on the boundary. The measurement perturbations will bring additional information about the absorption coefficient in the support of the displacement.

Consider a small displacement $v : \Omega \longrightarrow \mathbb{R}^d$, supported inside Ω for simplicity. The absorption coefficient become a_v implicitly defined by

$$a_v(x + v(x)) = a(x) \tag{2.6}$$

and the light fluence changes to Φ_v satisfying

$$\begin{cases} -\triangle \Phi_v + a_v \Phi_v = 0 & \text{in } \Omega \\ l\partial_\nu \Phi_v + \Phi_v = g & \text{on } \partial\Omega. \end{cases} \tag{2.7}$$

Now compute the cross correlation between Φ and Φ_v on $\partial\Omega$, the following formula

$$\frac{1}{l} \int_{\partial\Omega} g(\Phi_v - \Phi) = \int_\Omega (a_v - a)\Phi\Phi_v \tag{2.8}$$

holds. Assuming that the variation $\Phi_v - \Phi$ can be measured on the boundary, we define the variational measurement as

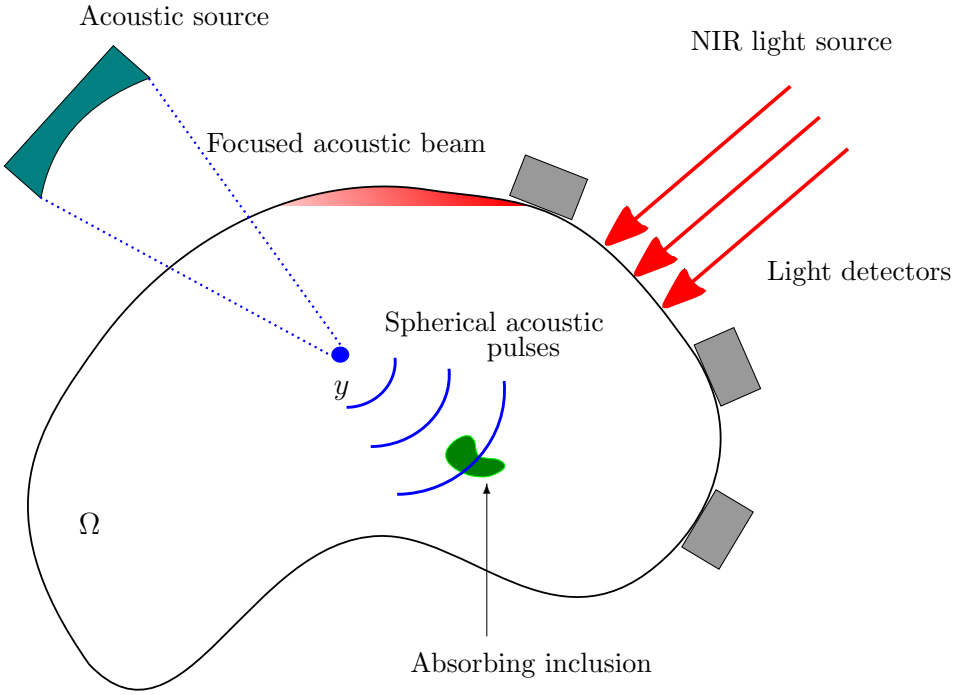

Figure 2.1: Diffusive optic imaging procedure perturbed by an acoustic displacement field. Light detectors detect variations of the outgoing light intensity.

$$M_v = \int_\Omega (a_v - a)\Phi\Phi_v. \tag{2.9}$$

As in Chapter 1, assume that the medium is mechanically homogeneous and consider a spherical type perturbation given in spherical coordinates by

$$v_{\eta,y,r}(y+\rho\xi) = \frac{\eta}{r} w\left(\frac{\rho - r}{\eta}\right)\xi, \qquad \forall(\rho,\xi) \in]\eta, +\infty[\times S^{d-1}, \tag{2.10}$$

where y is the center of the pulse, r its radius (proportional to the time) and η its size. The function w is the pulse shape supposed to be non negative of class $\mathcal{C}^\infty$ supported in $[-1,1]$ and satisfying $w < 1$ and $w' > -1$; see Chapter 1.

Assume that y can be moved around the domain of interest, we show that through an inversion of the spherical means Radon transform, we can reconstruct the curl-free part of the vectorial field $\Phi^2\nabla a$. This yields the equation (2.22) for a where the source term is computed from the data. Hence the functions a and Φ satisfy the coupled system of equations (2.23) and (2.24). This nonlinear coupling suggests the iterative algorithm (2.25)–(2.26) for reconstructing a. One of the main contributions of this chapter is to prove the convergence of the iterative scheme to the true image a_* using the contraction fixed point theorem. Moreover, the high resolution and the good stability properties of the reconstructed images are shown.

The chapter is organized as follows. In Section 2.1, we introduce some preliminary results. In Section 2.2, we present our reconstruction algorithm. In Section 2.3 we provide a proof of convergence for the algorithm. In Section 2.4 we illustrate the performance of the proposed algorithm in terms of resolution and stability. The chapter ends with a short discussion. Throughout the chapter, C is a universal constant depending only on known quantities and functions.

2.1 Preliminaries

In this section, we first recall two consequences of well-known regularity results. The propositions we present here are special cases in those papers but enough for us to study ultrasound-modulated optical tomography. The reader can find the following result in [76, 80].

Proposition 2.1.1 *Suppose that Ω is smooth. If $a \in L^\infty(\Omega)$, then any weak and bounded solution Φ of the equation*

$$-\Delta\Phi + a\Phi = 0, \tag{2.11}$$

is in $\mathcal{C}^1(\Omega)$ and

$$\|\Phi\|_{\mathcal{C}^1(\overline{\Omega}')} \leq c_1 \left(\|\Phi\|_{L^\infty(\Omega)}, \|a\|_{L^\infty(\Omega)}, \operatorname{dist}(\Omega', \partial\Omega)\right)$$

for all $\Omega' \Subset \Omega$.

The following proposition is from [59, 79].

Proposition 2.1.2 *Let D be a bounded smooth domain and λ, Λ, and M be positive constants. If $\Phi \in L^\infty(D)$ is such that*

$$0 < \lambda \leq \Phi \leq \Lambda \qquad \text{in } D$$

and if $f \in L^\infty(D)$ then the solution a of

$$\begin{cases} \nabla \cdot (\Phi^2 \nabla a) &= f \quad \text{in } D, \\ a &= 0 \quad \text{on } \partial D \end{cases} \tag{2.12}$$

is in $\mathcal{C}^1\left(\overline{D}\right)$ with

$$\|a\|_{\mathcal{C}^1\left(\overline{D}\right)} \leq c_2(\lambda, \Lambda, M). \tag{2.13}$$

Remark 2.1.3 *Assume that the constant c_2 in (2.13) is optimal (i.e., c_2 is the infimum of all of its possible values), then,*

$$c_2(\lambda, \Lambda, \delta M) \leq \delta c_2(\lambda, \Lambda, M) \tag{2.14}$$

for all $0 < \delta < 1$. This can be seen by multiplying both sides of (2.12) by δ.

We next establish the weak comparison principle and the strong maximum principle for Laplace equations with the Robin boundary condition under consideration. The main idea of the proof is based on the weak comparison principle in [82] for Dirichlet boundary conditions, with some suitable modifications. Although this might be a well-known result, we provide a proof here for the sake of completeness. Also, our strong maximum principle is somewhat different from the classical one.

Proposition 2.1.4 (weak comparison principle) *Let a be a nonnegative measurable function and assume that $\Phi \in H^1(\Omega)$ satisfies*

$$\begin{cases} -\Delta\Phi + a\Phi & \geq & 0 & \text{in } \Omega, \\ \partial_\nu\Phi + \Phi & \geq & 0 & \text{on } \partial\Omega. \end{cases} \tag{2.15}$$

Then $\Phi \geq 0$ a.e. in Ω.

Proof. Using $\Phi^- = \max\{0, -\Phi\} \geq 0$ as a test function in the variational formulation of (2.15) gives

$$\begin{aligned} 0 &\leq \int_\Omega \nabla\Phi \cdot \nabla\Phi^- dx - \int_{\partial\Omega} \partial_\nu\Phi\Phi^- d\sigma + \int_\Omega a\Phi\Phi^- dx \\ &\leq \int_\Omega \nabla\Phi \cdot \nabla\Phi^- dx + \int_{\partial\Omega} \Phi\Phi^- d\sigma + \int_\Omega a\Phi\Phi^- dx \\ &= -\int_\Omega |\nabla\Phi^-|^2 dx - \int_{\partial\Omega} |\Phi^-|^2 d\sigma - \int_\Omega a|\Phi^-|^2 dx. \end{aligned}$$

It follows that $\Phi^- = 0$. Note that Φ^- is admissible to be a test function because it belongs to $H^1(\Omega)$ (see [60]). □

Proposition 2.1.5 (strong maximum principle) *Let $g \not\equiv 0$ be a nonnegative smooth function defined on $\partial\Omega$. Let $D \Subset \Omega$ be smooth. For all $c > 0$, the solution Φ of*

$$\begin{cases} -\Delta\Phi + c\Phi & = & 0 & \text{in } \Omega, \\ \partial_\nu\Phi + \Phi & = & g & \text{on } \partial\Omega, \end{cases} \tag{2.16}$$

is bounded and positive in D.

We need the following lemma to prove this strong maximum principle [96].

Lemma 2.1.6 (Hopf lemma) *Let $\Phi \in \mathcal{C}^1\left(\overline{\Omega}\right) \cap \mathcal{C}^2(\Omega)$ satisfy*

$$-\Delta\Phi + c\Phi \geq 0$$

on Ω where c is a nonnegative constant. If there exists $x_0 \in \partial\Omega$ such that $\Phi(x_0) \leq 0$ and $\Phi(x) > \Phi(x_0)$ for all $x \in \Omega$, then

$$\partial_\nu\Phi(x_0) < 0.$$

Proof. [Proof of Proposition 2.1.5] Since g is nonnegative, so is Φ because of Proposition 2.1.4. On the other hand, applying Proposition 2.1.4 again for $\|g\|_{L^\infty(\partial\Omega)} - \Phi$, we can see that $\Phi \leq \|g\|_{L^\infty(\partial\Omega)}$. The boundedness of Φ in Ω and hence D has been verified. In order to use the Hopf lemma, we show that $\Phi \in \mathcal{C}^2(\Omega)$. In fact, for all $x_0 \in \Omega$, let D_1 and D_2 satisfying

$$D_1 \Subset D_2 \Subset \Omega$$

be two open neighbourhoods of x_0. The boundedness of Φ in the previous paragraph and Proposition 2.1.1 imply that Φ belongs to $\mathcal{C}^1(\overline{D}_2)$. On the other hand, Theorem 8.8 in [60]

helps us to see that $\Phi \in H^2(D_2)$. Hence, $\partial_{x_i}\Phi$, $i = 1, \cdots, d$, is in $H^1(D_2)$. It also satisfies the equation

$$-\Delta\partial_{x_i}\Phi + c\partial_{x_i}\Phi = 0.$$

Hence, $\partial_{x_i}\Phi$ belongs to $\mathcal{C}^1(\overline{D}_1)$ by Proposition 2.1.1. In other words, $\Phi \in \mathcal{C}^2(\overline{D}_1)$.

We claim that $\Phi > 0$ not only in $\overline{D}$ but also in Ω. Assume that $\Phi(x_0) = 0$ for some $x_0 \in \Omega$. Since g is not identically zero, neither is Φ. Hence, we can find a point $x_1 \in \Omega$ such that $\Phi(x_1) > 0$. Without loss of generality, we can suppose that $B(x_1, r) \subset \Omega$ with $r = |x_1 - x_0|$ and $\Phi(x) > 0$ for all $x \in B(x_1, r)$. Since $\Phi \in \mathcal{C}^2(\Omega)$, it belongs to $\mathcal{C}^1(\overline{B(x_1, r)}) \cap \mathcal{C}^2(B(x_1, r))$. We can apply the Hopf lemma for Φ in $B(x_1, r)$ to get

$$\nabla\Phi(x_0) \cdot (x_1 - x_0) < 0.$$

This is a contradiction because Φ attains its minimum value at x_0 and $\nabla\Phi(x_0) = 0$.

2.2 A reconstruction algorithm

Considering a small displacement field v in the domain Ω changing the light absorption a to $a_v = a \circ (Id + v)^{-1}$, we measure the variation of the light fluence $\Phi_v - \Phi$ on $\partial\Omega$. The aim is to reconstruct the optical absorption coefficient a from several measurements generated by several displacement field with a better resolution and stability than using pure optical tomography.

In Chapter 1, we have shown that the displacement function v at x caused by a short diverging spherical acoustic wave generated at $y \in \mathbb{R}^d \setminus \overline{D}$ is of the form

$$v_{\eta,y,r}(y + \rho\xi) = \frac{\eta}{r} w\left(\frac{\rho - r}{\eta}\right)\xi, \qquad \forall(\rho, \xi) \in]\eta, +\infty[\times S^{d-1}, \tag{2.17}$$

in spherical coordinates centered in y.

Now, by exactly the same arguments as in Chapter 1, it follows that

$$\|\Phi_v - \Phi\|_{H^1(\Omega)} \leq c\|a_v - a\|_{L^2(\Omega)},$$

for some positive constant c, and therefore,

$$\int_{\partial\Omega} g(\partial_\nu\Phi - \partial_\nu\Phi_v)\, d\sigma = \int_\Omega \Phi\Phi_v(a - a_v) \approx -\int_\Omega \Phi^2\nabla a \cdot v \tag{2.18}$$

Since $\partial_\nu\Phi$ and $\partial_\nu\Phi_v$ can be measured on $\partial\Omega$, it is possible to evaluate the quantity $\int_{\partial\Omega} g(\partial_\nu\Phi - \partial_\nu\Phi_v)\, d\sigma$ for all y, t. This quantity is nothing other than the cross-correlations between the boundary measurements in the perturbed and unperturbed media.

Next, from (2.18) we establish an equation for a. Using Helmholtz decomposition, we write

$$\Phi^2\nabla a = -\nabla\psi + \nabla \times \Gamma. \tag{2.19}$$

Here, in order to ensure the uniqueness of ψ and Γ we assume that Ω is simply connected, Γ is such that $\nabla \cdot \Gamma = 0$, and supply the boundary conditions $\partial_\nu\psi = -\Phi^2\partial_\nu a$ and $\Gamma \times \nu = 0$ on $\partial\Omega$.

Since v takes the radial form (2.17), integration by parts yields

$$\int_\Omega \nabla \times \Gamma \cdot v = 0,$$

and so, (2.18) can be rewritten as

$$\int_{\partial\Omega} g(\partial_\nu \Phi - \partial_\nu \Phi_v)\, d\sigma \approx \int_\Omega \nabla\psi \cdot v\, dx.$$

Hence, ψ can be constructed and considered as the given data by employing the spherical Radon transform, as is done in Chapter 1. Let

$$M_v(y,r) := \int_{\partial\Omega} g(x) \left(\partial_\nu \Phi(x) - \partial_\nu \Phi_v(x,y,r/c)\right) d\sigma(x), \tag{2.20}$$

where v_y is given by (2.17).

For $f \in \mathcal{C}^0(\mathbb{R}^d)$ and $E \subset \mathbb{R}^d$, define the spherical Radon transform of f over E by

$$\mathcal{R}[f](y,r) = \int_{S^{d-1}} f(y + r\xi)\, d\sigma(\xi) \quad y \in E,\ r > 0,$$

where $d\sigma$ is the surface measure over S^{d-1}.

From Chapter 1 the following lemma holds.

Lemma 2.2.1 *Fix $y \in \Omega \setminus \overline{D}$ and let $r_0 > 0$. Suppose that $a(x) = a_0$ for $x \in B(y, r_0)$, where B is the ball of center y and radius r_0. Suppose also that $a \in \mathcal{C}^{1,\beta}(\overline{\Omega})$ and η is small enough. Then, for all $r > r_0$ and $\eta \ll r$, we have*

$$\mathcal{R}[\psi](y,r) \approx -\frac{1}{\eta^2 \|w\|_{L^1} |S^{d-1}|} \int_{r_0}^r \frac{M_v(y,\rho)}{\rho^{d-2}} d\rho. \tag{2.21}$$

Having in hand ψ from the cross-correlations between boundary measurements using a spherical Radon transform inversion, we take the divergence of (2.19) to arrive at

$$-\nabla \cdot (\Phi^2 \nabla a) = \Delta\psi. \tag{2.22}$$

This allows us to recover a in D by solving the system of equations for the two unknowns Φ and q

$$\begin{cases} -\Delta\Phi + q\Phi &= 0 \quad \text{in } \Omega, \\ \partial_\nu \Phi + \Phi &= g \quad \text{on } \partial\Omega, \end{cases} \tag{2.23}$$

and

$$\begin{cases} -\nabla \cdot (\Phi^2 \nabla q) &= \Delta\psi \quad \text{in } D, \\ q &= a_0 \quad \text{on } \partial D. \end{cases} \tag{2.24}$$

This suggests the following algorithm:

1. Define the initial guess $q^{(0)} = a_0$.

2. Establish an iterating sequence $\{q^{(n)}\}$ as follows.

(a) For $n \geq 1$, solve

$$\begin{cases} -\Delta\Phi^{(n)} + \hat{q}^{(n-1)}\Phi^{(n)} &= 0 \quad \text{in } \Omega, \\ \partial_\nu\Phi^{(n)} + \Phi^{(n)} &= g \quad \text{on } \partial\Omega, \end{cases} \tag{2.25}$$

where

$$\hat{p} := \min\{\max\{p, \underline{q}\}, \overline{q}\}.$$

(b) Find $q^{(n)}$ by solving

$$\begin{cases} -\nabla\cdot((\Phi^{(n)})^2\nabla q^{(n)}) &= \Delta\psi \quad \text{in } D, \\ q^{(n)} &= a_0 \quad \text{on } \partial D, \end{cases} \tag{2.26}$$

and set $q^{(n)} = a_0$ in $\Omega \setminus D$.

3. The convergent function of $\{q^{(n)}\}$ is the true optical absorption coefficient a_*.

Remark 2.2.2 *The convergence of $\{q^{(n)}\}$, mentioned in Step 3, will be shown by the Banach fixed point theorem in the next section. This also implies the well-posedness of the system constituted by (2.23) and (2.24).*

Remark 2.2.3 *Problem (2.25) is uniquely solvable because we are able to avoid the case that $(\Phi^{(n)})^2$ approaches 0 or ∞ somewhere inside D in the next section; see Lemma 2.3.1.*

Remark 2.2.4 *We modify $q^{(n-1)}$ by $\hat{q}^{(n-1)}$ in (2.25) because of the obvious inequality*

$$|\hat{p} - a| \leq |p - a|,$$

which makes the proof of the algorithm easier and may increase the rate of convergence.

2.3 Iterative algorithm convergence

In this section, we first assume that the Born assumption holds, *i.e.*, the optical coefficient a_* takes the form

$$a_* = a_0(1 + \delta s_*). \tag{2.27}$$

Here δ is a small constant and s_* is a smooth function whose support is D.

Equation (2.22) together with (2.27) implies that

$$-\Delta\psi = \delta a_0 \nabla\cdot(\Phi^2\nabla s_*), \tag{2.28}$$

where δ and s_* were introduced in (2.27). Assume that a is bounded from below and above by two known positive constants $\underline{q}$ and $\overline{q}$ respectively. Since Φ solves problem (2.11) with a replacing p and Λ, which will be defined later in Lemma 2.3.1, replacing M, its $\mathcal{C}^1(\overline{D})$ norm is bounded. We assume further that δ is small and s_* is smooth, with known bound on its $\mathcal{C}^2(D)$ norm, to guarantee that $\|\Delta\psi\|_{L^\infty(D)}$ is bounded in the order of δ.

Define the open set of $L^\infty(\Omega)$,

$$\mathcal{Q} = \{p \in L^\infty(\Omega) : \underline{q} < p < \overline{q}\}, \tag{2.29}$$

and the map

$$\begin{array}{rcl} F_1 : \mathcal{Q} & \to & H^1(\Omega) \\ q & \mapsto & F_1[q] = \Phi, \end{array} \tag{2.30}$$

where Φ is the solution of (2.23).

We have the following result.

Lemma 2.3.1 *For all $q \in \mathcal{Q}$, $F_1[q]$ is in $L^\infty(\Omega)$. There exists a positive constant $\Lambda(\underline{q}, \overline{q})$ such that*

$$\left|F_1[q](x)\right| \leq \Lambda, \forall\, x \in \Omega. \tag{2.31}$$

Moreover, for any $D \Subset \Omega$, there exists a positive constant $\lambda(D, \underline{q}, \overline{q})$ such that

$$\lambda \leq F_1[q](x), \forall\, x \in D. \tag{2.32}$$

Proof. Let $\Phi_{\underline{q}}$ and $\Phi_{\overline{q}}$ be the solutions of (2.16) with c replaced by $\underline{q}$ and $\overline{q}$, respectively. It follows by Proposition 2.1.4 that

$$\Phi_{\overline{q}} \leq \Phi \leq \Phi_{\underline{q}} \text{in } \Omega.$$

On the other hand, we can apply Proposition 2.1.5 to see that

$$\Phi_{\overline{q}} > 0 \text{ in } D.$$

The lemma is proved by letting $\lambda = \inf_D \Phi_{\overline{q}}$ and $\Lambda = \sup_\Omega \Phi_{\underline{q}}$.

Lemma 2.3.2 *The map F_1 is Fréchet differentiable. Its derivative at q is given by*

$$DF_1[q](h) = \phi, \tag{2.33}$$

for $h \in L^\infty(\Omega)$, where ϕ solves

$$\left\{ \begin{array}{rcll} -\Delta\phi + q\phi & = & -h\Phi & \text{in } \Omega, \\ \partial_\nu \phi + \phi & = & 0 & \text{on } \partial\Omega, \end{array} \right. \tag{2.34}$$

with $\Phi = F_1[q]$. Moreover, $DF_1[q]$ can be continuously extended to the whole $L^2(\Omega)$ by the same formula in (2.34) with

$$\|DF_1[q]\|_{\mathcal{L}(L^2(\Omega), H^1(\Omega))} \leq C\Lambda, \tag{2.35}$$

where Λ was defined in Lemma 2.3.1.

Proof. Let Φ' be the solution of (2.23) with $q + h$ replacing q, assuming $\|h\|_{L^\infty(\Omega)} \ll 1$ so that $q + h \in \mathcal{Q}$ *a.e.* in Ω. Note that $\Phi' - \Phi$ solves

$$\left\{ \begin{array}{rcll} -\Delta(\Phi' - \Phi) + (q + h)(\Phi' - \Phi) & = & -h\Phi & \text{in } \Omega, \\ \partial_\nu(\Phi' - \Phi) + (\Phi' - \Phi) & = & 0 & \text{on } \partial\Omega. \end{array} \right.$$

Using $\Phi' - \Phi$ as a test function in the variational formulation of the problem above gives

$$\|\Phi' - \Phi\|_{H^1(\Omega)} \leq C\|h\|_{L^\infty(\Omega)}\|\Phi\|_{L^2(\Omega)}. \tag{2.36}$$

On the other hand, since $\Phi' - \Phi - \phi$ solves

$$\left\{ \begin{array}{rcll} -\Delta(\Phi' - \Phi - \phi) + q(\Phi' - \Phi - \phi) & = & -h(\Phi' - \Phi) & \text{in } \Omega, \\ \partial_\nu(\Phi' - \Phi - \phi) + (\Phi' - \Phi - \phi) & = & 0 & \text{on } \partial\Omega, \end{array} \right.$$

we can apply the argument above to obtain

$$\|\Phi' - \Phi - \phi\|_{H^1(\Omega)} \leq C\|h\|_{L^\infty(\Omega)}\|\Phi' - \Phi\|_{L^2(\Omega)}. \tag{2.37}$$

Combining (2.36) and (2.37) shows that

$$\|\Phi' - \Phi - \phi\|_{H^1(\Omega)} \leq C\|h\|^2_{L^\infty(\Omega)}\|\Phi\|_{L^2(\Omega)},$$

which implies

$$\lim_{\|h\|_{L^\infty(\Omega)} \to 0} \frac{\|\Phi' - \Phi - \phi\|_{H^1(\Omega)}}{\|h\|_{L^\infty(\Omega)}} = 0.$$

The first part of the lemma follows.

Because of Lemma 2.3.1 and Proposition 2.1.4, which shows that $\Phi \in L^\infty(\Omega)$, problem (2.34) is uniquely solvable for all $h \in L^2(\Omega)$ and therefore the extension $DF_1[q] : L^2(\Omega) \to H^1(\Omega)$ is well-defined. Its continuity and (2.35) can be deduced, using ϕ as a test function in the variational formulation of (2.34) and applying Lemma 2.3.1:

$$\|\phi\|_{H^1(\Omega)} \leq C\|h\|_{L^2(\Omega)}\|\Phi\|_{L^\infty(\Omega)}.$$

We next introduce another open set of $L^\infty(\Omega)$:

$$\mathcal{P} = \left\{ \rho \in L^\infty(\Omega) : \frac{\lambda}{2} < \rho < 2\Lambda \text{ in } D \right\}. \tag{2.38}$$

Let

$$\begin{array}{rcl} F_2 : \mathcal{P} & \to & H^1(\Omega) \\ \Phi & \mapsto & F_2[\Phi] = q, \end{array}$$

where q is the solution of (2.24) in D and $q = a_0$ on $\Omega \setminus \overline{D}$.

The following lemma can be proved in the same manner as Lemma 2.3.2.

Lemma 2.3.3 *The map F_2 is Fréchet differentiable. Its derivative at Φ is given by*

$$DF_2[\Phi](h) = Q, \tag{2.39}$$

for $h \in L^\infty(\Omega)$, where Q solves

$$\left\{ \begin{array}{rcll} -\nabla \cdot (\Phi^2 \nabla Q) & = & \nabla \cdot (2\Phi h \nabla q) & \text{in } D, \\ Q & = & 0 & \text{on } \partial D \end{array} \right. \tag{2.40}$$

with $q = F_2[\Phi]$ being the solution of (2.24) and $Q = 0$ in $\Omega \setminus D$. Moreover, $DF_2[\Phi]$ can be extended continuously to $L^2(\Omega)$ and

$$\|DF_2[\Phi]\|_{\mathcal{L}(L^2(\Omega),H^1(\Omega))} \leq \frac{2\delta\Lambda a_0}{\lambda^2} c_2(\lambda, \Lambda, M), \tag{2.41}$$

where M is an upper bound of $\|\nabla \cdot (\Phi \nabla s_*)\|_{L^\infty(D)}$.

Proof. Since evaluating the derivative of F_2 at Φ is similar to doing so in Lemma 2.3.2, we only verify the well-definedness of the extension of $DF_2[\Phi]$ and (2.41). Since $\Phi \in \mathcal{P}$, we can apply Proposition 2.1.2 to see that the solution q of (2.24) is in $\mathcal{C}^1(\overline{D})$ and

$$\|q - a_0\|_{\mathcal{C}^1(\overline{D})} \leq c_2(\lambda, \Lambda, \delta M).$$

As a consequence, since $q = a_0$ on $\Omega \setminus D$, we deduce that

$$\|\nabla q\|_{L^\infty(\Omega)} \leq c_2(\lambda, \Lambda, \delta M) \leq \delta a_0 c_2(\lambda, \Lambda, M). \tag{2.42}$$

Thus, (2.40) is uniquely solvable if $h \in L^2(\Omega)$. This shows how to extend $DF_2[\Phi]$ to $L^2(\Omega)$.

In order to prove (2.41), we use Q as a test function in the variational formulation of (2.40) and employ (2.42) to get

$$\begin{aligned} \lambda^2 \int_D |\nabla Q|^2 dx &\leq \int_D \Phi^2 |\nabla Q|^2 dx \\ &\leq 2\Lambda \|\nabla q\|_{L^\infty(D)} \int_D |h||\nabla Q| dx \\ &\leq 2\delta\Lambda c_2(\lambda, \Lambda, M) \|h\|_{L^2(D)} \|\nabla Q\|_{L^2(D)}. \end{aligned}$$

Therefore,

$$\|Q\|_{H_0^1(D)} \leq \frac{2\delta\Lambda a_0}{\lambda^2} c_2(\lambda, \Lambda, M),$$

and the proof is complete. □

The following result holds.

Theorem 2.3.4 *Assume that $\|s_*\|_{\mathcal{C}^2(D)} \leq M$ and $\underline{q}$, $\overline{q}$, and M are given. If δ is sufficiently small then the iteration sequence in the algorithm converges in $L^2(\Omega)$ to a, the unique solution of (2.23) and (2.24).*

Proof. Introduce the map

$$F[q] = F_2 \circ F_1[q]$$

defined on $\mathcal{Q}$. Thanks to (2.31) and (2.32), the range of F_1 is contained in the domain of F_2. This shows how the definition above makes sense. Considering F as the map $\mathcal{P} \to L^2(\Omega)$, using the standard chain rule in differentiation and the fact that $H^1(\Omega) \subset L^2(\Omega)$, we have

$$DF[q] : L^\infty(\Omega) \to L^2(\Omega)$$

given by

$$DF[q](h) = DF_2[F_1[q]](DF_1[q](h)) \tag{2.43}$$

is the Fréchet derivative of F. Moreover, by Lemmas 2.3.2 and 2.3.3, $DF[q]$ can be extended continuously to $L^2(\Omega)$ with

$$\|DF[q]\|_{\mathcal{L}(L^2(\Omega),L^2(\Omega))} \leq \|DF_1[q]\|_{\mathcal{L}(L^2(\Omega),H^1(\Omega))}\|DF_2[q]\|_{\mathcal{L}(L^2(\Omega),H^1(\Omega))} \leq C\delta.$$

Recall from the algorithm that $q^{(0)} = a_0$ is the initial guess for the true coefficient a_* and for $n \geq 1$, define

$$q^{(n)} = F[Tq^{(n-1)}], \quad n \geq 1,$$

where $T(p) = \min\{\max\{p, \underline{q}\}, \overline{q}\}$. Note that for all $m, n \geq 1$,

$$\begin{aligned} \|F[Tq^{(n)}] - F[Tq^{(m)}]\|_{L^2(\Omega)} &= \left\| \int_0^1 DF[(1-t)Tq^{(n)} + tTq^{(m)}](q^{(m)} - q^{(n)})dt \right\|_{L^2(\Omega)} \\ &\leq C\delta\|q^{(m)} - q^{(n)}\|_{L^2(\Omega)}. \end{aligned}$$

Thus, if δ is small enough then

$$F \circ T : L^2(\Omega) \to L^2(\Omega)$$

is a contraction map. Let q^* denote the fixed point of $F \circ T$ and hence the convergent point of $q^{(n)}$. Since a_*, the true absorption coefficient, is a fixed point of F and is in the interval $[\underline{q}, \overline{q}]$, it is the fixed point of $F \circ T$. Therefore, $q^* = a_*$ and the proof is complete.

Now we generalize Theorem 2.3.4 behind the Born approximation (2.27). Using exactly the same arguments as those in the proof of Theorem 2.3.4 we obtain our main result in this section.

Theorem 2.3.5 *If $\|\Delta\psi\|_{L^\infty(D)}$ is sufficiently small, then the iteration sequence in the algorithm converges in $L^2(\Omega)$ to a, the unique solution of (2.23) and (2.24).*

2.4 Numerical simulations

2.4.1 Forward problem

In this section we numerically illustrate the convergence of the fixed point scheme when $\delta|D| \ll |\Omega|$. In fact, if the support of $a_* - a_0$ is small, then δ can be taken quite large and we observe convergence to the true optical distribution behind the Born approximation. Note that if δ is small enough, then one iteration is enough to satisfactory reconstruct the optical absorption distribution.

As a two dimensional test case, we consider $\Omega =]-1, 1[^2$ and $a_0 = 1$. We set

$$a(x) = 1 + \delta \sum_i (a_i - 1)\mathbf{1}_{\Omega_i},$$

where Ω_i are smooth domains strictly included in Ω, a_i are smooth functions on Ω_i greater than -1 and δ is a positive constant. In this test, we consider the case were the inclusions Ω_i are three disks with $a_1 = 1.1$, $a_2 = 1.2$ and $a_3 = 1.3$ and $\delta = 10$; see Figure 2.2 (1).

To solve the direct problem, we use a finite element method implemented in Matlab with an adaptive mesh (see Figure 2.2 (2)) to fit the variations of the absorption distribution a. We compute the light fluence Φ solving the equation

$$\begin{cases} -\triangle\Phi + a\Phi = 0 & \text{in } \Omega, \\ l\partial_\nu\Phi + \Phi = g & \text{on } \partial\Omega \end{cases}$$

with $l = 1$ and an illumination from the left, *i.e.*, $g = 1$ on $\{x = -1\}$ and $g = 0$ elsewhere. The solution is represented in logarithmic scale in Figures 2.2 (3) and (4).

For some centers y taken on the unit circle and $r \in]0, 2[$, we compute a discrete form of the map

$$v_{y,r,\eta}(x) = \frac{\eta}{r} w\left(\frac{|x-y| - r}{\eta}\right) \frac{x-y}{|x-y|},$$

where the wave shape w is defined by

$$w(t) = \begin{cases} \exp\left(\dfrac{1}{t^2-1}\right) & t \in]-1, 1[, \\ 0 & \text{otherwise.} \end{cases}$$

From this map, we compute the displaced absorption as $a_v = a \circ (Id + v)^{-1}$ and the variation of the fluence $\Phi_v - \Phi$. Its cross correlation on the boundary leads to the measurement

$$M = \int_{\partial\Omega} (a_v - a)\Phi\Phi_v.$$

Figure 2.2 (5) represents the measurements for 64 centers y equidistributed on the unit circle and with $r \in]0, 2[$. Applying the asymptotic formula (2.21), we deduce an approximation of the spherical means Radon transform $\mathcal{R}[\Psi]$ of the internal data Ψ; see Figure 2.2 (6).

Using Lemma 2.2.1 and adopting the same numerical approach as in [12], we generate the data Ψ by inverting the spherical Radon transform. In the case where the number of sampling points y is small, the total variation regularization-type method developed in [12] can be used. Problems (2.25) and (2.26) are solved iteratively using a finite element code. We use a structured mesh with 10^4 nodes and $P1$-finite elements.

2.4.2 Inverse problem

From this point, we only keep the interpreted data $\mathcal{R}[\Psi]$ and the a prior knowledge of $a_0 = 1$. We don not employ the forward model for the inversion. We choose $D = D(0, 0.8)$ as a subdomain of interest and invert the spherical mean Radon transform using the filtered back-projection algorithm; see [12]. We plot this internal data Ψ on a fine uniform mesh on D; see Figure 2.3.

Now, we initialize the iterative procedure by computing Φ_0 the light fluence in the case of a contrast $\delta = 0$ and defining a_1 as the solution of

$$\begin{cases} -\nabla \cdot (\Phi_0^2 \nabla a_1) = \triangle\psi, & \text{in } D, \\ a_1 = a_0 & \text{on } \partial D; \end{cases}$$

see Figure 2.5. At the first iteration, the shapes of two over three inclusions are well reconstructed. However, a large error in the values of the parameters inside the inclusions occurs. Therefore, we continue the process using the iterative algorithm, by computing the illumination Φ_1 corresponding to a_1 to get a_2. We define the fixed point sequence:

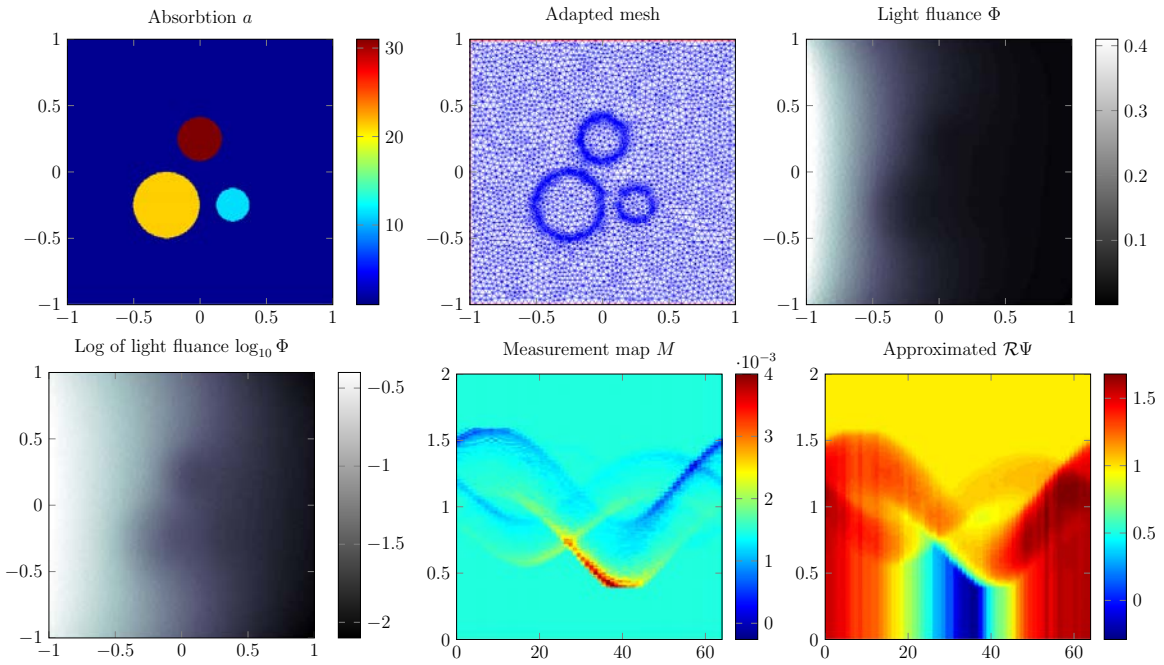

Figure 2.2: Numerical simulations for the forward problem. From left to right, top to bottom: (1) absorption map to be reconstructed with a contrast parameter $\delta = 10$; (2) Adapted mesh for solving the forward problem; (3) Light fluence Φ solution of (2.5); (4) Light fluence plotted in log scale: $\log_{10}(\Phi)$; (5) Measurements on the boundary computed with formula (2.20); (6) Approximated spherical means Radon transform of Ψ computed from the measurements by (2.21).

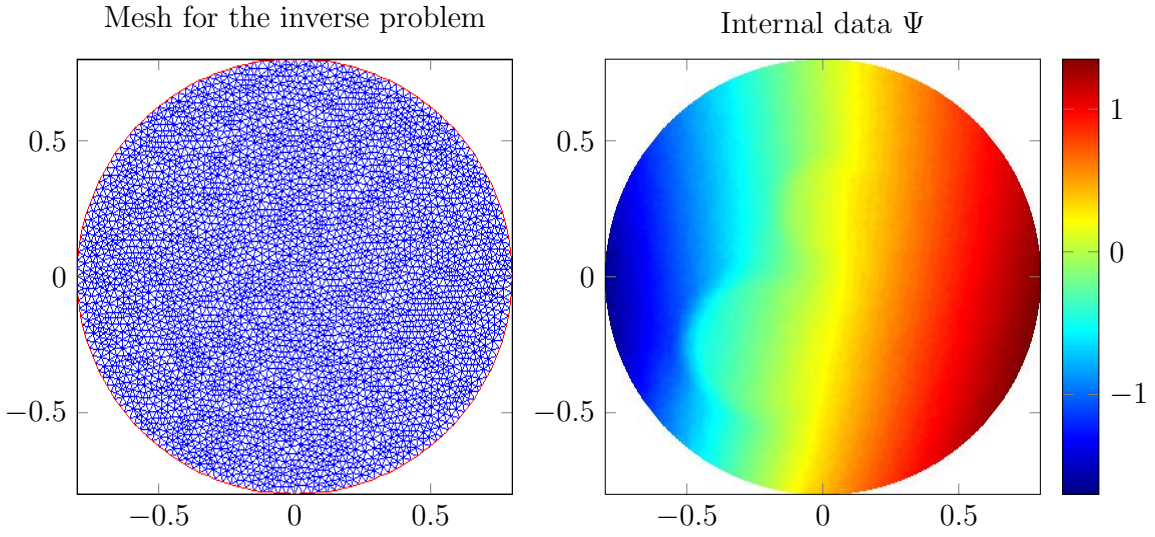

Figure 2.3: Uniform mesh on D and the internal data Ψ.

$$(a_{n+1}, \Phi_{n+1}) : \begin{cases} \begin{cases} \nabla \cdot (\Phi_n^2 \nabla a_{n+1}) = \triangle \Psi & \text{in } D, \\ a_{n+1} = a_0 & \text{on } \partial D, \\ a_{n+1} = a_0 & \text{on } \Omega \backslash D, \end{cases} \\ \begin{cases} -\triangle \Phi_{n+1} + a_{n+1} \Phi_{n+1} = 0 & \text{in } \Omega, \\ l \partial_\nu \Phi_{n+1} + \Phi_{n+1} = g & \text{on } \partial\Omega. \end{cases} \end{cases}$$

Figure 2.5 represents the iterations a_1, a_2, a_5, and a_{10}. Figure 2.6 shows the quadratic error of $a_1 0$. As expected, this error is concentrated on the inclusions boundaries. We also notice an instability located on the right part, which is due to the small value of the light fluence Φ in this region.

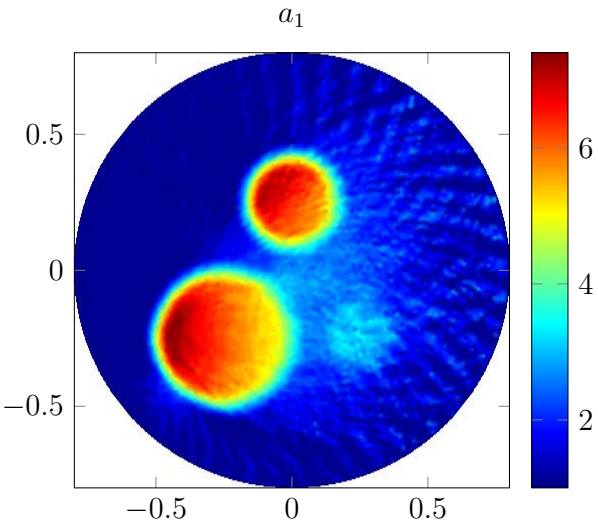

Figure 2.4: First reconstruction of the absorption a given in Figure 2.2 (1).

Remark 2.4.1 *Using $\triangle \Psi$ might seem numerically unstable because it uses two derivatives of the data. In fact, it only uses one derivative because this term has to be understood in the weak sense:*

$$\langle \triangle \Psi, \varphi \rangle_{H^{-1}(D), H_0^1(D)} = - \int_D \nabla \Psi \cdot \nabla \varphi, \qquad \forall \varphi \in H_0^1(D).$$

Nevertheless, the gradient $\nabla \Psi$ has to be stably reconstructed, which is the case here because of the smoothing effect of the wavefront. We will come back on this important item in Chapter **??***, in which we investigate the stability issues in a more general framework.*

In this numerical application we distinguish four regimes of convergence depending on the contrast of the absorption map. The first is the very low contrast case when $\Phi \approx \Phi_0$ and the first iteration a_1 of the fixed point algorithm is the best reconstruction that we can expect from the internal data. The second regime is characterized by a low contrast when $\Phi \approx \Phi_1$ and so the second iteration a_2 of the fixed point algorithm is the best reconstruction that we can expect from the internal data. The third regime is characterized by a high

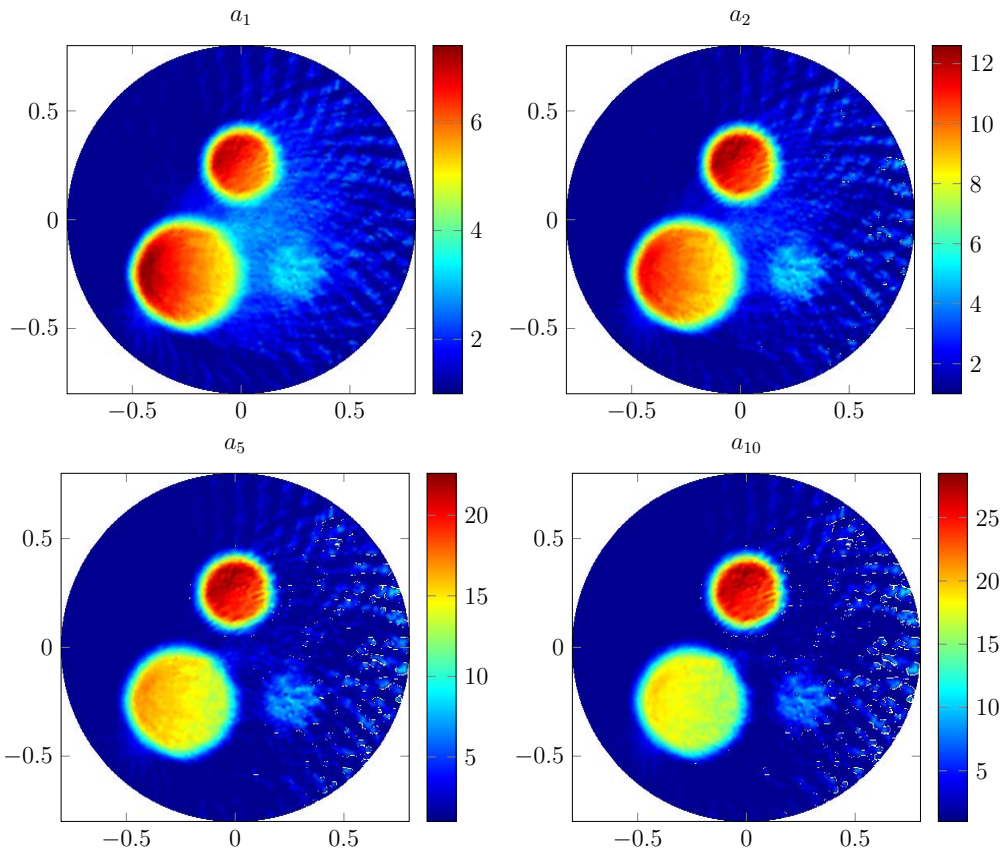

Figure 2.5: Iterations of the sequence (a_n) from the iterative fixed point algorithm.

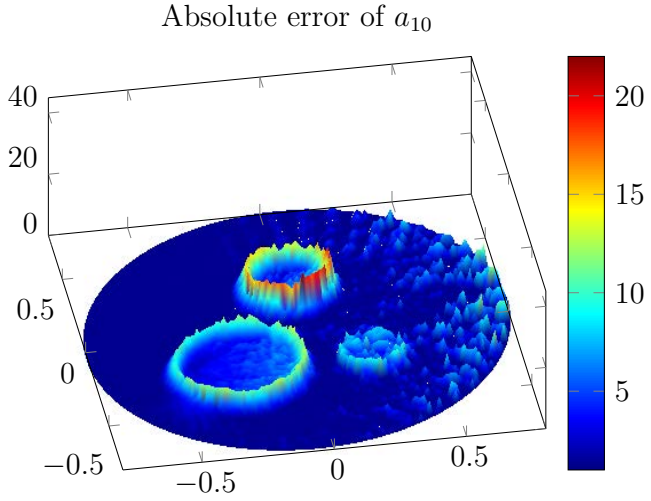

Figure 2.6: Absolute error of a_{10}, $E_{10} = |a_{10} - a|$.

absorption contrast and provide a relative slow convergence of the fixed point algorithm. Finally, the fourth regime is the very high contrast case when the fixed point algorithm does

not converge. These four regimes are illustrated in Figures 2.7 and 2.8.

When the contrast is too high, some high absorption area creates shadow zones in which the lack of light fluence inhibits any reconstruction. The minimum error is due to numerical factors (number of acoustic sources to invert the spherical means Radon transform for example) and the resolution factor η of the acoustic pulse. When η goes to zero, we get the same kind of convergence that the one shown in Chapter 1.

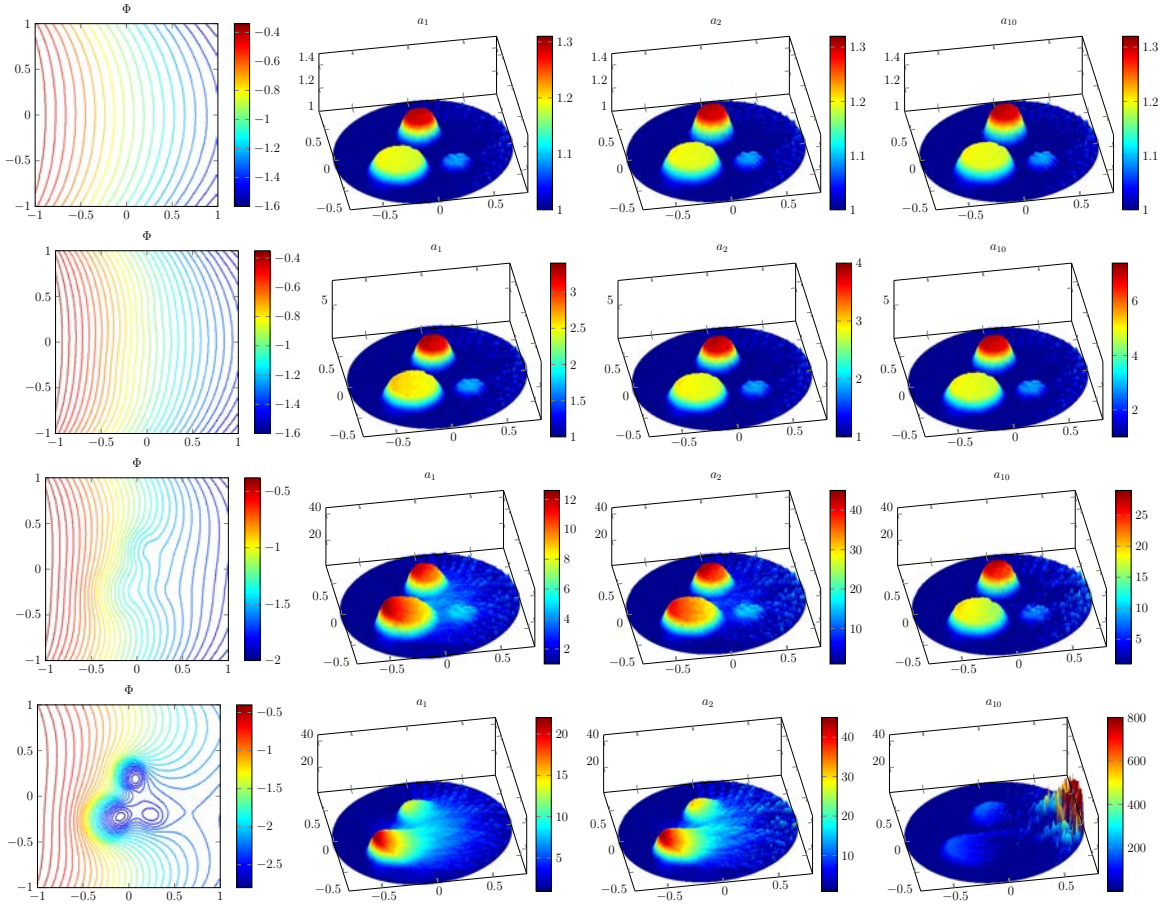

Figure 2.7: The four different regimes of convergence. From top to bottom: the contrast increases, $\delta = 0.1$, $\delta = 1$, $\delta = 10$ and $\delta = 100$. From left to right: the light fluence in Ω and the iterations of the reconstructed absorption a_1, a_2 and a_{10}.

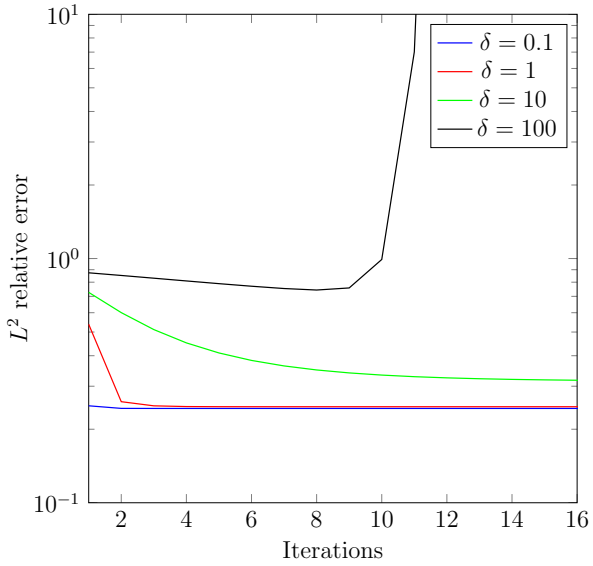

Figure 2.8: Convergence of the four regimes.

Chapter 3

Reconstruction of a piecewise smooth absorption coefficient by an acousto-optic process

Introduction

In Chapter 2 we have proposed an original method for reconstructing the optical absorption coefficient by using mechanical perturbations of the medium. While taking optical measurements the medium is perturbed by a propagating acoustic wave. Then cross-correlations between the boundary values of the optical energy density in the medium changed by the propagation of the acoustic wave and those of the optical energy density in the unperturbed one are computed. Finally, under some smoothness conditions, the use of a spherical Radon transform inversion yields a reconstructed image for a_*, which has a resolution of order the width of the wave front of the acoustic wave propagating in the medium.

This chapter aims to generalize the acousto-optic process for nonsmooth optical absorption distributions. We tackle the nonlinear optical reconstruction problem for optical inclusions. We develop a mathematical framework for the reconstruction problem in the case where the optical absorption distribution is a perturbation of a piecewise constant function. We introduce an iterative reconstructing algorithm of Landweber-type and prove its convergence and stability. For doing so, we introduce a weak Helmholtz decomposition and interpret in a weak sense the cross-correlation measurements.

To describe our approach, we employ several notations. Each smooth component of a_* is called an inclusion. The background of a_* is assumed to be a known positive constant and denoted by a_0. Assume further the knowledge of a lower bound $\underline{a}$ and an upper bound $\overline{a}$ of a_*, both of which are positive. Finally, let $D \Subset \Omega$ be known and such that

$$a_* = a_0 \quad \text{in } \Omega \setminus \overline{D}. \tag{3.1}$$

We next impose some conditions on the unknown inclusions. Let $k \geq 1$ denote the number of inclusions and A_i be occupied by the ith inclusion. Assume:

I_1. for any $i \in \{1, \ldots, k\}$, A_i is a smooth subdomain of Ω, ∂A_i is connected;

I_2. for any $j \neq i$, $\overline{A_i} \cap \overline{A_j} = \emptyset$;

I_3. $\cup_{i=1}^{k} \overline{A}_i \Subset D$.

All of the assumptions above suggest the definition of the class $(\mathcal{A}) \subset L^\infty(\Omega)$, which contains a_*.

Definition 3.0.1 *The function a is said to belong to class $(\mathcal{A})$ iff there exist $k \geq 1$, $A_1, \cdots, A_k \Subset D$ satisfying I_1, I_2 and I_3 and $a_1, \cdots, a_k \in \mathcal{C}^2(\overline{A}_i, [\underline{a}, \overline{a}])$ such that*

$$a = \sum_{i=0}^{k} a_i \mathbf{1}_{A_i}, \tag{3.2}$$

where, again, a_0 was introduced in (3.1), $A_0 = \Omega \setminus \cup_{i=1}^{k} \overline{A}_i$, and $\mathbf{1}_{A_i}$ denotes the characteristic function of A_i.

Our main results in this chapter can be summarized as follows. A spherical acoustic wave is generated at y outside Ω. Its propagation inside the medium Ω changes the optical absorption distribution. Due to the acoustic wave, any point $x \in \Omega$ moves to its new position $x + v^\eta_{y,r}(x)$, where $v^\eta_{y,r}$ is defined by (3.16) with r being the radius of the spherical wave impulsion. By linearization, the displacement field is approximately $v^\eta_{y,r}$ as the thickness η of the acoustic wavefront goes to zero. Hence, the optical absorption of the medium changed by the propagation of the acoustic wave is approximately $a_*(x + v^\eta_{y,r})$, up to an error of order η.

Using cross-correlations between the outgoing light intensities in the medium changed by the propagation of the acoustic wave and those of in the unperturbed one, we get the data $M_\eta(y, r)$ given by (3.20). In Propositions 3.3.2 and 3.3.3, we show that $M_\eta(y, r)$ converges in the sense of distributions to $M(y, r)$ as $\eta \to 0$. We refer to $M(y, r)$ as the ideal data. Making use of a weak Helmholtz decomposition, stated in Lemma 3.1.6, we relate in Theorem 3.4.1 the ideal data to the gradient of $\Phi_*^2 \nabla a_*$. Since a_* is piecewise smooth, ∇a_* can be defined only in the sense of distributions. Technical arguments and quite delicate estimates are needed in order to establish the fact that the gradient part of $\Phi_*^2 \nabla a_*$ can be obtained from the cross-correlation measurements using the inverse spherical Radon transform. Based on this, we propose an optimal control approach for reconstructing the values of a_* inside the inclusions. For doing so, we first detect the support of $a_* - a_0$ as the support of the gradient part of the data $\Phi_*^2 \nabla a_*$. In fact, Lemma 3.1.6 shows that the support of the data yields the support of the inclusions. Their boundaries are detected as the support of the discontinuities in the data. Proposition 3.5.1 provides a Lipschitz stability result for reconstructing piecewise constant optical absorption. In contrast with the recent results in [2, 35, 36], Proposition 3.5.1 uses only one measurement but the supports of the inclusions are known. Minimizing the discrepancy functional (3.37) we obtain the background constant values of the optical absorption inside the inclusions. Next, in order to recover spatial variations of a_* inside the inclusions, we minimize the discrepancy between the linear forms $F[a]$ and $\Delta\psi$ given by (3.40) and (3.47), respectively. We prove in Theorem 3.5.3 that the Fréchet derivative of the nonlinear discrepancy functional is well-defined and establish useful estimates as well. We introduce an iterative scheme of Landweber-type for minimizing the discrepancy functional and prove in Theorem 3.5.5 its convergence provided that the optical absorption coefficient is in the set K defined by (3.38).

3.1 Preliminaries

3.1.1 Basic properties

We first recall the following results from Chapter 2.

Proposition 3.1.1 (weak comparison principle) *Let $a \in L^\infty(\Omega)$ be a nonnegative function and assume that $\Phi \in H^1(\Omega)$ satisfies*

$$\begin{cases} -\Delta\Phi + a\Phi \geq 0 & \text{in } \Omega, \\ l\partial_\nu\Phi + \Phi \geq 0 & \text{on } \partial\Omega. \end{cases} \tag{3.3}$$

We have $\Phi \geq 0$ a.e. in Ω.

Lemma 3.1.2 (Lemma 2.3.1 in Chapter 2) *Let D be as in (3.1) and assume that $g \in H^{1/2}(\partial\Omega)$ is nonnegative and not identically zero. There exist two positive constants λ and Λ such that for all $a \in (\mathcal{A})$, the solution Φ of*

$$\begin{cases} -\triangle\Phi + a\Phi = 0 & \text{in } \Omega, \\ l\partial_\nu\Phi + \Phi = g & \text{on } \partial\Omega, \end{cases} \tag{3.4}$$

satisfies

$$\lambda \leq \Phi \leq \Lambda \quad \text{in } D. \tag{3.5}$$

Lemma 3.1.3 (Lemma 2.3.2 in Chapter 2) *Let T be the map that sends $a \in (\mathcal{A})$ into the unique solution of (3.4). Then, T is Fréchet differentiable. Its derivative at a is given by*

$$DT[a](h) = \Phi, \tag{3.6}$$

for $h \in L^\infty(\Omega)$, where Φ solves

$$\begin{cases} -\Delta\Phi + a\Phi = -hT[a] & \text{in } \Omega, \\ l\partial_\nu\Phi + \Phi = 0 & \text{on } \partial\Omega. \end{cases} \tag{3.7}$$

Moreover, $DT[a]$ can be continuously extended to $L^2(\Omega)$ by the same formula given in (3.6) and (3.7) with

$$\|DT[a]\|_{\mathcal{L}(L^2(\Omega),H^1(\Omega))} \leq C\Lambda, \tag{3.8}$$

where Λ is defined in Lemma 3.1.2 and $\mathcal{L}(L^2(\Omega), H^1(\Omega))$ is the set of bounded linear operators from $L^2(\Omega)$ into $H^1(\Omega)$.

The following lemma will be helpful to prove the uniqueness of the constructed coefficient. We refer to Appendix 3.6.1 for its proof.

Lemma 3.1.4 *Let Ω' be the union of several subdomains of Ω such that $\Omega \setminus \Omega'$ is path connected. If ϕ is a bounded solution to*

$$\begin{cases} -\Delta\phi + c\phi = 0 & \text{in } \Omega \setminus \Omega', \\ l\partial_\nu\phi + \phi = 0 & \text{on } \partial\Omega, \end{cases} \tag{3.9}$$

for some nonnegative constant c and $\partial_\nu\phi \equiv 0$ on $\partial\Omega$, then $\phi \equiv 0$ in $\Omega \setminus \Omega'$.

Corollary 3.1.5 *Let $A_0, A_1, \cdots, A_k$ be as in Definition 3.0.1 and let $a \in (\mathcal{A})$ be defined relative to these sets. Denote by Φ_j, $j = 1, \cdots, k$, the solution of*

$$\begin{cases} -\Delta\Phi_j + a\Phi_j &= \mathbf{1}_{A_j}\Phi \quad \text{in } \Omega, \\ l\partial_\nu\Phi_j + \Phi_j &= 0 \qquad \text{on } \partial\Omega \end{cases}$$

with Φ being the solution of (3.4). Then, the set $\{\partial_\nu\Phi_j|_{\partial\Omega}\}$ is linearly independent.

Proof. Define

$$\Phi = \sum_{j=1}^{k} \alpha_j \Phi_j \quad \text{in } \Omega,$$

for some $\alpha_1, \cdots, \alpha_k \in \mathbb{R}$, and assume that $\partial_\nu\Phi = 0$ on $\partial\Omega$. It is obvious that Φ is the solution of

$$\begin{cases} -\Delta\Phi + a\Phi &= \displaystyle\sum_{j=1}^{k} \alpha_j \mathbf{1}_{A_j}\Phi \quad \text{in } \Omega, \\ l\partial_\nu\Phi + \Phi &= 0 \qquad\qquad \text{on } \partial\Omega, \end{cases}$$

and, hence, satisfies (3.9) with $c = a_0$ and $\Omega' = \cup_{i=1}^{k} A_i$. Thus, by Lemma 3.1.4, $\Phi \equiv 0$ in A_0. On the other hand, for each $i \in \{1, \cdots, k\}$, Φ solves

$$\begin{cases} -\Delta\Phi + a_i\Phi &= \alpha_i \mathbf{1}_{A_i}\Phi \quad \text{in } A_i, \\ \Phi &= 0 \qquad \text{on } \partial A_i. \end{cases}$$

We can now apply the strong comparison principle (see, for instance, Lemma 3.1 in [82]) and the Hopf lemma to see that $\partial_\nu\Phi \neq 0$ on ∂A_i. This contradicts to the fact that $\Phi \equiv 0$ in A_0. □

3.1.2 Helmholtz decomposition in the sense of distributions

The Helmholtz decomposition plays a crucial role in Chapter 2 when we established a differential coupling system for a, where a was supposed to be in $\mathcal{C}^2(\overline{\Omega})$. Fortunately, when a is no longer smooth but $\Phi^2\nabla a$ belongs to $(H^1(\Omega)^d)^* \subset H^{-1}(\Omega)^d$ for all $\Phi \in \mathcal{C}^1(\Omega)$, a corresponding Helmholtz decomposition remains true. Note that for all $a \in (\mathcal{A})$ and $\Phi \in \mathcal{C}^1(\Omega)$, $\Phi^2\nabla a \in (H^1(\Omega)^d)^*$ in the sense that

$$\begin{aligned} \langle \Phi^2\nabla a, v\rangle_{(H^1(\Omega)^d)^*, H^1(\Omega)^d} &= \langle \Phi^2\nabla(a - a_0), v\rangle_{(H^1(\Omega)^d)^*, H^1(\Omega)^d} \\ &= -\int_D (a - a_0)\nabla\cdot(\Phi^2 v)\, dx. \end{aligned} \tag{3.10}$$

The domain of the integral above is written as D instead of Ω because $a - a_0 = 0$ in $\Omega \setminus D$, where D is introduced in (3.1). By the same reason, we do not require the test functions to vanish on the boundary $\partial\Omega$. The last equation in (3.10) suggests that it might be sufficient to impose $a \in \mathcal{C}^1(\overline{A}_i)$, instead of $\mathcal{C}^2(\overline{A}_i)$, $i = 1, \cdots, k$, as in Definition 3.0.1. However, we need the differentiability of a up to second order in each inclusion for some later regularity and estimation purposes.

The following result holds.

Lemma 3.1.6 *For any U in $H^2(\Omega)^d$ there exist $\psi \in L^2(\Omega)$ and $\Psi \in H^2(\Omega)^d$ such that*

$$U = \nabla\psi + \Psi$$

with $\nabla \cdot \Psi = 0$. In particular, if $U = \Phi^2\nabla a$ for some $a \in \mathcal{A}$ then ψ is continuous and discontinuous at the point where a is, respectively.

Proof. Letting $U = (U_1, \cdots, U_d) \in H^{-1}(\Omega)^d$, we denote by $u = (u_1, \cdots, u_d)$ the solution of

$$\begin{cases} -\Delta u &= U \quad \text{in } \Omega, \\ u &= 0 \quad \text{on } \partial\Omega. \end{cases} \tag{3.11}$$

The vector $u \in H_0^1(\Omega)^d$ is actually the Riesz representation of U in $H_0^1(\Omega)^d$. Applying the classical Helmholtz decomposition for u (see, for instance, [57]), we can find $f \in H^1(\Omega)$ and $G \in H(\text{curl}, \Omega) := \{w \in L^2(\Omega)^d : \nabla \times w \in L^2(\Omega)^d\}$ such that

$$u = \nabla f + \nabla \times G. \tag{3.12}$$

Here, $\nabla \cdot G = 0$ inside Ω and

$$G \times \nu = 0 \quad \text{on } \partial\Omega. \tag{3.13}$$

Moreover, f is a solution of

$$\begin{cases} \Delta f &= \nabla \cdot u \quad \text{in } \Omega, \\ \partial_\nu f &= 0 \qquad \text{on } \partial\Omega. \end{cases} \tag{3.14}$$

Since u belongs to $H^1(\Omega)^d$, $\nabla \cdot u \in L^2(\Omega)$. By standard regularity results, we see that $f \in H^2(\Omega)$.

In view of (3.11), taking the Laplacian of (3.12) yields

$$U = \nabla\psi + \Psi,$$

in the sense of distributions, where $\psi = -\Delta f \in L^2(\Omega)$ and Ψ is divergence free.

We next prove the second statement of the lemma in which $U = \Phi^2\nabla a$ for some $a \in (\mathcal{A})$. The main tools we use here are the H^2- and $\mathcal{C}^1$-regularity results. Fix $j \in \{1, \cdots, d\}$ and $i \in \{0, \cdots, k\}$. Denote by u_j the jth component of the vector u, defined in (3.11). Since $u_j \in H_0^1(\Omega)$, it belongs to $H^1(A_i)$. The function u_j solves

$$-\Delta u_j = \Phi^2 \partial_{x_j} a, \tag{3.15}$$

in A_i. Applying Theorem 8.8 in [60], we see that u_j is in $H^2(A_i')$ for all $A_i' \Subset A_i$. Hence, differentiating (3.15) gives

$$-\Delta \partial_{x_l} u_j = \partial_{x_l}(\Phi^2 \partial_{x_j} a)$$

in A_i' for all $l = 1, \cdots, d$. Since $\partial_{x_l} u_j \in H^1(A_i')$ and $\partial_{x_l}(\Phi^2\partial_{x_j} a) \in L^2(A_i')$, we can apply the $\mathcal{C}^1$-regularity result in [76] to see that $\partial_{x_l} u_j$ is in $\mathcal{C}^1(A_i'')$ for all $A_i'' \Subset A_i'$. This implies $u_j \in \mathcal{C}^2(A_i)$. Considering the differential equation in (3.14) in each inclusion and following the same regularity process, we see that $f \in \mathcal{C}^2(A_i)$. Hence $\psi = -\Delta f$ is continuous in A_i, which is also the set of continuous points of a. On the other hand, since $U = \Phi^2\nabla a$ involves Dirac distributions supported in $\cup_i \partial A_i$, $\nabla \cdot u$ is not continuous across $\cup_i \partial A_i$, neither is ψ. □

3.2 The set of measurements

In this section, we describe the set of data obtained by the acousto-optic process introduced in Chapter 2. The basic idea in achieving a resolution enhancement in imaging the optical absorption distribution is as follows. We generate a spherical acoustic wave inside the medium. The propagation of the acoustic wave changes the absorption parameter of the medium. During the propagation of the wave we measure the light intensity on $\partial\Omega$. The aim is now to reconstruct the optical absorption coefficient from such set of measurements.

Let $a \in (\mathcal{A})$ represent the true coefficient a_*. Let S^{d-1} be the unit sphere in $\mathbb{R}^d$. Let $\mu > 0$ and let $S_\mu = \mu S^{d-1}$, the sphere of radius μ and center 0, be such that Ω stays inside S_μ. We perturb the optical domain Ω by spherical acoustic waves generated at point sources $y \in S_\mu$. Let $r \in [r_0, R]$ be the radius of the spherical wave impulsion, where r_0 and R are the minimum and maximum radii so that the spherical waves generated at point sources on S_μ can intersect Ω. Let $\eta \ll 1$ be the acoustic impulsion typical length representing the thickness of the wavefront. Let the position function P be defined by

$$P : x \mapsto x + v^\eta_{y,r}(x), \quad x \in \Omega,$$

where

$$v^\eta_{y,r}(x) = \eta \frac{r_0}{r} w\left(\frac{r - |x-y|}{\eta}\right) \frac{x-y}{|x-y|}, \tag{3.16}$$

and w is a smooth function supported on $[-1,1]$ with $\|w\|_\infty = 1$. Here, $\| \|_\infty$ denotes $\| \|_{L^\infty(]-1,1[)}$.

In Chapter 1, we have shown that the displacement function at the point x caused by the short diverging spherical acoustic wave generated at y is given by

$$u^\eta_{y,r}(x) = P^{-1}(x) - x, \quad x \in \Omega. \tag{3.17}$$

Let C_0 be the cylinder $S_\mu \times (r_0, R)$. For each $(y,r) \in C_0$, $a_{u^\eta_{y,r}}(x)$ denotes $a(x + u^\eta_{y,r}(x))$ and $\Phi_{u^\eta_{y,r}}$ is the optical energy density in the displaced medium, which satisfies

$$\begin{cases} -\triangle \Phi_{u^\eta_{y,r}} + a_{u^\eta_{y,r}} \Phi_{u^\eta_{y,r}} = 0 \ \text{ in } \Omega, \\ \qquad l\partial_\nu \Phi_{u^\eta_{y,r}} + \Phi_{u^\eta_{y,r}} = g \ \text{ on } \partial\Omega. \end{cases} \tag{3.18}$$

Physically, the outgoing light intensities $\partial_\nu \Phi|_{\partial\Omega}$ and $\partial_\nu \Phi_{u^\eta_{y,r}}|_{\partial\Omega}$ are measured. We are thus able to assume the knowledge of the cross-correlation measurements:

$$\frac{1}{\eta^2} \int_{\partial\Omega} g(\partial_\nu \Phi_{u^\eta_{y,r}} - \partial_\nu \Phi) d\sigma, \qquad y \in S_\mu, r > 0. \tag{3.19}$$

Integration by parts shows that the quantity above is equal to

$$M_\eta(y,r) = \frac{1}{\eta^2} \int_\Omega (a_{u^\eta_{y,r}} - a) \Phi \Phi_{u^\eta_{y,r}} dx, \tag{3.20}$$

which is considered as our set of data. Here, the coefficient $1/\eta^2$ is put in front of the integral because both Φ and $\Phi_{u^\eta_{y,r}}$ are bounded (Lemma 3.1.2) and

$$\|a_{u^\eta_{y,r}} - a\|_{L^1(\Omega)} = O(\eta^2) \qquad \text{as } \eta \to 0^+, \tag{3.21}$$

provided that the following technical condition, named as $(\mathcal{H})$, is imposed: there exists $C > 0$ such that for any $y \in S_\mu$, $r > 0$, and $i = 1, \ldots, k$, we have

$$\sigma\big(\partial A_i \cap \Sigma_\eta(y, r)\big) \leq C\eta, \tag{3.22}$$

with

$$\Sigma_\eta(y, r) = \{z \in \mathbb{R}^d : r - \eta < |z - y| < r + \eta\}.$$

Condition $(\mathcal{H})$ ensures that the spheres centered on S_μ and the boundaries ∂A_i are not too close to be tangent. Let

$$V_\varepsilon(S) = \{x \in \mathbb{R}^d,\ \exists y \in S,\ |x - y| < \varepsilon\}, \tag{3.23}$$

for any smooth surface S of $\mathbb{R}^d$, and $\varepsilon > 0$. Since S is smooth, the volume of $V_\varepsilon(S)$ satisfies

$$|V_\varepsilon(S)| = 2\sigma(S)\varepsilon + O(\varepsilon^2).$$

Hence, condition $(\mathcal{H})$ guarantees that

$$|A_i \triangle P^{-1}(A_i)| + |A_i \triangle P(A_i)| \leq O(\eta^2), \tag{3.24}$$

where $\triangle$ denotes the symmetric area difference.

Fix now $(y, \eta) \in C_0$ and write

$$\begin{aligned} \left\|a_{u^\eta_{y,r}} - a\right\|_{L^1(\Omega)} &= \sum_{i=1}^n \int_{A_i \cup P^{-1}(A_i)} |a_{u^\eta_{y,r}} - a| dx \\ &= \sum_{i=1}^n \int_{A_i \cap P^{-1}(A_i)} |a_{u^\eta_{y,r}} - a| dx + \int_{A_i \triangle P^{-1}(A_i)} |a_{u^\eta_{y,r}} - a| dx. \end{aligned} \tag{3.25}$$

As $u^\eta_{y,r}$ is supported on $\Sigma_\eta(y, r)$ and $\left\|u^\eta_{y,r}\right\|_\infty = \eta$,

$$\begin{aligned} \int_{A_i \cap P^{-1}(A_i)} |a_{u^\eta_{y,r}} - a| dx &= \int_{\Sigma_\eta \cap A_i \cap P^{-1}(A_i)} |a_{u^\eta_{y,r}} - a| dx \\ &\leq \eta \left\|\nabla a_i\right\|_{L^\infty(A_i)} |\Sigma_\eta| \\ &\leq \left\|\nabla a_i\right\|_{L^\infty(A_i)} \sigma(S(0, R))\eta^2, \end{aligned}$$

where $\sigma(S(0, R))$ is the surface measure of the sphere of center O and radius R. The second integral in (3.25) is bounded by $O(\eta^2)$ because of (3.24) and the boundedness of a.

3.3 Asymptotic formula

Consider the open cylinder $C := S_\mu \times (0, R)$ with its standard product topology.

The construction of

$$\begin{aligned} M_\eta : C &\to \mathbb{R} \\ (y, r) &\mapsto \frac{1}{\eta^2} \int_\Omega (a_{u^\eta_{y,r}} - a) \Phi \Phi_{u^\eta_{y,r}} dx, \end{aligned}$$

has been described in this previous section. The knowledge of the function is obtained from those of g, $\partial_\nu \Phi$ and $\partial_\nu \Phi_{u^\eta_{y,r}}$ on $\partial\Omega$. In this section, we study the limit of M_η as $\eta \to 0^+$. This, together with a weak version of Helmholtz decomposition and the spherical Radon transform, will help us detect all inclusions.

Lemma 3.3.1 *For any $\eta > 0$, M_η is a continuous map on C.*

Proof. It is sufficient to consider only the case $r > r_0$ because $M_\eta(y,r) = 0$ for all $r \le r_0$ and $y \in S_\mu$. Fix $(y,r) \in S_\mu \times (r_0, R)$ and let $\{(y_n, r_n)\}_{n\ge1} \subset S_\mu \times (r_0, R)$ converge to (y,r). Noting that $a^\eta_{u_{y,r}}$ is continuous except on the measure zero set

$$\{x + u^\eta_{y,r}(x) : x \in \cup_{i=1}^n \partial A_i\},$$

we have

$$a(x + u^\eta_{y_n,r_n}(x)) \to a(x + u^\eta_{y,r}(x))$$

a.e. in Ω. On the other hand, since a is bounded,

$$|a(x + u^\eta_{y_n,r_n}(x)) - a(x + u^\eta_{y,r}(x))|^2$$

is uniformly bounded. Therefore, it follows by the Lebesgue dominated convergence theorem that

$$a_{u^\eta_{y_n,r_n}} \to a_{u^\eta_{y,r}} \qquad \text{in } L^2(\Omega)$$

as $n \to \infty$. This implies

$$\Phi_{u^\eta_{y_n,r_n}} \to \Phi_{u^\eta_{y,r}}$$

in both $H^1(\Omega)$ and $L^4(\Omega)$. Note that the L^4 convergence above is valid because d is either 2 or 3. A direct calculation yields

$$\begin{aligned}
&|\eta^2(M_\eta(y_n,r_n) - M_\eta(y,r))| \\
&\quad= \left|\int_\Omega [(a_{u^\eta_{y_n,r_n}} - a)\Phi\Phi_{u^\eta_{y_n,r_n}} - (a_{u^\eta_{y,r}} - a)\Phi\Phi_{u^\eta_{y,r}}]dx\right| \\
&\quad\le \int_\Omega |a_{u^\eta_{y_n,r_n}} - a|\Phi|\Phi_{u^\eta_{y_n,r_n}} - \Phi_{u^\eta_{y,r}}|dx + \int_\Omega |a_{u^\eta_{y_n,r_n}} - a_{u^\eta_{y,r}}|\Phi\Phi_{u^\eta_{y,r}}dx, \\
&\quad\le 2\overline{a}\|\Phi\|_{L^2(\Omega)}\|\Phi_{u^\eta_{y_n,r_n}} - \Phi_{u^\eta_{y,r}}\|_{L^2(\Omega)} \\
&\qquad\qquad + \|a_{u^\eta_{y_n,r_n}} - a_{u^\eta_{y,r}}\|_{L^2(\Omega)}\|\Phi\|_{L^4(\Omega)}\|\|\Phi_{u^\eta_{y,r}}\|_{L^4(\Omega)}.
\end{aligned}$$

The lemma follows. □

Lemma 3.3.1 guarantees that M_η is measurable. In the case that a is smooth, which has been studied in Chapters 1 and 2, $M_\eta(y,r) \approx \int_\Omega \nabla a \cdot u^\eta_{y,r}\Phi^2$ when η is small. However, when a is piecewise smooth, we need to establish a similar approximation in the weak sense. The following proposition holds. We refer to Appendix 3.6.2 for its proof.

Proposition 3.3.2 *Let $C = S_\mu \times (0,R)$. Let μ be such that $\Omega \Subset S_\mu$. For any $0 < \eta \ll 1$, define the continuous function*

$$\tilde{M}_\eta(y,r) = \frac{1}{\eta^2}\int_\Omega (a - a_0)\nabla\cdot(\Phi^2 v^\eta_{y,r})dx, \qquad (y,r) \in C, \tag{3.26}$$

where Φ is the solution of (3.4). Assume ($\mathcal{H}$) holds and, consequently, (3.24) is valid. Then there exists $c > 0$, independent of (y,r), such that

$$\left|M_\eta(y,r) - \tilde{M}_\eta(y,r)\right| \le c\eta, \quad \forall (y,r) \in C. \tag{3.27}$$

It follows from Proposition 3.3.2 that for each $(y,r) \in C$,

$$\lim_{\eta\to 0^+} M_\eta(y,r) = \lim_{\eta\to 0^+} \tilde{M}_\eta(y,r) := M_{y,r}. \tag{3.28}$$

We cannot expect that M is a smooth function on C because $u^\eta_{y,r}/\eta^2$, and hence $v^\eta_{y,r}/\eta^2$, converges to a distribution supported on the circle (or sphere) $S(y,r) = \{z : |z-y| = r\}$. The limit in (3.28) is understood as follows.

Let

$$G(C) = \left\{ f \in L^2(C) : \partial_r f \in L^2(C) \right\}$$

be a Hilbert space, endowed with the norm

$$\|\cdot\|_{G(C)} = \|\cdot\|_{L^2(C)} + \|\partial_r \cdot\|_{L^2(C)}.$$

Let γ be the (continuous) trace operator from C to $S_\mu \times \{0, R\}$ and denote

$$G_0(C) = \gamma^{-1}(0) = \{f \in G(C) : \gamma(f) = 0\}, \qquad G^{-1}(C) = G_0(C)^*,$$

where $G_0(C)^*$ is the dual of $G_0(C)$. We have the following relations

$$H^1_0(C) \subset G_0(C) \subset L^2(C), \qquad L^2(C) \subset G^{-1}(C) \subset H^{-1}(C).$$

Let $\|\ \|_1$ denote $\|\ \|_{L^1(]-1,1[)}$. The following is the main result of this section. It is a direct consequence of Proposition 3.3.2.

Proposition 3.3.3 *The function M_η converges to the ideal measurements M in $G^{-1}(C)$ as $\eta \to 0^+$ with*

$$\begin{aligned}&\langle M, \varphi\rangle_{(\mathcal{C}_0^\infty(C))^*, \mathcal{C}_0^\infty(C)} \\ &\quad = -r_0 \|w\|_1 \int_{S_\mu} \int_0^R \int_{S^{d-1}\cap\Omega_{y,r}} a(y+r\xi) \frac{\partial}{\partial r}\left(r^{d-2}\Phi^2(y+r\xi)\varphi(y,r)\right) d\xi dr dy, \end{aligned} \tag{3.29}$$

where

$$\Omega_{y,r} = \left\{ \frac{x-y}{r} : x \in \Omega \right\}.$$

Proof. For any φ in $G_0(C)$, we have

$$\begin{aligned}\left\langle \tilde{M}_\eta, \varphi \right\rangle &= -\int_{y\in S_\mu} \int_{r=0}^R \int_\Omega (a-a_0)(x) \nabla\cdot_x \left(\Phi^2(x) \frac{v^\eta_{y,r}(x)}{\eta^2} \varphi(y,r) \right) dx dr dy \\ &= -\int_{y\in S_\mu} \int_\Omega (a-a_0)(x) \nabla\cdot_x \left(\Phi^2(x) \int_{r=0}^R \frac{v^\eta_{y,r}(x)}{\eta^2} \varphi(y,r) dr \right) dx dy.\end{aligned}$$

Then by the change of variables $x = y + \rho\xi$ we get

$$\frac{v^\eta_{y,r}(x)}{\eta^2} = \frac{r_0}{r\eta} w\left(\frac{\rho - r}{\eta}\right)\xi.$$

Hence we can write

$$\left\langle \tilde{M}_\eta, \varphi \right\rangle = -$$
$$\int_{S_\mu} \int_{S^{d-1}} \int_{\rho=0}^{R} (a-a_0)(y+\rho\xi) \frac{\partial}{\partial \rho} \left(\rho^{d-1} \Phi^2(y+\rho\xi) \int_{r=0}^{R} \frac{r_0}{r\eta} w\left(\frac{\rho-r}{\eta}\right) \varphi(y,r) dr \right) d\rho d\xi dy$$

Since

$$\frac{1}{\eta} w\left(\frac{\rho-r}{\eta}\right) \overset{\eta\to 0}{\longrightarrow} \|w\|_1 \delta_\rho,$$

we deduce that

$$\int_{r=0}^{R} \frac{r_0}{r\eta} w\left(\frac{\rho-r}{\eta}\right) \varphi(y,r) dr \overset{\eta\to 0}{\longrightarrow} \frac{\|w\|_1 r_0}{\rho} \varphi(y,\rho),$$

and then

$$\left\langle \tilde{M}_\eta, \varphi \right\rangle \overset{\eta\to 0}{\longrightarrow}$$
$$- \|w\|_1 r_0 \int_{S_\mu} \int_{\rho=0}^{R} \int_{S^{d-1}} a(y+\rho\xi) \frac{\partial}{\partial \rho} \left(\rho^{d-2} \Phi^2(y+\rho\xi) \varphi(y,\rho) \right) d\rho d\xi dy,$$

as desired. □

3.4 Detecting the inclusions

Using the fact that $\Phi^2 \nabla a \in (H^1(\Omega)^d)^* \subset H^2(\Omega)^d$, we can employ Lemma 3.1.6 to write that

$$\Phi^2 \nabla a = \nabla \psi + \Psi, \tag{3.30}$$

where Ψ is a divergence free field and $\psi \in L^2(\Omega)$. Since both $\Phi^2 \nabla a$ and $\nabla \psi$ are in $(H^1(\Omega)^d)^*$, so is Ψ. Moreover, it follows from the usual integration by parts formula and the boundary condition (3.13) that

$$\langle \Psi, \nabla v \rangle = 0, \qquad \forall\, v \in \mathcal{C}^\infty(\overline{\Omega}). \tag{3.31}$$

For a distribution $f \in (\mathcal{C}_0^\infty(\Omega))^*$, we define its spherical Radon transform $\mathcal{R}[f]$ in the sense of distributions by

$$\langle \mathcal{R}[f], \varphi \rangle_{(\mathcal{C}_0^\infty(C))^*, \mathcal{C}_0^\infty(C)} = \langle f, \mathcal{R}^*[\varphi] \rangle_{(\mathcal{C}_0^\infty(\Omega))^*, \mathcal{C}_0^\infty(\Omega)},$$

where

$$\mathcal{R}^*[\varphi](x) = \int_C \varphi(y, |x-y|) dy \quad \text{for } \varphi \in \mathcal{C}_0^\infty(C).$$

We have the following result.

Theorem 3.4.1 *The spherical Radon transform $\mathcal{R}[\psi]$ of ψ satisfies the equation*

$$M = r_0 \|w\|_1 r^{d-2} \frac{\partial \mathcal{R}[\psi]}{\partial r} \tag{3.32}$$

in the sense of distributions.

Proof. Let $\varphi \in \mathcal{C}_0^\infty(C)$, and for a fixed $y \in S_\mu$ we define

$$F_y(x) = \varphi(y, |x-y|)\frac{x-y}{|x-y|^2} \qquad x \in \Omega.$$

For any $y \in S_\mu$, the vector F_y is in $H^1(\Omega)^d$ because $|x-y| \geq r_0$. Equation (3.30) yields

$$\langle \Phi^2 \nabla a, F_y \rangle = \langle \nabla \psi, F_y \rangle + \langle \Psi, F_y \rangle$$

and since F_y is the gradient of the function given by

$$x \longmapsto \int_0^{|x-y|} \frac{\varphi(y,\rho)}{\rho} d\rho,$$

it follows from (3.31) that $\langle \Psi, F_y \rangle = 0$. Here, $\langle\ ,\ \rangle$ denotes the duality pair between $H^1(\Omega)^d$ and $(H^1(\Omega)^d)^*$. Therefore,

$$\langle \Phi^2 \nabla a, F_y \rangle = \langle \nabla \psi, F_y \rangle. \tag{3.33}$$

A simple calculation shows

$$\begin{aligned} \langle \Phi^2 \nabla a, F_y \rangle &= \int_\Omega a \nabla \cdot (\Phi^2 F_y) dx \\ &= \int_0^R \int_{S^{d-1} \cap \Omega_{y,r}} \left[a \nabla \cdot (\Phi^2 F_y) \right](y + r\xi) r^{d-1} d\xi dr, \end{aligned}$$

and hence,

$$\langle \Phi^2 \nabla a, F_y \rangle = \int_0^R \int_{S^{d-1} \cap \Omega_{y,r}} a(y+r\xi) \frac{\partial}{\partial r} \left[\Phi^2(y+r\xi) \varphi(y,r) r^{d-2} \right] d\xi dr. \tag{3.34}$$

Combining (3.29), (3.33), and (3.34) implies

$$\begin{aligned} \langle M, \Phi \rangle &= \|w\|_{L^1(\Omega)} \int_{S_\mu} \langle \nabla \psi, F_y \rangle dy \\ &= -\|w\|_{L^1(\Omega)} \int_{S_\mu} \int_\Omega \psi \nabla \cdot (F_y) dx dy \\ &= -\|w\|_{L^1(\Omega)} \int_{S_\mu} \int_0^R \int_{S^{d-1} \cap \Omega_{y,r}} \left[\psi \nabla \cdot (F_y) \right](y + r\xi) r^{d-1} d\xi dr dy \\ &= -\|w\|_{L^1(\Omega)} \int_{S_\mu} \int_0^R \int_{S^{d-1} \cap \Omega_{y,r}} \psi(y+r\xi) \frac{\partial}{\partial r} \left[\varphi(y,r) r^{d-2} \right] d\xi dr dy \\ &= -r_0 \|w\|_{L^1(\Omega)} \int_{S_\mu} \int_0^R \mathcal{R}[\psi](y,r) \frac{\partial}{\partial r} \left[\varphi(y,r) r^{d-2} \right] dr dy \\ &= r_0 \|w\|_{L^1(\Omega)} \langle r^{d-2} \frac{\partial \mathcal{R}[\psi]}{\partial r}, \varphi \rangle, \end{aligned}$$

and the proof is complete. □

Remark 3.4.2 *Theorem 3.4.1 provides the knowledge of the derivative of the spherical Radon transform of ψ (see Appendix 3.6.3 for the reconstruction of $\mathcal{R}[\psi]$ from its derivative). Note that the function ψ itself can be reconstructed in a stable way from $\mathcal{R}[\psi]$ using an inversion (filtered) retroprojection formula for the spherical Radon transform. From this, all inclusions are detected by the second statement in Lemma 3.1.6, noticing that ∂A_i is the set of discontinuous points of ψ.*

3.5 A reconstruction algorithm of the true coefficient

With all inclusions $A_1, A_2, \cdots, A_k$ in hand, we are able to find an initial guess for a_* using the unique continuation property (Lemma 3.1.4) and then employ a Landweber type iteration to reconstruct a_*. As an initial guess, we reconstruct constant values inside each inclusion by minimizing the discrepancy between computed and measured boundary data. We prove a Lipschitz stability result for the reconstruction of the optical absorption coefficient in the class of piecewise constant distributions provided that the support of the inclusions is known.

3.5.1 The data of boundary measurements and an initial guess

Define

$$\mathcal{S} = \left\{ \sum_{i=0}^{k} \alpha_i \mathbf{1}_{A_i} : \alpha_0 = a_0 \text{ and } \alpha_1, \cdots, \alpha_k \in [\underline{a}, \overline{a}] \right\}.$$

Let a_1 and a_2 be in $\mathcal{S}$. Their difference can be written as

$$a_2 - a_1 = \sum_{i=1}^{k} h_i \mathbf{1}_{A_i},$$

for some $h = (h_1, \cdots, h_k) \in B = [\underline{a} - \overline{a}, \overline{a} - \underline{a}]^k$. Note that B can be considered as a closed ball of $\mathbb{R}^k$ with respect to the $\infty-$norm of $\mathbb{R}^k$ given by

$$|h| = \max\{|h_1|, \cdots, |h_k|\}.$$

The compactness of B plays an important role in our analysis. Suppose that $l \neq 0$. Denote by Φ_1 and Φ_2 the optical energy density functions that correspond to a_1 and a_2. The function $\phi = \Phi_1 - \Phi_2$ solves

$$\begin{cases} -\Delta\phi + a_1\phi &= \displaystyle\sum_{i=1}^{k} h_i \mathbf{1}_{A_i} \Phi_2 \quad \text{in } \Omega, \\ l\partial_\nu\phi + \phi &= 0 \qquad\qquad\qquad\quad \text{on } \partial\Omega. \end{cases} \tag{3.35}$$

Using ϕ as the test function in the variational form of (3.35), we see that

$$\int_\Omega (|\nabla\phi|^2 + \underline{a}\phi^2) dx + l \int_{\partial\Omega} (\partial_\nu\phi)^2 \, d\sigma \leq |h| \Lambda \int_\Omega |\phi| dx,$$

where Λ is defined in Lemma 3.1.2. This implies

$$\|\partial_\nu\phi\|_{L^2(\partial\Omega)} \leq C|h|$$

and, therefore, the continuity of the map $h \mapsto \partial_\nu\phi|_{\partial\Omega}$. Since the map $h \in \partial_{\mathbb{R}^k} B \mapsto \|\partial_\nu\phi\|_{L^2(\partial\Omega)}$ is continuous and nonzero (due to Corollary 3.1.5), we can employ the compactness of $\partial_{\mathbb{R}^k} B$ in $\mathbb{R}^k$ to see that

$$c(a_1) = \min_{h \in \partial_{\mathbb{R}^k} B} \|\partial_\nu\phi\|_{L^2(\partial\Omega)} > 0.$$

Identifying $\mathcal{S}$ with a compact subset of $\mathbb{R}^k$, we can conclude that

$$c = \inf_{a_1 \in \mathcal{S}} c(a_1) > 0.$$

Properly scaling the inequality

$$\|\partial_\nu \phi\|_{L^2(\partial\Omega)} \geq c$$

for all $h \in \partial_{\mathbb{R}^k} B$, we arrive at the following Lipschitz stability result using only one measurement. Note here that the support of the inclusions is known and only the value of the optical absorption coefficient inside each inclusion is to be determined.

Proposition 3.5.1 *There exists $c > 0$ such that for all $a_1, a_2 \in \mathcal{S}$,*

$$\|\partial_\nu \Phi_1 - \partial_\nu \Phi_2\|_{L^2(\partial\Omega)} \geq c\|a_1 - a_2\|_{L^\infty(\Omega)}, \tag{3.36}$$

where Φ_1 and Φ_2 are the solutions of (3.4) with a replaced by a_1 and a_2, respectively.

Remark 3.5.2 *Inequality (3.36) guarantees the uniqueness of the reconstruction for $a_* \in \mathcal{S}$ if $\partial_\nu \Phi_*|_{\partial\Omega}$ is considered as the data given. It, moreover, implies the stability in the sense that small noise does not cause large error.*

Proposition 3.5.1 suggests us to minimize the quadratic misfit functional:

$$J(a) = \frac{1}{2}\|\partial_\nu \Phi - \partial_\nu \Phi_*\|^2_{L^2(\partial\Omega)}, \tag{3.37}$$

where a varies in $\mathcal{S}$ and Φ_* is the true optical energy density. This is possible since $\mathcal{S}$ is identical with a compact subset of $\mathbb{R}^k$. By (3.36), the function $a_I = \operatorname{argmin} J$ is close to a_* provided that a_* is a perturbation of a constant on each inclusion A_i. Therefore, a_I can be considered as the background constant optical absorption distribution in the inclusions. For simplicity, we propose the following exhaustion method: for each fine partition P of the interval $[\underline{a}, \overline{a}]$, try all values of α_i such that α_i equals each element of P, and finally choose the $k-$tuple $(\alpha_1, \cdots, \alpha_k)$ that gives the smallest $\|\partial_\nu \Phi - \partial_\nu \Phi_*\|_{L^2(\partial\Omega)}$.

3.5.2 Internal data map and its differentiability

Recall that the true optical absorption coefficient a_* is of the form (3.2). Suppose that $a_* = (a_1^*, \cdots, a_k^*)$ belongs to

$$K := \{a \in \prod_{j=1}^k W_0^{1,4}(A_j) : \underline{a} \leq a_i \leq \overline{a} \text{ and } \|\nabla a_i\|_{L^4(A_j)} \leq \theta, i = 1, \cdots, k\}, \tag{3.38}$$

where θ will be determined later in (3.42). It is obvious that K is closed and convex in H where $H = \prod_{j=1}^k H_0^1(A_j)$ is a Hilbert space with the usual inner product

$$\langle u, v\rangle_H = \sum_{i=1}^k \int_{A_j} \nabla u_j \cdot \nabla v_j dx$$

for all $u = (u_1, \cdots, u_k)$ and $v = (v_1, \cdots, v_k)$ in H.

Now, let the map $F : K \to H^*$ with H^* being the dual of H be defined as follows. For all $(a_1, \cdots, a_k) \in K$, let

$$a = \sum_{i=0}^k a_i \mathbf{1}_{A_i}, \tag{3.39}$$

and

$$F[a](v) = \sum_{j=1}^{k} \int_{A_j} T[a]^2 \nabla a_j \cdot \nabla v \quad \text{for all } v \in H, \tag{3.40}$$

where $T[a]$ was defined in Lemma 3.1.3. Note that from the acoustic-optic measurements we can construct $F[a_*]$, where a_* is the true optical absorption coefficient. We call F the *internal data* map.

Theorem 3.5.3 *The map F is Fréchet differentiable in K and*

$$DF[a](h, v) = \sum_{i=1}^{k} \int_{A_i} (2T[a]DT[a](h)\nabla a_i + T[a]^2 \nabla h_i)\nabla v_i dx \tag{3.41}$$

for all $a = (a_1, \cdots, a_k) \in K$, $h = (h_1, \cdots, h_k) \in \prod_{j=1}^{k} W_0^{1,4}(A_j) \cap L^\infty(A_j)$ and $v = (v_1, \cdots, v_k) \in H$. Assume further

$$0 < \theta < \frac{C_{\Omega'}\lambda^2}{\Lambda^2}, \tag{3.42}$$

where $\Omega' = \cup_{j=1}^{k} A_j$ and $C_{\Omega'}$ is the norm of the embedding map of $H^1(\Omega')$ into $L^4(\Omega')$, multiplied with the constant in (3.8). Then, $DF[a]$ is well-defined on H and there exists a positive constant C such that for all $h \in H$,

$$\|DF[a](h)\|_{H^*} \geq C\|h\|_H. \tag{3.43}$$

Here, $DF[a](h) : v \in H \mapsto DF[a](h, v)$.

Remark 3.5.4 *The term $DT[a](h)$ in (3.41) is understood as $DT[a]$ acting on the function that is equal to 0 in A_0 and to h_j in A_j, $j = 1, \cdots, k$.*

Proof of Theorem 3.5.3. The Fréchet differentiability of F and the expression (3.41) of DF can be deduced from Lemma 3.1.3 and the standard rules in differentiation. We only prove (3.43). In fact, for all $h \in H$,

$$\begin{aligned} DF[a](h,h) &= \sum_{j=1}^{k} \int_{A_j} \left(T[a]^2|\nabla h_j|^2 + 2T[a]DT[a](h)\nabla a_j \nabla h_j\right) dx \\ &\geq \sum_{j=1}^{k} \left[\int_{A_j} \left(T[a]^2|\nabla h_j|^2\right) dx - \int_{A_j} |2T[a]DT[a](h)\nabla a_j \nabla h_j| dx\right] \\ &\geq \lambda^2 \left(\|h\|_H^2 - \sum_{j=1}^{k} \frac{\Lambda}{\lambda^2} \|DT[a](h)\|_{L^4(A_j)} \|\nabla a_j\|_{L^4(A_j)} \|\nabla h_j\|_{L^2(A_j)}\right). \end{aligned}$$

It follows from the continuous embedding of $H^1(\Omega')$ into $L^4(\Omega')$ and (3.8) that

$$DF[a](h,h) \geq \lambda^2 \left(1 - \frac{C_{\Omega'}\Lambda^2\theta}{\lambda^2}\right) \|h\|_H^2.$$

Therefore, the bilinear form $DF[a] : (h, v) \in H \times H \mapsto DF[a](h, v)$ is coercive, which shows that inequality (3.43) holds true with $C = \lambda^2(1 - \frac{C_{\Omega'}\Lambda^2\theta}{\lambda^2})$. □

We now make use of Theorem 3.5.3 in order to prove a local Landweber condition which guarantees the convergence of the reconstruction algorithm [64].

Let a and a' be in K. We can find $t \in [0,1]$ such that

$$\|F[a] - F[a']\|_{H^*} = \|DF[ta + (1-t)a'](a-a')\|_{H^*} \geq C\|a - a'\|_H \tag{3.44}$$

by (3.43). Hence, if $\|a-a'\|_H$ is small enough, then F satisfies the local Landweber condition:

$$\|F[a] - F[a'] - DF[a](a-a')\|_{H^*} \leq \eta\|F[a] - F[a']\|_{H^*} \tag{3.45}$$

for some $\eta < \frac{1}{2}$.

3.5.3 Landweber iteration

Going back to equation (3.30), we have

$$\nabla \cdot \Phi^2 \nabla a = \Delta\psi \tag{3.46}$$

in the sense of distributions. However, the equation above can be understood in the classical sense in each inclusion A_i. This observation plays an important role in reconstructing the true coefficient from the initial guess given in Subsection 3.5.1.

Considering $\Delta\psi$ as an element of H^* defined by

$$-\Delta\psi(v) = \sum_{j=1}^{k} \int_{A_j} \nabla\psi \cdot \nabla v_j dx, \tag{3.47}$$

for all $v = (v_1, \cdots, v_k)$, we rewrite (3.46) as

$$F[a] = \Delta\psi. \tag{3.48}$$

Recalling that K is closed and convex in H, we can employ the classical Hilbert projection theorem to define the projection from H onto K as

$$P : H \ni h \mapsto \operatorname{argmin}\{\|h - a\|_H : a \in K\}. \tag{3.49}$$

It is not hard to verify that

$$\|P(h) - a\|_H \leq \|h - a\|_H \tag{3.50}$$

for all $a \in K$.

We next solve (3.48) using the Landweber method to minimize

$$I(a) = \frac{1}{2}\|F[a] - \Delta\psi\|^2_{H^*},$$

where a varies in K with the initial guess $a_I = (\alpha_1, \cdots, \alpha_k)$, obtained in Subsection 3.5.1. The corresponding guess for the coefficient is

$$a_I = \sum_{i=1}^{k} \alpha_i \mathbf{1}_{A_i}.$$

There is a gap if we minimize I by the classical Landweber sequence given by

$$\begin{aligned} a^{(0)} &= a_I, \\ a^{(n+1)} &= a^{(n)} - \mu DF[a^{(n)}]^*(F[a^{(n)}] - \Delta\psi) \end{aligned}$$

because $a^{(1)}$ may not belong to K and $F[a^{(1)}]$ is not well-defined. Motivated by (3.50), which implies $P(a^{(n)})$ is closer to a_* than $a^{(n)}$ is, we modify this formula as

$$a^{(n+1)} = P(a^{(n)}) - \mu DF[P(a^{(n)})]^*(F[P(a^{(n)})] - \Delta\psi) \tag{3.51}$$

with $\mu > 0$ being a relaxation parameter. We have the following convergence result.

Theorem 3.5.5 *Suppose that the true optical distribution a_* belongs to K and μ is sufficiently small. Let $a^{(n)}$ be defined by (3.51) with $a^{(0)}$ being the initial (piecewise constant) guess obtained as the minimizer of (3.37). Then the sequence $a^{(n)}$ converges in H to a_* as $n \to \infty$.*

Noting that F satisfies the local Landweber condition (see (3.45)), we can repeat the proof of Proposition 2.2 in [64] to see that

$$\|a^{(n+1)} - a_*\|_H^2 + (1 - 2\eta)\|F[P(a^{(n)}) - \Delta\psi]\|_{H^*}^2 \le \|P(a^{(n)}) - a_*\|_H^2.$$

This and (3.50) imply

$$\|P(a^{(n+1)}) - a_*\|_H^2 - \|P(a^{(n)}) - a_*\|_H^2 \le (2\eta - 1)\|F[P(a^{(n)}) - \Delta\psi]\|_{H^*}^2 \le 0. \tag{3.52}$$

It follows that

$$\sum_{i=1}^{\infty} \|F[P(a^{(n)})] - \Delta\psi\|_{H^*}^2 \le \frac{1}{1 - 2\eta}\|a_*\|_H^2,$$

and hence

$$F[P(a^{(n)})] \to \Delta\psi \text{ in } H^* \text{ as } n \to \infty. \tag{3.53}$$

On the other hand, we can see from (3.52) that the sequence $(P(a^{(n)}))_{n\ge1}$ is bounded in H. Assume that $P(a^{(n)})$ converges weakly to a' for some $a' \in H$. Since K is closed and convex, it is weakly closed and therefore $a' \in K$. Passing to a subsequence if necessary, this sequence converges to a' *a.e.* and also converges strongly to a' in $\prod_{j=1}^k L^2(A_j)$. So, $T[P(a^n)]$ converges to $T[a']$ in $H^1(\Omega)$ and hence in $L^4(\Omega)$. For all $v \in H$, we have

$$\begin{aligned} &\sum_{j=1}^{k} \int_{A_j} (T[P(a^{(n)})]^2 \nabla P(a^{(n)}) - T[a']^2 \nabla a')\nabla v dx \\ &= \sum_{j=1}^{k} \left[\int_{A_j} (T[P(a^{(n)})]^2 - T[a']^2)\nabla P(a^{(n)})\nabla v dx + \int_{A_j} T[a']^2(\nabla P(a^{(n)}) - \nabla a')\nabla v dx \right], \end{aligned}$$

which goes to 0 by the dominated convergence theorem and the weak convergence of $P(a^{(n)})$ to a' in H. We have obtained $F[a'] = \Delta\psi = F[a_*]$. Using (3.43) gives $a' = a_*$.

In summary, if the true coefficient a_* is a perturbation of a constant on each inclusion then the coefficient a_I obtained in Section 3.5.1 is quite closed to a_*. Moreover, the misfit between the initial guess a_I and the true distribution a_* can be properly corrected by the sequence in (3.51).

3.6 Appendix

3.6.1 Proof of Lemma 3.1.4

The boundedness of ϕ together with the assumption that $\phi \equiv 0$ on $\partial\Omega$ imply by standard regularity results that $\phi \in \mathcal{C}^1(\partial\Omega \cup \Omega \setminus \overline{\Omega}')$. Arguing similarly to Proposition 2.1.4 in Chapter 1, we see that $\phi \in \mathcal{C}^2(\Omega \setminus \overline{\Omega}')$. Define

$$\mathcal{U} = \{x \in \Omega \setminus \overline{\Omega}' : u(x) \neq 0\}.$$

The continuity of ϕ shows that $\mathcal{U}$ is open. Assume, on contrary, that $\mathcal{U}$ is nonempty.

Noting that $\mathcal{U}$ can be decomposed as the union of its connected open subsets. Denote by $\mathcal{O}$ the connected component of $\mathcal{U}$, which is closest to $\partial\Omega$. Without loss of generality, assume that $\phi > 0$ in $\mathcal{O}$. Let

$$\delta = \operatorname{dist}(\mathcal{O}, \partial\Omega).$$

The distance above is understood as the length of the shortest curve, contained in $\Omega \setminus \overline{\Omega}'$ and connecting $\overline{\mathcal{O}}$ and $\partial\Omega$.

In the case that $\delta = 0$, $\partial\mathcal{O}$ and $\partial\Omega$ have a common point x_0. Applying the Hopf lemma for the equation

$$\begin{cases} -\Delta\phi + c\phi &= 0 \quad \text{in } \mathcal{O}, \\ \phi &> 0 \quad \text{on } \partial\mathcal{O}, \end{cases}$$

gives $\partial_\nu\phi(x_0) < 0$, which is impossible.

When $\delta > 0$, it is easy to see that $\phi \equiv 0$ in a neighborhood of $\partial\Omega$. Assume that such a neighborhood and $\mathcal{O}$ have a common boundary point x_0. Noting that $\nabla\phi(x_0) = 0$, we can apply the Hopf lemma again to get the contradiction. □

3.6.2 Proof of Proposition 3.3.2

For simplicity, we write u and v when referring to $u^\eta_{y,r}$ and $v^\eta_{y,r}$, respectively. Using (3.24) and the same arguments when estimating $\|a_v - a\|_{L^1(\Omega)}$ in the previous section yields

$$\|a_u - a\|_{L^2(\Omega)} \leq O(\eta).$$

This, together with standard H^2-regularity results (see, for instance, [60, Theorems 8.8 and 8.12]) and the embedding of $H^2(\Omega)$ into $L^\infty(\Omega)$, gives

$$\|\Phi_v - \Phi\|_{L^\infty(\Omega)} \leq O(\eta).$$

Hence, it follows from (3.21) that

$$\begin{aligned} \left| \int_\Omega (a_v - a)\Phi\Phi_v dx - \int_\Omega (a_v - a)\Phi^2 dx \right| &\leq \int_\Omega \Phi |a_v - a||\Phi_v - \Phi| dx \\ &\leq \|\Phi\|_{L^\infty(\Omega)} \|a_v - a\|_{L^1(\Omega)} \|\Phi_v - \Phi\|_{L^\infty(\Omega)} \\ &\leq c\eta^3. \end{aligned} \tag{3.54}$$

The constant c depends only on $\overline{a} = \max a$ and $\underline{a} = \min a$, both of which are assumed to be known. The independence of c on $||\Phi||_{L^\infty(\Omega)}$ can be deduced from Lemma 3.1.2. Now, note that the second integral in the left hand side of (3.54) can be rewritten as

$$\begin{aligned}\int_\Omega (a_v - a)\Phi^2 dx &= \sum_{i=1}^n \int_{A_i \cup P(A_i)} (a_v - a)\Phi^2 dx \\ &= \sum_{i=1}^n \left[\int_{A_i \cap P(A_i)} (a_v - a)\Phi^2 dx + \int_{A_i \triangle P(A_i)} (a_v - a)\Phi^2 dx \right],\end{aligned}$$

and that the integral in (3.26) is equal to

$$\begin{aligned}\int_\Omega (a - a_0)\nabla \cdot (\Phi^2 v) dx &= \sum_{i=1}^n \int_{A_i} (a - a_0)\nabla \cdot (\Phi^2 v) dx \\ &= \sum_{i=1}^n \left[\int_{\partial A_i} (a_i - a_0)\Phi^2 v \cdot \nu_i d\sigma - \int_{A_i} \Phi^2 \nabla a \cdot v dx \right] \\ &= \sum_{i=1}^n \left[\int_{\partial A_i} (a_i - a_0)\Phi^2 v \cdot \nu_i d\sigma \right. \\ &\qquad \left. - \int_{A_i \cap P(A_i)} \Phi^2 \nabla a \cdot v dx - \int_{A_i \setminus P(A_i)} \Phi^2 \nabla a \cdot v dx \right].\end{aligned}$$

Therefore, we have

$$\begin{aligned}&\left| \int_\Omega (a_v - a)\Phi^2 dx - \int_\Omega (a - a_0)\nabla \cdot (\Phi^2 v) dx \right| \\ &\quad \leq \sum_{i=1}^n \left| \int_{A_i \cap P(A_i)} (a_v - a + \nabla a \cdot v)\Phi^2 dx \right| + \left| \int_{A_i \setminus P(A_i)} \Phi^2 \nabla a_i \cdot v dx \right| \\ &\qquad + \left| \int_{A_i \triangle P(A_i)} (a_v - a)\Phi^2 dx - \int_{\partial A_i} (a_i - a_0)\Phi^2 v \cdot \nu_i d\sigma \right|.\end{aligned}$$

Denote by α_i, β_i and γ_i the last three quantities in the inequality above. We need to prove that they all are bounded by $O(\eta^3)$ to complete the proof.

(i) Since for all $i = 1, \cdots, k$, $a_i \in \mathcal{C}^2(\overline{A}_i)$ and $\|D^2 a_i\|_{L^\infty(A_i)}$ are bounded by some known constants, we can find a constant c such that

$$\left| \int_{A_i \cap P(A_i)} (a_v - a - \nabla a \cdot u)\Phi^2 dx \right| \leq \|\Phi\|^2_{L^\infty(A_i)} \left\| D^2 a \right\|_{L^\infty(A_i)} \eta^2 |\Sigma_\eta| \leq c_1^i \eta^3.$$

On the other hand, using the classical substitution method in integration gives

$$\begin{aligned}
&\left|\int_{A_i\cap P(A_i)\cap\Sigma_\eta} \nabla a\cdot(u+v)\Phi^2 dx\right| \\
&\quad\le \left|\int_{S(y,r)} (\Phi^2\nabla a)(\xi)\cdot\int_{-\eta}^{\eta}(\mathbf{1}_{A_i}(u+v))\left((1+\frac{\rho}{r})\xi\right)d\rho d\xi\right| \\
&\qquad+\left|\int_{S(y,r)}\int_{-\eta}^{\eta}\left[(\Phi^2\nabla a)\left((1+\frac{\rho}{r})\xi\right)-(\Phi^2\nabla a)(\xi)\right].(\mathbf{1}_{A_i}(u+v))\left((1+\frac{\rho}{r})\xi\right)d\rho d\xi\right| \\
&\quad\le 0+2\eta^2\left\|\partial_r(\Phi^2\nabla a)\right\|_{L^\infty(A_i)}|\Sigma_\eta| \\
&\quad\le c\eta^3.
\end{aligned}$$

The quantity α_i is bounded from above by $O(\eta^3)$ because

$$\alpha_i\le\left|\int_{A_i\cap P(A_i)}(a_v-a-\nabla a\cdot u)\Phi^2dx\right|+\left|\int_{A_i\cap P(A_i)\cap\Sigma_\eta}\nabla a\cdot(u+v)\Phi^2dx\right|.$$

(ii) The fact that $\beta_i\le O(\eta^3)$ can be deduced from the boundedness of the integrand and (3.24).

(iii) The main point of the proof is the estimate of γ_i. In order to deal with the integral over $A_i\triangle P(A_i)$, we introduce a change of parametrization involving ∂A_i. Let us first define the set

$$E=\{(z,t)\in\partial A_i\times[0,\eta[,\ v(z)\neq 0,\ t<|v(z)|\}$$

and then the map

$$\begin{aligned}\chi: E&\longrightarrow A_i\triangle P(A_i)\\ (z,t)&\longmapsto z+t\tilde v(z),\end{aligned}$$

where $\tilde v(z)=v(z)/|v(z)|$. This map is well-defined for η small enough. For any $x\in A_i\triangle P(A_i)$, we call z the intersection between $[y,x]$ and ∂A_i. The whole segment $[z,z+v(z)]$ is included in $A_i\triangle P(A_i)$ and there exists a unique t such that $x=z+t\tilde v(z)$. Hence, this map is a bijection. We denote $T(z)$ the tangent plane to ∂A_i in z, in a basis adapted to the decomposition $\mathbb{R}^d=T(z)\oplus\mathbb{R}\tilde v(z)$, the derivative of χ take the form:

$$d\chi(z,t)=\begin{bmatrix}I_{d-1}+td\tilde v(z) & 0\\ * & 1\end{bmatrix}$$

and, as $\tilde v(z)=(z-y)/|z-y|$, the operator $d\tilde v(z)$ does not depend on η and $td\tilde v(z)=O(\eta)$ with a constant depending on r_0. Then,

$$\det(d\chi(z,t))=1+t\ \nabla\cdot(\tilde v)(z)+O(\eta^2)=1+O(\eta).$$

As $B(z)$ is not orthonormal, the differential volume written with the variables (z,t) depends on the angle between $\tilde v(z)$ and $\nu(z)$ called $\theta(z)$. This volume at the point $z+t\tilde v(z)$ is $(1+O(\eta))\cos(\theta(z))dtdz$. We denote by

$$(\partial A_i)^\pm=\{z\in\partial A_i,\ \pm\theta(z)>0\}$$

and write

$$\int_{P(A_i)\setminus A_i}(a_v-a)\Phi^2dx = \int_{(\partial A_i)^+}\int_0^{|v(z)|}(a_v-a_0)\Phi^2(z+t\tilde{v}(z))(1+O(\eta)) \times\cos(\theta(z))dtdz$$

and, as a_i and Φ are $\mathcal{C}^1(\overline{A}_i)$, we can write that for any $z\in(\partial A_i)^+$, and $t\in[0,|v(z)|]$,

$$|(a_v-a_0)\Phi^2(z+t\tilde{v}(z))-(a_i-a_0)\Phi^2(z)|\leq O(\eta).$$

Then,

$$\left|\int_0^{|v(z)|}(a_v-a_0)\Phi^2(z+t\tilde{v}(z))(1+O(\eta))dt-(a_i-a_0)\Phi^2(z)|v(z)|\right|\leq O(\eta^2).$$

Now, noticing that $\cos(\theta)|v(z)|=v(z)\cdot\nu(z)$ and that $\sigma((\partial A_i)^+\cap\Sigma_\eta)$, the surface measure of $(\partial A_i)^+\cap\Sigma_\eta$, is of order $O(\eta)$, we have

$$\left|\int_{P(A_i)\setminus A_i}(a_v-a)\Phi^2-\int_{(\partial A_i)^+}(a_i-a_0)\Phi^2v\cdot\nu\right|\leq O(\eta^3).$$

We also get

$$\left|\int_{A_i\setminus P(A_i)}(a_v-a)\Phi^2-\int_{(\partial A_i)^-}(a_i-a_0)\Phi^2v\cdot\nu\right|\leq O(\eta^3)$$

by the same arguments. □

3.6.3 Construction of $\mathcal{R}[\psi]$ from formula (3.32)

In order to construct $\mathcal{R}[\psi]$ from formula (3.32), we need to invert the operator $\frac{\partial}{\partial r}:L^2(C)\longrightarrow G^{-1}(C)$ and prove the stability of the inversion. For any $f\in L^2(C)$, by Fubini's theorem, the function $F(y,r)=\int_0^r f(y,\rho)d\rho$ is well-defined and in $G(C)$ but not in $G_0(C)$. Since this operator is acting on distributions which are zero on $S_\mu\times]0,r_0[$, we introduce

$$\begin{aligned}p:L^2(C)&\longrightarrow G_0(C)\\ \varphi&\longmapsto\left[(y,r)\mapsto-\int_0^r\left(\varphi(y,\rho)-\frac{R}{r_0}\chi_{]0,r_0[}(\rho)\varphi(y,\rho R/r_0)\right)d\rho\right]\end{aligned}$$

and its dual

$$p^*:G^{-1}(C)\longrightarrow L^2(C). \tag{3.55}$$

The following result holds.

Proposition 3.6.1 *For all $f\in L^2(C)$ such that $f=0$ on $S_\mu\times]0,r_0[$, we have the inversion formula*

$$p^*[\frac{\partial f}{\partial r}]=f.$$

Proof. For any $\varphi \in L^2(C)$, we have $\frac{\partial}{\partial r} p[\varphi] = -\varphi$ on $S_\mu \times [r_0, R[$ and therefore,

$$\int_C p^* \left[\frac{\partial f}{\partial r}\right] \varphi = \left\langle \frac{\partial f}{\partial r}, p[\varphi] \right\rangle_{G^{-1}(C), G_0^1(C)} = -\int_C f \frac{\partial}{\partial r} p[\varphi] = \int_C f\varphi,$$

which yields the claimed result. □

Proposition 3.6.2 *For all* $u \in \mathcal{M} := \left\{v \in G^{-1}(C) : \mathrm{supp}(v) \subset S_\mu \times [r_0, R[\right\}$,

$$\|p^* u\|_{L^2(C)} \leq \|u\|_{G^{-1}(C)}.$$

Proof. We first note that $p^*[u] = 0$ on $S_\mu \times]0, r_0[$. Then, for any $\varphi \in L^2(C)$, we get

$$\begin{aligned}
\left|\int_C p^*[u]\,\varphi\right| = \left|\int_C p^*[u]\,\chi_{[r_0,R[}\varphi\right| &\leq \|u\|_{G^{-1}(C)} \left\|p[\chi_{[r_0,R[}\varphi]\right\|_{G_0^1(C)} \\
&\leq \|u\|_{G^{-1}(C)} \left\|\frac{\partial}{\partial r} p[\chi_{[r_0,R[}\varphi]\right\|_{L^2(C)} \\
&\leq \|u\|_{G^{-1}(C)} \left\|\chi_{[r_0,R[}\varphi\right\|_{L^2(C)} \\
&\leq \|u\|_{G^{-1}(C)} \|\varphi\|_{L^2(C)},
\end{aligned}$$

and the proof is complete. □

Finally, we deduce the following result.

Corollary 3.6.3 *From formula (3.32), we have*

$$\mathcal{R}[\psi] = \frac{1}{r_0 \|w\|_1} p^*(r^{d-2} M).$$

Moreover, for η *small, if* $\mathcal{R}[\psi_\eta] = \frac{1}{r_0\|w\|_1} p^*(r^{d-2} M_\eta)$, *then*

$$\|\mathcal{R}[\psi - \psi_\eta]\|_{L^2(C)} \leq \frac{R^{d-2}}{r_0 \|w\|_1} \|M - M_\eta\|_{G^{-1}(C)},$$

which ensures the stability of the construction of $\mathcal{R}[\psi]$ *from the measurements* M_η.

Chapter 4

Reconstruction and stability in acousto-optic imaging for absorption maps with bounded variation

Introduction

In Chapters 2,1, and 3, an original mathematical and numerical framework for modeling biomedical imaging modalities based on mechanical perturbations of the medium is developed. The objective is to enhance the resolution and stability of tissue property imaging.

Many kinds of waves propagate in biological tissues over certain frequency ranges. Each one of them can be used to provide an image of a specific physical parameter. Low-frequency electromagnetic waves are sensitive to electrical conductivity; optical waves tell about optical absorption, ultrasonic waves reveal tissue's density, mechanical shear waves indicate how tissues respond to shear forces. However, single-wave imaging modalities are known to suffer from low specificity as well as intrinsic instabilities and low resolution; see [3, 105]. These fundamental deficiencies are impossible to eliminate, unless additional a priori information is incorporated. Single-wave imaging modalities can only be used for anomaly detection. Expansions techniques for data analysis, which reduce the set of admissible solutions and the number of unknowns, allow robust and accurate reconstruction of the location and of some geometric features of the anomalies, even with moderately noisy data.

One promising way to overcome the inherent limits of single-wave imaging and provide a stable and quantitative reconstruction of a distribution of physical parameters is to combine different wave-imaging modalities; see [3, 105]. A variety of multi-wave imaging approaches are being introduced and studied. In such approaches, two or more types of physical waves are involved in order to overcome the individual deficiencies of each one of them and to combine their strengths. Because of the way the waves are combined, multi-wave imaging can produce a single image with the best contrast and resolution properties of the two waves.

Three different types of wave interaction can be exploited in multi-wave imaging [55]: (i) the interaction of one kind of wave with tissue can generate a second kind of wave; (ii) a low-frequency wave that carries information about the desired contrast can be locally modulated by a second wave that has better spatial resolution; (iii) a fast propagating wave can be used to acquire a spatio-temporal sequence of the propagation of a slower transient wave.

In Chapters 2 and 3, by mechanically perturbing the medium we prove both analytically

and numerically the stability and resolution enhancement for reconstructing optical tissue parameters. We show how the high contrast of optical tomography [27] can be coupled to the high resolution of the acoustic propagation in soft tissues. The use of mechanical perturbations of the medium modeled by acoustics equations in fluids enhance the resolution to the order of the front width of the acoustic wave, which propagates inside the object. It dramatically increases the low resolution of optical tomography [102].

This chapter is a continuation and an extension of the work started in Chapters 2 and 3. We keep here the same models for the diffusive light propagation [38] and for the acoustic perturbations. Our aim is to extend the reconstruction algorithm developed in Chapter 2 to a large class of non smooth functions taken in a subclass of BV(Ω), the set of functions with bounded variation.

The reconstruction and the stability of the inversion are shown in this general case. Such an extension is essential for applying the proposed hybrid method to biological tissues. Indeed, the physiologic parameters that we want to recover cannot be considered smooth or piecewise smooth as assumed in Chapter 3.

Under this natural assumption, new mathematical difficulties rise to prove that the acousto-optic data contain enough information for reconstructing the absorption map. The lack of smoothness also causes difficulties to ensure the stability of the algorithm. This chapter resolves these challenging issues. It provides both an original reconstruction formula and a new stability result in the general setting. As far as we know, together with the recent work [91], it is the first work in imaging discontinuous parameter distributions from internal measurements.

Throughout this chapter, we denote by $\mathcal{S}$ the space of Schwartz and by $\mathcal{S}'$ its dual. We use the notation H^s for the usual Sobolev spaces and set $\mathcal{D}$ to be the set of $\mathcal{C}^\infty$ compactly supported functions.

As in Chapters 2 and 3, we consider a smooth bounded domain Ω of $\mathbb{R}^d$, for $d \in \{2, 3\}$, and a light fluence field defined as the unique solution of the diffusion equation

$$\begin{cases} -\triangle\Phi + a\Phi = 0 & \text{in } \Omega, \\ l\partial_\nu\Phi + \Phi = g & \text{on } \partial\Omega, \end{cases} \tag{4.1}$$

where $a \in L^\infty(\Omega)$ satisfying $a \geq \underline{a} > 0$ and $\mathrm{supp}(a - a_0) \subset \Omega$ is the absorption parameter to be recovered; see [27, 102]. The extrapolation length l, and the bounds $\underline{a}$ and a_0 are known positive constants. The incoming illumination $g \in H^{1/2}(\partial\Omega)$ is a non negative non zero map and is also supposed to be known.

The acoustic perturbations are assumed to be generated by spherical pressure waves. Let η be the front width of the acoustic wave and let w be the wave shape. The acoustic perturbations take the form:

$$v_{y,r,\eta}(x) = \frac{\eta}{r} w\left(\frac{|x-y| - r}{\eta}\right) \frac{x-y}{|x-y|}, \qquad \forall\, x \in \mathbb{R}^d \backslash \{y\}, \tag{4.2}$$

where $y \in Y \subset \mathbb{R}^d$, $\eta > 0$ and $r \in]\eta, +\infty[$; see Chapter 1. Here, $Y \subset \Omega$ is a smooth surface. Moreover, the map $w \in \mathcal{D}(\mathbb{R})$ is non negative and satisfies $\mathrm{supp}(w) \subset [-1, 1]$, $w' > -1$ and $\|w\|_{L^1} = 1$. This last assumption ensures that the map $x \longmapsto x + v(x)$ is a diffeomorphism.

The effect of the displacement v on the absorption map is assumed to be only a shifting effect, that is, to say that a becomes a_v implicitly defined on $\Omega_v = (Id + v)(\Omega)$ by

$$a_v(x + v(x)) = a(x), \qquad \forall\, x \in \Omega_v, \tag{4.3}$$

or equivalently, by the formula $a_v = a \circ (Id + v)^{-1}$. We introduce the displaced light fluence as the unique solution of

$$\begin{cases} -\triangle \Phi_v + a_v \Phi_v = 0 & \text{in } \Omega, \\ l\partial_\nu \Phi_v + \Phi_v = g & \text{on } \partial\Omega, \end{cases} \tag{4.4}$$

by extending a_v by a_0 if necessary. Computing now the cross-correlation on the boundary $\partial\Omega$ between Φ and Φ_v it follows that

$$\frac{1}{l}\int_{\partial\Omega}(\Phi - \Phi_v)g = \int_\Omega (a_v - a)\Phi\Phi_v. \tag{4.5}$$

Assume that the term in the left-hand side of the above identity can be measured. We define the measurement as the real quantity given by

$$M_v = \frac{1}{\eta^2}\int_\Omega (a_v - a)\Phi\Phi_v. \tag{4.6}$$

Throughout this chapter, we assume that M_v is known for any displacement field v given by (4.2).

For a smooth surface $Y \subset \Omega$ and $\eta > 0$, we assume that we are in possession of

$$M_\eta(y, r) = \frac{1}{\eta^2}\int_\Omega (a_{v_{y,r,\eta}} - a)\Phi\Phi_{v_{y,r,\eta}}, \qquad \forall\, (y, r) \in Y \times]\eta, +\infty[. \tag{4.7}$$

The imaging problem considered in this chapter is to reconstruct a from the measurement data M_η given by (4.7). The aim is to prove that the reconstruction algorithm from acousto-optic differential measurements presented in Chapter 2 can be extended for a very general class of discontinuous absorption maps. For doing so, we start from the same differential boundary measurements (4.7) and consider the case where a has bounded variations. Under some additional hypothesis, we correctly interpret the first order term in the asymptotic formula when $\|v\|_{L^\infty}$ goes to zero. Then, by giving a weak definition of the spherical means Radon transform $\mathcal{R}$, we show how the internal data Ψ satisfying

$$\Phi^2 \mathrm{D}a = \mathrm{D}\Psi + \nabla \times G,$$

can be reconstructed stably in $H^s(D)$ with $s < 1/2$ and D being a smooth domain. This is done through a stable reconstruction of $\mathcal{R}[\Psi]$ in $H^{(d-1)/2+s}$. Here, Da and DΨ are defined by (4.8).

The second part is to show that a stable reconstruction of the absorption map a is possible from this internal data Ψ. We give a system of two coupled elliptic equations solved by (a, Φ) and prove that a can be found as a solution of a fixed point problem. As the system depends on Ψ, we show that the solution depends continuously on Ψ in order to verify the global stability of the reconstruction.

Finally, we present numerical illustrations to substantiate the potential of the proposed method. We consider the imaging of a highly discontinuous absorption map, chosen from a real biological tissue data.

4.1 Preliminaries

In order to work with a wide set of discontinuous functions, we introduce $BV(\Omega)$ and several subspaces of $BV(\Omega)$.

4.1.1 Some subclasses of functions with bounded variation

Definition 4.1.1 *A function $u \in L^1(\Omega)$ is with bounded variation if its weak derivative Du is a finite Radon measure. For any $\varphi \in \mathcal{C}_c^1(\Omega)^d$, we have*

$$\int_\Omega u(x)\nabla \cdot \varphi(x)dx = -\int_\Omega \varphi(x) \cdot Du(dx).$$

A Radon measure can be uniquely decomposed into three singular measures as follows:

$$\mathrm{D}u = \mathrm{D}_l u + \mathrm{D}_j u + \mathrm{D}_c u, \tag{4.8}$$

which are respectively called the Lebesgue part, the jump part, and the Cantor part of Da. The Lebesgue part is absolutely continuous with respect to the Lebesgue measure and is identified to $\mathrm{D}_l u \in L^1(\Omega)^d$, which is called the smooth variation of u. The jump part $\mathrm{D}_j u$ is such that there exists a set $S \subset \Omega$ of Hausdorff dimension $d-1$, rectifiable admitting the existence of a generalized normal vector $\nu_S(x)$ for almost every $x \in S$. The jump part is written $\mathrm{D}_j u = [u]_S \nu_S \cdot \mathcal{H}_S^{d-1}$, where $[u]_S \in L^1(S, \mathcal{H}_S^{d-1})$ is called the jump of a over S and $\mathcal{H}_S^{d-1}$ is the Hausdorff measure on S. The cantor part $\mathrm{D}_c u$ is supported on a set of Hausdorff dimension less that $d-1$, which means that its $d-1$ Hausdorff-measure is zero; see [1].

In many cases it is very difficult to deal with such a general measure derivative. We introduce the special class of functions of bounded variation $SBV(\Omega)$. This class stays a very large set of discontinuous functions.

Definition 4.1.2 *A function $u \in BV(\Omega)$ is in the special class of bounded variation if $D_c u = 0$. We denote by*

$$SBV(\Omega) = \{u \in BV(\Omega),\ D_c u = 0\}.$$

In some cases, we shall work in some specific L^p framework. Hence, we use the following spaces.

Definition 4.1.3 *For any $p \in [1, +\infty]$, we define*

$$SBV^p(\Omega) = \left\{u \in SBV(\Omega) \cap L^p(\Omega),\ D_l u \in L^p(\Omega)^d,\ [u]_S \in L^p(S, \mathcal{H}_S^{d-1})\right\}.$$

Roughly speaking, a function $u \in SBV^p(\Omega)$ is a function of class $W^{1,p}$ admitting surface discontinuities. In the following, we state some Sobolev regularity results for functions of bounded variation. The classic embedding rule for $BV(\Omega)$ in the Sobolev spaces is that this space behaves like $W^{1,1}(\Omega)$.

Proposition 4.1.1 ($BV(\Omega)$ embedding in Sobolev) *For any $s \in \mathbb{R}^+, p \geq 1$, if $W^{1,1}(\Omega) \hookrightarrow W^{s,p}(\Omega)$ continuously, then $BV(\Omega) \hookrightarrow W^{s,p}(\Omega)$ continuously.*

If a function is in $SBV^\infty(\Omega)$ we can expect a better Sobolev regularity. We give the following embedding result.

Proposition 4.1.2 *For any $0 \leq \alpha < \frac{1}{2}$, $SBV^\infty(\Omega) \hookrightarrow H^\alpha(\Omega)$.*

Proof. Consider $u \in SBV^\infty(\Omega)$. $\mathrm{D}u = \mathrm{D}_l u + [u]_S \nu_S \mathcal{H}_S^{d-1}$ where S is a rectifiable surface, $\mathrm{D}_l u \in L^\infty(\Omega)^d$ and $[u]_S \in L^\infty(S, \mathcal{H}_S^{d-1})$. We introduce a continuous trace operator $\gamma_S : H^{1-\alpha}(\Omega) \longrightarrow L^2(S)$ and consider a test function $\varphi \in DD(\Omega)^d$ to write

$$\begin{aligned}
\langle \mathrm{D}u, \varphi \rangle_{\mathcal{D}'(\Omega)^d, \mathcal{D}(\Omega)^d} &= \int_\Omega \mathrm{D}_l u \cdot \varphi + \int_S [u]_S \nu_S \cdot \varphi \mathcal{H}_S^{d-1} \\
\left| \langle \mathrm{D}u, \varphi \rangle_{\mathcal{D}'(\Omega)^d, \mathcal{D}(\Omega)^d} \right| &\leq \|\mathrm{D}_l u\|_{L^\infty(\Omega)} \|\varphi\|_{L^2(\Omega)} + \|[u]_S\|_{L^\infty(S)} \|\varphi\|_{L^2(S)} \\
&\leq \|\gamma_S\|_{\mathcal{L}(H^{1-\alpha}(\Omega), L^2(\Omega))} \left(\|\mathrm{D}_l u\|_{L^\infty(\Omega)} + \|[u]_S\|_{L^\infty(S)} \right) \|\varphi\|_{H^{1-\alpha}(\Omega)}.
\end{aligned}$$

This proves that $\mathrm{D}u \in H^{\alpha-1}(\Omega)^d$ and so, $u \in H^\alpha(\Omega)$. □

4.1.2 The light fluence operator

The light fluence Φ associated to the absorption a is defined as the solution of

$$\begin{cases} -\triangle \Phi + a\Phi = 0 & \text{in } \Omega, \\ l\partial_\nu \Phi + \Phi = g & \text{on } \partial\Omega, \end{cases} \tag{4.9}$$

where $g \in H^{1/2}(\partial\Omega)$ is non negative and non zero. This problem is well posed if $a \in L^\infty(\Omega)$ and admits a positive lower bound. Throughout this chapter, we assume that there exist three constants $0 < \underline{a} \leq a_0 \leq \overline{a} < +\infty$ such that $\underline{a} \leq a \leq \overline{a}$ in Ω and $\mathrm{supp}(a - a_0) \subset D$. Under this condition, the light fluence Φ is uniquely determined in $H^2(\Omega)$. We define the set of the admissible absorption maps by

$$\mathcal{A}_0 = \left\{ a \in L^2(\Omega),\ \underline{a} \leq a \leq \overline{a},\ \mathrm{supp}(a - a_0) \subset D \right\} \tag{4.10}$$

and the light fluence operator as follows.

Definition 4.1.4 *Let the light fluence operator F be given by*

$$\begin{aligned} F : \mathcal{A}_0 &\longrightarrow H^2(\Omega) \\ a &\longmapsto \Phi, \end{aligned}$$

where Φ is the unique solution of (4.9).

As in dimensions 2 and 3, $H^2(\Omega) \hookrightarrow L^\infty(\Omega)$ we define the following two quantities in $\overline{\mathbb{R}}$

$$\begin{aligned} \underline{\Phi} &= \inf_{a \in \mathcal{A}_0} \inf_{x \in \Omega} F[a](x), \\ \overline{\Phi} &= \sup_{a \in \mathcal{A}_0} \sup_{x \in \Omega} F[a](x). \end{aligned} \tag{4.11}$$

The following result is from Chapter 2.

Proposition 4.1.3 *The quantity $\overline{\Phi}$ is finite and depends only on g, l, Ω and $\underline{a}$. Moreover, if $g \geq 0$ and $g \neq 0$ in $\partial\Omega$, then $\underline{\Phi} > 0$ and depends only on g, l, Ω, and $\overline{a}$.*

The following proposition is a direct application of standard elliptic regularity results [60] on the equation satisfied by $F[a] - F[a']$.

Proposition 4.1.4 *The operator F is Lipschitz continuous from $\mathcal{A}_0$ to $H^2(\Omega)$ in the sense that there exists a constant $C > 0$ depending only on Ω such that for any a and a' in $\mathcal{A}$, we have*

$$\|F[a] - F[a']\|_{H^2(\Omega)} \leq C\overline{\Phi}\, \|a' - a\|_{L^2(\Omega)}\,.$$

In the following, we will suppose that a is in $SBV^\infty(\Omega)$ and get from that a little Sobolev regularity enhancement due to Proposition 4.1.2. We have $a \in H^s(\Omega)$ for $s \in]0, \frac{1}{2}[$. For such number s, we define a new admissible set for the absorption map:

$$\mathcal{A}_s = \left\{ a \in \mathcal{A}_0 \cap H^s(\Omega),\ \|a\|_{H^s(\Omega)} \leq R_{\mathcal{A}_s} \right\}, \tag{4.12}$$

where $R_{\mathcal{A}_s}$ is a positive real number called the radius of $\mathcal{A}_s$. This gain of regularity for a implies a gain of regularity for $\Phi = F[a]$.

The following result is easy to prove. It follows immediately from standard regularity estimates.

Proposition 4.1.5 *Assume that $g \in H^1(\partial\Omega)$. Then for any $s \in]0, \frac{1}{2}[$ and any $a \in \mathcal{A}_s$, $F[a] \in H^{2+s}(\Omega)$. Moreover, the map*

$$F : \mathcal{A}_s \longrightarrow H^{2+s}(\Omega)$$

is Lipschitz continuous in the following sense: There exists a constant $C > 0$ depending only on Ω and s such that, for any a and a' in $\mathcal{A}_s$, we have

$$\|F[a] - F[a']\|_{H^{2+s}(\Omega)} \leq C(\overline{\Phi} + ||\nabla\Phi||_{L^\infty})\, \|a' - a\|_{H^s(\Omega)}\,.$$

4.1.3 Spherical means Radon transform

Here, we introduce the spherical means Radon transform $\mathcal{R}$ and the normalized spherical flow operator $\vec{\mathcal{R}}$. We extend their definition to tempered distributions in order to deal with derivative of non smooth functions. We also give several useful properties of these operators. We denote by $\Sigma = Y \times]0, +\infty[$.

Definition 4.1.5 (Spherical means Radon transform) *For any function $f \in \mathcal{C}^0(\mathbb{R}^d)$, we define its spherical means Radon transform $\mathcal{R}[f] \in \mathcal{C}^0(Y \times]0, +\infty[)$ by*

$$\mathcal{R}[f](y, r) = \int_{S^{d-1}} f(y + r\xi)\sigma(d\xi), \quad \forall\ (y, r) \in \Sigma,$$

where σ is the surface measure of the unit sphere. To extend this definition to distributions, we introduce the dual operator $\mathcal{R}^* : \mathcal{S}(\Sigma) \longrightarrow \mathcal{S}(\mathbb{R}^d)$ defined for any $\varphi \in \mathcal{S}(\Sigma)$ by

$$\mathcal{R}^*[\varphi](x) = \int_Y \frac{\varphi(y, |x-y|)}{|x-y|^{d-1}} \sigma(dy).$$

Then, for any tempered distribution $u \in \mathcal{S}'(\mathbb{R}^d)$, we define its spherical mean Radon transform $\mathcal{R}[u] \in \mathcal{S}'(\Sigma)$ as follows:

$$\langle \mathcal{R}[u], \varphi \rangle_{\mathcal{S}'(\Sigma),\mathcal{S}(\Sigma)} = \langle u, \mathcal{R}^*[\varphi] \rangle_{\mathcal{S}'(\mathbb{R}^d),\mathcal{S}(\mathbb{R}^d)}, \quad \forall\, \varphi \in \mathcal{S}(\mathbb{R}^d).$$

Injectivity and invertibility issues for $\mathcal{R}$ have been studied in several works; see, for instance, [94]. In [94, Corollary 6.4], the continuity of $\mathcal{R}$ and its inverse is proved. The following result holds.

Theorem 4.1.6 *Consider $s \in \mathbb{R}$ and suppose that for some $\alpha < s$ and any $u \in H^\alpha(\Omega)$ compactly supported, $\mathcal{R}[u] = 0$ implies $u = 0$. Then there exist two positive constants c_1 and c_2 such that*

$$\|u\|_{H^\alpha(\Omega)} \leq c_1 \|\mathcal{R}[u]\|_{H^{\alpha+\frac{d-1}{2}}(\Sigma)} \leq c_2 \|u\|_{H^\alpha(\Omega)}.$$

In the following, we always suppose that we are in the context where this theorem applies. Injectivity issues are essentially controlled by the set of centers Y; see, for instance, [97].

Definition 4.1.6 (Spherical flow operator) *For any function $F \in \mathcal{C}^0(\mathbb{R}^d)^d$, we define its normalized flow through the sphere $S(y,r)$, $\vec{\mathcal{R}}[F] \in \mathcal{C}^0(Y \times]0, +\infty[)$ by*

$$\vec{\mathcal{R}}[F](y,r) = \int_{S^{d-1}} f(y + r\xi)\sigma(d\xi), \quad \forall\, (y,r) \in \Sigma,$$

where σ is the surface measure of the unit sphere. To extend this definition to distributions, we introduce the dual operator $\mathcal{R}^* : \mathcal{S}(\Sigma) \longrightarrow \mathcal{S}(\mathbb{R}^d)$ defined for any $\varphi \in \mathcal{S}(\Sigma)$ by

$$\vec{\mathcal{R}}^*[\varphi](y,r) = \int_Y \frac{\varphi(y, |x-y|)}{|x-y|^d}(x-y)\sigma(dy).$$

Then, for any tempered distribution $U \in \mathcal{S}'(\mathbb{R}^d)^d$, we define its normalized flow through the sphere $S(y,r)$ denoted by $\vec{\mathcal{R}}[U] \in \mathcal{S}'(\Sigma)$ as

$$\left\langle \vec{\mathcal{R}}[u], \varphi \right\rangle_{\mathcal{S}'(\Sigma),\mathcal{S}(\Sigma)} = \left\langle u, \vec{\mathcal{R}}^*[\varphi] \right\rangle_{\mathcal{S}'(\mathbb{R}^d),\mathcal{S}(\mathbb{R}^d)}, \quad \forall\, \varphi \in \mathcal{S}(\mathbb{R}^d),$$

$$\vec{\mathcal{R}}[F](y,r) = \int_{S^{d-1}} F(y + \rho\xi) \cdot \xi \sigma(d\xi), \quad \forall\, (y,r) \in \Sigma. \tag{4.13}$$

The following result holds.

Proposition 4.1.7 *For any $u \in \mathcal{S}'(\mathbb{R}^d)$, $U \in \mathcal{S}'(\mathbb{R}^d)^d$, we have the following identities in the sense of distributions:*

$$\vec{\mathcal{R}}[\nabla u] = \partial_r \mathcal{R}[u], \tag{4.14}$$

$$\vec{\mathcal{R}}[\nabla \times U] = 0, \tag{4.15}$$

$$\mathcal{R}[\nabla \cdot U] = \frac{1}{r}\partial_r \left(r\vec{\mathcal{R}}[U] \right), \tag{4.16}$$

and

$$\mathcal{R}[\triangle u] = \frac{1}{r}\partial_r \big(r\partial_r \mathcal{R}[u] \big). \tag{4.17}$$

4.2 Recovering the internal data

The aim of this section is to recover the internal data Ψ with enough stability in order to use it in the next section to recover the absorption map a. The section is divided into five steps.

In the first step, we prove that when a belongs to $SBV^\infty(\Omega)$, the approximation

$$M_\eta(y,r) = -\frac{1}{\eta^2}\int_\Omega \Phi^2(x) v_{y,r,\eta}(x) \cdot \mathrm{D}a(dx) + \mathcal{O}\left(\eta^{\frac{d-1}{2d}}\right)$$

holds as η goes to zero. In the second step, we link the approximated measurement to $\vec{\mathcal{R}}[\Phi^2 \mathrm{D}a]$ through the exact formula:

$$\frac{1}{\eta^2}\int_\Omega \Phi^2(x) v_{y,r,\eta}(x) \cdot \mathrm{D}a(dx) = \left(\left[\vec{\mathcal{R}}[\Phi^2 \mathrm{D}a] \right] * \left[r^{d-2} w_\eta \right] \right)(y,r),$$

where $*$ is the convolution product with respect to the variable r and $w_\eta(r) = \frac{1}{\eta} w(r/\eta)$. In the third step, we give a weak Helmholtz decomposition of

$$\Phi^2 \mathrm{D}a = \mathrm{D}\Psi + \nabla \times G,$$

where $\Psi \in H^s_{loc}(\mathbb{R}^d)$ with $s \in [0, 1/2[$ and is of class $\mathcal{C}^\infty$ outside of $\mathrm{supp}(\mathrm{D}a)$ and satisfies $\Psi|_Y = 0$. In the fourth step, we prove that its spherical means Radon transform $\mathcal{R}[\Psi]$ is stably approximated in the space $H^{(d-1)/2}(\Sigma)$ in order to satisfy the assumptions of the Palamodov theorem. We conclude by proving the stable reconstruction of Ψ in $L^2(D)$, where D is a smooth subdomain of interest containing $\mathrm{supp}(\mathrm{D}a)$ and is such that $Y \subset \partial D$.

4.2.1 Step 1: From physical to ideal measurements

Definition 4.2.1 (Ideal measurements) *We call the ideal measurement function associated to the absorption $a \in SBV^\infty(\Omega)$ the function defined on Σ by*

$$\tilde{M}_\eta(y,r) = -\frac{1}{\eta^2}\int_\Omega \Phi^2(x) v_{y,r,\eta}(x) \cdot Da(dx). \tag{4.18}$$

In order to prove that M_η is close to $\tilde{M}_\eta$ when η goes to zero, we need several definitions.

Definition 4.2.2 (Wrap condition) *We say that the surface Y satisfies the wrap condition around Ω' if there exists a constant $C > 0$ such that for any $x \in \Omega' \subset \Omega$, $\Gamma \subset S^{d-1}$ measurable, we have*

$$\sigma\left(Y \cap \mathrm{Cone}(x,\Gamma)\right) \leq C\ \sigma(\Gamma),$$

where $\mathrm{Cone}(x,\Gamma) = \{x + t\xi,\ \xi \in \Gamma,\ t \in \mathbb{R}^+\}$.

Theorem 4.2.1 *Let $a \in SBV^\infty(\Omega)$ and let Ω' be such that $dist(\Omega', Y) \geq r_0 > 0$. Suppose that Y satisfies the wrap condition around Ω'. Then, there exists a constant $C > 0$ depending on Ω, Φ, $|Y|$, $|Da|(\Omega)$, r_0 and the wrap constant such that*

$$\left\| M_\eta - \tilde{M}_\eta \right\|_{L^2(\Sigma)} \leq C\eta^{\frac{d-1}{2d}},$$

and

$$\left\| P[M_\eta] - P[\tilde{M}_\eta] \right\|_{H^1(\Sigma)} \leq C\eta^{\frac{d-1}{2d}},$$

where P is the operator defined by

$$P[\varphi](y,r) = -\int_0^r \frac{\varphi(y,\rho)}{\rho^{d-2}} d\rho.$$

To prove this result, we need several lemmas. The first one is a spherical density result for the Radon measure $|\mathrm{D}a|$. Its proof uses some measure density results and is given in Appendix 4.6.1.

Lemma 4.2.2 *Consider $a \in SBV^\infty(\Omega)$ constant out of the subdomain $D \subset \Omega$ and let the mollifier sequence $w_\eta(r) = \frac{1}{\eta} w\left(\frac{1}{\eta}\right)$, where w is given by (4.2). Suppose that Y satisfies the wrap condition around D. Then, the sequence of functions defined on Σ by*

$$\varphi_\eta(y,r) = \int_\Omega w_\eta(|x-y| - r)|Da|(dx)$$

satisfies

$$\|\varphi_\eta\|_{L^2(\Sigma)} \leq C\eta^{-\frac{1}{2d}}$$

with C depending on $|Da|(\Omega)$, $|Y|$, and the wrap constant.

In the next lemma, we rewrite the measurement map M_η.

Lemma 4.2.3 *For any $(y,r) \in \Sigma$, we have*

$$M_\eta(y,r) = -\frac{1}{\eta^2} \int_\Omega T[v_{y,r,\eta}](x,y) v_{y,r,\eta}(x) \cdot Da(dx),$$

where

$$T[v](x,y) = \int_0^1 (\Phi\Phi_v)(x + tv(x)) \left(1 + t\frac{|v(x)|}{|x-y|}\right)^{d-1} dt.$$

Proof. Since we fix y (supposed to be zero) $r > r_0$ and $\eta > 0$, we will not write the dependence with respect to these variables. We first introduce an approximation sequence of $(a^\varepsilon)_{\varepsilon>0}$ such that $\mathrm{supp}(a^\varepsilon - a_0) \subset \Omega'$ and $a^\varepsilon \to a$ in $L^2(\Omega)$. Note that its derivative ∇a^ε converges to $\mathrm{D}a$ for the $H^{-1}(\Omega)^d$ norm.

We define now a flow $\varphi(x,t) = x + tv(x)$, $\varphi \in \mathcal{C}^\infty\left(\mathbb{R}^d \times [0,1], \mathbb{R}^d\right)$. The condition $w' > -1$ ensures that this flow is invertible in the sense that there exists a flow $\varphi^{-1}(x,t)$ of class $\mathcal{C}^\infty$

such that $\varphi(\varphi^{-1}(x,t),t) = \varphi^{-1}(\varphi(x,t),t) = x$ for all $(x,t) \in \mathbb{R}^d \times [0,1]$. In particular, it satisfies for any $x \in \mathbb{R}^d$, $\varphi^{-1}(x,0) = x$ and $\varphi^{-1}(x,1) = (Id+v)^{-1}(x)$. For all $x \in \mathbb{R}^d$, $\varepsilon > 0$, we have

$$\begin{aligned} a^\varepsilon \circ (Id+v)^{-1}(x) - a^\varepsilon(x) &= \int_0^1 \nabla a^\varepsilon(\varphi^{-1}(x,t)) \cdot \partial_t \varphi^{-1}(x,t) dt \\ \int_\Omega (a_v^\varepsilon - a^\varepsilon)p &= \int_\Omega \int_0^1 \nabla a^\varepsilon(\varphi^{-1}(x,t)) \cdot \partial_t \varphi^{-1}(x,t) p(x) dt dx \\ \int_\Omega (a_v^\varepsilon - a^\varepsilon)p &= \int_0^1 \int_\Omega \nabla a^\varepsilon(\varphi^{-1}(x,t)) \cdot \partial_t \varphi^{-1}(x,t) p(x) dx dt, \end{aligned}$$

where $p = \Phi\Phi_v$.

Hence, using the change of variables $x \mapsto \varphi(x,t)$, we get

$$\begin{aligned} \int_\Omega (a_v^\varepsilon - a^\varepsilon)p &= \int_0^1 \int_\Omega \nabla a^\varepsilon(x) \cdot \partial_t \varphi^{-1}(\varphi(x,t),t) p \circ \varphi(x,t) \det(d_x\varphi(x,t)) dx dt \\ &= -\int_\Omega F \cdot \nabla a^\varepsilon, \end{aligned}$$

where

$$F(x) = -\int_0^1 \partial_t \varphi^{-1}(\varphi(x,t),t) p \circ \varphi(x,t) \det(d_x\varphi(x,t)) dt.$$

As $p \in H^2(\Omega)$, the function F belongs to $H^1(\Omega)^d$. Passing to the limit when ε goes to zero in the previous equation, the term in the left-hand side goes to $\int_\Omega (a_u - a)p$ and as $F \in H^1(\Omega)^d$ and $\operatorname{supp}\big(\nabla a^\varepsilon\big) \subset \Omega' \subset\subset \Omega$, the right-hand side converges to $\int_\Omega F(x) \cdot \mathrm{D}a(dx)$. Hence, the formula

$$M = \int_\Omega (a_v - a)p = -\int_\Omega F(x) \cdot \mathrm{D}a(dx)$$

holds. In order to simplify the writing of F, we recall two useful properties satisfied by φ and φ^{-1}. Deriving the identity $\varphi^{-1}(\varphi(x,t),t) = x$ with respect to t and x, we get

$$\begin{aligned} d_x\varphi^{-1}(\varphi(x,t),t)\partial_t\varphi(x,t) + \partial_t\varphi^{-1}(\varphi(x,t),t) &= 0, \\ d_x\varphi^{-1}(\varphi(x,t),t) d_x\varphi(x,t) &= Id. \end{aligned}$$

We recall that $d_x\varphi(x,t) = Id + t dv(x)$. Now noticing that $\partial_t\varphi^{-1}(\varphi(x,t),t) = -(Id+tdv(x))$, we rewrite F as follows:

$$F(x) = -\int_0^1 p\big(x+tv(x)\big) \det\big(Id+tdv(x)\big)\big(Id+tdv(x)\big)^{-1} v(x) dt.$$

Fortunately, $dv(x)$ is diagonal in the spherical orthonormal basis $\mathcal{B} = (\xi, e_2, \cdots, e_d)$, where $\xi = x/|x|$ and $(e_2, \cdots, e_d)$ is an orthonormal basis of $\xi^\perp$, the hyperplane orthogonal to ξ. Its matrix in this basis is given by

$$\operatorname{mat}_{\mathcal{B}}(dv(x)) = \begin{bmatrix} \frac{r_0}{r} w'\left(\frac{|x|-r}{\eta}\right) & 0 \\ 0 & \frac{|v(x)|}{|x|} I_{d-1} \end{bmatrix}.$$

Then,

$$\mathrm{mat}_{\mathcal{B}}(Id + tdv(x)) = \begin{bmatrix} 1 + t\frac{r_0}{r} w'\left(\frac{|x|-r}{\eta}\right) & 0 \\ 0 & \left(1 + t\frac{|v(x)|}{|x|}\right) I_{d-1} \end{bmatrix},$$

and from this matrix we deduce that

$$\det\big(Id + tdv(x)\big) = \left[1 + t\frac{r_0}{r} w'\left(\frac{|x|-r}{\eta}\right)\right]\left[1 + t\frac{|v(x)|}{|x|}\right]^{d-1}$$
$$\big(Id + tdv(x)\big)^{-1} v(x) = \frac{v(x)}{1 + t\frac{r_0}{r} w'\left(\frac{|x|-r}{\eta}\right)}.$$

Therefore,

$$F(x) = \int_0^1 p\big(x + tv(x)\big)\left[1 + t\frac{|v(x)|}{|x|}\right]^{d-1} dt\ v(x).$$

Replacing $|x|$ by $|x-y|$ and rewriting the dependence in y, r, and η, we finally get the expected formula. □

The next result shows that the shifted absorption map a_v stays close to a in $L^1(\Omega)$ if η is small. The key result is optimal in the sense that it requires that a to be of bounded variation. In fact, it shows that any reconstruction would be impossible without this minimal regularity.

Proposition 4.2.4 *Consider $a \in \mathcal{A}_0 \cap BV(\Omega)$ and let the internal displacement v be given by (4.2). We have the following estimate:*

$$\|a_v - a\|_{L^1(\Omega)} \leq C|Da|(\Omega)\eta$$

with C depending only on the space dimension d.

Proof. Let us consider an approximation sequence $(a^\varepsilon)_{e>0} \subset \mathcal{C}^0(\Omega)$ such that $\mathrm{supp}(a^e - a) \subset D$ and $\|a^\varepsilon - a\|_{L^1(\Omega)} \leq \varepsilon$. Now, we define the flow $\varphi \in \mathcal{C}^\infty\big(\mathbb{R}^d \times [0,1]\big)$ by $\varphi(x,t) = x + tv_\eta(x)$. The condition $w' > -1$ ensures that this flow is invertible in the sense that there exists a flow $\varphi^{-1}(x,t)$ of class $\mathcal{C}^\infty$ such that $\varphi(\varphi^{-1}(x,t),t) = \varphi^{-1}(\varphi(x,t),t) = x$ for all $(x,t) \in \mathbb{R}^d \times [0,1]$. In particular, it satisfies for any $x \in \mathbb{R}^d$, $\varphi^{-1}(x,0) = x$ and $\varphi^{-1}(x,1) = (Id + v_\eta)^{-1}(x)$.

For all $x \in \mathbb{R}^d$, $\varepsilon > 0$, we get

$$a^\varepsilon_{v_\eta}(x) - a^\varepsilon(x) = a^\varepsilon \circ \varphi^{-1}(x,1) - a^\varepsilon \circ \varphi^{-1}(x,0) = \int_0^1 \nabla a^\varepsilon \circ \varphi^{-1}(x,t)\partial_t\varphi^{-1}(x,t)dt$$
$$\left\|a^\varepsilon_{v_\eta}(x) - a^\varepsilon(x)\right\|_{L^1(\Omega)} \leq \int_0^1 \int_\Omega \left|\nabla a^\varepsilon \circ \varphi^{-1}(x,t) \cdot \partial_t\varphi^{-1}(x,t)\right| dxdt$$
$$\leq \int_0^1 \int_\Omega \left|\nabla a^\varepsilon(x) \cdot \partial_t\varphi^{-1}(\varphi(x,t),t)\right| |\det d_x\varphi(x,t)|dxdt.$$

A similar computation to the one in the proof of (4.2.3) leads to

$$|\partial_t\varphi^{-1}(\varphi(x,t),t) \det d_x\varphi(x,t)| \leq \left(1 + \frac{d(d-1)}{2}\right)|v_\eta(x)|$$

and so,

$$\left\|a^{\varepsilon}_{v_\eta}(x) - a^{\varepsilon}(x)\right\|_{L^1(\Omega)} \leq \left(1 + \frac{d(d-1)}{2}\right)\eta \int_\Omega |\nabla a^{\varepsilon}|.$$

Passing now to the limit when ε goes to zero, we get the expected result. □

As a consequence of Proposition 4.2.4, we deduce that the modified light fluence Φ_v is close to Φ in $H^2(\Omega)$ when η is small.

By combining (4.2.4) and (4.1.4), the following result holds.

Corollary 4.2.5 *Consider $a \in \mathcal{A}_0 \cap BV(\Omega)$ and the internal displacement v given by (4.2). We have the following estimate:*

$$\|\Phi_v - \Phi\|_{H^2(\Omega)} \leq C\overline{\Phi}(\overline{a} - \underline{a})^{\frac{1}{2}} |Da|(\Omega)^{\frac{1}{2}} \eta^{\frac{1}{2}},$$

where C depends on d and Ω.

Lemma 4.2.6 *Consider a subdomain $\Omega' \subset \Omega$ such that $dist(\Omega', Y) \geq r_0 > 0$. There exists a constant $C > 0$ depending on Ω, Φ and a such that*

$$\left\|T[v_{y,r,\eta}](.,y) - \Phi^2\right\|_{L^\infty(\Omega')} \leq C\eta^{\frac{1}{2}}.$$

Proof. For fixed $\eta > 0$ and $(y,r) \in \Sigma$, for $t \in [0,1]$ and $x \in \Omega'$,

$$\begin{aligned}
|(\Phi\Phi_v)(x + tv(x)) - \Phi^2(x)| &\leq |\Phi^2(x + tv(x)) - \Phi^2(x)| + |(\Phi\Phi_v)(x + tv(x)) - \Phi^2(x + tv(x))| \\
&\leq 2\overline{\Phi}|\Phi(x + tv(x)) - \Phi(x)| + \overline{\Phi}|(\Phi_v(x + tv(x)) - \Phi(x + tv(x))| \\
&\leq 2\overline{\Phi}\,\|\Phi\|_{\mathcal{C}^{0,\frac{1}{2}}(\overline{\Omega})}\,\eta^{\frac{1}{2}} + \overline{\Phi}C_1\eta^{\frac{1}{2}} \\
&\leq C\eta^{1/2}.
\end{aligned}$$

Recalling that for $x \in \Omega'$, $|x - y| \geq r_0$, we use the previous inequality in (4.19) to get the desired result. □

Now, we are ready to prove Theorem 4.2.1.

Proof. (of Theorem 4.2.1) For any $(y,r) \in \Sigma$,

$$\begin{aligned}
|M_\eta - \tilde{M}_\eta|(y,r) &\leq \int_\Omega |T[v_{y,r,\eta}](x,y) - \Phi^2(x)| \frac{|v_{y,r,\eta}(x)|}{\eta^2} |\mathrm{D}a|(dx) \\
&\leq \left\|T[v_{y,r,\eta}] - \Phi^2\right\|_{L^\infty(\Omega')} \int_\Omega w_\eta(|x-y| - r)|\mathrm{D}a|(dx).
\end{aligned}$$

Applying Lemmas 4.2.6 and 4.2.2, we get the first inequality,

$$\left\|M_\eta - \tilde{M}_\eta\right\|_{L^2(\Sigma)} \leq C\eta^{\frac{d-1}{2d}}.$$

Next, taking the derivative with respect to the variable y, it follows that

$$d_y(M_\eta - \tilde{M}_\eta)(y,r) = \int_\Omega d_y\left(\left(T[v_{y,r,\eta}](x,y) - \Phi^2(x)\right)\frac{v_{y,r,\eta}(x)}{\eta^2}\right) \cdot \mathrm{D}a(dx)$$

with

$$d_y\left(\left(T[v_{y,r,\eta}](x,y)-\Phi^2(x)\right)\frac{v_\eta(x,y,r)}{\eta^2}\right)=d_vT[v_{y,r,\eta}](x,y)\cdot d_yv_{y,r,\eta}(x)\frac{v_{y,r,\eta}(x)}{\eta^2}$$
$$+\left(T[v_{y,r,\eta}](x,y)-\Phi^2(x)\right)\frac{d_yv_{y,r,\eta}(x)}{\eta^2}$$
$$+d_yT[v_{y,r,\eta}](x,y)\frac{v_{y,r,\eta}(x)}{\eta^2}.$$

The vector field $v_{y,r,\eta}$ satisfies

$$d_yv_{y,r,\eta}=\partial_rv_{y,r,\eta}+|v_{y,r,\eta}|B(y,r,x),$$

where $B(y,r,x)$ is a matrix uniformly bounded with respect to all variables. Moreover,

$$d_yT[v_{y,r,\eta}](x,y)=\mathcal{O}(\eta)$$

with reminder uniform with respect to all variables. Thus we write

$$d_y\left(\left(T[v_{y,r,\eta}](x,y)-\Phi^2(x)\right)\frac{v_\eta(x,y,r)}{\eta^2}\right)$$
$$=\partial_r\left(\left(T[v_{y,r,\eta}](x,y)-\Phi^2(x)\right)\frac{v_{y,r,\eta}(x)}{\eta^2}\right)\frac{(x-y)^T}{|x-y|}$$
$$+R(y,r,x)\frac{|v_{y,r,\eta}(x)|}{\eta^2},$$

where the reminder $R(y,r,x)=\mathcal{O}(\eta^{1/2})$ uniformly with respect to all variables. Here, T denotes the transpose.

Using this identity, we can integrate by parts with respect to r to get

$$\int_0^r\frac{1}{\rho^{d-2}}d_y\left(\left(T[v_\eta(y,\rho)](x,y)-\Phi^2(x)\right)\frac{v_\eta(y,\rho)(x)}{\eta^2}\right)d\rho$$
$$=\frac{1}{r^{d-2}}\left(\left(T[v_{y,r,\eta}](x,y)-\Phi^2(x)\right)\frac{v_{y,r,\eta}\nabla(x)}{\eta^2}\right)\frac{(x-y)^T}{|x-y|}$$
$$+(d-2)\int_0^r\frac{1}{\rho^{d-1}}\left(\left(T[v_\eta(y,\rho)](x,y)-\Phi^2(x)\right)\frac{v_\eta(y,\rho)(x)}{\eta^2}\right)d\rho\frac{(x-y)^T}{|x-y|}$$
$$+\int_0^rR(y,\rho,x)\frac{|v_\eta(y,\rho)(x)|}{\eta^2}d\rho.$$

Finally, we integrate over Ω and use Lemma 4.2.2 in order to control these three terms. We control all of these by $\eta^{\frac{d-1}{2d}}$. □

4.2.2 Step 2: Linking the measurement and $\Phi^2\mathbf{D}a$

In the previous subsection, we have shown that the measurement M_η is approximated by

$$\tilde{M}_\eta(y,r) = -\frac{1}{\eta^2}\int_\Omega \Phi^2(x) v_{y,r,\eta}(x)\cdot \mathrm{D}a(dx)$$

in a certain sense when η goes to zero. We propose here a rewriting of $\tilde{M}_\eta$ using the spherical operators defined in subsection 4.1.3. As $\mathrm{D}a$ is a finite measure compactly supported, it is a tempered distribution on $\mathbb{R}^d$. Since $\Phi \in \mathcal{C}^0\big(\overline{\Omega}\big)$, the vector field $\Phi^2\mathrm{D}a$ is a tempered distribution on $\mathbb{R}^d$ defined by

$$\big\langle \Phi^2\mathrm{D}a, \varphi\big\rangle_{S'(\mathbb{R}^d)^d, S(\mathbb{R}^d)^d} = \int_\Omega \Phi^2\varphi\cdot \mathrm{D}a.$$

The following result holds.

Proposition 4.2.7 *For any $a\in\mathcal{A}$, $\eta>0$ we have the formula*

$$\tilde{M}_\eta = -\frac{1}{r}\left[\left(r^{d-1}\vec{\mathcal{R}}[\Phi^2 Da]\right) * w_\eta(-.)\right] \qquad \text{in } \Sigma, \tag{4.19}$$

where $*$ is the one dimensional convolution product with respect to the variable r and $w_\eta(r) = \frac{1}{\eta}w\left(\frac{r}{\eta}\right)$.

Proof. Consider a test function $\varphi\in\mathcal{S}(\Sigma)$. We have

$$\begin{aligned}
-\int_\Sigma \tilde{M}_\eta\varphi &= -\int_Y\int_0^\infty M_\eta(y,r)\varphi(y,r)\sigma(dy)dr\\
&= \frac{1}{\eta^2}\int_\Omega \Phi^2(x)\left(\int_Y\int_0^\infty v_{y,r,\eta}(x)\varphi(y,r)\sigma(dy)dr\right)\cdot \mathrm{D}a(dx)\\
&= \int_\Omega \Phi^2(x)\left(\int_Y\int_0^\infty \frac{1}{r}w_\eta\left(|x-y|-r\right)\varphi(y,r)dr\frac{x-y}{|x-y|}\sigma(dy)\right)\cdot \mathrm{D}a(dx)\\
&= \int_\Omega \Phi^2(x)\left(\int_Y\left(w_\eta * \frac{\varphi(y,.)}{r}\right)(|x-y|)\frac{x-y}{|x-y|}\sigma(dy)\right)\cdot \mathrm{D}a(dx)\\
&= \int_\Omega \Phi^2(x)\vec{\mathcal{R}}^*\left[r^{d-1}\left(w_\eta * \frac{\varphi(y,.)}{r}\right)\right](x)\cdot \mathrm{D}a(dx)\\
&= \left\langle \Phi^2\mathrm{D}a, \vec{\mathcal{R}}^*\left[r^{d-1}\left(w_\eta * \frac{\varphi(y,.)}{r}\right)\right]\right\rangle_{\mathcal{S}'(\mathbb{R}^d),\mathcal{S}(\mathbb{R}^d)}\\
&= \left\langle \vec{\mathcal{R}}[\Phi^2\mathrm{D}a], r^{d-1}\left(w_\eta * \frac{\varphi(y,.)}{r}\right)\right\rangle_{\mathcal{S}'(\Sigma),\mathcal{S}(\Sigma)}\\
&= \left\langle \frac{1}{r^{d-1}}\vec{\mathcal{R}}[\Phi^2\mathrm{D}a], w_\eta * \frac{\varphi(y,.)}{r}\right\rangle_{\mathcal{S}'(\Sigma),\mathcal{S}(\Sigma)}\\
&= \left\langle \frac{1}{r}\left(r^{d-1}\vec{\mathcal{R}}[\Phi^2\mathrm{D}a]\right) * w_\eta(-.), \varphi\right\rangle_{\mathcal{S}'(\Sigma),\mathcal{S}(\Sigma)}.
\end{aligned}$$

□

4.2.3 Step 3: Helmholtz decomposition of $\Phi^2 \mathrm{D}a$

Since $\Phi^2 \mathrm{D}a$ is a tempered distribution, we can consider its Fourier transform. As $a \in H^s(\Omega)$ with $s \in [0, 1/2[$ and $\mathrm{D}a$ is compactly supported, it follows that $\mathrm{D}a \in H_K^{s-1}(\Omega)^d$. Moreover, as Φ^2 is in $H^2(\Omega)$, we also have that $\Phi^2 \mathrm{D}a \in H_K^{s-1}(\Omega)^d$. From Appendix 4.6.2, we deduce that $\widehat{\Phi^2 \mathrm{D}a}$ belongs to $L^1_{loc}(\mathbb{R}^d)^d$ and satisfies

$$\int_{\mathbb{R}^d} \left| \widehat{\Phi^2 \mathrm{D}a} \right|^2 (\xi) \left(1 + |\xi|^2\right)^{(s-1)} d\xi < +\infty.$$

Let the Sobolev space $H^{\alpha+1}_{\mathrm{curl}}(\mathbb{R}^d)^d$ be defined by

$$H^{\alpha+1}_{\mathrm{curl}}(\mathbb{R}^d) := \left\{ A \in H^\alpha(\mathbb{R}^d)^d,\ \nabla \times A \in H^\alpha(\mathbb{R}^d)^d \right\}.$$

The following proposition gives a generalization of the Helmholtz decomposition for some compactly supported distributional vector fields.

Proposition 4.2.8 *Consider $\alpha \in \mathbb{R}$ and $U \in H^\alpha_K(\Omega)^d$, where K is a compact of Ω. There exists $u \in H^{\alpha+1}(\mathbb{R}^d)$ and $A \in H^{\alpha+1}_{\mathrm{curl}}(\mathbb{R}^d)$ such that*

$$U = Du + \nabla \times A$$

in the sense of distributions.

Proof. As $U \in H^\alpha_K(\Omega)$, $\widehat{U} \in L^1_{loc}(\mathbb{R}^d)^d$. We define now $\widehat{u} = \frac{\widehat{U} \cdot \xi}{i|\xi|^2} \in L^1_{loc}(\mathbb{R}^d)$ and $\widehat{A} = \frac{\widehat{U} \wedge \xi}{i|\xi|^2} \in L^1_{loc}(\mathbb{R}^d)^d$. We have the decomposition $\widehat{U} = i\widehat{u}\xi + i\xi \wedge \widehat{A}$. As $i\widehat{u}\xi$ is the Fourier transform of ∇u where u is the inverse Fourier transform of $\widehat{u}$ and has the same integrability than $\widehat{U}$, we deduce that $u \in H^{\alpha+1}(\mathbb{R}^d)$ and A, the inverse Fourier transform of $\widehat{A}$, is in $H^{\alpha+1}_{\mathrm{curl}}(\mathbb{R}^d)$.□

Using this last result, we write

$$\Phi^2 \mathrm{D}a = \mathrm{D}\Psi + \nabla \times G \tag{4.20}$$

with $\psi \in H^s(\mathbb{R}^d)$ and therefore, we get

$$\vec{\mathcal{R}}[\Phi^2 \nabla a] = \partial_r \mathcal{R}[\psi] \tag{4.21}$$

in the sense of distributions. Using this last identity in (4.19) we obtain that

$$\tilde{M}_\eta = -\frac{1}{r} \left[\left(r^{d-1} \partial_r \mathcal{R}[\Psi] \right) * w_\eta(-.) \right] \qquad \text{in } \Sigma. \tag{4.22}$$

The proof is then complete. □

4.2.4 Step 4: Approximating $\mathcal{R}[\Psi]$

We can show now that from the previous identity, the quantity $\mathcal{R}[\Psi]$ can be approximated up to a function depending only in y in $H^{\frac{d-1}{2}}(\Sigma)$ in order to apply Palamodov's theorem (see [94]).

Theorem 4.2.9 *Let $s \in \left]\frac{1}{3}, \frac{1}{2}\right[$ and $\alpha > 0$ and consider $a \in \mathcal{A}_{s+\alpha}$. Then $P[\tilde{M}_\eta]$ converges to $\mathcal{R}[\Psi] - g$ in $H^{\frac{d-1}{2}+s}(\Sigma)$ where g is a function depending only on y. More precisely, there exists a constant C depending on d, s, α and Σ such that*

$$\left\| P[\tilde{M}_\eta] - \mathcal{R}[\Psi] + g \right\|_{H^{\frac{d-1}{2}+s}(\Sigma)} \leq C\eta^{\frac{\alpha}{\alpha+1}} \left\|\Psi\right\|_{H^{s+\alpha}(\Sigma)}.$$

Proof. Starting from (4.22) and integrating by parts, we write

$$\tilde{M}_\eta(y,r) = \int_{\mathbb{R}} \mathcal{R}[\Psi](y,\rho)\partial_\rho \left(\frac{1}{r} w_\eta(\rho - r)\rho^{d-1} \right) d\rho.$$

Now, applying P to $\tilde{M}_\eta$, we get

$$P[\tilde{M}_\eta](y,r) = -\int_{\mathbb{R}} \mathcal{R}[\Psi](y,\rho)\partial_\rho \left(\int_{r_0}^{r} w_\eta(\rho - s)\frac{\rho^{d-1}}{s^{d-1}} ds \right) d\rho.$$

Let us develop the test function

$$\partial_\rho \int_{r_0}^{r} w_\eta(\rho - s)\frac{\rho^{d-1}}{s^{d-1}} ds = w_\eta(\rho - r_0)\frac{\rho^{d-1}}{r_0^{d-1}} - w_\eta(\rho - r)\frac{\rho^{d-1}}{r^{d-1}} - \theta_\eta(\rho, r)$$

with

$$\theta_\eta(\rho, r) = (d-1)\int_{r_0}^{r} w(\rho - s)(s - \rho)\frac{\rho^{d-2}}{s^d} ds.$$

which satisfies $\left\|\theta_\eta\right\|_{H^1(]0,R[^2)} \leq C\eta^{1/2}$ with C depending on r_0, R, and d. Finally, we write

$$\begin{aligned} P[\tilde{M}_\eta](y,r) = \frac{1}{r^{d-1}} \int_0^R \rho^{d-1}\mathcal{R}[\Psi](y,\rho) w_\eta(\rho - r) d\rho - \frac{1}{r_0^{d-1}} \int_0^R \rho^{d-1}\mathcal{R}[\Psi](y,\rho) w_\eta(\rho - r_0) d\rho \\ + \int_0^R \mathcal{R}[\Psi](y,\rho)\theta_\eta(\rho, r) d\rho. \end{aligned}$$

Using Lemma 4.6.3, we bound the $H^{\frac{d-1}{2}}(\Sigma)$ norm of the third term by $C\eta^{\frac{1}{2}} \left\|\mathcal{R}[\Psi]\right\|_{H^{\frac{d-1}{2}}(\Sigma)}$. Moreover, using Lemma 4.6.4, we say that as $\mathcal{R}[\Psi] \in H^{\frac{d-1}{2}+s+\alpha}(\Sigma)$, the first term converges to $\mathcal{R}[\Psi]$ for the norm of $H^{\frac{d-1}{2}+s}(\Sigma)$ with an error controlled by $\eta^{\frac{\alpha}{\alpha+1}} \left\|\mathcal{R}[\Psi]\right\|_{H^{\frac{d-1}{2}+s+\alpha}(\Sigma)}$. Using the same argument, the second term goes to $g(y) = \mathcal{R}[\Psi](y, r_0)$ in the same manner. We finally obtain that

$$\left\| P[\tilde{M}_\eta] - \mathcal{R}[\Psi] + g \right\|_{H^{\frac{d-1}{2}+s}(\Sigma)} \leq C\eta^{\frac{\alpha}{\alpha+1}} \left\|\mathcal{R}[\Psi]\right\|_{H^{\frac{d-1}{2}+s+\alpha}(\Sigma)},$$

where C depends on d and the manifold Σ. □

4.2.5 Step 5: Approximating Ψ

We recall here that we have assumed the invertibility of the spherical means Radon transform. We apply $\mathcal{R}^{-1}$ to the inequality given in Theorem 4.2.9 to get

$$\left\|\mathcal{R}^{-1}\circ P[\tilde{M}_\eta]-\Psi+\mathcal{R}^{-1}[g]\right\|_{H^s(D)}\leq \eta^{\frac{\alpha}{\alpha+1}}\left\|\Psi\right\|_{H^{s+\alpha}(\Sigma)}. \tag{4.23}$$

The problem that we have here is that we do not know the map $h=\mathcal{R}^{-1}[g]$. Nevertheless, this function is harmonic because $\partial_r\mathcal{R}[h]=0$ and so using Proposition 4.1.7, $\mathcal{R}[\triangle h]=0$ we get $\triangle h=0$. We can change Ψ to $\tilde{\Psi}=\Psi-h$ in the Helmholtz decomposition of $\Phi^2\mathrm{D}a$. Indeed, ∇h is divergence-free and there exists a smooth vector field A such that $\nabla h=\nabla\times A$. We write

$$\begin{aligned}\Phi^2\mathrm{D}a&=\mathrm{D}\Psi+\nabla\times G,\\ \Phi^2\mathrm{D}a&=\mathrm{D}(\Psi-h)+\nabla\times(G-A),\\ \Phi^2\mathrm{D}a&=\mathrm{D}\tilde{\Psi}+\nabla\times\tilde{G},\end{aligned}$$

where $\tilde{\Psi}$ can be approximated in $H^s(D)$ and satisfies $\tilde{\Psi}|_Y=0$.

To summarize the five steps of this section, we state the following theorem.

Theorem 4.2.10 *Consider $a\in\mathcal{A}_0\cap SBV^\infty(\Omega)$ satisfying supp$(Da)\subset D\subset\overline{D}\subset\Omega$ and assume that Y satisfies the wrap condition around D. Then there exists $\Psi\in H^s(\mathbb{R}^d)$ with $s\in]0,1/2[$ and of class $\mathcal{C}^\infty$ outside of supp(Da) satisfying $\Psi|_Y=0$ and*

$$\Phi^2 Da=D\Psi+\nabla\times G, \tag{4.24}$$

where $G\in H^s_{curl}(\mathbb{R}^d)^d$ and $\Phi=F[a]$. Moreover, $\mathcal{R}^{-1}\circ P[M_\eta]$ converges strongly to Ψ in $H^s(D)$ when η goes to zero at a speed bounded by $\mathcal{O}\left(\eta^{\frac{1}{4}}\right)$.

This map Ψ will be now the starting point of the reconstruction procedure. In the next section, we assume that Ψ is known in $H^s(D)$ up to a small error in $H^s(D)$. We will see how to approximate the absorption parameter a from this data.

4.3 Stable reconstruction of the absorption map

In this section, we assume that the assumptions of Theorem 4.2.10 are satisfied and suppose in addition that $Y=\partial D$. As a consequence, we assume the knowledge of $\Psi\in H^s(D)$ of class $\mathcal{C}^\infty$ in a neighborhood of ∂D, which satisfies $\Psi|_{\partial D}=0$. The goal of this section is to present a method to estimate the absorption map a from the knowledge of Ψ. We choose s such that $H^{s+1}(\Omega)$ is embedded in $L^\infty(\Omega)$ in dimensions 2 and 3. This is true for any $s\in]1/3,1/2[$.

Let us take the divergence of (4.24) in the sense of distributions to get

$$\nabla\cdot(\Phi^2\mathrm{D}a)=\triangle\Psi,$$

which looks like an elliptic equation with unknown a. There are two difficulties here. The first one is that we do not have enough regularity to deal with this equation using a variational approach. To do so, we should have Ψ in $H^1(D)$ and look for a solution a in $H^1(D)$. The second difficulty is that the diffusion term Φ^2 is unknown here and depends on a by $\Phi^2 = F[a]^2$, where F is the light fluence operator.

Finally, we recall the definition of the set of admissible absorption distributions:

$$\mathcal{A}_s = \left\{ a \in \mathcal{A}_0 \cap H^s(\Omega),\ \|a\|_{H^s(\Omega)} \leq R_{\mathcal{A}_s} \right\}$$

and define

$$\mathcal{B}_s = \left\{ \Phi \in W^{1,\infty}(D),\ \underline{\Phi} \leq \Phi\overline{\Phi}, \|\nabla\Phi\|_{L^\infty} \leq R_{\mathcal{B}_s} \right\},$$

where $R_{\mathcal{B}_s} = \sup_{a\in\mathcal{A}_s} \|\nabla F[a]\|_{L^\infty(D)}$. Note that F maps $\mathcal{A}_s$ into $\mathcal{B}_s$.

4.3.1 The change of function argument

The main idea is to introduce a new variable:

$$\tilde{a} = a - a_0 - \frac{\Psi}{\Phi^2}, \tag{4.25}$$

which is well defined in $H^s(D)$ since $\Phi \geq \overline{\Phi}$.

Proposition 4.3.1 *For all $a \in \mathcal{A}_s$ and $\Phi = F[a]$, we have $\tilde{a} \in H_0^1(D)$.*

Proof. In the sense of distributions, we have

$$\begin{aligned}
\mathrm{D}\tilde{a} &= \mathrm{D}a - \frac{\mathrm{D}\Psi}{\Phi^2} + 2\Psi\frac{\nabla\Phi}{\Phi^3},\\
\Phi^2\mathrm{D}\tilde{a} &= \Phi^2\mathrm{D}a - \mathrm{D}\Psi + 2\Psi\nabla\log\Phi,\\
\nabla\cdot(\Phi^2\mathrm{D}\tilde{a}) &= \nabla\cdot(2\Psi\nabla\log\Phi),\\
\Phi^2\triangle\tilde{a} &= \nabla\cdot(2\Psi\nabla\log\Phi) - \nabla(\Phi^2)\cdot\mathrm{D}\tilde{a},\\
\triangle\tilde{a} &= \frac{1}{\Phi^2}\nabla\cdot(2\Psi\nabla\log\Phi) - 2\nabla(\log\Phi)\cdot\mathrm{D}\tilde{a}.
\end{aligned}$$

Consider a test function $\varphi \in \mathcal{D}(D)$ and using the fact that $\nabla\Phi \in L^\infty(D)$, which follows from the fact that $\Phi \in H^{2+s}(\Omega)$, we have

$$\begin{aligned}
&\left\langle \frac{1}{\Phi^2}\nabla\cdot(2\Psi\nabla\log\Phi), \varphi \right\rangle_{\mathcal{D}'(D),\mathcal{D}(D)} = \left\langle \nabla\cdot(2\Psi\nabla\log\Phi), \frac{\varphi}{\Phi^2} \right\rangle_{H^{-1}(D),H_0^1(D)}\\
&= -2\int_D \frac{\Psi}{\Phi^2}\nabla(\log\Phi)\cdot(\nabla\varphi - 2\varphi\nabla(\log\Phi))\\
&\leq \frac{2}{\underline{\Phi}^3}\|\Psi\|_{L^2(D)}\|\nabla\Phi\|_{L^\infty(D)}\left(\|\nabla\varphi\|_{L^2(D)} + \frac{2}{\underline{\Phi}}\|\nabla\Phi\|_{L^\infty(D)}\|\varphi\|_{L^2(D)}\right)\\
&\leq C\|\varphi\|_{H_0^1(D)}
\end{aligned}$$

and so $\frac{1}{\Phi^2}\nabla\cdot(2\Psi\nabla\log\Phi) \in H^{-1}(D)$. We also have

$$
\begin{aligned}
&\langle 2\nabla(\log\Phi)\cdot \mathrm{D}\tilde{a},\varphi\rangle_{\mathcal{D}'(D),\mathcal{D}(D)} = \langle \mathrm{D}\tilde{a}, 2\nabla(\log\Phi)\varphi\rangle_{H^{-1}(D),H^1_0(D)}\\
&= -2\int_D \tilde{a}\big(\varphi\triangle(\log\Phi)+\nabla(\log\Phi)\cdot\nabla\varphi\big)\\
&= -2\int_D \tilde{a}\left(a\varphi - \frac{|\nabla\Phi|^2}{\Phi^2}\varphi + \nabla(\log\Phi)\cdot\nabla\varphi\right)\\
&\leq 2\left\|\tilde{a}\right\|_{L^2(D)}\left(\overline{a}\left\|\varphi\right\|_{L^2(D)} + \frac{\left\|\nabla\Phi\right\|^2_{L^\infty(D)}}{\underline{\Phi}^2}\left\|\varphi\right\|_{L^2(D)} + \frac{\left\|\nabla\Phi\right\|_{L^\infty(D)}}{\underline{\Phi}}\left\|\nabla\varphi\right\|_{L^2(D)}\right)\\
&\leq C\left\|\varphi\right\|_{H^1_0(D)}
\end{aligned}
$$

and so $2\nabla(\log\Phi)\cdot\mathrm{D}\tilde{a}\in H^{-1}(D)$. Finally, since $\triangle\tilde{a}\in H^{-1}(D)$ and $\tilde{a}$ is smooth in a neighborhood of ∂D and satisfies $\tilde{a}|_{\partial D}=0$, it follows from the standard regularity theory that $\tilde{a}\in H^1_0(D)$. □

From the previous computation, it follows that $\tilde{a}$ is defined as the unique solution of

$$
\begin{cases}
\nabla\cdot(\Phi^2\nabla\tilde{a}) = \nabla\cdot(2\Psi\nabla\log\Phi) & \text{in } D,\\
\tilde{a}=0 & \text{on } \partial D.
\end{cases}
\tag{4.26}
$$

This system allows us to define an operator

$$
\begin{aligned}
\tilde{G}_\Psi : \mathcal{B}_s &\longrightarrow H^1_0(\Omega)\\
\Phi &\longmapsto \tilde{a}
\end{aligned}
\tag{4.27}
$$

and the one which gives a from Φ,

$$
\begin{aligned}
G_\Psi : \mathcal{B}_s &\longrightarrow H^s(\Omega)\\
\Phi &\longmapsto \begin{cases} a_0 + \tilde{G}_\Psi[\Phi] + \dfrac{\Psi}{\Phi^2} & \text{in } D,\\ a_0 & \text{in } \Omega\backslash\overline{D}. \end{cases}
\end{aligned}
\tag{4.28}
$$

The global problem that we have to solve now is to find a pair $(\tilde{a},\Phi)\in H^1(D)\times\mathcal{B}_s$ such that

$$
\begin{cases}
-\triangle\Phi + \left(a_0+\tilde{a}+\dfrac{\Psi}{\Phi^2}\mathbf{1}_D\right)\Phi = 0 & \text{in } \Omega,\\
\nabla\cdot(\Phi^2\nabla\tilde{a}) = \nabla\cdot(2\Psi\nabla\log\Phi) & \text{in } D,\\
l\partial_\nu\Phi+\Phi = g & \text{on } \partial\Omega,\\
\tilde{a}=0 & \text{on } \partial D,\\
\tilde{a}=0 & \text{in } \partial\Omega\backslash\overline{D}.
\end{cases}
$$

4.3.2 Fixed point algorithm

We look for a solution a as the fixed point of the map $G_\Psi \circ F : \mathcal{A}_s \longrightarrow H^s(\Omega)$. In order to cycle this operator, we introduce the truncation operator

$$\begin{aligned} T : H^s(\Omega) &\longrightarrow H^s(\Omega) \\ a &\longmapsto \max\left(\min(a, \overline{a}), \underline{a}\right) \end{aligned}$$

and look for a fixed point of the operator $T \circ G_\Psi \circ F : \mathcal{A}_s \longrightarrow H^s(\Omega)$.

Theorem 4.3.2 *Consider Ψ in $H^s(D)$. The operator $T \circ G_\Psi \circ F : \mathcal{A}_s \longrightarrow H^s(\Omega)$ is H^s-Lipschitz and, for any a, $a' \in \mathcal{A}$, we have*

$$\|T \circ G_\Psi \circ F\|_{Lip(H^s(\Omega))} \leq c(s, d, \Omega, \underline{\Phi}, \overline{\Phi}, R_{\mathcal{B}_s}) \, \|\Psi\|_{H^s(\Omega)}$$

and if $\|\Psi\|_{H^s(\Omega)}$ is small enough, $T \circ G_\Psi \circ F$ is a contraction from $\mathcal{A}_s$ into $\mathcal{A}_s$ and admits a unique fixed point in $\mathcal{A}_s$ called a_Ψ.

Proof. Reconsidering the Lipschitz estimate of the system 4.9 with $a \in H^s(\Omega)$ and taking into account that $H^{2+s}(\Omega)$ is embedded in $W^{1,\infty}(\Omega)$ we can deduce that $F : H^s(\Omega) \longrightarrow W^{1,\infty}(D)$ is Lipschitz and obtain that

$$\|F\|_{Lip(H^s(\Omega), W^{1,\infty}(D))} \leq c(s, d, \Omega) \left(R_{\mathcal{B}_s} + \overline{\Phi}\right).$$

Consider now Φ and Φ' in $\mathcal{B}_s$, then

$$|\nabla \log \Phi - \nabla \log \Phi'| \leq \frac{1}{\underline{\Phi}} |\nabla(\Phi - \Phi')| + \frac{|\nabla \Phi'|}{\underline{\Phi}^2} |\Phi - \Phi'|,$$

and so

$$\|\nabla \log \Phi - \nabla \log \Phi'\|_{L^\infty(\Omega)} \leq \frac{1}{\underline{\Phi}} \left(1 + \frac{R_{\mathcal{B}_s}}{\underline{\Phi}}\right) \|\Phi - \Phi'\|_{W^{1,\infty}(\Omega)}.$$

This inequality proves that $\tilde{G}_\Psi : \mathcal{B}_s \longrightarrow H_0^1(\Omega)$ is Lipschitz and that

$$\left\|\tilde{G}_\Psi\right\|_{Lip\left(W^{1,\infty}(D), H_0^1(\Omega)\right)} \leq \frac{1}{\underline{\Phi}^3} \left(1 + \frac{R_{\mathcal{B}_s}}{\underline{\Phi}}\right) \|\Psi\|_{L^2(D)}.$$

We can now control the Lipschitz norm of G_Ψ. Noticing that

$$\left\|\frac{1}{\Phi^2} - \frac{1}{\Phi'^2}\right\|_{W^{1,\infty}(D)} \leq \frac{1}{\underline{\Phi}^3} \left(2 + 3\frac{R_{\mathcal{B}_s}}{\underline{\Phi}} \left(\frac{\overline{\Phi}}{\underline{\Phi}}\right)^2\right) \|\Phi - \Phi'\|_{W^{1,\infty}(D)},$$

we get

$$\begin{aligned} \|G_\Psi \Phi - G_\Psi \Phi'\|_{H^s(\Omega)} &\leq \left\|\tilde{G}_\Psi \Phi - \tilde{G}_\Psi \Phi'\right\|_{H_0^1(\Omega)} + \|\Psi\|_{H^s(\Omega)} \left\|\frac{1}{\Phi^2} - \frac{1}{\Phi'^2}\right\|_{W^{1,\infty}(D)} \\ &\leq \frac{1}{\underline{\Phi}^3} \left[3 + 3\frac{R_{\mathcal{B}_s}}{\underline{\Phi}} \left(1 + \left(\frac{\overline{\Phi}}{\underline{\Phi}}\right)^2\right)\right] \|\Psi\|_{H^s(\Omega)} \|\Phi - \Phi'\|_{W^{1,\infty}(D)} \end{aligned}$$

and finally,

$$\|G_\Psi\|_{Lip(W^{1,\infty}(D),H^s(\Omega))} \leq \frac{1}{\underline{\Phi}^3}\left[3+3\frac{R_{\mathcal{B}_s}}{\underline{\Phi}}\left(1+\left(\frac{\overline{\Phi}}{\underline{\Phi}}\right)^2\right)\right]\|\Psi\|_{H^s(\Omega)}\,.$$

The truncation operator $T : H^s(\Omega) \longrightarrow H^s(\Omega)$ satisfies

$$\|T\|_{Lip(H^s(\Omega),H^s(\Omega))} = 1.$$

The proof is then complete. □

In the case of a contraction map, the iterative algorithm converges exponentially to the fixed point a_Ψ and yields a map

$$\begin{aligned} I : H^s(D) &\longrightarrow \mathcal{A}_s \\ \Psi &\longmapsto a_\Psi. \end{aligned}$$

From the Lipschitz continuity of $\tilde{G}_\Psi$ with respect to Ψ, the following stability result holds.

Proposition 4.3.3 *For all $\Psi, \Psi' \in H^s(D)$ such that $G_\Psi \circ F$ and $G_{\Psi'} \circ F$ are contractions, we have*

$$\|I[\Psi] - I[\Psi']\|_{H^s(D)} \leq C\|\Psi - \Psi'\|_{H^s(D)}$$

for some positive constant C.

Proof. Consider $\Psi, \Psi' \in H^s(D)$ such that $G_\Psi \circ F$ and $G_{\Psi'} \circ F$ are contractions and call a_Ψ and $a_{\Psi'}$ their fixed points. We have for any $\Phi \in \mathcal{B}_s$,

$$\|G_\Psi[\Phi] - G_{\Psi'}[\Phi]\|_{H^s(\Omega)} \leq \left\|\tilde{G}_\Psi[\Phi] - \tilde{G}_{\Psi'}[\Phi]\right\|_{H^s(\Omega)} + \left\|\frac{\Psi-\Psi'}{\Phi^2}\right\|_{H^s(\Omega)}.$$

Remarking that $u := G_\Psi[\Phi] - G_{\Psi'}[\Phi]$ satisfies

$$\begin{cases} \nabla\cdot(\Phi^2\nabla u) = 2\nabla\cdot[(\Psi-\Psi')\nabla\log\Phi] & \text{in } D, \\ u = 0 \quad \text{on } \partial D, \end{cases}$$

it follows that

$$\left\|\tilde{G}_\Psi[\Phi] - \tilde{G}_{\Psi'}[\Phi]\right\|_{H^s(\Omega)} \leq \frac{2R_{\mathcal{B}_s}}{\underline{\Phi}^3}\|\Psi-\Psi'\|_{L^2(\Omega)}$$

and so

$$\|G_\Psi[\Phi] - G_{\Psi'}[\Phi]\|_{H^s(\Omega)} \leq \frac{4R_{\mathcal{B}_s}}{\underline{\Phi}^3}\|\Psi-\Psi'\|_{H^s(\Omega)}\,.$$

We can now estimate

$$\begin{aligned}\|a_\Psi - a_{\Psi'}\|_{H^s(\Omega)} &= \|G_\Psi \circ F[a_\Psi] - G_{\Psi'} \circ F[a_{\Psi'}]\|_{H^s(\Omega)} \\ &\leq \|G_\Psi \circ F[a_\Psi] - G_{\Psi'} \circ F[a_\Psi]\|_{H^s(\Omega)} + \|G_{\Psi'} \circ F[a_\Psi] - G_{\Psi'} \circ F[a_{\Psi'}]\|_{H^s(\Omega)} \\ &\leq \|G_\Psi - G_{\Psi'}\|_{H^s(\Omega)} + \|G_{\Psi'} \circ F[a_\Psi] - G_{\Psi'} \circ F[a_{\Psi'}]\|_{H^s(\Omega)} \\ &\leq \frac{4R_{\mathcal{B}_s}}{\underline{\Phi}^3} \|\Psi - \Psi'\|_{H^s(\Omega)} + \|G_{\Psi'} \circ F\|_{Lip(H^s(\Omega))} \|a_\Psi - a_{\Psi'}\|_{H^s(\Omega)} .\end{aligned}$$

Let $\kappa := \|G_{\Psi'} \circ F\|_{Lip(H^s(\Omega))} < 1$. It follows that

$$\|a_\Psi - a_{\Psi'}\|_{H^s(\Omega)} \leq \frac{4R_{\mathcal{B}_s}}{\underline{\Phi}^3(1-\kappa)} \|\Psi - \Psi'\|_{H^s(\Omega)} ,$$

which completes the proof. □

4.4 Numerical simulations

In this section, we show how this new technique allows a very good reconstruction of highly discontinuous absorption map. We consider here a realistic absorption map taken from a blood vessels picture.

4.4.1 Forward problem

As we said in introduction, the main application of this acousto-optic method would be the imaging of red light absorption which has high contrast in tumors due to the high level of vascularization.

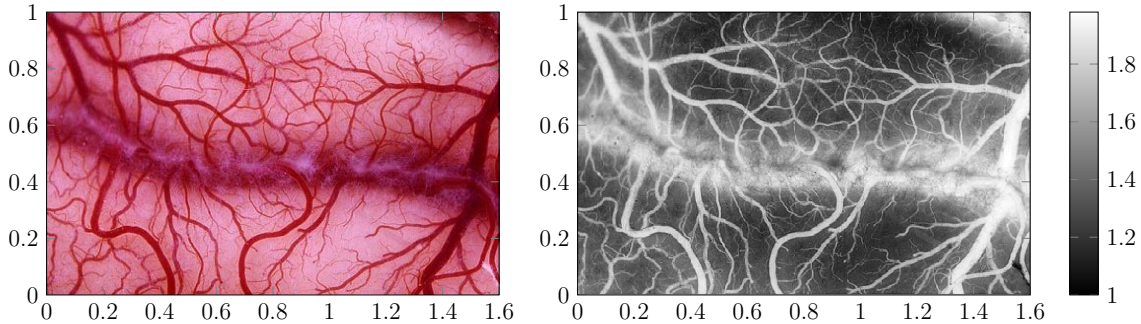

Figure 4.1: Realistic biological light absorption map. (1) A real picture of living membrane by transparency. (2) The absorption map chosen for the numerical experiments. The resolution is about 132k pixels.

In the following, the domain is fixed to $\Omega =]0, 1.6[\times]0, 1[$ and we consider the absorption map a given by Figure 4.1 (2). We define our domain D as a disk strictly included in Ω represented by the red circle in Figure 4.2.

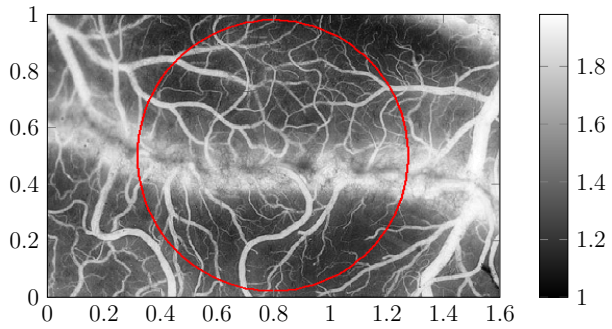

Figure 4.2: Absorption map in Ω and the domain of interest $D := D\big((0.8, 0.5), 0.48\big)$ in red.

Using the same method than for the numerical simulation in Chapter 2 we compute the forward problem in order to generate virtual measurements. For some centers y taken on $Y := \partial D$, $r > 0$ and $\eta = 10^{-4}$ fixed, we compute a discrete form of the map

$$v_{y,r,\eta}(x) = \frac{\eta}{r} w\left(\frac{|x-y| - r}{\eta}\right) \frac{x-y}{|x-y|},$$

where the wave shape w is defined by

$$w(t) = \begin{cases} \exp\left(\dfrac{1}{t^2-1}\right) & t \in]-1, 1[, \\ 0 & \text{otherwise.} \end{cases}$$

From this map, we compute the displaced absorption as $a_v = a \circ (Id + v)^{-1}$ and the variation of the fluence $\Phi_v - \Phi$. Its cross correlation on the boundary leads to the measurement

$$M_\eta(y, r) = \int_\Omega (a_{v_{y,r,\eta}} - a)\Phi\Phi_{v_{y,r,\eta}},$$

represented in Figure 4.3 (1). From that, we apply Theorems 4.2.1 and 4.2.9 to get an approximation of $\mathcal{R}[\Psi]$ up to a function depending only on y.

The non vertical visible lines on the illustration of $\mathcal{R}[\Psi]$ are due to the presences of blood vessels. The vertical lines are just numerical artifacts due to the integration. As we only need to know $\mathcal{R}[\Psi]$ up to a function depending only on y to theoretically reconstruct the absorption, this last numerical issue is not important. Now, from numerical spherical means Radon transform inversion, we compute the internal data map Ψ inside D.

As we can observe the blood vessels in the representation of the map Ψ, we shall confirm that there is a good information about the absorption map. If we try the algorithm presented in Chapter 2, we take the derivative of the data map Ψ in order to compute the source term $\triangle\Psi$ which destroys the information due to the numerical noise. It is even worse with additional measurement noise. Here, we use the fixed point algorithm proposed in Theorem 4.3.2. We compute the fixed point sequence $(a_n, \Phi_n)_{n\in\mathbb{N}}$ defined by

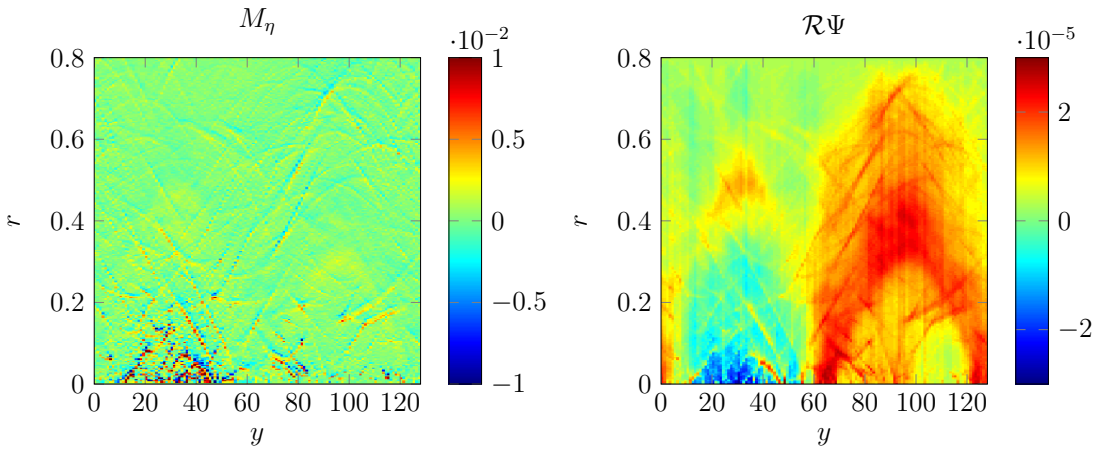

Figure 4.3: Computed measurement $M_\eta(y, r)$ and the deduced approximation of $\mathcal{R}[\Psi]$. We used 128 acoustic centers on ∂D.

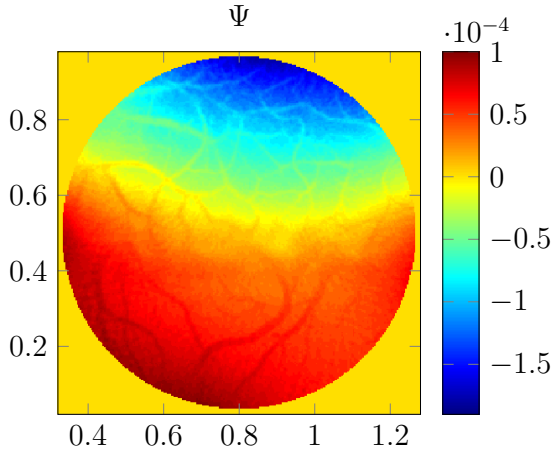

Figure 4.4: Internal data map Ψ computed inside the domain of interest D.

$$(a_0, \Phi_0) : \begin{cases} a_0 = 1 & \text{in } \Omega, \\ \Phi_0 : \begin{cases} -\triangle \Phi_0 + a_0 \Phi_0 = 0 & \text{in } \Omega, \\ l\partial_\nu \Phi_0 + \Phi_0 = g & \text{on } \partial\Omega, \end{cases} \end{cases}$$

and

$$\forall\, n \in \mathbb{N}, \qquad (a_{n+1}, \Phi_{n+1}) : \begin{cases} \tilde{a}_{n+1} : \begin{cases} \nabla \cdot (\Phi_n^2 \nabla \tilde{a}_{n+1}) = 2\nabla \cdot (\Psi \nabla \log \Phi_n) & \text{in } D, \\ \tilde{a}_{n+1} = -\dfrac{\Psi}{\Phi_n^2} & \text{on } \partial D, \end{cases} \\ a_{n+1} : \begin{cases} 1 + \dfrac{\Psi}{\Phi_n^2} + \tilde{a}_{n+1} & \text{in } D, \\ 1 \quad \text{in } \Omega \backslash \overline{D}, \end{cases} \\ \Phi_{n+1} : \begin{cases} -\triangle \Phi_{n+1} + a_n \Phi_{n+1} = 0 & \text{in } \Omega, \\ l\partial_\nu \Phi_{n+1} + \Phi_{n+1} = g & \text{on } \partial\Omega. \end{cases} \end{cases}$$

After few iterations of this sequence, we get a good reconstruction of the absorption map a. To fix the ideas, let us say that the variational information about a is in the map Ψ/Φ^2. We correct it with a smooth function $\tilde{a}$ in order to reach the map a. The difference of these two functions gives an approximation of $a - 1$ at each iteration.

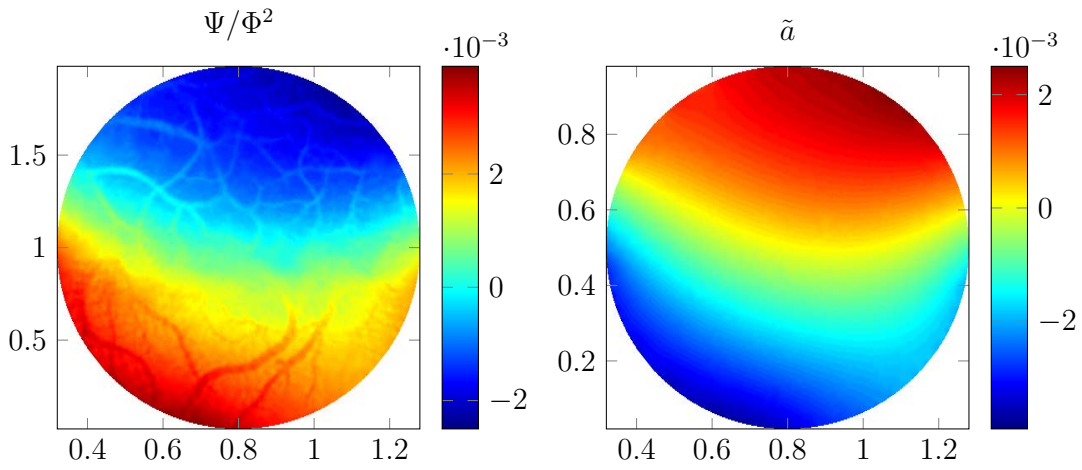

Figure 4.5: The map Ψ/Φ^2 where the blood vessels are visible and the map $\tilde{a}$ after 10 iterations of the fixed point algorithm.

Remark 4.4.1 *The power of this algorithm is that we avoid the derivation of the data map Ψ and we only solve elliptic equation for smooth solutions Φ_n and $\tilde{a}$. This provides a good reconstruction of the discontinuities of the absorption map a and illustrates the fixed point Theorem 4.3.2 which works for functions in $H^s(\Omega)$ with $s < 1/2$.*

Remark 4.4.2 *Our finest reconstruction is given in Figure 4.6 (4). Even if the vessels are easy to recognize, two problems occur. The first one is that the reconstructed solution is lightly attenuated. This is due to the approximation made using the asymptotic formula given in Theorem 4.2.9. A nice improvement would be to solve a deconvolution problem instead of the asymptotic formula. The second problem is the strong attenuation close to the boundary ∂D. This phenomenon is normal and is due to the fact that the measurements have no sense for small radius r. In the mathematical part, we have supposed that $a = a_0$*

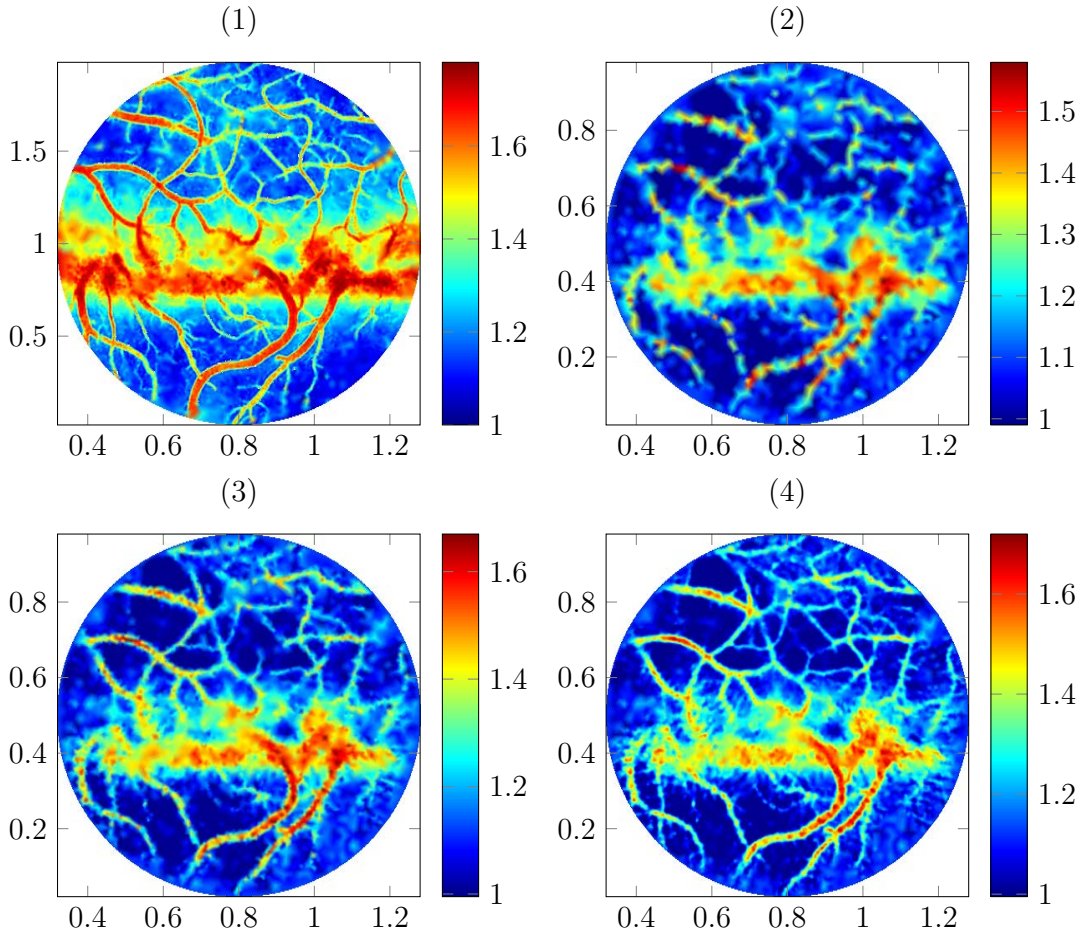

Figure 4.6: Reconstruction of the absorption map after 10 iterations of the fixed point sequence. (1) The true absorption. (2) Reconstruction using uniform mesh of 5k triangles. (3) Reconstruction with non uniform mesh of 13k triangles. (4) Reconstruction with non uniform mesh of 106k triangles.

in a neighborhood of ∂D. In this numerical example, this hypothesis is not respected and the consequence is that the reconstruction is not valid close to ∂D. Nevertheless, the inside part of the reconstruction is quite satisfying.

4.5 Concluding remarks

In this chapter we have introduced for the first time a mathematical and numerical framework for reconstructing highly discontinuous contrast distributions from internal measurements. The framework yields stable and accurate reconstructions. We have illustrated our approach on a highly discontinuous absorption map, chosen from a real biological tissue data. Many challenging problems are still open. It would be very interesting to develop an optimal control scheme for reconstructing highly discontinuous contrast distributions and prove its convergence, starting from a good initial guess. Another challenging problem is to estimate

the resolution of the developed approach in terms of the signal-to-noise ratio in the data.

4.6 Appendices

4.6.1 Spherical density of Da

Lemma 4.6.1 *Consider $a \in SBV^\infty(\Omega)$ constant out of the convex $< D \subset \Omega$ and the mollifier sequence $w_\eta(r) = \frac{1}{\eta} w\left(\frac{1}{\eta}\right)$. Suppose that Y satisfies the wrap condition around D, then the sequence of functions defined on Σ*

$$\varphi_\eta(y, r) = \int_\Omega w_\eta(|x - y| - r)|Da|(dx)$$

satisfies

$$\|\varphi_\eta\|_{L^2(\Sigma)} \leq C\eta^{-\frac{1}{2d}},$$

where C depends on $|Da|(\Omega)$, $|Y|$, and the wrap constant.

Proof. We develop $\|\varphi_\eta\|^2_{L^2(\Sigma)}$ norm as

$$\begin{aligned}
\|\varphi_\eta\|^2_{L^2(\Sigma)} &= \int_\Sigma \int_\Omega \int_\Omega w_\eta(|x - y| - r) w_\eta(|x' - y| - r)|\mathrm{D}a|(dx)|\mathrm{D}a|(dx')dydr \\
&= \int_Y \int_\Omega \int_\Omega \int_0^R w_\eta(|x - y| - r) w_\eta(|x' - y| - r)dr|\mathrm{D}a|(dx)|\mathrm{D}a|(dx')dy \\
&= \int_Y \int_\Omega \int_\Omega \overline{w}_\eta(|x - y| - |x' - y|)|\mathrm{D}a|(dx)|\mathrm{D}a|(dx')dy,
\end{aligned}$$

where

$$\overline{w}_\eta(r) = \int_{\mathbb{R}} w_\eta(r - \rho) w_\eta(-\rho)d\rho$$

satisfies $\mathrm{supp}(\overline{w}_\eta) \subset [-2\eta, 2\eta]$, $\|\overline{w}_\eta\|_{L^1(\mathbb{R})} \leq 1$ and $\overline{w}_\eta \leq \frac{1}{\eta}$. Let us fix $\varepsilon > 0$ and define $Z_\varepsilon = \{(x, x') \in \Omega^2,\ |x - x'| \leq \varepsilon\}$. First, we have

$$\begin{aligned}
\int_Y \int_{Z_\varepsilon} \overline{w}_\eta(|x - y| - |x' - y|)|\mathrm{D}a|(dx)|\mathrm{D}a|(dx')dy &\leq \frac{1}{\eta}|Y| \int_\Omega \int_{B(x,\varepsilon)} |\mathrm{D}a|(dx')|\mathrm{D}a|(dx) \\
&\leq \frac{1}{\eta}|Y| \int_\Omega |\mathrm{D}a|(B(x, \varepsilon))|\mathrm{D}a|(dx).
\end{aligned}$$

Using the fact that $a \in SBV^\infty(\Omega)$, the Radon measure $|\mathrm{D}a|$ can be decomposed as

$$|\mathrm{D}a| = |\nabla_l a|\mathcal{L}^d + |[a]_S|\mathcal{H}^{d-1}_S,$$

where $|\nabla_l a| \in L^\infty(\Omega)$ and $|[a]_S| \in L^\infty(S)$. Thus, we can control the upper (d-1)-densities of $|\mathrm{D}a|$ using that for any $x \in \Omega'$

$$\frac{1}{\varepsilon^{d-1}}|\mathrm{D}a|(B(x,\varepsilon)) \leq \|\nabla_l a\|_{L^\infty(\Omega)}\,\omega^d\varepsilon + \|[A]_S\|_{L^\infty(S)}\,\frac{1}{\varepsilon^{d-1}}\mathcal{H}^{d-1}(S\cap B(x,\varepsilon)).$$

In fact, [**?**, Theorem 6.2] says that for any $x \in S$,

$$\limsup_{\varepsilon\to 0}\frac{1}{\varepsilon^{d-1}}\mathcal{H}^{d-1}(S\cap B(x,\varepsilon)) \leq 2^{d-1} \qquad a.e.\ \text{ on } S,$$
$$\limsup_{\varepsilon\to 0}\frac{1}{\varepsilon^{d-1}}\mathcal{H}^{d-1}(S\cap B(x,\varepsilon)) = 0 \qquad a.e.\ \text{ on } \Omega'\backslash S,$$

which implies for $|\mathrm{D}a|$ that

$$\limsup_{\varepsilon\to 0}\frac{1}{\varepsilon^{d-1}}|\mathrm{D}a|(B(x,\varepsilon)) \leq \|[A]_S\|_{L^\infty(S)}\,2^{d-1} \qquad a.e.\ \text{ on } S,$$
$$\limsup_{\varepsilon\to 0}\frac{1}{\varepsilon^{d-1}}|\mathrm{D}a|(B(x,\varepsilon)) = 0 \qquad a.e.\ \text{ on } \Omega'\backslash S.$$

Using Fatou lemma, it follows that

$$\begin{aligned}\limsup_{\varepsilon\to 0}\int_{\Omega'}\frac{1}{\varepsilon^{d-1}}|\mathrm{D}a|(B(x,\varepsilon))|\mathrm{D}a|(dx) &\leq \int_{\Omega'}\limsup_{\varepsilon\to 0}\frac{1}{\varepsilon^{d-1}}|\mathrm{D}a|(B(x,\varepsilon))|\mathrm{D}a|(dx)\\ &\leq \|[A]_S\|_{L^\infty(S)}\,2^{d-1}\mathcal{H}^{d-1}(S).\end{aligned}$$

That simply shows that the left-hand integral is bounded when ε goes to zero. We finally arrive at

$$\int_Y\int_{Z_\varepsilon}\overline{w}_\eta(|x-y|-|x'-y|)|\mathrm{D}a|(dx)|\mathrm{D}a|(dx')dy \leq C_1\frac{\varepsilon^{d-1}}{\eta}, \tag{4.29}$$

where the constant C_1 depends on $|\mathrm{D}a|(\Omega)$ and $|Y|$. The second integral that we have to control is

$$\int_Y\int_{\Omega'^2\backslash Z_\varepsilon}\overline{w}_\eta(|x-y|-|x'-y|)|\mathrm{D}a|(dx)|\mathrm{D}a|(dx')dy.$$

For that, we define for any $(x,x') \in \Omega^2$ the set

$$Y_\eta(x,x') = \{y\in Y,\ ||x-y|-|x'-y|| \leq 2\eta\}.$$

As Y satisfies the wrap condition around Ω', a computation leads to

$$\mathcal{H}^{d-1}\left(Y_\eta(x,x')\right) \leq 2C_2\frac{\eta}{\varepsilon} \quad \forall\,(x,x') \in \Omega'^2\backslash Z_\varepsilon,$$

where C_2 is the wrap constant relative to Y and Ω'. We can now control the second term,

$$\begin{aligned}\int_Y\int_{\Omega'^2\backslash Z_\varepsilon}\overline{w}_\eta(|x-y|-|x'-y|)|\mathrm{D}a|(dx)|\mathrm{D}a|(dx')dy &\leq \frac{1}{\eta}\int_{\Omega'^2}\mathcal{H}^{d-1}\left(Y_\eta(x,x')\right)|\mathrm{D}a|(dx)|\mathrm{D}a|(dx')\\ &\leq \frac{C_2}{\varepsilon}|\mathrm{D}a|(\Omega)^2.\end{aligned} \tag{4.30}$$

Finally, putting together (4.29) and (4.30), we obtain

$$\|\varphi_\eta\|^2_{L^2(\Sigma)} \leq C_1\frac{\varepsilon^{d-1}}{\eta} + 2\frac{C_2}{\varepsilon}|\mathrm{D}a|(\Omega)^2,$$

which is true for any choice of $\varepsilon > 0$. So, we fix it at the best choice $\varepsilon = \eta^{1/d}$ to obtain

$$\|\varphi_\eta\|^2_{L^2(\Sigma)} \leq (C_1 + 2C_2|\mathrm{D}a|(\Omega)^2)\eta^{-\frac{1}{d}},$$

which concludes the proof. □

4.6.2 Sobolev spaces with fractional order and Helmholtz decomposition

On the smooth open domain D of $\mathbb{R}^d$, for any $\alpha \geq 0$ the Sobolev space $H^\alpha(D)$ is defined as usual. We shall also consider the space of functions of $H^\alpha(D)$ supported in a compact K denoted $H^\alpha_K(D)$. As the functions of $H^\alpha_K(D)$ can be extended by zero outside of D, we can define their Fourier transform and use the following characterization,

Definition 4.6.1 *For any $\alpha \geq 0$, $K \subset D$ compact we define*

$$H^\alpha_K(D) = \left\{ f \in L^2(D),\ supp(u) \subset K,\ \int_{\mathbb{R}^d} |\widehat{u}|^2(\xi)(1+|\xi|^2)^\alpha d\xi < +\infty \right\}$$

and for any $f \in H^\alpha_K(D)$ we will denote

$$\|f\|_{H^\alpha(D)} = \left(\frac{1}{(2\pi)^d} \int_{\mathbb{R}^d} |\widehat{u}|^2(\xi)(1+|\xi|^2)^\alpha d\xi \right)^{\frac{1}{2}}.$$

We define now $H^{-\alpha}_K(D)$ by duality.

Definition 4.6.2 *For any $\alpha > 0$, $K \subset D$ compact we define*

$$H^{-\alpha}_K(D) = \{u \in H^\alpha(D)',\ supp(u) \subset K\}$$

endowed with the continuity norm.

Fortunately, these spaces have also a Fourier characterization. For any $u \in H^{-\alpha}_K(D)$, u is a compact supported distribution i.e. an element of $\mathcal{E}'(D)$ which naturally embeds in $\mathcal{S}'(\mathbb{R}^d)$. So the Fourier transform $\widehat{u}$ is defined in $\mathcal{S}'(\mathbb{R}^d)$.

Proposition 4.6.2 *For any $\alpha > 0$, $K \subset D$ compact,*

$$H^{-\alpha}_K(D) = \left\{ u \in \mathcal{E}'(D),\ supp(u) \subset K,\ \widehat{u} \in L^1_{loc}\big(\mathbb{R}^d\big),\ \int_{\mathbb{R}^d} |\widehat{u}|^2(\xi)(1+|\xi|^2)^{-\alpha} d\xi < +\infty \right\}$$

Proof. Let us take $u \in H^{-\alpha}_K(D)$. As $u \in \mathcal{S}'(R^d)$, we take $\widehat{u} \in \mathcal{S}'(\mathbb{R}^d)$, $\varphi \in \mathcal{S}'(\mathbb{R}^d)$ and we compute

$$\begin{aligned}
\left| \left\langle (1+|\xi|^2)^{-\alpha/2}\widehat{u}, \varphi \right\rangle_{\mathcal{S}'(\mathbb{R}^d),\mathcal{S}(\mathbb{R}^d)} \right| &= \left| \left\langle u, [\widehat{(1+|x|^2)^{-\alpha/2}\varphi}] \right\rangle_{\mathcal{S}'(\mathbb{R}^d),\mathcal{S}(\mathbb{R}^d)} \right| \\
&\leq \|u\|_{H^\alpha(D)'} \left\| [\widehat{(1+|x|^2)^{-\alpha/2}\varphi}] \right\|_{H^\alpha(D)} \\
&\leq (2\pi)^{d/2} \|u\|_{H^\alpha(D)'} \|\varphi\|_{L^2(D)},
\end{aligned}$$

which proves that $(1+|\xi|^2)^{-\alpha/2}\widehat{u} \in L^2(\mathbb{R}^d)$ and

$$\left(\frac{1}{(2\pi)^d}\int_{\mathbb{R}^d} |\widehat{u}|^2(\xi)(1+|\xi|^2)^{-\alpha}d\xi\right)^{1/2} \leq \|u\|_{H^\alpha(D)'}.$$

Conversely, if u satisfies these conditions, we show that it is in $H^\alpha(D)'$ and that

$$\|u\|_{H^\alpha(D)'} \leq \left(\frac{1}{(2\pi)^d}\int_{\mathbb{R}^d} |\widehat{u}|^2(\xi)(1+|\xi|^2)^{-\alpha}d\xi\right)^{1/2}.$$

Then the proof is complete. □

We can now define the Helmholtz decomposition of a distribution vectorial field in the Sobolev sense for fractional order greater than -1. This allows to precise the regularity of Ψ depending on the regularity of a.

4.6.3 Kernel operators in Sobolev spaces of fractional order

In this appendix, we give two useful results about some kernel operators acting on one variable of a function. These results are given for functions defined in $\mathbb{R}^d$ in order to use the Fourier transform. They stay valid for functions defined on any manifold isomorphic to an open domain of $\mathbb{R}^d$ up to a multiplicative constant depending on the isomorphism.

Lemma 4.6.3 *Consider a kernel $\theta \in L^2(\mathbb{R}^2)$ and the operator $T : L^2(\mathbb{R}^d) \longrightarrow L^2(\mathbb{R}^d)$ defined by*

$$T[f](x) = \int_{\mathbb{R}} f(t,\tilde{x})\theta(t,x_1)dt$$

for a.e. $x \in \mathbb{R}^d$ with $\tilde{x} = (x_2,\ldots,x_d)$. If, for $s>0$, $f \in H^s(\mathbb{R}^d)$ and $\theta \in H^s(\mathbb{R}^2)$, then $T[f] \in H^s(\mathbb{R}^d)$ and we have

$$\|T[f]\|_{H^s(\mathbb{R}^d)} \leq \|\theta\|_{H^s(\mathbb{R}^2)} \|f\|_{H^s(\mathbb{R}^d)}.$$

Proof. Let us compute the Fourier transform of $T[f]$,

$$\begin{aligned}\widehat{T[f]}(\xi) &= \int_{\mathbb{R}}\int_{\mathbb{R}}\int_{\mathbb{R}^{d-1}} f(t,\tilde{x})\theta(t,x_1)e^{-ix_1\xi_1}e^{-i\tilde{x}\cdot\tilde{\xi}}d\tilde{x}dx_1dt \\ &= \int_{\mathbb{R}} \overset{\tilde{x}}{\widehat{f}}(t,\tilde{\xi})\overset{x_1}{\widehat{\theta}}(t,\xi_1)dt\end{aligned}$$

so

$$|\widehat{T[f]}|^2(\xi) \leq \int_{\mathbb{R}} |\overset{\tilde{x}}{\widehat{f}}(t,\tilde{\xi})|^2dt \int_{\mathbb{R}} |\overset{x_1}{\widehat{\theta}}(t,\xi_1)|^2dt.$$

Then, using Plancherel theorem,

$$\int_{\mathbb{R}} |\overset{\tilde{x}}{\widehat{f}}(t,\tilde{\xi})|^2dt = \frac{1}{2\pi}\int_{\mathbb{R}} |\widehat{f}(\xi)|^2d\xi_1$$

and

$$\int_{\mathbb{R}} |\widehat{\theta}^{x_1}(t,\xi_1)|^2 dt = \frac{1}{2\pi}\int_{\mathbb{R}} |\widehat{\theta}(\tau,\xi_1)|^2 d\tau.$$

Hence,

$$|\widehat{T[f]}|^2(\xi) \leq \frac{1}{(2\pi)^2}\int_{\mathbb{R}} |\widehat{f}(\xi)|^2 d\xi_1 \int_{\mathbb{R}} |\widehat{\theta}(\tau,\xi_1)|^2 d\tau$$

$$|\widehat{T[f]}|^2(\xi)\left(1+|\xi|^2\right)^s \leq \frac{1}{(2\pi)^2}\int_{\mathbb{R}} |\widehat{f}(\xi)|^2\left(1+|\tilde{\xi}|^2\right)^s d\xi_1 \int_{\mathbb{R}} |\widehat{\theta}(\tau,\xi_1)|^2\left(1+\xi_1^2\right)^s d\tau$$

$$\frac{1}{(2\pi)^d}\int_{\mathbb{R}^d} |\widehat{T[f]}|^2(\xi)\left(1+|\xi|^2\right)^s d\xi \leq$$

$$\frac{1}{(2\pi)^d}\int_{\mathbb{R}^d} |\widehat{f}(\xi)|^2\left(1+|\xi|^2\right)^s d\xi \frac{1}{(2\pi)^2}\int_{\mathbb{R}^2} |\widehat{\theta}(\tau,\xi_1)|^2\left(1+\xi_1^2+\tau^2\right)^s d\tau d\xi_1,$$

which completes the proof. □

In the case where the kernel is approaching a delta function, it is useful to understand how the operator is approaching the identity.

Lemma 4.6.4 *Consider $w \in \mathcal{C}_c^\infty(\mathbb{R})$ supported in $[-1,1]$, non negative and satisfying $\|w\|_{L^1(\mathbb{R})} = 1$. For any $\eta > 0$, $t \in \mathbb{R}$ we denote $w_\eta(t) = \frac{1}{\eta} w\left(\frac{t}{\eta}\right)$. Let us consider the sequence of operator $T_\eta : L^2(\mathbb{R}^d) \longrightarrow L^2(\mathbb{R}^d)$ defined by*

$$T_\eta[f](x) = \int_{\mathbb{R}} f(t,\tilde{x}) w_\eta(x_1 - t) dt.$$

For all $\alpha \geq 0$ and $\eta > 0$, T_η is continuous operator $T_\eta : H^\alpha(\mathbb{R}^d) \longrightarrow H^\alpha(\mathbb{R}^d)$ and for all $\beta > 0$, $f \in H^{\alpha+\beta}(\mathbb{R}^d)$, $T_\eta[f]$ converges to f in $H^\alpha(\mathbb{R}^d)$. More precisely,

$$\|T_\eta[f] - f\|_{(H^\alpha(\mathbb{R}^d)} \leq 2\eta^{\frac{\beta}{\beta+1}} \|f\|_{H^{\alpha+\beta}(\mathbb{R}^d)}.$$

Proof. Let us compute the Fourier transform of $T[f]$,

$$\begin{aligned}
\widehat{T[f]}(\xi) &= \int_{\mathbb{R}}\int_{\mathbb{R}}\int_{\mathbb{R}^{d-1}} f(t,\tilde{x}) w_\eta(x_1 - t) e^{-ix_1\xi_1} e^{-i\tilde{x}\cdot\tilde{\xi}} d\tilde{x} dx_1 dt \\
&= \int_{\mathbb{R}}\int_{\mathbb{R}}\int_{\mathbb{R}^{d-1}} f(t,\tilde{x}) w_\eta(u) e^{-iu\xi_1} e^{-it\xi_1} e^{-i\tilde{x}\cdot\tilde{\xi}} d\tilde{x} du dt \\
&= \widehat{f}(\xi)\widehat{w_\eta}(\xi_1),
\end{aligned}$$

where $\widehat{w_\eta} \leq 1$. This proves that $\|T_\eta[f]\|_{H^\alpha(\mathbb{R}^d)} \leq \|f\|_{H^\alpha(\mathbb{R}^d)}$. Now consider $\beta > 0$ and $f \in H^{\alpha+\beta}(\mathbb{R}^d)$, we have

$$\left(\widehat{T[f]} - \widehat{f}\right)(\xi) = f(\xi)\int_{\mathbb{R}} w_\eta(t)(e^{-it\xi 1} - 1) dt,$$

$$\left|\widehat{T_\eta[f]} - \widehat{f}\right|^2(\xi) \leq |\widehat{f}|^2(\xi)\int_{\mathbb{R}} w_\eta(t)|e^{-it\xi_1} - 1|^2 dt$$

by convexity, and we write,

$$\left|\widehat{T_\eta[f]} - \widehat{f}\right|^2(\xi) = |\widehat{f}|^2(\xi) \sup_{|t|\leq\eta} |e^{-it\xi_1} - 1|^2.$$

A study of the function $\xi_1 \mapsto \sup_{|z|\leq\eta} |e^{-iz\xi_1} - 1|^2$ gives us that

$$\sup_{|t|\leq\eta} |e^{-it\xi_1} - 1|^2 \leq 4\eta^{\frac{2\beta}{\beta+1}} \left(1 + |\xi|^2\right)^\beta,$$

and we finally get

$$\int_{\mathbb{R}^d} \left|\widehat{T_\eta[f]} - \widehat{f}\right|^2(\xi) \left(1 + |\xi|^2\right)^\alpha d\xi \leq 4\eta^{\frac{2\beta}{\beta+1}} \int_{\mathbb{R}^d} |\widehat{f}|^2(\xi) \left(1 + |\xi|^2\right)^{\alpha+\beta} d\xi,$$

which is equivalent to

$$\|T_\eta[f] - f\|_{H^\alpha(\mathbb{R}^d)} \leq 2\eta^{\frac{\beta}{\beta+1}} \|f\|_{H^{\alpha+\beta}(\mathbb{R}^d)}.$$

Hence, the proof is complete. □

Chapter 5

Acoustically induced Lorentz force electric impedance tomography

Introduction

Ultrasonic imaging is currently used in a wide range of medical diagnostic applications. Its high spatial resolution, combined with a real-time imaging capability, lack of side effects, and relatively low cost make it an attractive technique. However, it can be difficult to differentiate soft tissues because acoustic impedance varies by less than 10% among muscle, fat, and blood [62]. In contrast, electrical conductivity varies widely among soft tissue types and pathological states [56, 88] and its measurement can provide information about the physiological and pathological condition of tissue [16]. Several techniques have been developed to map electrical conductivity. The most well known is electrical impedance tomography, in which electrodes are placed around the organ of interest, a voltage difference is applied, and the conductivity distribution can be reconstructed from the measurement of the induced current at the electrodes [3, 24, 45]. This technique is harmless to the patient if low currents are used. However, the ill-posed character of the inverse problem results in lower spatial resolution than that achieved by ultrasound imaging, and any speckle information is lost.

The Lorentz force plays a key role in acousto-magnetic tomographic techniques [99]. Several approaches have been developed with the aim of providing electrical impedance information at a spatial resolution on the scale of ultrasound wavelengths [14, 63, 78, 84, 87, 99, 100, 109]. These include Hall effect imaging, magneto-acoustic current imaging, magneto-acoustic tomography with magnetic induction, and ultrasonically-induced Lorentz force imaging. Acousto-magnetic tomographic techniques have the potential to detect small conductivity inhomogeneities, enabling them to diagnose pathologies such as cancer by detecting tumorous tissues when other conductivity imaging techniques fail to do so.

In ultrasonically-induced Lorentz force method (experimental apparatus presented in Figure 5.1) an ultrasound pulse propagates through the medium to be imaged in the presence of a static magnetic field. The ultrasonic wave induces Lorentz' force on the ions in the medium, causing the negatively and positively charged ions to separate. This separation of charges acts as a source of electrical current and potential. Measurements of the induced current give information on the conductivity in the medium. A 1 *Tesla* magnetic field and a 1 *MPa* ultrasonic pulse induce current at the *nanoampere* scale. Stronger magnetic fields

and ultrasonic beams can be used to enhance the signal-to-noise ratio [63].

This chapter provides a rigorous mathematical and numerical framework for ultrasonically-induced Lorentz force electrical impedance tomography. We develop two efficient methods for reconstructing the conductivity in the medium from the induced electrical current. As far as we know, this is the first mathematical and numerical modeling of the experiment conducted in [63] to illustrate the feasibility of ultrasonically-induced Lorentz force electrical impedance tomography. Earlier attempts to model mathematically this technique were made in [14, 74]. The ultrasonically-induced Lorentz force electrical impedance tomography investigated here can be viewed as a new hybrid technique for conductivity imaging. It has been experimentally tested [63], and was reported to produce images of quality comparable to those of ultrasound images taken under similar conditions.

The chapter is organized as follows. We start by describing the ionic model of conductivity. From this model we derive the current density induced by an ultrasonic pulse in the presence of a static magnetic field. We then find an expression of the measured current. The inverse problem is to image the conductivity distribution from such measurements corresponding to different pulse sources and directions. A virtual potential used with simple integrations by parts can relate the measured current to the conductivity distribution and the velocity of the ultrasonic pulse. A Wiener deconvolution filter can then reduce the problem to imaging the conductivity from the internal electric current density. The internal electric current density corresponds to that which would be induced by a constant voltage difference between one electrode and another with zero potential. We introduce two reconstruction schemes for solving the imaging problem from the internal data. The first is an optimal control method; we also propose an alternative to this scheme via the use of a transport equation satisfied by the internal current density. The second algorithm is direct and can be viewed as a PDE-based reconstruction scheme. We prove that solving such a PDE yields to the true conductivity distribution as the regularization parameter tends to zero. In doing so, we prove the existence of the characteristic lines for the transport equation under some conditions on the conductivity distribution. We finally test numerically the two proposed schemes in the presence of measurement noise, and also quantify their stability and resolution.

5.1 Electric measurements from acousto-magnetic coupling

Let a physical object to be imaged occupy a three-dimensional domain Ω with a smooth boundary $\partial\Omega$. Assume that this body is placed in a constant magnetic field B in the direction e_3 where $\{e_1, e_2, e_3\}$ denotes the standard orthonormal basis of $\mathbb{R}^3$. We are interested in recovering the electrical conductivity of this body $\sigma \in L^\infty(\Omega)$ with the known lower and upper bounds:

$$0 < \underline{\sigma} \leq \sigma \leq \overline{\sigma} < \infty.$$

An acoustic transducer sends a short acoustic pulse from $y \in \mathbb{R}^3$ in the direction $\xi \in S^2$, with S^2 being the unit sphere, such that $\xi \cdot e_3 = 0$. This pulse generates the velocity field $v(x,t)\xi$ with $v(x,t)$ taking the following form:

$$v(x,t) = w\big(z - ct\big)\ A\big(z, |r|\big), \tag{5.1}$$

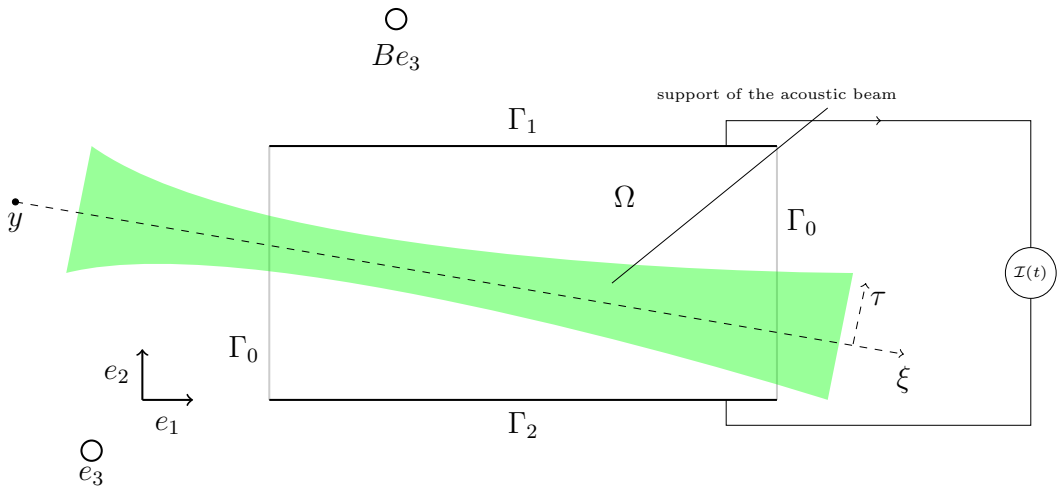

Figure 5.1: Basic experiment scheme. An acoustic transducer in y sends focal acoustic pulses in the direction ξ. While the pulse is traveling in the electrolytic medium embedded in a constant magnetic field Be_3, a small current is detected and measured in the wire between the two electrodes Γ_1 and Γ_2.

where

$$z = (x-y)\cdot\xi \quad \text{and} \quad r = x - y - z\xi \ \in \Upsilon_\xi := \{\zeta \in \mathbb{R}^3 \ : \ \zeta\cdot\xi = 0\}.$$

Here, $w \in \mathcal{C}_c^\infty(\mathbb{R})$, supported in $]-\eta, 0[$, is the ultrasonic pulse profile; $A \in \mathcal{C}^\infty(\mathbb{R}\times\mathbb{R}^+)$, supported in $\mathbb{R}^+ \times [0, R]$, is the cylindrical profile distribution of the wave corresponding to the focus of the acoustic transducer; and R is the maximal radius of the acoustic beam.

5.1.1 The ionic model of conductivity

We describe here the electrical behavior of the medium as an electrolytic tissue composed of ions capable of motion in an aqueous tissue. We consider k types of ions in the medium with charges of q_i, $i \in \{1, \dots, k\}$. The corresponding volumetric density n_i is assumed to be constant. Neutrality in the medium is described as

$$\sum_i q_i n_i = 0. \tag{5.2}$$

The Kohlrausch law defines the conductivity of such a medium as a linear combination of the ionic concentrations

$$\sigma = e^+ \sum_i \mu_i q_i n_i, \tag{5.3}$$

where e^+ is the elementary charge, and the coefficients μ_i denote the ionic mobility of each ion i; see, for example, [87, 95].

5.1.2 Ion deviation by Lorentz force

We embed the medium in a constant magnetic field B with direction e_3, and perturb it mechanically using the short, focused, ultrasonic pulses v defined in (5.1). The motion of the charged particle i inside the medium is deviated by the Lorentz force

$$F_i = q_i v\xi \times B. \tag{5.4}$$

This force accelerates the ion in the orthogonal direction $\tau = \xi \times e_3$. Then, almost immediately, the ion reaches a constant speed given by

$$v_{\tau,i} = \mu_i |B| v$$

at the first order; see [87, 95] for more details. Finally, the ion i has a total velocity

$$v_i = v\xi + \mu_i |B| v\tau.$$

The current density generated by the displacement of charges can be described as follows:

$$j_S = \sum_i n_i q_i v_i = \left(\sum_i n_i q_i \right) v\xi + \left(\sum_i n_i \mu_i q_i \right) |B| v\tau.$$

Using the neutrality condition (5.2) and the definition of σ in (5.3), we get the following simple formula for j_S:

$$j_S = \frac{1}{e^+} |B| \sigma v \tau, \tag{5.5}$$

which is in accordance with the formula used in [14].

This electrolytic description of the tissue characterizes the interaction between the ultrasonic pulse and the magnetic field through a small deviation of the charged particles embedded in the tissue. This deviation generates a current density j_S orthogonal to ξ and to B, locally supported inside the domain. At a fixed time t, j_S is supported in the support of $x \mapsto v(x,t)$. This current is proportional to σ, and is the source of the current that we measure on the electrodes placed at $\partial\Omega$. In the next section, a formal link is substantiated between j_S and the measured current I.

5.1.3 Internal electrical potential

Because the characteristic time of the acoustic propagation is very long compared with the electromagnetic wave propagation characteristic time, we can adopt the electrostatic frame. Consequently, the total current j in Ω at a fixed time t can be formulated as

$$j = j_S + \sigma \nabla u, \tag{5.6}$$

where u is the electrical potential. It satisfies

$$\nabla \cdot (j_S + \sigma \nabla u) = \nabla \cdot j = 0. \tag{5.7}$$

Figure 5.2 shows the configuration under consideration. Let Γ_1 and Γ_2 be portions of the boundary $\partial\Omega$ where two planner electrodes are placed. Denote $\Gamma_0 = \partial\Omega \setminus (\Gamma_1 \cup \Gamma_2)$.

Figure 5.2: Imaging system configuration. An ultrasonic wave propagates in a medium of electrical conductivity σ comprised between electrodes Γ_1 and Γ_2.

As we measure the current between the two electrodes Γ_1 and Γ_2, the electrical potential is the same on both electrodes, and can be fixed to zero without loss of generality. Further, it is assumed that no current can leave from Γ_0. The potential u can then be defined as the unique solution in $H^1(\Omega)$ of the elliptic system

$$\begin{cases} -\nabla \cdot (\sigma \nabla u) = \nabla \cdot j_S & \text{in } \Omega, \\ u = 0 & \text{on } \Gamma_1 \cup \Gamma_2, \\ \partial_\nu u = 0 & \text{on } \Gamma_0. \end{cases} \tag{5.8}$$

Throughout this chapter ∂_ν denotes the normal derivative. Note that the source term j_S depends on the time $t > 0$, the position of the acoustic transducer $y \in \mathbb{R}^3$, and the direction $\xi \in S^2$. The electrical potential u also depends on these variables.

The measurable intensity I is the current flow through the electrodes. Integrating (5.8) by parts gives

$$\int_{\Gamma_1} \sigma \partial_\nu u + \int_{\Gamma_2} \sigma \partial_\nu u = 0,$$

which is the expression of current flow conservation. We define the intensity I by

$$I = \int_{\Gamma_2} \sigma \partial_\nu u. \tag{5.9}$$

5.1.4 Virtual potential

In order to link I to σ, we introduce a virtual potential $U \in H^1(\Omega)$ defined as the unique solution of

$$\begin{cases} -\nabla \cdot (\sigma \nabla U) = 0 & \text{in } \Omega, \\ U = 0 & \text{on } \Gamma_1, \\ U = 1 & \text{on } \Gamma_2, \\ \partial_\nu U = 0 & \text{on } \Gamma_0. \end{cases} \tag{5.10}$$

Then we multiply (5.8) by U and integrate by parts. Assuming that the support of v does not intersect the electrodes Γ_1 and Γ_2, we obtain

$$-\int_\Omega \sigma \nabla u \cdot \nabla U + \int_{\Gamma_2} \sigma \partial_\nu u = \int_\Omega j_S \cdot \nabla U.$$

From the property of U in (5.10) and the definition of I in (5.9), the above identity becomes

$$I = \int_\Omega j_S \cdot \nabla U.$$

The above identity links the measured intensity I to an internal information of σ using the expression of j_S in (5.5):

$$I = \frac{|B|}{e^+} \int_\Omega v(x,t)\sigma(x)\nabla U(x)dx \cdot \tau.$$

According to (5.1), v depends on y, ξ, and t, so does I. We define the measurement function as

$$M_{y,\xi}(z) = \int_\Omega v(x, z/c)\sigma(x)\nabla U(x)dx \cdot \tau(\xi) \tag{5.11}$$

for any $y \in \mathbb{R}^3$, $\xi \in S^2$ and $z > 0$. We assume the knowledge of this function in a certain subset of $\mathbb{R}^3 \times S^2 \times \mathbb{R}^+$ denoted by $Y \times \mathfrak{S} \times]0, z_{max}[$. We will discuss later the assumptions we have to impose on this subset in order to make the reconstruction accurate and stable.

5.2 Construction of the virtual current

For simplicity, let us restrict ourselves to the two dimensional case where both the conductivity σ and the virtual potential U do not change in e_3-direction. For convenience, the same notations will be used as in the three dimensional case.

In order to obtain the information of σ contained in $M_{y,\xi}$, we need to separate the contribution of the displacement term v from this measurement function. Using the cylindrical symmetry of this integration we write for any $z \in]0, z_{max}[$,

$$\begin{aligned} M_{y,\xi}(z) &= \int_{\mathbb{R}} \int_{\Upsilon_\xi} w(z - z')(\sigma\nabla U)(y + z'\xi + r)A(z', |r|)drdz' \cdot \tau(\xi), \\ &= \int_{\mathbb{R}} w(z - z') \int_{\Upsilon_\xi} (\sigma\nabla U)(y + z'\xi + r)A(z', |r|)drdz' \cdot \tau(\xi), \\ &= \left(W \star \Phi_{y,\xi}\right)(z) \cdot \tau(\xi), \end{aligned} \tag{5.12}$$

where $W(z) = w(-z)$, $\star$ denotes the convolution product, and

$$\Phi_{y,\xi}(z) = \int_{\Upsilon_\xi} \sigma(y + z\xi + r)A(z, |r|)\nabla U(y + z\xi + r)dr.$$

As will be shown in section 5.5, through a one dimensional deconvolution problem that can be stably solved using, for instance, a Wiener-type filtering method, we get access to the function $\Phi_{y,\xi} \cdot \tau(\xi)$. Now the question is about the reconstruction of σ from $\Phi_{y,\xi} \cdot \tau(\xi)$. We can notice that $\Phi_{y,\xi}$ is a weighted Radon transform applied to the virtual current field $\sigma\nabla U$. The weight $A(z, |r|)$ is critical for the choice of the method that we can use. Closer this weight is to a Dirac mass function, better is the stability of the reconstruction. In this case, if the field $\sigma\nabla U$ does not have too large variations, we can recover a first-order approximation; as discussed in the rest of this section.

In order to make the reconstruction accurate and stable, we make two assumptions on the set of parameters $Y \times D \times]0, z_{max}[$. For any $x \in \Omega$, we define

$$\mathfrak{S}_x = \left\{ \xi \in \mathfrak{S} \ : \ \xi = \frac{x - y}{|x - y|} \ \text{ for some } \ y \in Y \right\}.$$

The first assumption is

$$\text{(H1)} \quad \forall x \in \Omega, \ \ \exists\, \xi_1, \xi_2 \in \mathfrak{S}_x \quad \text{s.t.} \quad |\xi_1 \times \xi_2| \neq 0,$$

and the second one reads

$$\text{(H2)} \quad \forall x \in \Omega, \ \ \forall \xi \in \mathfrak{S}_x, \ \ \exists \text{ unique } \ y \in Y \quad \text{s.t.} \quad \xi = \frac{x - y}{|x - y|}.$$

From the assumption (H2), we can define a distance map $|x-y|$ as a function of x and ξ. We will denote $d_Y(x,\xi) = |x-y|$. By a change of variables, we rename our data function Σ as

$$\begin{aligned}\psi(x,\xi) &= \Phi_{y,\xi}\big(d_Y(x,\xi)\big)\cdot\tau(\xi)\\ &= \int_{\Upsilon_\xi}(\sigma\nabla U)(x+r)A\big(d_Y(x,\xi),|r|\big)dr\cdot\tau(\xi).\end{aligned} \tag{5.13}$$

Now if we denote by

$$\gamma(x,\xi) = \int_{\Upsilon_\xi} A\big(d_Y(x,\xi),|r|\big)dr\ \tau(\xi), \tag{5.14}$$

then we expect that

$$\psi(x,\xi)\approx(\sigma\nabla U)(x)\cdot\gamma(x,\xi),$$

provided the supp(A) is small enough and $\sigma\nabla U$ does not vary too much. The following lemma makes this statement precise.

Lemma 5.2.1 *Consider a fixed direction $\xi\in\mathfrak{S}$ and consider the domain covered by the pulses of direction ξ defined by $\Omega_\xi=\{x\in\Omega\ :\ \xi\in\mathfrak{S}_x\}$. Suppose that the virtual current $\sigma\nabla U$ has bounded variations, then*

$$\|\psi(\cdot,\xi)-\sigma\nabla U\cdot\gamma(\cdot,\xi)\|_{L^1(\Omega_\xi)}\le cR\|\sigma\nabla U\|_{TV(\Omega)^2},$$

where R is the maximum radius of the cylindrical support of the envelope A and $c>0$ depends on the shape of A. Here, $\|\ \|_{TV(\Omega)^2}$ denotes the total variation semi-norm.

Proof. For a.e. $x\in\Omega_\xi$, we have

$$\begin{aligned}&|\psi(x,\xi)-(\sigma\nabla U)(x)\cdot\gamma(x,\xi)|\le\\ &\int_{\Upsilon_\xi}|(\sigma\nabla U)(x+r)-(\sigma\nabla U)(x)|\,A\big(d_Y(x,\xi),|r|\big)dr,\end{aligned}$$

and so

$$\begin{aligned}&\|\psi(\cdot,\xi)-\sigma\nabla U\cdot\gamma(\cdot,\xi)\|_{L^1(\Omega_\xi)}\\ &\le\int_{\Upsilon_\xi}\int_{\Omega_\xi}|(\sigma\nabla U)(x+r)-(\sigma\nabla U)(x)|\,A\big(d_Y(x,\xi),|r|\big)dxdr\\ &\le\|\sigma\nabla U\|_{TV(\Omega)^2}\int_{\Upsilon_\xi}|r|\sup_{0<z<z_{max}}A(z,|r|)dr\\ &\le 2\pi R\|\sigma\nabla U\|_{TV(\Omega)^2}\int_{\mathbb{R}+}\sup_{0<z<z_{max}}A(z,\rho)d\rho.\end{aligned}$$

□

Note that in the most interesting cases, $\sigma\nabla U$ has bounded variations. For example, if σ has a piecewise $W^{1,\infty}$ smoothness on smooth inclusions, then $\sigma\nabla U$ has bounded variations. This also holds true for σ in some subclasses of functions of bounded variations. In the following, we make the assumption, as in Lemma 5.2.1, that $\sigma\nabla U$ has bounded variations.

In conclusion, our data approximates the quantity $(\sigma\nabla U)(x)\cdot\gamma(x,\xi)$ for any $x\in\Omega$, $\xi\in\mathfrak{S}_x$ where the vector $\gamma(x,\xi)$ is supposed to be known. To get the current $(\sigma\nabla U)(x)$, we simply consider data from two linearly independent directions. Using assumption (H1), for a fixed $x\in\Omega$, there exist $\xi_1,\xi_2\in\mathfrak{S}_x$ such that $\det(\xi_1,\xi_2)\neq 0$. We construct the 2×2 invertible matrix

$$\Gamma(x,\xi_1,\xi_2)=\begin{bmatrix}\gamma(x,\xi_1)^\perp\\ \gamma(x,\xi_2)^\perp\end{bmatrix},$$

and the data column vector

$$\Psi(x,\xi_1,\xi_2)=\begin{bmatrix}\psi(x,\xi_1)\\ \psi(x,\xi_2)\end{bmatrix}.$$

We approximate the current $\sigma\nabla U(x)$ by the vector field

$$V(x,\xi_1,\xi_2)=\Gamma(x,\xi_1,\xi_2)^{-1}\Psi(x,\xi_1,\xi_2).$$

Indeed, for any open set $\widetilde{\Omega}\subset\Omega_{\xi_1}\cap\Omega_{\xi_2}$, the following estimate holds:

$$\begin{aligned}&\|V(\cdot,\xi_1,\xi_2)-\sigma\nabla U\|_{L^1(\widetilde{\Omega})^2}\\ &\leq\sup_{x\in\widetilde{\Omega}}\left\|\Gamma(x,\xi_1,\xi_2)^{-1}\right\|_{\mathcal{L}(\mathbb{R}^2)}\left(\sum_{i=1}^{2}\|\psi(\cdot,\xi_i)-\sigma\nabla U\cdot\gamma(\cdot,\xi_i)\|_{L^1(\Omega_{\xi_i})}\right)^{1/2}\\ &\leq cR\|\sigma\nabla U\|_{TV(\Omega)^2}.\end{aligned}$$

It is worth mentioning that if more directions are available, then we can use them to enhance the stability of the reconstruction. The linear system becomes over-determined and we can get the optimal approximation by using a least-squares method.

5.3 Recovering the conductivity by optimal control

In this section we assume that, according to the previous one, we are in the situation where we know a good approximation of the virtual current $D:=\sigma\nabla U$ in the sense of $L^1(\Omega)^2$. The objective here is to provide efficient methods for separating σ from D.

For $a<b$, let us denote by $L^\infty_{a,b}(\Omega):=\{f\in L^\infty(\Omega)\ :\ a<f<b\}$ and define the operator $\mathcal{F}:L^\infty_{\underline{\sigma},\overline{\sigma}}(\Omega)\longrightarrow H^1(\Omega)$ by

$$\mathcal{F}[\sigma]=U:\begin{cases}\nabla\cdot(\sigma\nabla U)=0 & \text{in }\Omega,\\ U=0 & \text{on }\Gamma_1,\\ U=1 & \text{on }\Gamma_2,\\ \partial_\nu U=0 & \text{on }\Gamma_0.\end{cases}\tag{5.15}$$

The following lemma holds.

Lemma 5.3.1 *The operator $\mathcal{F}$ is Fréchet differentiable and for any $\sigma\in L^\infty_{\underline{\sigma},\overline{\sigma}}(\Omega)$ and $h\in L^\infty(\Omega)$ such that $\sigma+h\in L^\infty_{\underline{\sigma},\overline{\sigma}}(\Omega)$ we have*

$$d\mathcal{F}[\sigma](h) = v : \quad \begin{cases} \nabla \cdot (\sigma \nabla v) = -\nabla \cdot (h \nabla \mathcal{F}[\sigma]) & \text{in } \Omega, \\ v = 0 & \text{on } \Gamma_1 \cup \Gamma_2, \\ \partial_\nu v = 0 & \text{on } \Gamma_0. \end{cases} \tag{5.16}$$

Proof. Let us denote by $w = \mathcal{F}[\sigma + h] - \mathcal{F}[\sigma] - v$. This function is in $H^1(\Omega)$ and satisfies the equation

$$\nabla \cdot (\sigma \nabla w) = -\nabla \cdot (h \nabla (\mathcal{F}[\sigma + h] - \mathcal{F}[\sigma]))$$

with the same boundary conditions as v. We have the elliptic global control:

$$\|\nabla w\|_{L^2(\Omega)} \leq \frac{1}{\underline{\sigma}} \|h\|_{L^\infty(\Omega)} \|\nabla (\mathcal{F}[\sigma + h] - \mathcal{F}[\sigma])\|_{L^2(\Omega)}.$$

Since

$$\nabla \cdot (\sigma \nabla (\mathcal{F}[\sigma + h] - \mathcal{F}[\sigma])) = -\nabla \cdot (h \nabla \mathcal{F}[\sigma + h]),$$

we can also control $\mathcal{F}[\sigma + h] - \mathcal{F}[\sigma]$ with

$$\|\nabla (\mathcal{F}[\sigma + h] - \mathcal{F}[\sigma])\|_{L^2(\Omega)} \leq \frac{1}{\underline{\sigma}} \|h\|_{L^\infty(\Omega)} \|\nabla \mathcal{F}[\sigma + h]\|_{L^2(\Omega)}.$$

Then, there is a positive constant C depending only on Ω such that

$$\|\nabla \mathcal{F}[\sigma + h]\|_{L^2(\Omega)} \leq C \frac{\overline{\sigma}}{\underline{\sigma}}.$$

Finally, we obtain

$$\|\nabla w\|_{L^2(\Omega)} \leq C \frac{\overline{\sigma}}{\underline{\sigma}^3} \|h\|^2_{L^\infty(\Omega)}.$$

□

We look for the minimizer of the functional

$$J[\sigma] = \frac{1}{2} \int_\Omega |\sigma \nabla \mathcal{F}[\sigma] - D|^2. \tag{5.17}$$

In order to do so, we compute its gradient. The following lemma holds.

Lemma 5.3.2 *For any $\sigma \in L^\infty_{\underline{\sigma},\overline{\sigma}}(\Omega)$,*

$$dJ[\sigma] = (\sigma \nabla \mathcal{F}[\sigma] - D - \nabla p) \cdot \nabla \mathcal{F}[\sigma],$$

where p is defined as the solution to the adjoint problem:

$$\begin{cases} \nabla \cdot (\sigma \nabla p) = \nabla \cdot (\sigma^2 \nabla \mathcal{F}[\sigma] - \sigma D) & \text{in } \Omega, \\ p = 0 & \text{on } \Gamma_1 \cup \Gamma_2, \\ \partial_\nu p = 0 & \text{on } \Gamma_0. \end{cases} \tag{5.18}$$

Proof. As $\mathcal{F}$ is Fréchet differentiable, so is J. For $\sigma \in L^\infty_{\underline{\sigma},\overline{\sigma}}(\Omega)$ and $h \in L^\infty(\Omega)$ such that $\sigma + h \in L^\infty_{\underline{\sigma},\overline{\sigma}}(\Omega)$, we have

$$dJ[\sigma](h) = \int_\Omega (\sigma \nabla \mathcal{F}[\sigma] - D) \cdot (h \nabla \mathcal{F}[\sigma] + \sigma \nabla d\mathcal{F}[\sigma](h)).$$

Now, multiplying (5.18) by $d\mathcal{F}[\sigma](h)$, we get

$$\int_\Omega \sigma \nabla p \cdot \nabla d\mathcal{F}[\sigma](h) = \int_\Omega (\sigma^2 \nabla \mathcal{F}[\sigma] - \sigma D) \cdot \nabla d\mathcal{F}[\sigma](h).$$

On the other hand, multiplying (5.16) by p we arrive at

$$\int_\Omega \sigma \nabla p \cdot \nabla d\mathcal{F}[\sigma](h) = -\int_\Omega h \nabla \mathcal{F}[\sigma] \cdot \nabla p,$$

and therefore,

$$dJ[\sigma](h) = \int_\Omega h(\sigma \nabla \mathcal{F}[\sigma] - D - \nabla p) \cdot \nabla \mathcal{F}[\sigma].$$

□

Lemma 5.3.2 allows us to implement a numerical gradient descent method in order to find σ. A regularization term can also be added to $J[\sigma]$ in order to avoid instability. As we are seeking discontinuous σ with smooth variations out of the discontinuity set, a good choice would be the minimization of the regularized functional:

$$J_\varepsilon[\sigma] = \frac{1}{2} \int_\Omega |\sigma \nabla \mathcal{F}[\sigma] - D|^2 + \varepsilon ||\sigma||_{TV(\Omega)}, \tag{5.19}$$

where $\varepsilon > 0$ is the regularization parameter.

5.4 The orthogonal field method

In this section, we present an alternative direct method to optimal control for reconstructing the conductivity σ from the internal data $\sigma \nabla U$. It is based on solving a transport equation. The following approach may be extended to the three dimensional case. However, several proofs would need to be revisited.

Given a vector field $D = \sigma \nabla U$ which is parallel to ∇U everywhere, we may construct the vectorial field $F = (D_2, -D_1)^T$ which is everywhere orthogonal to D. Here, T denotes the transpose. The flow of F may define the level sets of U. Assuming that the variations of the conductivity σ are far enough from Γ_0, we can assume that $U(x) = x_2$ on this boundary part. Then U is a solution of the following transport equation:

$$\begin{cases} F \cdot \nabla u = 0 & \text{in } \Omega, \\ u = x_2 & \text{on } \partial\Omega. \end{cases} \tag{5.20}$$

In the case where (5.20) is well posed and can be solved, we can reconstruct the virtual potential U. The conductivity σ is deduced from U and D by the following identity

$$\sigma = \frac{D \cdot \nabla U}{|D|^2}. \tag{5.21}$$

Despite to its very simple form, this first-order equation is really tricky. Existence and uniqueness are both difficult challenges in the general case. Our main difficulty here is due to the fact that F is discontinuous. As the function U that we are looking for is a natural solution of this equation, we are only concerned here with the uniqueness of a solution to (5.20).

5.4.1 Uniqueness result for the transport equation

The uniqueness of a solution to (5.20) is directly linked to the existence of outgoing characteristic lines defined by the dynamic system:

$$\begin{cases} X'(t) = F(X(t)),\ t \geq 0, \\ X(0) = x,\ x \in \Omega, \end{cases} \tag{5.22}$$

which usually needs the continuity of F. As σ is in general not continuous, F is not continuous, which makes the classical existence results useless. Nevertheless, under some assumptions on σ, we can insure the existence of the characteristic lines.

Definition 5.4.1 *For any $k \in \mathbb{N}$, $\alpha \in]0,1[$, for any curve $\mathcal{C}$ of class $\mathcal{C}^{1,\alpha}$ such that $\Omega \setminus \mathcal{C}$ is a union of connected domains $\Omega_i, i = 1, 2, \cdots n$, we define $C^{k,\alpha}_{\mathcal{C}}(\overline{\Omega})$ to be the class of functions $f : \Omega \longrightarrow \mathbb{R}$ satisfying*

$$f|_{\Omega_i} \in \mathcal{C}^{k,\alpha}(\overline{\Omega_i}) \quad \forall i = 1, \cdots n.$$

Definition 5.4.2 *A conductivity σ is said to be admissible if there exists a constant $\alpha \in]0,1[$ and a curve $\mathcal{C}$ of class $\mathcal{C}^{1,\alpha}$ such that $\sigma \in C^{0,\alpha}_{\mathcal{C}}(\overline{\Omega}) \cap L^{\infty}_{\underline{\sigma},\overline{\sigma}}(\Omega)$ and*

$$\inf_{\Omega \setminus \mathcal{C}} \sigma \nabla \mathcal{F}[\sigma] \cdot e_2 \ > \ 0.$$

If σ is admissible and belongs to $C^{0,\alpha}_{\mathcal{C}}(\overline{\Omega})$, then the solution U of (5.10) belongs to $C^{1,\alpha}_{\mathcal{C}}(\overline{\Omega})$ and the field $F = (\sigma \nabla U)^{\perp}$ satisfies

$$F \in C^{0,\alpha}_{\mathcal{C}}(\overline{\Omega}) \quad \text{and} \quad \inf_{\Omega \setminus \mathcal{C}} F \cdot e_1 \ > \ 0.$$

Moreover, as F is orthogonal to $\sigma \nabla U$, we can describe the jump of F at the curve $\mathcal{C}$. Defining the normal and tangential unit vectors ν and τ and also the local sides (+) and (-) with respect to ν, we can write F on both sides as

$$\begin{aligned} F^+ &= \sigma^+ \partial_\nu U^+ \tau + \sigma^+ \partial_\tau U^+ \nu, \\ F^- &= \sigma^- \partial_\nu U^- \tau + \sigma^- \partial_\tau U^- \nu \end{aligned}$$

with the transmission conditions, $\sigma^+ \partial_\nu U^+ = \sigma^- \partial_\nu U^-$ and $\partial_\tau U^+ = \partial_\tau U^-$. Finally, we characterize the discontinuity of F by

$$[F] = [\sigma] \partial_\tau U \nu,$$

where $[\,]$ denotes the jump across $\mathcal{C}$.

With all of these properties for the field F, we can prove the existence of the characteristic lines for (5.22).

Theorem 5.4.1 *(Local existence of characteristics) Assume that $F \in C^{0,\alpha}_{\mathcal{C}}(\overline{\Omega})$ with $\mathcal{C}$ of class $\mathcal{C}^{1,\alpha}$ for $\alpha \in]0,1[$. Assume that the discontinuity of F on $\mathcal{C}$ satisfies*

$$F^+ = f\tau + \sigma^+ g\nu,$$
$$F^- = f\tau + \sigma^- g\nu$$

with $f, g, \sigma^+, \sigma^- \in \mathcal{C}^{0,\alpha}(\mathcal{C})$ where σ^+, σ^- are positive and g is locally signed. Then, for any $x_0 \in \Omega$, there exists $T > 0$ and $X \in \mathcal{C}^1\big([0,T[,\Omega\big)$ such that $t \mapsto F(X(t))$ is measurable and

$$X(t) = x_0 + \int_0^t F(X(s))ds, \quad \forall t \in [0,T[.$$

Proof. If $x_0 \notin \mathcal{C}$, then F is continuous in a neighborhood of x_0 and the Cauchy-Peano theorem can be applied.

If $x_0 \in \mathcal{C}$, then we choose a disk $B \subset \Omega$ centered at x_0. The oriented line $\mathcal{C}$ separates B in two simply connected open domains called B^+ and B^-. For ease of explanation, we may assume that $\mathcal{C} \cap B$ is straight line (since we can flatten the curve using a proper $\mathcal{C}^{0,\alpha}$-diffeomorphism).

Assume that $g(x_0) > 0$. Up to rescaling B, we can assume that $g(x) > 0$ for all $x \in \mathcal{C} \cap B$. We extend $F|_{B^+}$ to a continuous field $\tilde{F} \in \mathcal{C}^0(B)$ by even reflection. The Cauchy-Peano theorem insures the existence of $T > 0$ and $X \in \mathcal{C}^1\big([0,T[,\Omega\big)$ such that $X(0) = x_0$ and $X'(t) = \tilde{F}(X(t))$ for all $t \in [0,T[$. As $g(x_0) > 0$, we have $X'(0) \cdot \nu(x_0) > 0$ and $X(t) \in \overline{B^+}$ in a neighborhood of 0. Thus, for a small enough t, $X'(t) = F(X(t))$. If $g(x_0) < 0$, then we apply the same argument by interchanging B^- and B^+.

Suppose now that $g(x_0) = 0$. The field F is now tangent to the discontinuity line. If $f(x_0) = 0$, then $X(t) = x_0$ is a solution. We assume here that $f(x_0) > 0$. As g is assumed to be locally signed, we can suppose that $g \geq 0$ in a small sub-curve of $\mathcal{C}$ satisfying $(x - x_0) \cdot \tau(x_0) > 0$. Again, we extend $F|_{B^+}$ to a continuous field $\tilde{F} \in \mathcal{C}^0(B)$ by even reflection and use the Cauchy-Peano theorem to show that there exists $T > 0$ and $X \in \mathcal{C}^1\big([0,T[,\Omega\big)$ such that $X(0) = x_0$ and $X'(t) = \tilde{F}(X(t))$ for all $t \in [0,T[$. In order to complete the proof, we should show that $X(t)$ belongs to $\overline{B^+}$ for t small enough. If not, there exists a sequence $t_n \searrow 0$ such that $X(t_n) \in B^-$. By the mean value theorem, there exists $\tilde{t}_n \in (0, t_n)$ such that $F(X(\tilde{t}_n)) \cdot \nu(x_0) = X'(\tilde{t}_n) \cdot \nu(x_0) < 0$. Thus, $X(t)$ belongs to $\overline{B^+}$ and $X'(t) = F(X(t))$ for t small enough.

Note that the local monotony of g is satisfied in many cases. For instance if $\mathcal{C}$ is analytic and σ is piecewise constant, then ∇U is analytic on $\mathcal{C}$ and hence, g is locally signed. □

It is worth mentioning that existence of a solution for the Cauchy problem (5.22) has been proved in [40] provided that $F \cdot \nu > 0$ on $\mathcal{C}$. Here, we have made a weaker assumption. In fact, we only need that $F \cdot \nu$ is locally signed.

Corollary 5.4.2 *(Existence of outgoing characteristics) Consider $F \in C^{0,\alpha}_{\mathcal{C}}(\Omega)$ satisfying the same conditions as in Theorem 5.4.1 and the condition*

$$\inf_{\Omega \setminus \mathcal{C}} F \cdot e_1 \geq c,$$

where c is a positive constant. Then for any $x_0 \in \Omega$ there exists $0 < T < T_{\max}$ where $T_{\max} = \frac{1}{c} diam(\Omega)$ and $X \in \mathcal{C}^0\big([0,T[,\Omega\big)$ satisfying

$$\begin{aligned} X(t) &= x_0 + \int_0^t F(X(s))ds, \quad \forall t \in [0,T[, \\ \lim_{t\to T} X(t) &\in \partial\Omega. \end{aligned}$$

This result means that from any point $x_0 \in \Omega$, the characteristic line reaches $\partial\Omega$ in a finite time.

Proof. Let $x_0 \in \Omega$ and $X \in \mathcal{C}^0\big([0,T[,\Omega\big)$ a maximal solution of (5.22). Using $F \cdot e_1 \geq c$ we have that $X'(t) \cdot e_1 \geq c$ and so $X(t) \cdot e_1 \geq x_0 \cdot e_1 + ct$ and as $X(t) \in \Omega$ for all $t \in [0,T[$, it is necessary that $T < T_{\max}$. As $F \in C^{0,\alpha}_{\mathcal{C}}(\Omega)$, F is bounded, X is Lipschitz, and the limit of $X(t)$ when t goes to T exists in $\overline{\Omega}$ and is called $X(T)$. Let us show that $X(T) \in \partial\Omega$. Suppose that $X(T) \in \Omega$, then applying Theorem 5.4.1 at $X(T)$, we can continuously extend X on $[T, T+\varepsilon[$ for some positive ε which contradicts the fact that X is a maximal solution.$\square$

Corollary 5.4.3 *(Uniqueness for the transport problem) Consider $F \in C^{0,\alpha}_{\mathcal{C}}(\Omega)$ satisfying the same conditions as in Corollary 5.4.2 and consider $u \in \mathcal{C}^0\big(\overline{\Omega}\big) \cap \mathcal{C}^1 C\big(\overline{\Omega}\big)$. If u is a solution of the system*

$$\begin{cases} F \cdot \nabla u = 0 & \text{in } \Omega, \\ u = 0 & \text{on } \partial\Omega, \end{cases} \tag{5.23}$$

then $u = 0$ in Ω.

Proof. Consider $x_0 \in \Omega$ and a characteristic $X \in \mathcal{C}^0\big([0,T[,\Omega\big)$ satisfying

$$\begin{aligned} X(t) &= x_0 + \int_0^t F(X(s))ds, \quad \forall t \in [0,T[, \\ \lim_{t\to T} X(t) &\in \partial\Omega. \end{aligned}$$

We define $f \in \mathcal{C}^0\big([0,T],\mathbb{R}\big)$ by $f(t) = u(X(t))$. We show that f is constant. Let us define $I = X^{-1}(\mathcal{C})$ then f is differentiable in $[0,T]\backslash I$ and $f'(t) = \nabla u(X(t)) \cdot F(X(t)) = 0$. Let us take $t \in I$. If t is not isolated in I, using the fact that $\partial_\tau u^+$ and $\partial_\tau u^-$ are locally signed, $F(X(t))$ is parallel to $\mathcal{C}$ and for an $\varepsilon > 0$, $X(s) \in \overline{B^+}$ (or $\overline{B^-}$) for $s \in [t, t+\varepsilon[$. Then, $f(s) = u(x(s))$ is differentiable on $[t, t+\varepsilon[$ with $f'(s) = \nabla u^+(X(s)) \cdot F(X(s))$. This proves that f is right differentiable at t and $(f')^+(t) = 0$. By the same argument, f is left differentiable at t and $(f')^-(t) = 0$ and so f is differentiable at t with $f'(t) = 0$. Finally, except for a zero measure set of isolated points, f is differentiable on $[0,T]$ and $f' = 0$ almost everywhere. This is not enough to conclude because there exists continuous increasing functions whose derivative is zero almost everywhere. Since for all $t, s \in [0,T]$,

$$|f(t) - f(s)| \leq \sup|\nabla u||X(t) - X(s)| \leq \sup|\nabla U| \sup|F||t-s|,$$

f is Lipschitz and thus absolutely continuous which implies, since $f' = 0$ a.e., that f is constant on $[0,T]$. We finally have $u(x_0) = f(0) = f(T) = u(X(T)) = 0$. □

Hence we conclude that if σ is admissible, then U is the unique solution to (5.20) and we can recover σ by (5.21).

Remark 5.4.4 *The characteristic method can be used to solve the transport problem. However, it suffers from poor numerical stability which is exponentially growing with the distance to the boundary. To avoid this delicate numerical issue, we propose a regularized approach for solving (5.20). Our approach consists in forming from (5.20) a second-order PDE and adding to this PDE a small elliptic term of order two.*

5.4.2 The viscosity-type regularization

In this subsection we introduce a viscosity approximation to (5.20). Let $\varepsilon > 0$. We regularize the transport equation (5.20) by considering the well-posed elliptic problem

$$\begin{cases} \nabla \cdot \left[\left(\varepsilon I + FF^T \right) \nabla u_\varepsilon \right] = 0 & \text{in } \Omega, \\ u_\varepsilon = x_2 & \text{on } \partial\Omega. \end{cases} \tag{5.24}$$

The main question is to understand the behavior of u_ε when ε goes to zero. Or more precisely, whether u_ε converges to the solution U of the transport equation (5.20) for a certain topology. The following result holds.

Theorem 5.4.5 *The sequence $(u_\varepsilon - U)_{\varepsilon>0}$ converges strongly to zero in $H_0^1(\Omega)$.*

Proof. We first prove that the sequence $(u_\varepsilon - U)_{\varepsilon>0}$ converges weakly to zero in $H_0^1(\Omega)$ when ε goes to zero. For any $\varepsilon > 0$, $\tilde{u}_\varepsilon := u_\varepsilon - U$ is in $H_0^1(\Omega)$ and satisfies

$$\nabla \cdot \left[\left(\varepsilon I + FF^T \right) \nabla \tilde{u}_\varepsilon \right] = -\varepsilon \triangle U \quad \text{in } \Omega. \tag{5.25}$$

Multiplying this equation by $\tilde{u}_\varepsilon$ and integrating by parts over Ω, we obtain

$$\varepsilon \int_\Omega |\nabla \tilde{u}_\varepsilon|^2 + \int_\Omega |F \cdot \nabla \tilde{u}_\varepsilon|^2 = -\varepsilon \int_\Omega \nabla U \cdot \nabla \tilde{u}_\varepsilon \tag{5.26}$$

and so,

$$\|\tilde{u}_\varepsilon\|^2_{H_0^1(\Omega)} \leq \int_\Omega |\nabla u \cdot \nabla \tilde{u}_\varepsilon| \leq \|U\|_{H^1(\Omega)} \|\tilde{u}_\varepsilon\|_{H_0^1(\Omega)}.$$

Then $\|\tilde{u}_\varepsilon\|_{H_0^1(\Omega)} \leq \|U\|_{H^1(\Omega)}$. The sequence $(u_\varepsilon)_{\varepsilon>0}$ is bounded in $H_0^1(\Omega)$ and so by Banach-Alaoglu's theorem, we can extract a subsequence which converges weakly to u^* in $H_0^1(\Omega)$. Multiplying (5.25) by u^* and integrating by parts, we get

$$\int_\Omega (F \cdot \nabla \tilde{u}_\varepsilon)(F \cdot \nabla u^*) = -\varepsilon \int_\Omega \nabla U \cdot \nabla u^* - \varepsilon \int_\Omega \nabla \tilde{u}_\varepsilon \cdot \nabla u^*.$$

Taking the limit when ε goes to zero,

$$\|F \cdot \nabla u^*\|_{L^2(\Omega)} = 0.$$

So u^* is a solution of the transport equation (5.23), and by Corollary 5.4.3, $u^* = 0$ in Ω. Actually, there is no need for the extraction of a subsequence to get the weak convergence result. Indeed, zero is the only accumulation point for u_ε for the weak topology. Consider a subsequence $u_{\phi(\varepsilon)}$. It is still bounded in $H_0^1(\Omega)$. Therefore, using the same argument as above, zero is an accumulation point of this subsequence.

Now, we are ready to prove the strong convergence. From (5.26) we get that

$$\int_\Omega |\nabla \tilde{u}_\varepsilon|^2 \leq -\int_\Omega \nabla U \cdot \nabla \tilde{u}_\varepsilon,$$

and as $\tilde{u}_\varepsilon \rightharpoonup 0$ in $H_0^1(\Omega)$, the term in the right-hand side goes to zero when ε goes to zero. Hence, $\|\tilde{u}_\varepsilon\|_{H_0^1(\Omega)} \to 0$. □

Finally, using Theorem 5.4.5 we define the approximate resistivity by

$$\frac{1}{\sigma_\varepsilon} = \frac{D \cdot \nabla u_\varepsilon}{|D|^2},$$

which strongly converges to $\dfrac{1}{\sigma}$ in $L^2(\Omega)$.

5.5 Numerical results

In this section we first discuss the deconvolution step. Then we test both the optimal control and the orthogonal field reconstruction schemes.

5.5.1 Deconvolution

In this subsection, we consider the problem of recovering $\Phi_{y,\xi}$ from the measurements $M_{y,\xi}$ in the presence of noise. From (5.12), it is easy to see that this can be done by deconvolution. However, deconvolution is a numerically very unstable process. In order to render stability we use a Wiener filter [83]. We assume that the signal $M_{y,\xi}(.)$ is perturbed by a random white noise:

$$\widetilde{M}_{y,\xi}(z) = M_{y,\xi}(z) + \mu(z), \tag{5.27}$$

where μ is a white Gaussian noise with variance ν^2. Equation (5.27) can be written as

$$\widetilde{M}_{y,\xi}(z) = \left(W \star \Phi_{y,\xi}\right)(z) + \mu(z).$$

Denote by $S(\Sigma) = \int_{\mathbb{R}} |\mathcal{F}(\Phi_{y,\xi})(\omega)| d\omega$ the mean spectral density of Σ, where $\mathcal{F}$ is the Fourier transform. The Wiener deconvolution filter can be written in the frequency domain as

$$\widehat{L}(\omega) = \frac{\overline{\mathcal{F}(W)}(\omega)}{|\mathcal{F}(W)|^2(\omega) + \frac{\nu}{S(\Sigma)}}.$$

The quotient $\nu/S(\Sigma)$ is the signal-to-noise ratio. So, in order to use the filter, we need to have an a priori estimate of the signal-to-noise ratio. We then recover Σ up to a small error by

$$\widetilde{\Sigma}_{y,\xi} = \mathcal{F}^{-1}\left(\mathcal{F}(\widetilde{M})\widehat{L}\right).$$

5.5.2 Conductivity reconstructions

In the numerical simulations, we choose $\Omega =]0,2[\times]0,1[$. Figure 5.3 (1) shows the true conductivity map in the medium. The simulations are done using a PDE solver. The data is simulated numerically on a fine mesh. For the orthogonal field method, in order to solve (5.24), we use a coarse mesh. Then we reconstruct an initial image of the conductivity. Based on the initial image, an adaptive mesh refinement for solving (5.24) yields a conductivity image of a better quality. Figure 5.3 (2) shows the used meshes for solving the viscosity approximation.

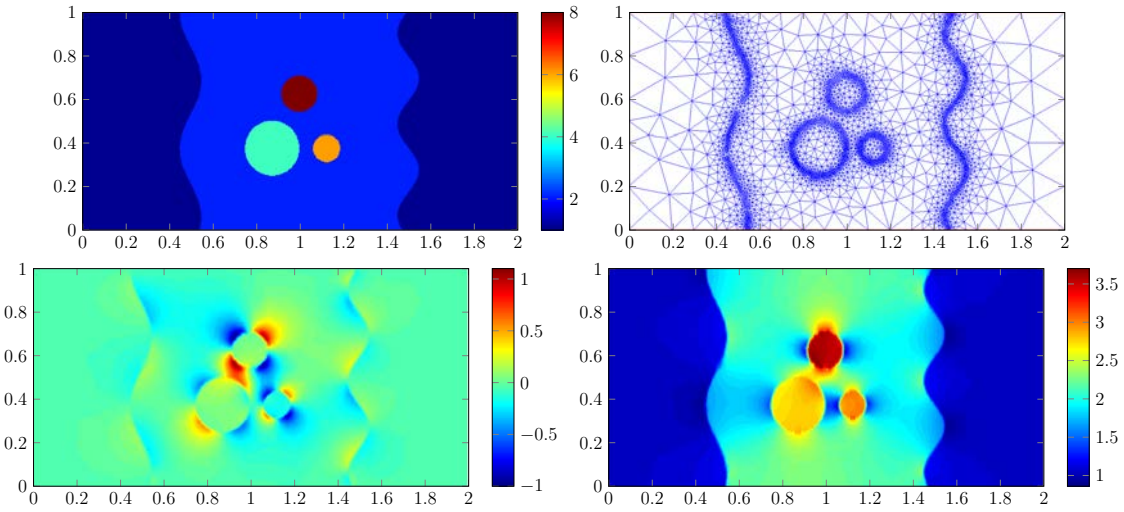

Figure 5.3: From left to right, top to bottom. (1) The conductivity map σ to be reconstructed. (2) The adapted mesh used to solve the direct problem. (2) the first component of the virtual current $\sigma\nabla U$. (3) the second component of the virtual current $\sigma\nabla U$.

The optimal control method

The minimization procedure gives a decent qualitative reconstruction. The main interfaces are easy to see, yet this method, due to its regularizing effect, fails to show details in weaker contrasts zones.

Transport equation method.

To find the solution of problem (5.24), we fix $\varepsilon = 10^{-3}$, and solve the equation on a uniform mesh on Ω. We reconstruct an approximation of σ, and adapt the mesh to this first reconstruction. We do this procedure several times in order to get refined mesh near the conductivity jumps. We can see that besides being computationally lighter than the minimization method, the orthogonal field method allows a quantitative reconstruction of σ and shows details even in the low contrast zones. It is relatively stable with respect to measurement noise. Figures **??**, **??**, and **??** show the reconstruction with different measurement noise levels. Figure **??** shows the L^2 norm of the error with respect to measurement noise,

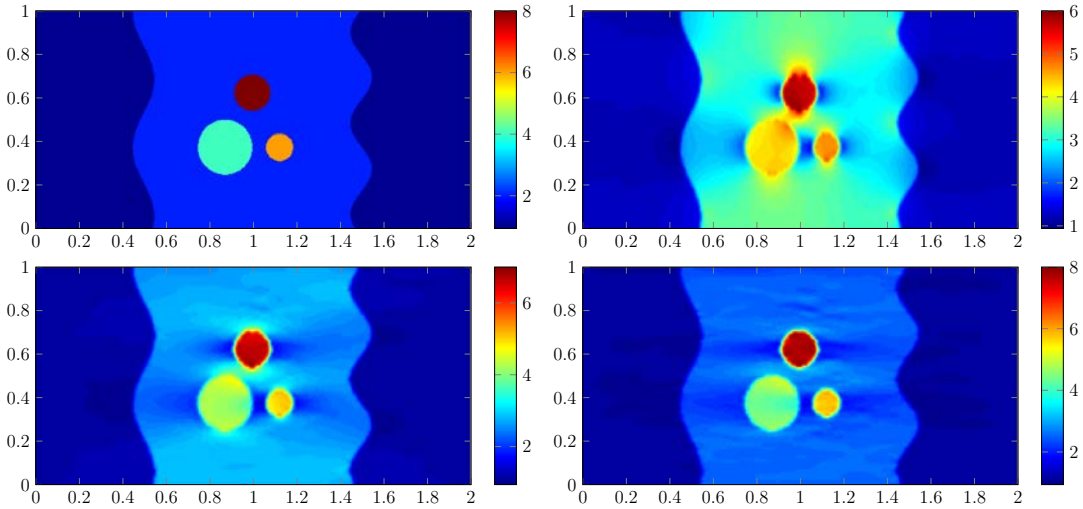

Figure 5.4: Reconstruction of the conductivity by optimization method. (1) The true conductivity. (2) Reconstruction after 5 iteration, (3) after 10 iterations and (5) after 20 iterations.

with ε fixed at 10^{-3}. A smaller ε increases the noise sensibility at higher noise levels, but also improves the details and reduces the smoothing effect of the $\varepsilon\Delta$ term in (5.24).

5.6 Concluding remarks

In this paper we have provided the mathematical basis of ultrasonically-induced Lorentz force electrical impedance tomography. We have designed two efficient algorithms and tested them numerically. The resolution of the reconstructed images is fixed by the ultrasound wavelength and the width of the ultrasonic beam. The orthogonal field method performs much better than the optimization scheme in terms of both computational time and accuracy. In a forthcoming work, we intend to generalize our approach for imaging anisotropic conductivities by ultrasonically-induced Lorentz force [107]. We will also propose an algorithm to find $\sigma\nabla U$ from the data function ψ using (5.13) and correct the leading-order approximation (5.14). This will enhance the resolution of the reconstructed conductivity images. Another challenging problem under consideration is to interpret the high-frequency component of $M_{y,\xi}$ in terms of speckle conductivity contrasts.

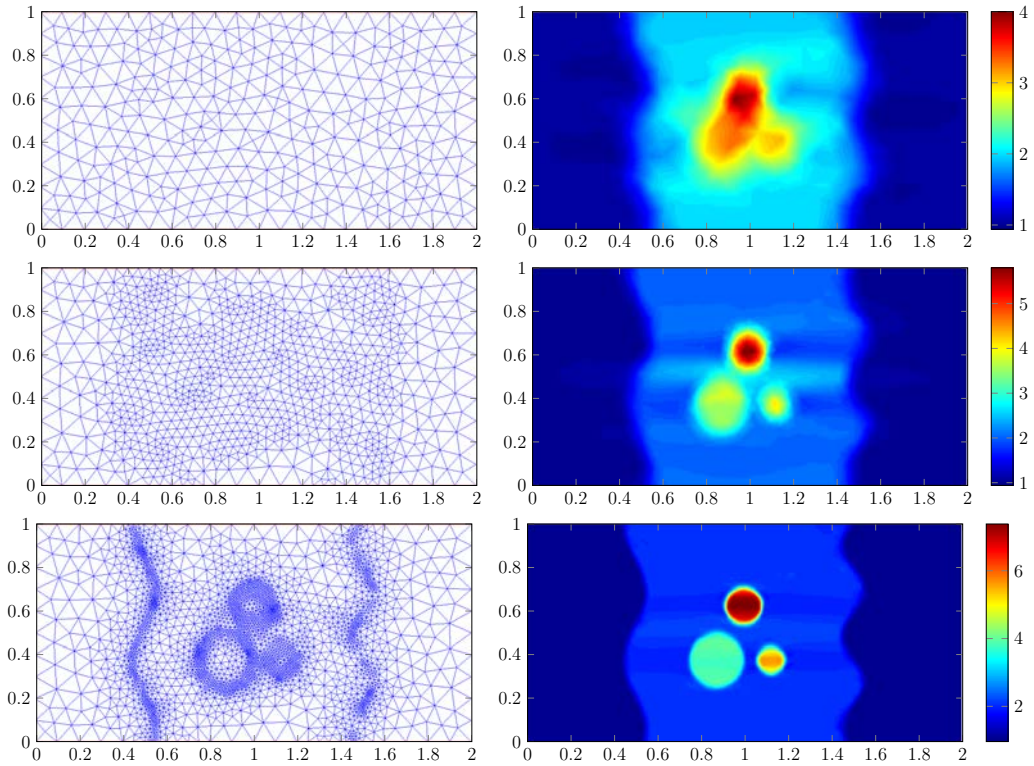

Figure 5.5: Reconstruction of the conductivity σ using the transport equation method with a viscosity parameter $\varepsilon = 10^{-3}$. To get a good resolution without any a priori informations about σ, we used an iterative mesh adaptation algorithm which refine the mesh around the highest variation of σ. Here is the reconstruction without mesh adaptation, with one adaptation and after three adaptations.

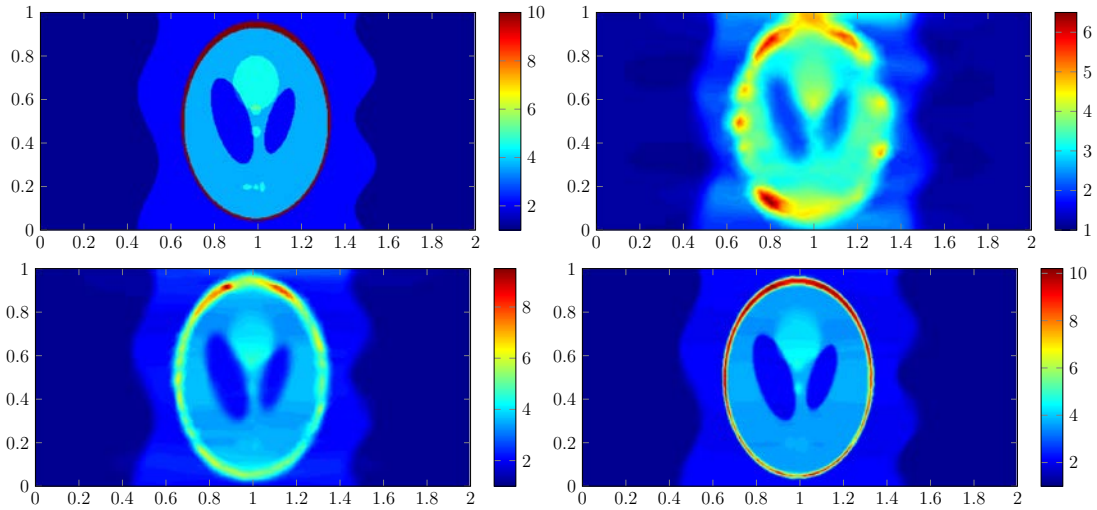

Figure 5.6: Reconstruction of the conductivity σ using the transport equation method with a viscosity parameter $\varepsilon = 10^{-3}$ and an adaptative mesh algorithm. (1) The original picture. (2) The reconstruction after one iteration. (3) After two iteration. (4) after five iterations.

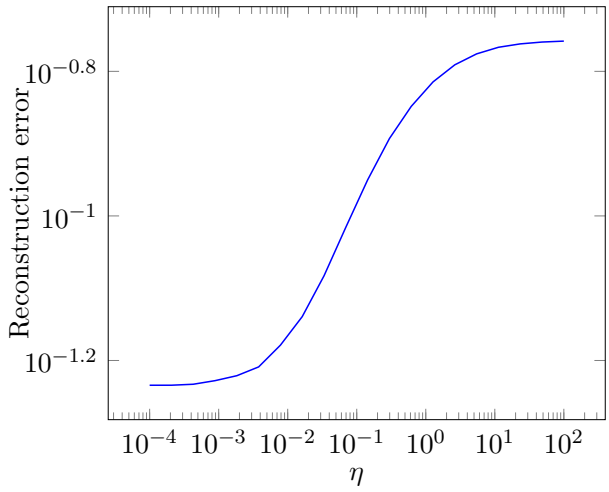

Figure 5.7: Reconstruction relative error with respect to the regularization parameter ε. The reconstruction is done with five mesh adaptation iterations.

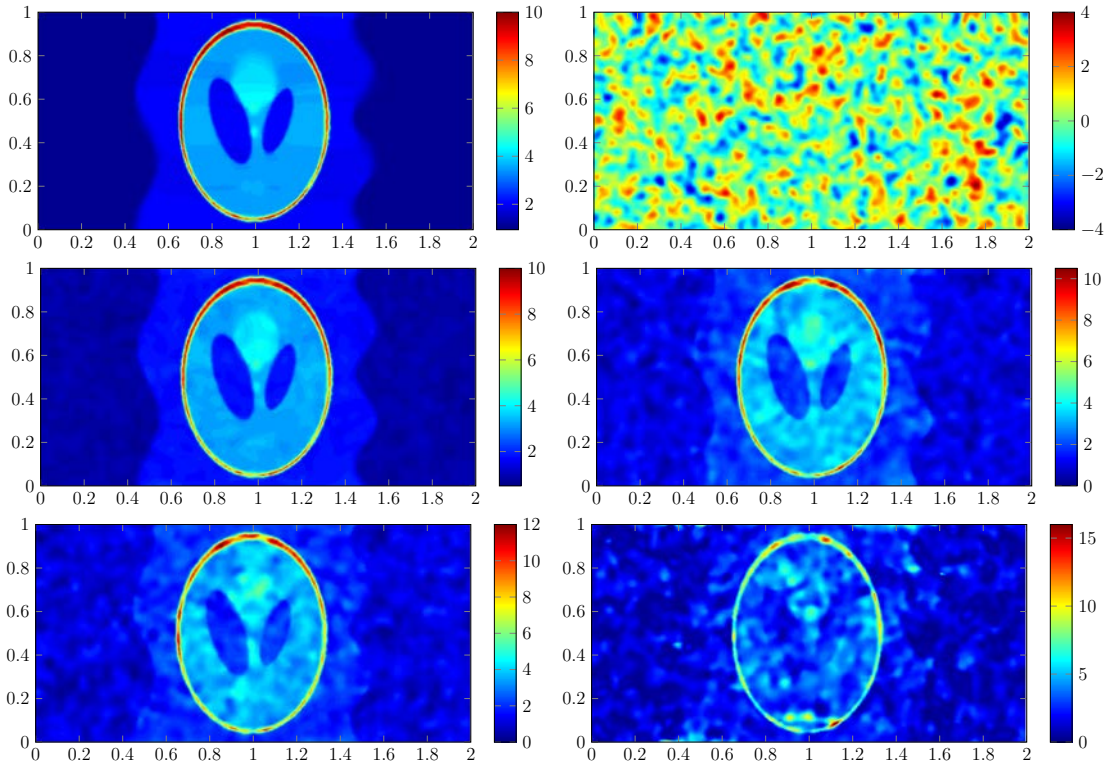

Figure 5.8: Reconstruction of the conductivity σ using the transport equation method with a viscosity parameter $\varepsilon = 10^{-3}$ with an additive medium noise. From left to right, top to bottom. (1) The reconstruction without noise. (2) The medium noise added to the internal current. (3) The reconstruction with a relative noise of 0.05. (4) The reconstruction with a relative noise of 0.1. (5) The reconstruction with a relative noise of 0.2. (6) The reconstruction with a relative noise of 0.5.

Concluding remarks

In this thesis, we have introduced new electrical and optical multi-wave imaging approaches. By mechanically perturbing the medium we have proved both analytically and numerically stability and resolution enhancement for reconstructing electrical and optical tissue parameters.

In Chapter 1 we have presented a mathematical framework and an efficient reconstruction technique based on spherical means Radon transform inversion for acousto-electromagnetic imaging. The Born approximation has been used. Both the analytical and numerical results illustrate the significant resolution enhancement in reconstructing the dielectric permittivity of the medium. Note that if we have at our disposal cross-correlation measurements for source points y on part of the unit circle only, then the inversion of formula (1.4.5) needs to be regularized. As shown in [12], a regularization with a total variation term is well adapted to smooth solutions with front discontinuous. The variant of Beck and Teboulle [34] accelerates the convergence of the inversion algorithm [12]. We have assumed that the acoustic wave propagates in a homogeneous medium and the amplitude of the background solution is constant. It would be interesting to exploit both the dielectric and elastic contrasts for enhancing specificity, specially in imaging tumors. Another important problem is to extend the mathematical framework to the case where the Born approximation is not valid or/and the amplitude of the background solution is constant.

In Chapter 2 we have presented a new algorithm for ultrasound-modulated optical diffuse tomography. The modulation of light is due to the propagation of spherical acoustic waves. It leads to a coupled system of equations. Iteratively solving such a system yields a resolved image for the optical absorption coefficient under the Born approximation. The algorithm has good stability properties. Its performance depends on the boundary data. In order to obtain optimal images in the sense of resolution and stability, the boundary data has to be chosen in such a way that the interior of the domain is illuminated.

The result of Chapter 2 can be extended to acousto-electromagnetic tomography developed in Chapter 1. In Chapter 1, the background solution, being a plane wave, has constant amplitude. Even though there is no maximum principle for the Helmholtz equation, the present approach applies to acousto-electromagnetic tomography if one can explicitly check that the amplitude of the background solution has a positive lower bound in the domain. This is the case, for example, when the background solution is a spherical wave emitted at a point outside the domain or in its boundary.

In Chapter 3 we have introduced a Landweber scheme for reconstructing piecewise smooth optical absorption distributions from opto acoustic measurements and proved its convergence. Because of the jumps in the absorption coefficient, we have used weak formulations for the Helmholtz decomposition for $\Phi_*^2 \nabla a_*$ and the relation between the spherical Radon transform of its gradient part ψ and the cross-correlation measurements $M_\eta(y, r)$. The res-

olution of the acousto-optic images is of order of η, the thickness of the acoustic wavefront. An interesting and challenging problem is to prove statistical stability of the proposed reconstruction with respect to a measurement noise by combining Fourier techniques together with statistical tools [17]. The magnitude of the additive noise should be much smaller than η^2. This yields a resolution limit for the acousto-optic process.

Note that we can enrich the set of data as follows. For $f \in L^2(\partial\Omega)$ such that $f \geq 0$ *a.e.* on $\partial\Omega$, compute instead of (3.19) the quantity

$$M_\eta^{f,g}(y,r) = \frac{1}{\eta^2}\int_{\partial\Omega}(f\partial_\nu\Phi^g_{u^\eta_{y,r}} - g\partial_\nu\Phi^f)\,d\sigma, \qquad y \in S_\mu, r > 0.$$

Similarly to (3.20), integration by parts yields

$$M_\eta^{f,g}(y,r) = \frac{1}{\eta^2}\int_\Omega (a_{u^\eta_{y,r}} - a)\Phi^f\Phi^g_{u^\eta_{y,r}}\,dx, \tag{5.28}$$

where Φ^f is the solution of (3.4) with g replaced by f. Note that the auxiliary data set is measured without medium perturbation.

The enriched data (5.28) may be used in order to generalize our approach to the case of measurements of the outgoing light intensities on only part of $\partial\Omega$ by choosing f supported only on the accessible part of the boundary.

In Chapter **??** we have extended the reconstruction and stability results of Chapters 2 and 3 to a very general class of optical absorption distributions.

In Chapter 5 we have provided the mathematical basis of ultrasonically-induced Lorentz force electrical impedance tomography. We have designed two efficient algorithms and tested them numerically. The resolution of the reconstructed images is fixed by the ultrasound wavelength and the width of the ultrasonic beam. The orthogonal field method performs much better than the optimization scheme in terms of both computational time and accuracy. A challenging problem is to generalize our approach for imaging anisotropic conductivities by ultrasonically-induced Lorentz force [107]. A second one is to propose an algorithm to find $\sigma\nabla U$ from the data function ψ using (5.13) and correct the leading-order approximation (5.14). This will enhance the resolution of the reconstructed conductivity images. A third one is to interpret the high-frequency component of $M_{y,\xi}$ in terms of speckle-type conductivity contrasts.

Bibliography

[1] G. Alberti and C. Mantegazza. A note on the theory of SBV functions. *Boll. Un. Mat. Ital.*, B (7) 11 (1997), no. 2, 375–382.

[2] G. Alessandrini and S. Vessella. Lipschitz stability for the inverse conductivity problem. *Adv. Appl. Math.*, 35 (2005), 207–241.

[3] H. Ammari. *An Introduction to Mathematics of Emerging Biomedical Imaging*. Vol. 62, Mathematics and Applications, Springer-Verlag, Berlin, 2008.

[4] H. Ammari, M. Asch, V. Jugnon, L. Guadarrama Bustos, and H. Kang. Transient imaging with limited-view data. *SIAM J. Imaging Sci.*, 4 (2011), 1097–1121.

[5] H. Ammari, E. Bonnetier, and Y. Capdeboscq. Enhanced resolution in structured media. *SIAM J. Appl. Math.*, 70 (2009), 1428–1452.

[6] H. Ammari, E. Bonnetier, Y. Capdeboscq, M. Tanter, and M. Fink. Electrical impedance tomography by elastic deformation. *SIAM J. Appl. Math.*, 68 (2008), 1557–1573.

[7] H. Ammari, E. Bossy, J. Garnier, W. Jing, and L. Seppecher. Radiative transfer and diffusion limits for wave field correlations in locally shifted random media. J. Math. Phys. 54 (2013), no. 2, 021501, 18 pp.

[8] H. Ammari, E. Bossy, J. Garnier, L. H. Nguyen and L. Seppecher. A reconstruction algorithm for ultrasound-modulated diffuse optical tomography. *Proc. Amer. Math. Soc.*, S 0002-9939(2014)12090-9.

[9] H. Ammari, E. Bossy, J. Garnier, and L. Seppecher. Acousto-electromagnetic tomography. *SIAM J. Appl. Math.*, 72 (2012), 1592–1617.

[10] H. Ammari, E. Bossy, V. Jugnon, and H. Kang. Mathematical modeling in photoacoustic imaging of small absorbers. SIAM Rev., 52 (2010), 677–695.

[11] H. Ammari, E. Bossy, V. Jugnon, and H. Kang. Qualitative photoacoustic imaging of small absorbers. *SIAM J. Appl. Math.*, 71, 676–693, 2011.

[12] H. Ammari, E. Bretin, V. Jugnon, and A. Wahab. Photoacoustic imaging for attenuating acoustic media, in *Mathematical Modeling in Biomedical Imaging II*. Lecture Notes in Mathematics, Vol. 2035, 57–84, Springer-Verlag, Berlin, 2011.

[13] H. Ammari, Y. Capdeboscq, F. de Gournay, A. Rozanova, and F. Triki. Microwave imaging by elastic perturbation. *SIAM J. Appl. Math.*, 71 (2011), 2112–2130.

[14] H. Ammari, Y. Capdeboscq, H. Kang, and A. Kozhemyak. Mathematical models and reconstruction methods in magneto-acoustic imaging. *European J. Appl. Math.*, 20 (2009), 303–317.

[15] H. Ammari, P. Garapon, H. Kang, and H. Lee. A method of biological tissues elasticity reconstruction using magnetic resonance elastography measurements. Quart. Appl. Math., 66 (2008), 139–175.

[16] H. Ammari, J. Garnier, L. Giovangigli, W. Jing, and J.K. Seo. Spectroscopic imaging of a dilute cell suspension. *arXiv* 1310.1292.

[17] H. Ammari, J. Garnier, and W. Jing. Resolution and stability analysis in acousto-electric imaging. *Inverse Problems*, 28 (2012), 084005.

[18] H. Ammari, J. Garnier, L.H. Nguyen, L. Seppecher, and M.P. Tran. 5.Convergence analysis of an image reconstruction algorithm from acousto-optic data. Preprint.

[19] H. Ammari, J. Garnier, L.H. Nguyen, and L. Seppecher. Reconstruction of a piecewise smooth absorption coefficient by an acousto-optic process. *Comm. Part. Differ. Equat.*, 38 (2013), no. 10, 1737–1762.

[20] H. Ammari, J. Garnier, and W. Jing. Resolution and stability analysis in acousto-electric imaging. *Inverse Problems*, 28 (2012), no. 8, 084005, 20 pp.

[21] H. Ammari, J. Garnier, H. Kang, M. Lim, and K. Sølna. Multistatic imaging of extended targets. *SIAM J. Imaging Sci.*, 5 (2012), 564–600.

[22] H. Ammari, J. Garnier, and K. Sølna. Resolution and stability analysis in full-aperture, linearized conductivity and wave imaging. *Proc. Amer. Math. Soc.*, 141 (2013), no. 10, 3431–3446.

[23] H. Ammari and H. Kang. Expansion Methods. *Handbook of Mathematical Methods in Imaging*, 447–499, Springer, New York, 2011.

[24] H. Ammari, O. Kwon, J.K. Seo, and E.J. Woo. T-Scan electrical impedance imaging system for anomaly detection. *SIAM J. Appl. Math.*, 65 (2004), 252–266.

[25] H. Ammari and A. Ramm. Recovery of small electromagnetic inhomogeneities from partial boundary measurements. *C. R. Acad. Sci. II*, 330 (2002), 199–205.

[26] H. Ammari and G. Uhlmann. Reconstruction of the potential from partial Cauchy data for the Schrödinger equation. *Indiana Univ. Math. J.*, 53 (2004), 169–183.

[27] S.R. Arridge. Optical tomography in medical imaging. *Inverse Problems*, 15 (1999), R41–R93.

[28] G. Bal, K. Ren, G. Uhlmann, and T. Zhou. Quantitative thermo-acoustics and related problems. *Inverse Problems*, 27 (2011), 055007 (15 pp).

[29] G. Bal and J.C. Schotland. Inverse scattering and acousto-optic imaging. *Phys. Rev. Letters*, 104 (2010), 043902.

[30] G. Bao, S. Hou, and P. Li. Inverse scattering by a continuation method with initial guesses from a direct imaging algorithm. *J. Comput. Phys.*, 227 (2007), 755–762.

[31] G. Bao and P. Li. Inverse medium scattering problems for electromagnetic waves. *SIAM J. Appl. Math.*, 65 (2005), 2049–2066.

[32] G. Bao and P. Li. Inverse medium scattering for the Helmholtz equation at fixed frequency. *Inverse Problems*, 21 (2005), 1621–1641.

[33] D. A. Boas, D. H. Brooks, E.L. Miller, C. A. DiMarzio, M. Kilmer, R. J. Gaudette, and Quan Zhang. Imaging the body with diffuse optical tomography. *Signal Processing Magazine, IEEE*, 18 (2001), 57–75.

[34] A. Beck and M. Teboulle. A fast iterative shrinkage-thresholding algorithm for linear inverse problems. *SIAM J. Imaging Sci.*, 2 (2009), 183–202.

[35] E. Beretta and E. Francini. Lipschitz stability for the electrical impedance tomography problem: the complex case. *Comm. Part. Differ. Equat.*, 36 (2011), 1723–1749.

[36] E. Beretta, M. V. De Hoop, and L. Qiu. Lipschitz stability of an inverse boundary value problem for a Schrödinger-type equation. *SIAM J. Math. Anal.*, 45 (2013), 679–699.

[37] E.J. Bond, S. Hagness, and B.D. Van Veen. Microwave imaging via space-time beamforming for early detection of breast cancer. *IEEE Trans. Antennas Propag.*, 51 (2003), 1690–1705.

[38] M. Born and E. Wolf. *Principles of Optics*. Cambridge University Press, Cambridge, 1999.

[39] E. Bossy, A.R. Funke, K. Daoudi, A.C. Boccara, M. Tanter, and M. Fink. Transient optoelastography in optically diffusive media. *Appl. Phys. Lett.*, 90 (2007), 174111.

[40] A. Bressan and W. Shen. On discontinuous differential equations. *Differential Inclusions and Optimal Control*, J. Andres, L. Gorniewicz and P. Nistri Eds., Julius Schauder Center, Lecture Notes in Nonlinear Analysis 2 (1998), 73–87.

[41] A. Buerkle and K. Sarabandi. Non-destructive evaluation of elastic targets using acousto-electromagnetic wave interaction and time reversal focusing. *IEEE Trans. Antennas Propag.* 57 (2009), 3628–3637.

[42] A.E. Bulyshev, A.E. Souvorov, S.Y. Semenov, R.H. Sevenson, A.G. Nazarov, Y.E. Sizov, and G.P. Tatsis. Three-dimensional microwave tomography. Theory and computer experiments in scalar approximation. *Inverse Problems*, 16 (2000), 863–875.

[43] Y. Capdeboscq, J. Fehrenbach, F. de Gournay, and O. Kavian. Imaging by modification: numerical reconstruction of local conductivities from corresponding power density measurements. *SIAM J. Imaging Sci.*, 2 (2009), 1003–1030.

[44] S.N. Chandler-Wilde and P. Monk. Wave-number-explicit bounds in time-harmonic scattering. *SIAM J. Math. Anal.*, 39 (2008), 1428–1455.

[45] M. Cheney, D. Isaacson, and J.C. Newell. Electrical impedance tomography. *SIAM Rev.*, 41 (1999), 85–101.

[46] D. Colton and R. Kress. *Inverse Acoustic and Electromagnetic Scattering Theory*. Vol. 93, *Applied Math. Sci.*, Springer-Verlag, New York, 1992.

[47] F. Delbary, M. Brignone, G. Bozza, R. Aramini, and M. Piana. A visualization method for breast cancer detection using microwaves. *SIAM J. Appl. Math.*, 70 (2010), 2509–2533.

[48] D. S. Elson, R. Li, C. Dunsby, R. Eckersley, and M. X. Tang. Ultrasound mediated optical tomography: a review of current methods. *Interface Focus*, doi:10.1098/rsfs.2011.0021.

[49] M. Fatemi and J.F. Greenleaf. Ultrasound stimulated vibro-acoustic spectroscopy. *Science*, 280 (1998), 82–85.

[50] E.C. Fear and M.A. Stuchly. Microwave detection of breast cancer. *IEEE Trans. Microwave Th. Tech.*, 48 (2000), 1854–1863.

[51] E.C. Fear, S.C. Hagness, P.M. Meaney, M. Okoniewski, and M.A. Stuchly. Enhancing breast tumor detection with near-field imaging. *IEEE Microwave Magazine*, 3 (2002), 48–56.

[52] D. Finch and Rakesh. The spherical mean value operator with centers on a sphere. *Inverse Problems*, 23 (2007), S37–S49.

[53] D. Finch, M. Haltmeier, and Rakesh. Inversion of spherical means and the wave equation in even dimensions. *SIAM J. Appl. Math.*, 68 (2007), 392–412.

[54] D. Finch, S. Patch, and Rakesh. Determining a function from its mean-values over a family of spheres. *SIAM J. Math. Anal.*, 35 (2004), 1213–1240.

[55] M. Fink and M. Tanter. Multiwave imaging and super resolution. *Phys. Today*, 63 (2010), 28–33.

[56] K.R. Foster and H.P. Schwan. Dielectric properties of tissues and biological materials: a critical review. *Critical Rev. Biomed. Eng.*, 17 (1989), 25–104.

[57] G. P. Galdi. *An Introduction to the Mathematical Theory of the Navier-Stokes Equations, Vol. I, Linearized Steady Problems*. Springer-Verlag, New York, 1994.

[58] B. Gebauer and O. Scherzer. Impedance-acoustic tomography. *SIAM J. Appl. Math.*, 69 (2008), 565–576.

[59] M. Giaquinta and E. Giusti. *Global $C^{1,\alpha}$ - regularity for second-order quasilinear elliptic equations in divergence form*, Research Report. Centre for Mathematical Analysis, Australian National University, 1983.

[60] D. Gilbarg and N. S. Trudinger. *Elliptic partial differential equations of second order.* Springer-Verlag, Berlin, 1977.

[61] P. González-Rodríguez and A. D. Kim. Reflectance optical tomography in epithelial tissues. *Inverse Problems*, 25 (2009), 015001, 24 pp.

[62] S.A. Goss, R.L. Johnston, and F. Dunn. Comprehensive compilation of empirical ultrasonic properties of mammalian tissues. *J. Acous. Soc. Amer.*, 64 (1978), 423.

[63] P. Grasland-Mongrain, J.-M. Mari, J.-Y. Chapelon, and C. Lafon. Lorentz force electrical impedance tomography. *IRBM*, 34 (2013), 357—360.

[64] M. Hanke, A. Neubauer, and O. Scherzer. A convergence analysis of the Landweber iteration for nonlinear ill-posed problems. *Numer. Math.*, 72 (1995), 21–37.

[65] D. Hyde, M. Kilmer, D. H. Brooks, and E. Miller. Analysis and exploitation of matrix structure arising in linearized optical tomographic imaging. *SIAM J. Matrix Anal. Appl.*, 29 (2007), 1065–1082.

[66] N. Irishina, D. Álvarez, O. Dorn, and M. Moscoso. Structural level set inversion for microwave breast screening. *Inverse Problems*, 26 (2010), 035015 (26pp).

[67] N. Irishina, O. Dorn, and M. Moscoso. A level set evolution strategy in microwave imaging for early breast cancer detection. *Comput. Math. Appl.*, 56 (2008), 607–618.

[68] K. Kilgore, S. Moskow, and J. C. Schotland. Inverse Born series for diffuse waves. *Contemp. Math.*, 494 (2009), 113–122.

[69] S. Kim, O. Kwon, J.K. Seo, and J.R. Yoon. On a nonlinear partial differential equation arising in magnetic resonance electrical impedance imaging. *SIAM J. Math. Anal.*, 34 (2002), 511–526.

[70] P. Kunchment and L. Kunyansky. Mathematics of thermoacoustic tomography. *Europ. J. Appl. Math.*, 19 (2008), 191–224.

[71] P. Kuchment and L. Kunyansky. Synthetic focusing in ultrasound modulated tomography. *Inverse Problems and Imaging*, 4 (2010) 655–673.

[72] P. Kuchment and L. Kunyansky. 2D and 3D reconstructions in acousto-electric tomography. *Inverse Problems*, 27 (2011), 055013.

[73] L. Kunyansky. A mathematical model and inversion procedure for Magneto-Acousto-Electric Tomography (MAET). *Inverse Problems*, 28 (2012), 035002.

[74] L. Kunyansky. A mathematical model and inversion procedure for magneto-acousto-electric tomography. *Inverse Problems*, 28 (2012), 035002.

[75] O. Kwon, J. Lee and J. Yoon. Equipotential line method for magnetic resonance electrical impedance tomography. *Inverse Problems*, 18 (2002), 1089–1100.

[76] O. A. Ladyzhenskaya and N. N. Ural'tseva. *Linear and Quasilinear Elliptic Equations.* Translated from the Russian by Scripta Technica, Inc. Translation editor: Leon Ehrenpreis, Academic Press, New York - London, 1968.

[77] E. Lee, J. K. Seo, E. J. Woo, and T. Zhang. Mathematical framework for a new microscopic electrical impedance tomography system. *Inverse Problems*, 27 (2011), p. 055008.

[78] X. Li, Y. Xu, and B. He. Imaging electrical impedance from acoustic measurements by means of magnetoacoustic tomography with magnetic induction (MAT-MI). *IEEE Trans. Bio. Eng.*, 2007 (54), 323–330.

[79] G. M. Lieberman. Boundary regularity for solutions of degenerate elliptic equations, *Nonlinear Anal.*, 12 (1988), 1203–1219.

[80] G. M. Lieberman. The natural generalization of the natural conditions of Ladyzhenskaya and Ural'tseva for elliptic equations. *Comm. Part. Diff. Equat.*, 16 (1991), 311–361.

[81] Q.H. Liu, Z.Q. Zhang, T. Wang, J.A. Bryan, G. Ybarra, L.W. Nolte, and W.T. Joines. Active microwave imaging I: 2-D forward and inverse scattering methods. *IEEE Trans. Microwave Th. Tech.*, 50 (2002), 123–133.

[82] N. H. Loc and K. Schmitt. On positive solutions of quasilinear elliptic equations. *Diff. Integral Equat.*, 22 (2009), 829–842.

[83] S. Mallat. *A Wavelet Tour of Signal Processing: the Sparse Way.* Academic Press, 2008.

[84] L. Mariappan and B. He. Magnetoacoustic tomography with magnetic induction: Bioimepedance reconstruction through vector source imaging. *IEEE Trans. Med. Imag.*, 32 (2013), 619–627.

[85] V. A. Markel and J. C. Schotland. Symmetries, inversion formulas, and image reconstruction for optical tomography. *Phys. Rev. E*, 70 (2004), 056616.

[86] J.M. Melenk and S. Sauter. Convergence analysis for finite element discretization of the Helmholtz equation with Dirichlet-to-Neumann boundary conditions. *Math. Comp.*, 79 (2010), 1871–1914.

[87] A. Montalibet. *Etude du couplage acousto-magnétique: détection des gradients de conductivité électrique en vue de la caractérisation tissulaire.* PhD., Dissertation, University of Lyon, 2002.

[88] T. Morimoto, S. Kimura, Y. Konishi, K. Komaki, T. Uyama, Y. Monden, D.Y. Kinouchi, and D. T. Iritani. A study of the electrical bio-impedance of tumors. *Investigative Surgery*, 6 (1993), 25–32.

[89] S. Moskow and J. C. Schotland. Convergence and stability of the inverse scattering series for diffuse waves. *Inverse Problems*, 24 (2008), 065005.

[90] A. Nachman, A. Tamasan, and A. Timonov. Reconstruction of planar conductivities in subdomains from incomplete data. *SIAM J. Appl. Math.*, 70 (2010), 3342–3362.

[91] W. Naetar and O. Scherzer. Quantitative photoacoustic tomography with piecewise constant material parameters. *arXiv*: 1403.2620.

[92] F. Natterer. An error bound for the Born approximation. *Inverse Problems*, 20 (2004), 447–452.

[93] J-C. Nédélec. *Acoustic and Electromagnetic Equations - Integral Representations for Harmonic Problems. Applied Mathematical Sciences*, Vol. 144, Springer, 2001.

[94] V. Palamodov. Remarks on the general Funk transform and thermoacoustic tomography. *Inverse Probl. Imaging*, 4 (2010), no. 4, 693–702.

[95] S. Pride. Governing equations for the coupled electromagnetics and acoustics of porous media. *Phys. Rev. B*, 50 (1994), 15678.

[96] M. H. Protter and H. F. Weinberger. *Maximum Principles in Differential Equations.* Prentice-Hall, 1967.

[97] E.T. Quinto. Support theorems for the spherical Radon transform on manifolds. *Int. Math. Res. Lett.*, 2006, 1–17 (Article ID 67205).

[98] M. C. W. van Rossum and Th. M. Nieuwenhuizen. Multiple scattering of classical waves: microscopy, mesoscopy, and diffusion. *Rev. Modern Phys.*, 71 (1999), 313–371.

[99] B.J. Roth. The role of magnetic forces in biology and medicine. *Soc. Exp. Bio. Med.*, 236 (2011), 132–137.

[100] B.J. Roth and K. Schalte. Ultrasonically-induced Lorentz force tomography. *Medical Bio. Eng. Comp.*, 47 (2009), 573–577.

[101] L. Ryzhik, G. Papanicolaou, and J. B. Keller. Transport equations for elastic and other waves in random media. *Wave Motion*, 24 (1996), 327–370.

[102] J. C. Schotland. Direct reconstruction methods in optical tomography. *Lecture Notes in Math.*, Vol. 2035, 1–29, Springer-Verlag, Berlin, 2011.

[103] J. C. Schotland and V. A. Markel. Inverse scattering with diffusing waves. *J. Opt. Soc. Amer. A*, 18 (2001), 2767–2777.

[104] J.K. Seo and E.J. Woo. Magnetic resonance electrical impedance tomography (MREIT). *SIAM Rev.*, 53 (2011), 40–68.

[105] J.K. Seo and E.J. Woo. *Nonlinear Inverse Problems in Imaging*. Wiley, 2013.

[106] F. Triki. Uniqueness and stability for the inverse medium problem with internal data. *Inverse Problems*, 26 (2010), 095014.

[107] N. Tseng and B.J. Roth. The potential induced in anisotropic tissue by the ultrasonically-induced Lorentz force. *Med. Bio. Eng. Compt.*, 46 (2008), 195–197.

[108] L. V. Wang. Mechanisms of ultrasonic modulation of multiply scattered coherent light: an analytic model. *Phys. Rev. Lett.*, 87 (2001), 043903.

[109] H. Wen, J. Shah, and R.S. Balaban. Hall effect imaging. *IEEE Trans. Biomedical Eng.*, 45 (1998), 119–124.

[110] T. Widlak and O. Scherzer. Hybrid tomography for conductivity imaging. *Inverse Problems*, 28 (2012), 084008.

[111] M. Zhao, J.D. Shea, S.C. Hagness, D.W. van der Weide, B.D. Van Veen, and T. Varghese. Numerical study of microwave scattering in breast tissue via coupled dielectric and elastic contrasts. *IEEE Trans. Wireless Prop. Lett.*, 7 (2008), 247–250.